CRANFIELD INSTITUTE OF TECHNOLOGY

COLLEGE OF AERONAUTICS

Ph. D Thesis

Academic Year 1991-1992

S. H. M. Macci

Structural and Mechanical Feasibility Study of a Variable Camber Wing (VCW) for a transport Aircraft

Supervisor: Dr J. P. Fielding

August 1992

ABSTRACT

Aerodynamic investigations have shown that variable camber wings (VCW) for transport aircraft have considerable potential in terms of improving aircraft performance and enhancing their operational flexibility. In order to justify these benefits it is essential that the camber varying system is structurally and mechanically feasible.

This research examined the feasibility of providing variable camber to two supercritical aerofoil sections of different characteristics. The unique method of camber variation was applied by rotating the forward and aft regions of the aerofoil on a circular arc and keeping the surface continuous and matching at their attachment to the main wing box. The change in camber thus increased the chord due to translational motion of the aforementioned regions.

The geometries required for varying the forward camber by this method presented formidable design difficulties and no immediate solutions could be found. As a result, an alternative geometry was devised which accepts camber by simply drooping the nose region.

A novel idea was developed for aft camber variation, which is considered to be universal for all supercritical aerofoil sections. The system utilises a tracking mechanism which guides a trailing edge element on a continuous arc. Surface continuity is provided by a flexible skin on the upper side and a spring loaded hinged panel on the under side. The flexible skin remains attached to the trailing edge element through a series of roller link arrangement which locate the skin in a separate guide rail. The large moment arm and therefore the increased torsional loads created due to the translational motion of the trailing edge element necessitated investigation of alternative deployment geometries. As a result two additional geometries were schemed. One had reduced radius of rotation and therefore reduced extension, while the other changed camber by drooping the aft region without any chordal extension. Since there was no aerodynamic evidence on the possible benefits offered by these geometries it was decide to postpone them until such information was available.

Some detailed aspects of the proposed concept for aft camber variation were considered by applying the system to a modern transport aircraft wing. This resulted in a design which is practically feasible. Justification of this concept was made by designing and testing a half scale structural model of one trailing edge segment. Three dimensional (3-D) geometric investigation showed that the camber-varying elements ride on a

frustum of a cone and therefore their deployment is skewed to the line of flight. The 3-D geometric implications of variable camber clearly suggested that the camber variation by rotation on a circular arc, on a tapered wing can be possible if the rotating element is made to flex and twist or it utilises a pin jointed arrangement. To provide the necessary flexibility to the trailing edge element, its structural box best be made from fibre reinforced plastic material. The deployment of the trailing edge element on the structural model was made possible by designing it in laminated wood.

Comparison of the proposed variable camber system with a conventional single slotted flap arrangement suggests that the two systems could be equally complex but the variable camber could be slightly heavier.

Further systems investigations are required to quantify overall aerodynamic, mass, and cost implications of the use of VCW on transport aircraft.

ACKNOWLEDGMENT

This project would not have been possible without the help of many people. I would like to express my sincere thanks to all of them including:

Dr. John Fielding for his supervision of the project and for providing me with the much needed guidance.

Professor John Spillman the originator of the variable camber concept for his advice and for taking a keen interest in this project. His enthusiasm and conviction provided the source of inspiration.

Alex Mackinnon who worked on the aerodynamic aspect of the concept. His thoughts and ideas together with our 'round the clock' discussions were of immense value.

Maurice Crook of the composite laboratory at the College of Aeronautics for helping with the manufacture of the composite skin and assembling of the structural model and also for his sane conversations regarding philosophical matters in life.

Malcolm Goodridge and the College of Aeronautics workshop boys for manufacturing the various components of the structural model.

Ian Stockman for proof reading the manuscript and improving my English in doing so.

My brother *Mushtaque* for his support and encouragement during the past years.

My dear wife *Shillu* for her understanding over the last twelve months and for giving me confidence to complete this work.

Mengé Omboko from Cameroon for the words of wisdom from the back of the pavilion.

All my *Friends* from Cranfield for providing *Many Magical Moments*.

Finally I would like to thank the Department of Trade and Industry and British Aerospace (Commercial Aircraft) Limited for awarding a joint contract to Cranfield Institute of Technology to carry out the variable camber wing research. It provided a unique opportunity to blend the extensive design experience of British Aerospace and Cranfield's research and testing facilities to produce a workable design solution.

TO SOPHIA MARIAM

CONTENTS

LIST OF FIGURES

CHAPTER THREE

APPENDIX B

APPENDIX C

LIST OF TABLES

NOTATION

The notation used in this thesis is as defined in the main text.

ABBREVIATIONS

ATVCW	Advanced Technology Variable Camber Wing
BAe	British Aerospace
BM	Bending moment
CFRP	Carbon fibre reinforced plastics
cofg	Centre of gravity
DOC	Direct operating cost
FE	Finite element
FEA	Finite element analysis
FLA	Future large aircraft
FRP	Fibre reinforced plastics
GLA	Gust load alleviation
H/L	Hinge-line
I/B	Inboard
LE	Leading edge
L/D	Lift to drag ratio
MAW	Mission adaptive wing
MBB	Messerschmitt-Bolkow-Blokom
MLC	Manoeuvre load control
O/B	Outboard
PTFE	PolyTetro Floro Ethylene
RAEVAM	Royal Aircraft Variable camber Mechanism
SF	Shear force
TE	Trailing edge
VC	Variable camber
VCW	Variable camber wing
WRBM	Wing root bending moment
2-D	Two dimensional
3-D	Three dimensional
$[90/0_2]_s$	Orientation, No. and lay-up of carbon fibres. Subscript 's' refers to symmetric lay

The two dimensional geometries and schemes described in Chapter Two and Seven are labelled as follows:-

Label Name	Figure No.	Details
LESA1	2.3a	LE VC geometry of Section A
LESA2	2.3b	LE VC design scheme for Section A
LESA3	2.3c	VC LE track details for Section A
LESB1	2.4a	First LE VC geometry for Section B
LESB2	2.4b	Second LE VC geometry for Section B
LESB3	2.5	LE VC design scheme one for Section B
LESB4	2.6	LE VC design scheme two for Section B
TESA1	2.7a	TE VC geometry one for Section A
TESB1	2.7b	TE VC geometry one for Section B
TESA2	2.8a	TE VC scheme one for Section A
TESB2	2.8c	TE VC scheme one for Section B
TESA3	2.10a	TE VC scheme two for Section A
TESB3	2.11a	TE VC scheme three for Section B
LESA4	2.12	LE VC scheme one with slat on Section A
TESA4	2.13	TE VC scheme one with flap on Section A
LESB5	2.14a	LE VC drooped nose geometry on Section B
LESB6	2.14b	LE VC with Kruieger flap on Section B
TESB4	7.1a	TE VC geometry two on Section B
TESB5	7.2	TE VC geometry three on Section B

CHAPTER ONE

INTRODUCTION

1.1 GENERAL

The mission profile of a transport aircraft consists of take-off, climb, cruise, descent, hold, and approach to touch down. During these phases the wing experiences a change in camber when it is configured from a low cambered high speed setting to low speed, take off and landing settings. This results in aerofoil sections which could only be optimum for one flight condition[1]. The change in wing profile is primarily made at the leading edges (LE) and trailing edges (TE) by deploying slat and flap systems respectively. In general these systems move in large increments away from the main wing section, creating undesirable sudden changes to the curvature of the camber line (Figure 1.1).

In service the aircraft often operates away from the design point, for example at cruise at different altitudes, when undergoing manoeuvres initiated by the pilot, or during atmospheric gust conditions. Conventional wings with 'discrete' camber changing systems similar to the one described above are not designed to have optimum lift characteristics during operations under these conditions. This results in a non optimum flight which has a marked effect on the performance and therefore on the fuel efficiency.

Variable camber (VC) implies changing the profile of the wing throughout the flight, while keeping the curvature of the camber line continuous, such that the aircraft operates at near optimum conditions. By varying the wing camber in this manner it is possible to continuously optimise the lift to drag (L/D) ratio and therefore improve performance, and reduce the direct operating cost (DOC) by increasing the fuel efficiency.

The economic success of a transport aircraft depends highly on its operational flexibility, the ability to operate over a wide and varying range of flight missions. For instance, during the lifespan of a commercial aircraft frequent requirements arise for increasing the payload or range to suit the market needs. In case of, say, the military air-lifters the varying mission requirement call for the aircraft to have long range strategic and short range tactical airlift capabilities. With the VC system it is possible to give such a flexibility in operation by improving the L/D which would assist in either increasing the fuel range or the payload mass.

Because of flexural deformation of wings under load, the LE and TE devices have to be divided into several spanwise sections. It follows that if each section is individually controlled, the camber can be varied across the span to suit the spanwise lift distribution required for different flight conditions, both in steady level flight and whilst manoeuvring. The ability to alter the spanwise lift distribution assists in reducing wing structural weight by reducing wing root bending moments (WRBM) associated with the gust and manoeuvre loads.

A smooth VC system therefore promises to contribute towards:-
1) Increasing fuel efficiency and reducing DOC,
2) Improving operational flexibility, and
3) Reducing WRBM,
These are the major goals in wing design for future transport aircraft.

The aerodynamic benefits listed above can only be justified if the variable camber wing (VCW) system represents a practically (structurally and mechanically) viable solution. This research explores the practical possibilities of achieving continuous camber variation on transport aircraft wings by examining:-

- Geometric implications on both the two dimensional (2-D) aerofoil sections, and the three dimensional (3-D) swept and tapered wings,
- The kinematic design of the system for achieving the camber,
- The possible complexities involved in the design of mechanical and structural components,
- The increase in structural weight as a result of these complexities, and
- The possible changes in the structural design of the wing.

1.2 HISTORICAL OVERVIEW OF VCW MECHANICAL FEATURES

The ability to optimise the aircraft wing so that it would suit all flight conditions has been a problem for aircraft designers since the early days of aviation. In order to achieve near perfect flight with a relatively light structure, it is necessary to design the wing, such that its profile can be altered continuously, in a manner similar to birds. Such variations could be realised if the wing is made from a skin that can flex and warp, and at the same time is sufficiently stiff to operate efficiently under aerodynamic loads.

Indeed, one may view the Wright Brother's attempt to alter the lift characteristics of their wing as a possible step towards achieving camber variation. A cable connected to the wing was hooked to a truss around the pilots hips, and when the hips moved the wing warped out of shape. This was a rudimentary form of camber control for banking the aircraft.

A number of aircraft thereafter had in-flight camber varying devices in one form or the other. Lack of material and mechanical technologies prevented designers from developing automatically flexing wings. Therefore the camber controlling devices on these aircraft (although automatically controlled) were limited in their applications and were designed to operate at certain flight conditions. An example of one such design is the 1914 Sopwith Baby[2], which incorporates the Fairey Aviation Company's "Patent camber gear". This consisted of full-span hinged trailing edge (TE) flaps that could be used either in opposition as ailerons or symmetrically as devices to increase lift. The flap deflections were controlled directly by the pilot through bungee chords, to provide increase in camber for low speeds.

It was not until the emergence of graphite based and fibre reinforced plastic (FRP) materials in the aerospace industry (some 25 years ago), that it became possible to implement flexible skin technology in high performance aircraft wing. Aircraft structural designers now had materials that could be tailored to have variable stiffness and flexibility. An important practical application of flexible skin using FRP materials was for the design of the leading edge (LE) variable camber (VC) Krueger flap on the Boeing 747[3]. The term 'VC' is used to describe the camber change that occurs to the flap panel as it is extended from its relatively flat shape, when stowed as part of the wing lower surface, to its fully cambered shape in the extended high lift position. Schematic diagram of the concept is shown in Figure 1.2. The flexible panel provides a smooth, gradually curved LE device with spanwise camber variation.

The successful use of flexible skin VC takeoff and landing flaps on the Boeing 747 was a breakthrough for the advancement of flexible skin concept to devices that could 'continuously' change the wing profile. In addition to the flexible skin systems, development in the areas of variable geometry mechanisms and actuation and drive systems has helped to progress research into the VC systems.

The references which describe the above schemes also include mechanical aspects such as linkage systems, variable geometry trusses with variable length members, cam and follower concepts, hinged multiple section devices, reinforced rubber extensible skins,

fibreglass skins, carbon fibre reinforced plastic (CFRP) skins, graphite epoxy skins, conventional hydraulic actuators, power hinges, rotary planetary gear units, pinion gear units and screw jacks.

1.2.1 Variable Camber by Drooping the Aerofoil

The most common method of achieving variable camber has been by 'drooping' the forward and aft regions of the aerofoil. Indeed, this method is so widely accepted that it has become the design norm. The first concept accepting this type of variation was an invention of a simple mechanical system for a LE geometry by Pierce and Treadgold[4]. An illustration of this idea is given in Figure 1.3a. The 'Royal Aircraft Establishment Variable Camber Mechanism' or RAEVAM as it is known consists of a flexible plate which is constrained by a series of swinging links attached to a rigid plate fixed to the spar. Drooping the LE nose in this fashion reduces the effective chord. In order to retain the chord length several variation to the basic scheme are possible. One such method is illustrated in Figure 1.3b. The rigid plate sits in a track and is made to translate by a separate jack. Moss, Haines and Jordan[5] report on the aerodynamic benefits gained by using the RAEVAM type of system for improving high speed stalling characteristics of an aerofoil.

Since the RAEVAM concept, several inventors have filed patents for systems that provide profile changes by drooping either the LE or trailing edge (TE) or both. Some of the most significant ideas include inventions by:-

1) Rowarth[6] (For achieving a VC at the TE),
2) Brown and Statkus[7] (a VC wing tip by a power hinge actuator), and
3) Cole[8] (a VC LE device having a movable nose section and an upper flexible panel).

Military aircraft have been the prime target for developing practical application of VC technology. The first extensive study of conformly varying camber was made on a fighter aircraft[9][10]. A new advanced technology variable camber wing (ATVCW) was designed around the F-8 which utilized the flexible skin technology derived from the Boeing 747 camber Krueger flap. Figure 1.4 illustrates the details of the system. The camber variation is obtained by drooping the LE and the TE of the aerofoil. One edge of each flexible panel is supported by the front or real spar or by the nose beam or the TE assembly at the other edge. The flexible skin of the TE is supported by transverse stringers and links to provide rigidity.

Davice[11] produced a report describing several possibilities of camber variation on a supercritical aerofoil section by drooping the LE and TE elements in a similar way to the ATVCW.

Current flying examples of continuous cambering systems are the F111 Mission Adaptive Wing (MAW)[12] and the X-29 Advanced Technology Demonstrator[13].

An illustration of the MAW is given in Figure 1.5. It has the ability to change both the chordwise and spanwise camber, while maintaining a continuous aerofoil shape. The LE system consists of a two bay link system supporting a rigid aluminium nose cap and upper and lower flexible skins. The fibreglass skins are designed to permit a continuous contour at the LE without sliding joints or gaps at the nose and upper surface, while a faired sliding joint exists on the lower surface in front of the spar. The TE mechanism has a three-bay variable geometry. The upper and lower skins are continuous (root to tip) glass reinforced plastic with no sliding joints at the upper or lower contours. A slip joint is provided at the TE. The skins are supported on spanwise beams. The steel-constructed linkages are moved by a rotary actuator gear box. Each flexible section is assigned its own torque tube, which is driven by a pair of high-speed hydraulic motors. Glass fibre material for flexible skins is used[14] because it has a good modulus and fatigue properties.

The system on the X-29 is a discrete VC system, as opposed to a smooth type, consisting of the 25% chord, full-span, double-hinged flaperon/lead tab-flap arrangement depicted in Figure 1.6.

The development and application of VCW on commercial transport aircraft has been very limited. Boeing Aircraft Co[15] carried out investigations to examine the potential attractiveness of varying the camber of a transport aircraft wing during flight, to continuously optimize the lift to drag (L/D) ratio and thereby reduce the fuel usage and operating costs. The VC concept developed in this study incorporated sharp altering devices to deflect and smoothly re-contour the LE and the TE of the wing. The mechanical devices to provide the wing with the capability for variable geometry are shown in Figure 1.7. At the LE, an 'A' frame is actuated to provide the required deflection. As the LE moves down, the upper surface becomes longer while the lower surface becomes shorter. The overall length of the skin remains the same without breakup. A basic mechanism of a four-bar linkage driven by a rotary actuator is used at the TE. The fibre skins are attached to the linkages with spanwise stringers, and short links.

1.2.2 Variable Camber by Drooping the Aerofoil and Extending the Chord

An alternative to simply drooping the LE and TE regions, VC is possible by increasing the chord through translational motion of these areas. This feature is considered to be very useful for providing extra lift to the wing while the aircraft is operating at optimum lift coefficient (C_L) and equivalent air speed.

Amongst the patented ideas:-

1) Hill[16] invented a mechanism that provided a change in profile across an untapered and unswept wing.

2) Sharrock[17] achieved chordal extension by carrying an aft flap and an intermediate wing portion on a tilting arm, depicted in Figure 1.8a. The upper surface is made continuous by an inextensible skin which is anchored to the main wing box and the intermediate wing. The tilting of the arm causes the upper surface skin to draw the intermediate wing away from the flap element. The skin effectively slides over the flap element and defines a smooth and continuous surface between the main wing and the flap element.

3) Halliday and Sharrock[18] suggest a way to anchor the flexible VC upper surface skin to a fixed wing box (Figure 1.8b) by pushing the skin on the flap body using a cam track arrangement. This arrangement includes a lower surface panel which is pulled towards the upper surface thus remaining attached to the flap body on small camber deflections.

Assessments of VC through increment in chord were carried out by Messerschmitt-Bolkow-Blokom (MBB) in Germany to study VCW for commercial transport aircraft (A330/340 type). Details include aerodynamic implications, performance improvements, mechanical realisation and engine/airframe integration. As a result, a concept was developed[19][20][21][22][23] which relied on the use of existing high lift devices to provide camber variation. The design principle of the system is shown in Figure 1.9. At the LE a partially flexible auxiliary flap at the lower surface prevents a slot opening during low lift, high speed slat settings. At the TE the corresponding operation of the flaps and spoilers/air-brakes provide the necessary camber variation. The TE track system is designed such that after the maximum camber position, any further deflection results in a Fowler motion suitable for low speed setting. The shape of the upper surface of the flap and the control track have to be such that there are minor discontinuities during VC operations[22]. The system is projected across a typical transport aircraft wing by segmentising it in-to four sections, as depicted in Figure 1.10a. If a spanwise variation is required, the two neighbouring flap supports have to

be driven by individual flap drive units, the principle system suggested is depicted in Figure 1.10b. The independent input commands would result in the flap being twisted between the two support stations[21].

1.3 BACKGROUND TO THIS RESEARCH

In his quest to assess the aerodynamic benefits of VC, Spillman[1] suggested a method of increasing camber by increasing the aerofoil chord. In view of the objective to enhance the cruise and field performance of a transport aircraft, Rao[24] furthered the work of Spillman[1] by carrying out low speed computational (theoretical) and experimental investigations. These studies showed improvements in aerofoil performance from 2-D camber variations and suggested possible reductions in WRBM by varying the camber across the span.

Lunn[25] used the preliminary 2-D experimental results by Rao[24] to estimate the possible weight savings by reducing WRBM, and reported that the overall wing weight for a 150 seat transport airliner could be reduced by 10%.

These preliminary investigations indicated that the VCW had considerable potential, however the feasibility of applying the concept to a transport aircraft wing required further research in the areas of high speed aerodynamics, and detailed structural/mechanical design. A research contract was awarded to Cranfield Institute of Technology in 1989 (reference [26]) by the Department of Trade and Industry (United Kingdom) and British Aerospace (Commercial Aircraft Division) to continue this work.

Mackinnon[27] explored the aerodynamic avenues by carrying out computational and experimental studies.

The research presented here concentrates on the investigations made to assess the practical, structural and mechanical aspects of VC on a transport aircraft wing.

1.4 RESEARCH OBJECTIVES AND THESIS OUTLINE

The objectives for this research were to:

1) Examine the practical possibilities of achieving the VC by rotating the forward and aft regions of the aerofoil section on a circular arc while keeping the upper surface continuous, which as far as could be ascertained has not previously been attempted.

The method of deflection adapted by Rao[24] necessitated translation as well as rotation of the moving elements, thus increasing the overall chord. Mackinnon[27] designed an aerofoil section specifically for VC application and achieved chordal extension in a similar way. This method is considered to be novel in that both the forward and aft sections of the aerofoil are rotated on a circular arc, which provides a continuous change in profile giving an ideal roof-top pressure distribution for minimum drag[24]. Illustration of the design devised for the wind tunnel model used by Rao[24] is given in Figure 1.11. The upper surface is kept continuous by sliding the solid LE and TE devices on top of solid sections which are part of the wing box, while on the lower surface, flexible plates are provided which keep the underside unbroken. It is believed that such a change in camber can be used to an advantage by implementing large extensions of chord suitable for low speed (high lift - take off) settings. None of the ideas disclosed in the literature search provided this benefit.

The objective was to design schemes around the aerofoil sections and the deployment profiles developed by Rao[24] and Mackinnon[27].

2) Explore the possibility of changing the deployment geometry.

The majority of the ideas reviewed in the literature search obtained camber variation by drooping the front and rear parts of the aerofoil without increasing the chord. The objective was to scheme geometries which provide forward and aft VC in a similar way around a thick supercritical aerofoil section (commonly used for transport aircraft wings).

3) Consider the geometric implications of spanwise variation of camber on a typical transport aircraft wing and extend the 2-D concepts to a real 3-D wing.

On a 3-D wing, ideal aerodynamic requirements (reference [24] and [27]) called for the camber controlling devices to be split in-to several spanwise segments, similar to the

high lift devices on a conventional wing of high aspect ratio, high sweep and high taper.

The objective was to assess the possibilities of achieving the required camber variation across the wing span.

4) Design and develop a 3-D structural/mechanical model and carry-out tests for design verification, and thereby establish the practical feasibility of the concept at a level commensurate with a real aircraft.

5) Consider the application of the VCW system to a transport aircraft and compare its performance with a conventional wing.

The objective was to consider the overall aspect of applying VC systems to a transport aircraft wing and compare its gains and losses with a wing that has conventional control systems.

1.1.4 Thesis Outline

The work towards meeting the first and second objectives is described in Chapters Two. 2-D geometric and aerodynamic considerations and practical ideas are presented and evaluated for their implementation. The geometric implications of spanwise camber variation are covered in Chapter Three.

Chapter Four discusses the application of the VC system to a transport aircraft. Details are given of a conceptual design study made to establish a base line aircraft configuration for VC operation. Geometric details and wing planform dimensions are outlined. The proposed scheme for aft camber variation is extended to a 3-D mechanical solution. Calculations made to carry out these investigations are presented in Appendix A, B and C.

Chapter Five contains the design, manufacturing and assembling details of the structural model. Chapter Six outlines the test procedure and discusses the test results. Stress calculations made to size the major components are contained in Appendix D. Appendix E includes the drawings made to manufacture the structural model.

Chapter Seven draws together the ideas and results discussed in previous chapters. An attempt is made to compare the proposed VC concept with a typical conventional high lift device concept.

Conclusions drawn from this research and recommendations for further work are given in Chapter Eight.

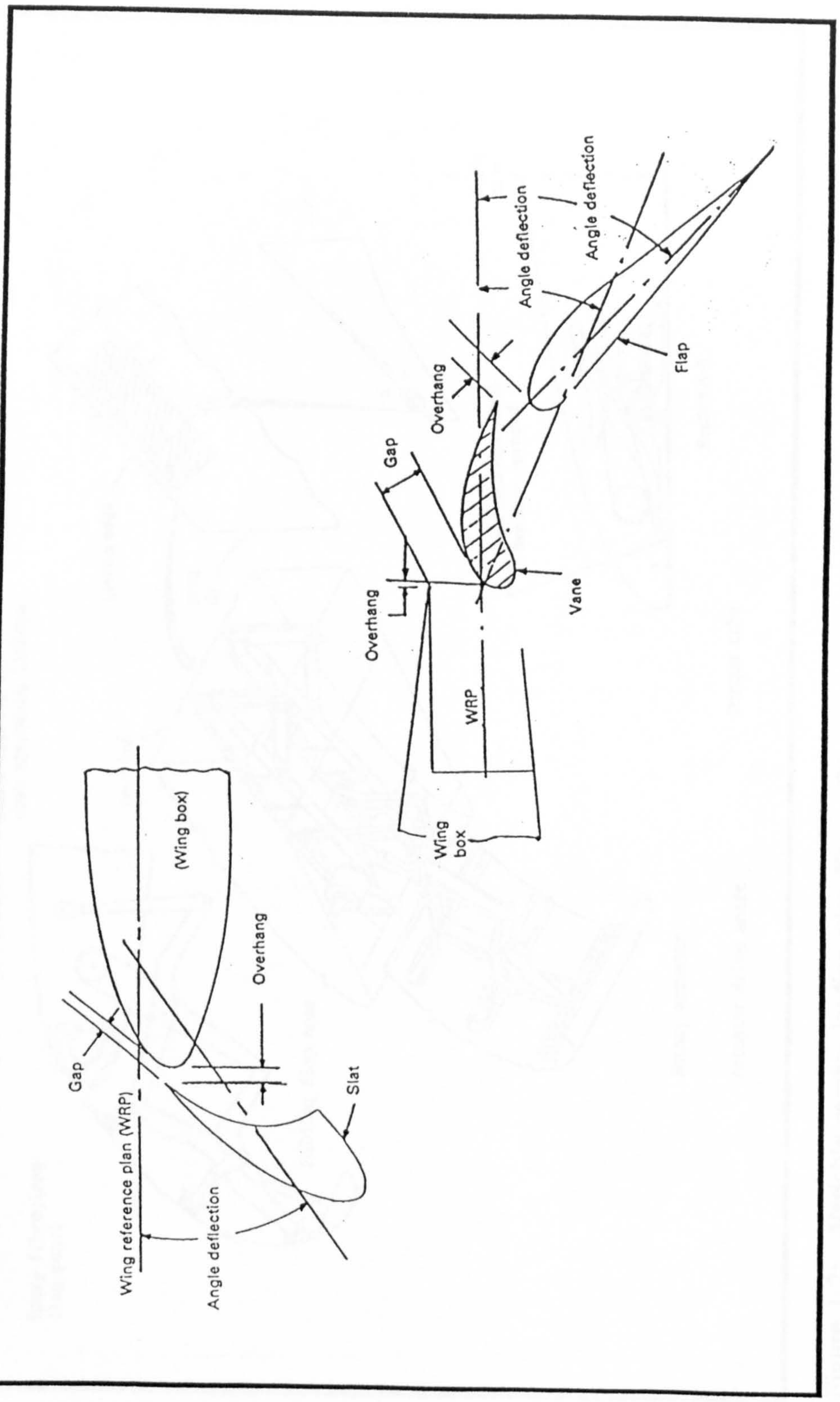

Figure 1.1: Typical low speed high lift camber setting with leading edge slat and trailing edge flap

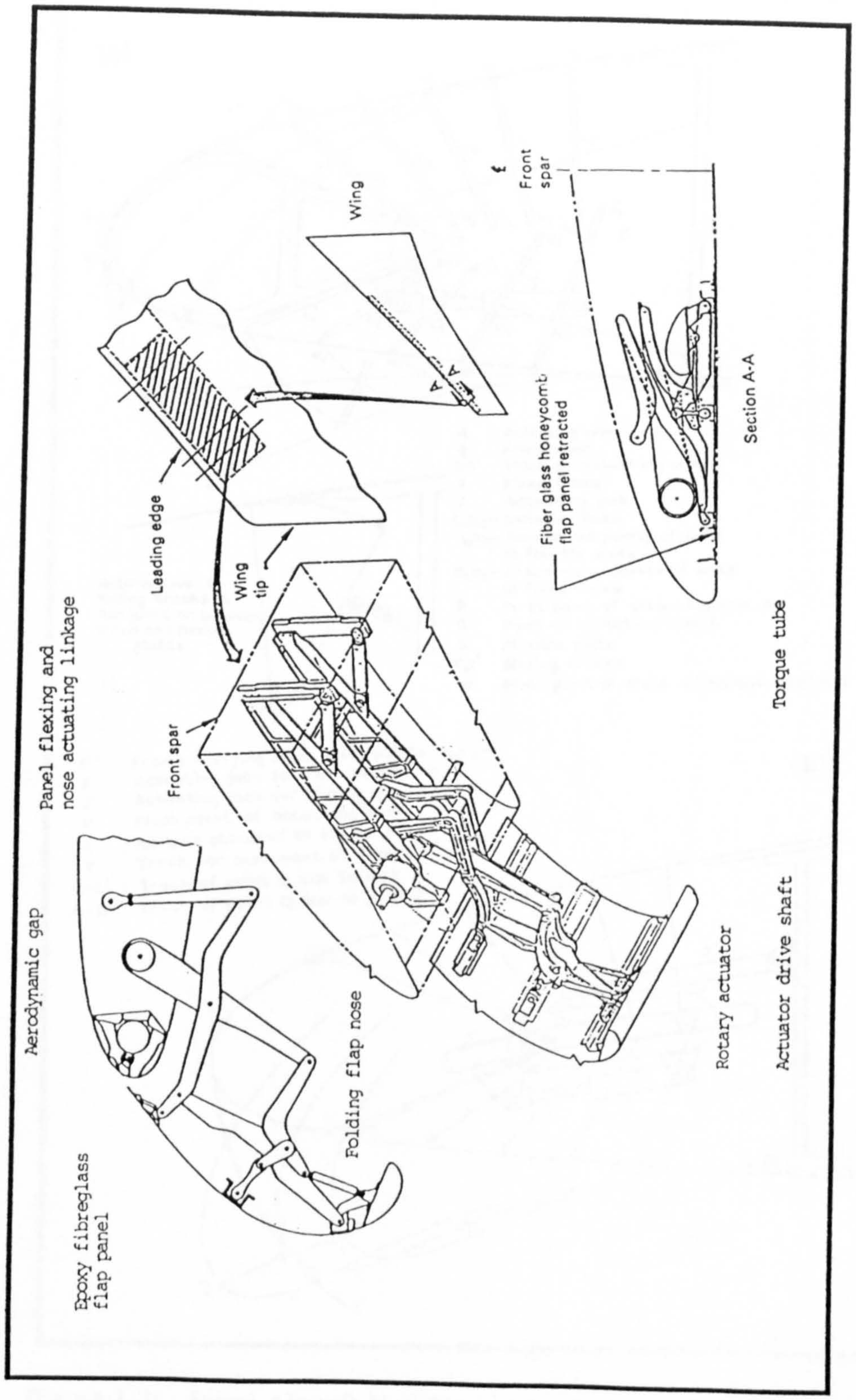

Figure 1.2: Variable camber leading edge Kruger flap

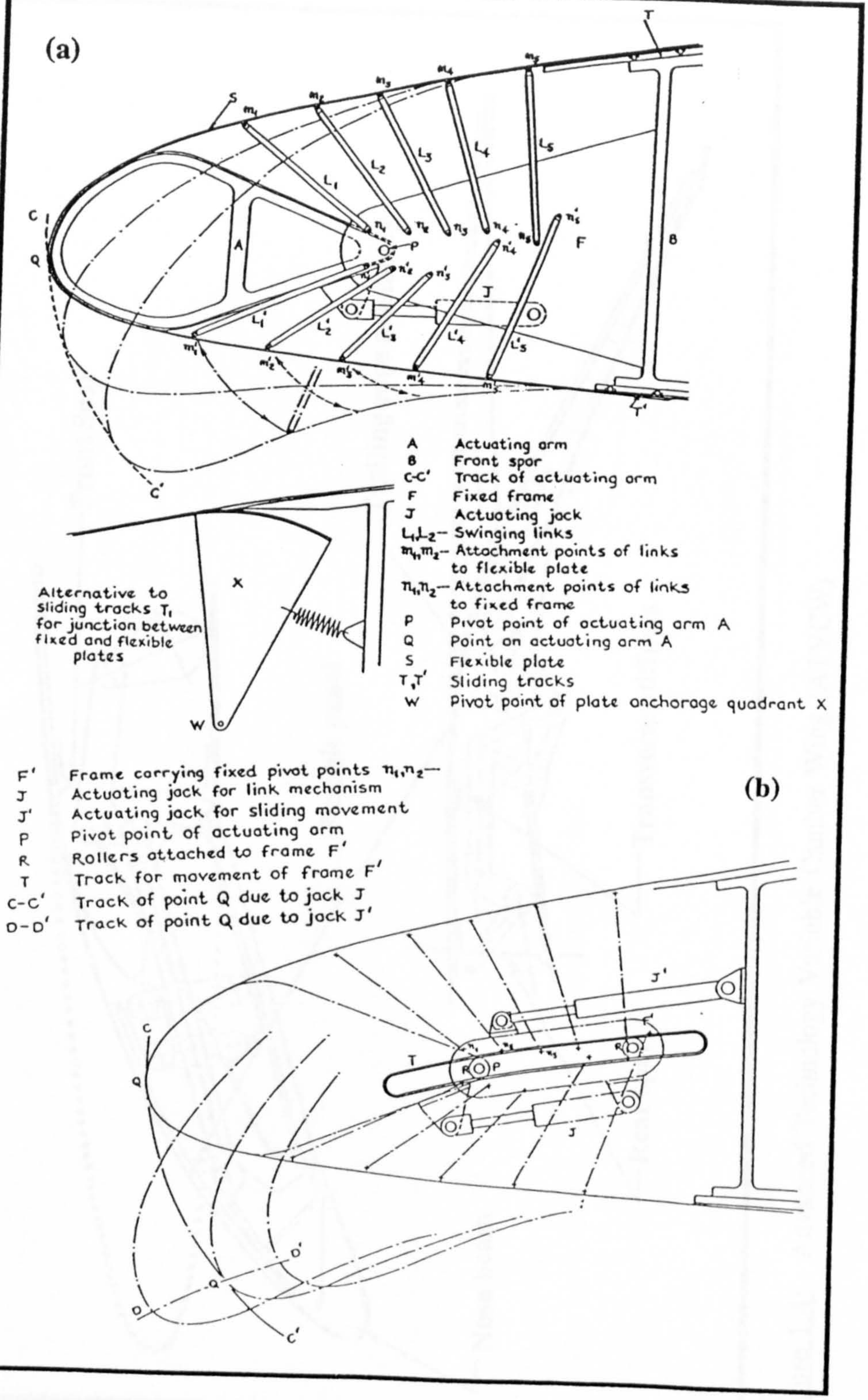

Figure 1.3: Royal Aircraft Variable camber Mechanism (RAEVAM)

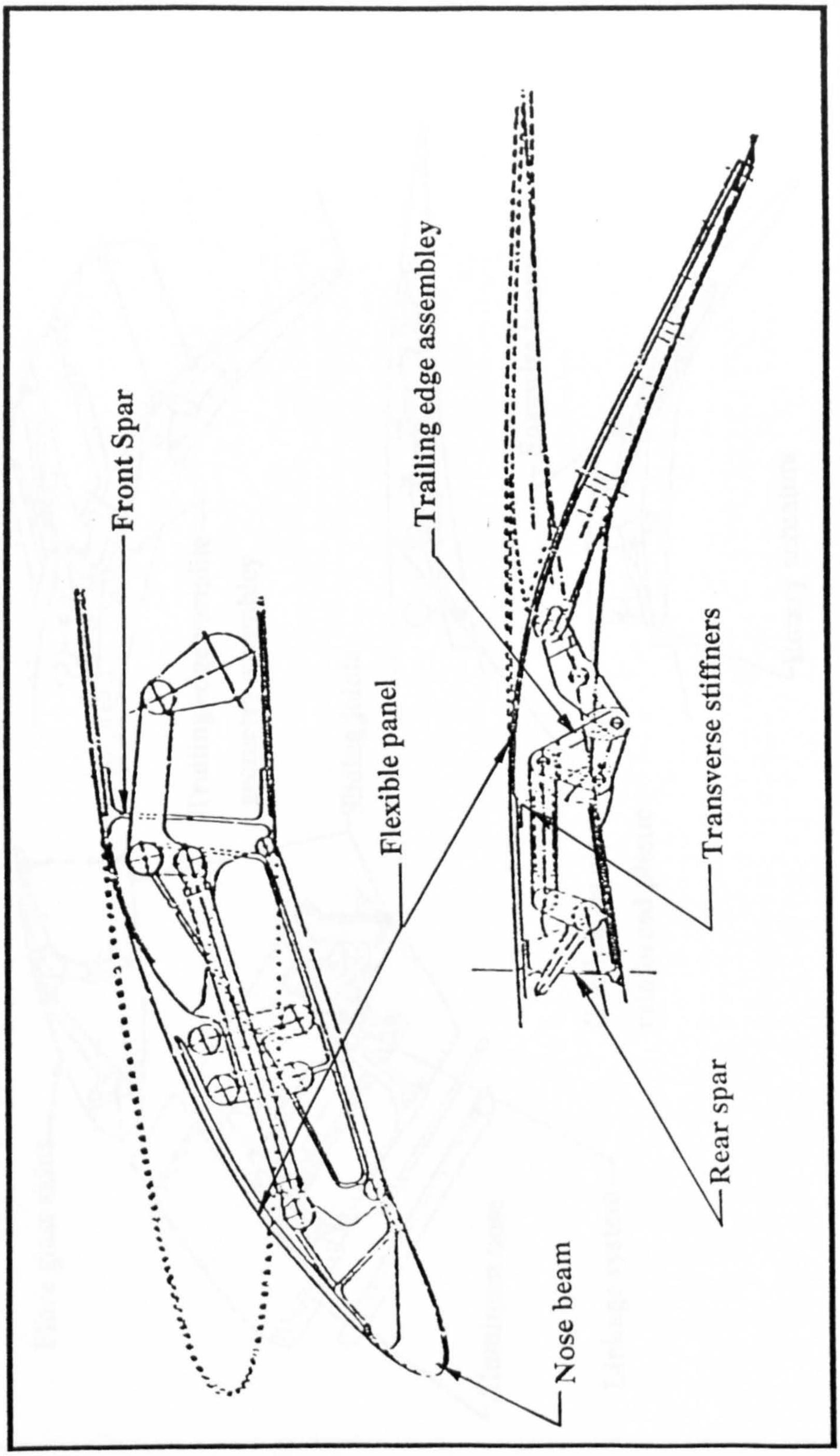

Figure 1.4: Advanced Technology Variable Camber Wing (ATVCW)

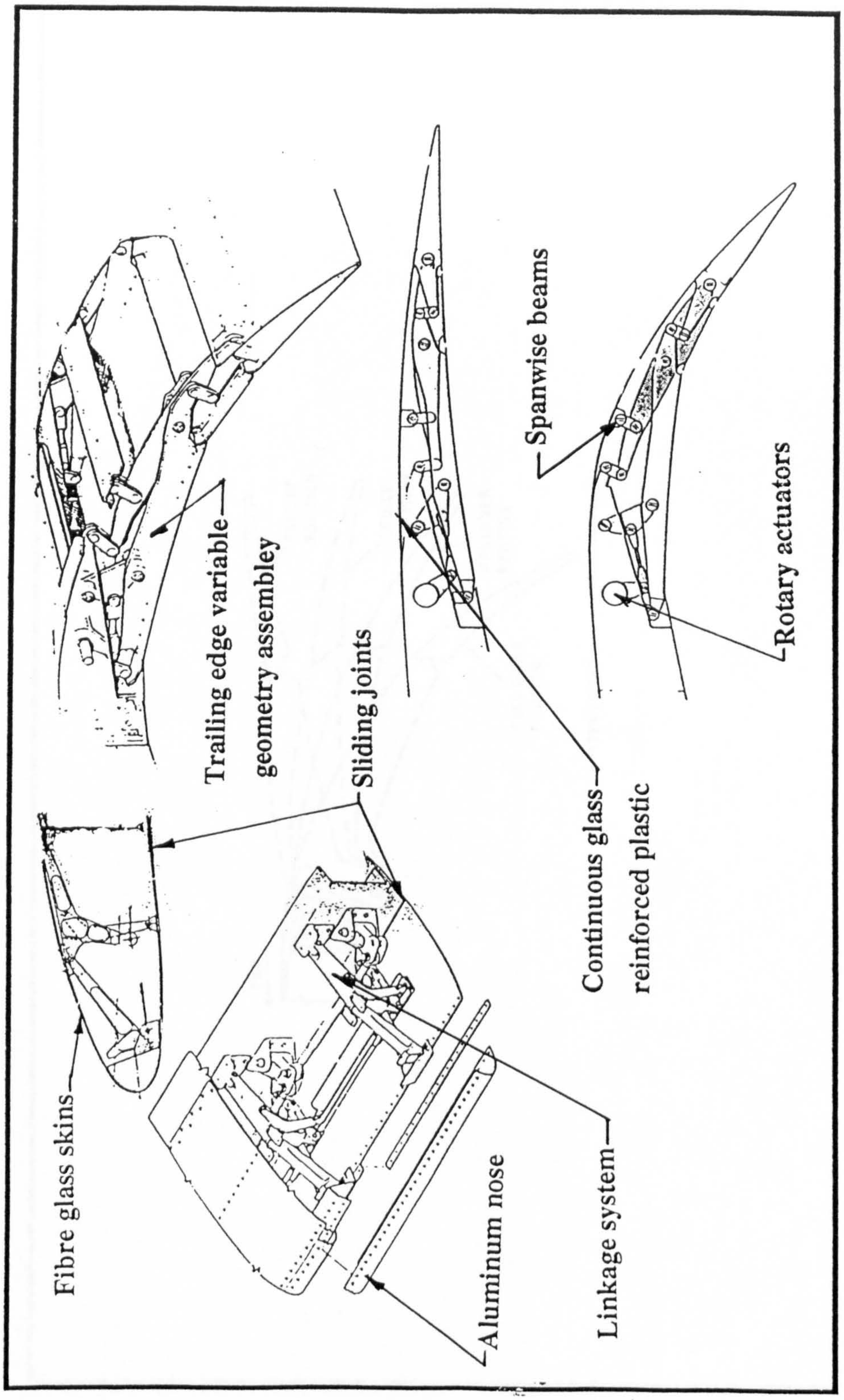

Figure 1.5: Mission Adaptive Wing (MAW)

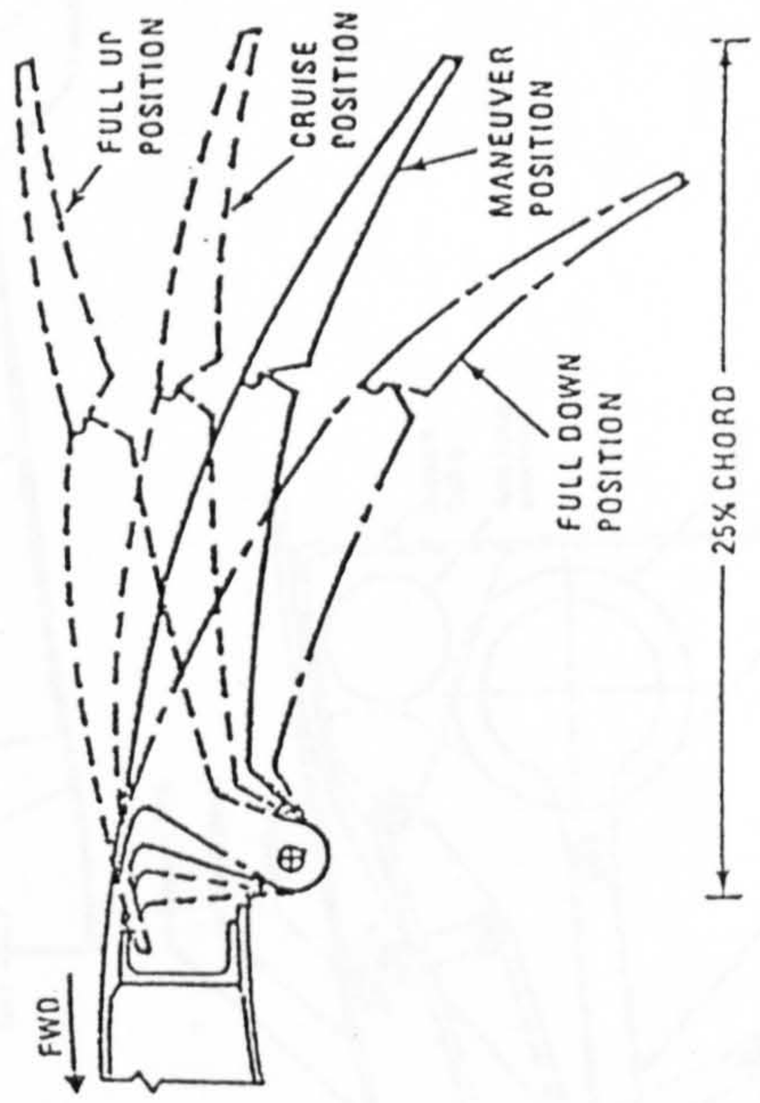

Figure 1.6: Discrete camber variation on the X-29 - Advanced Technology Demonstrator

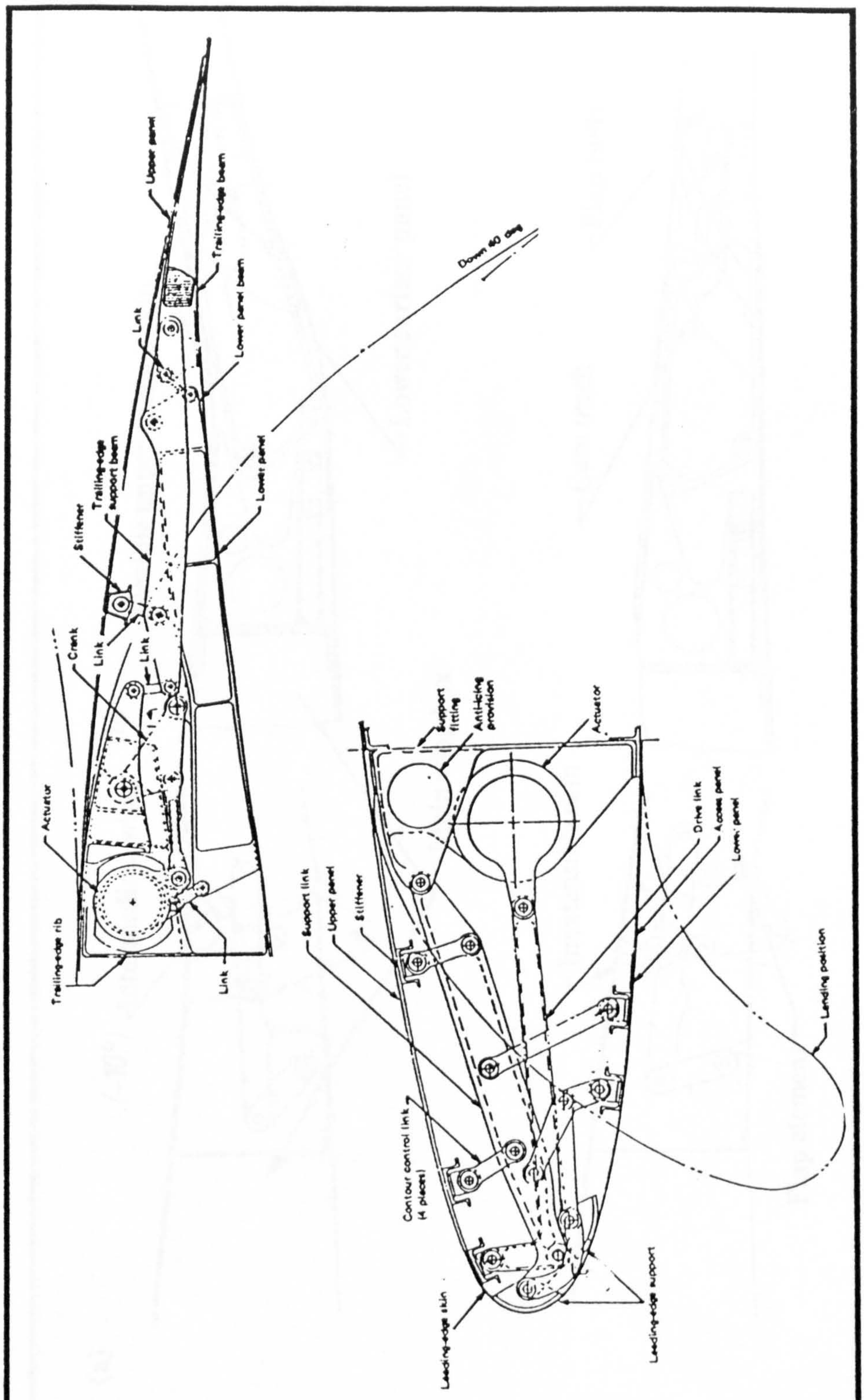

Figure 1.7: Variable camber for transport aircraft by drooping the forward and aft regions of the aerofoil

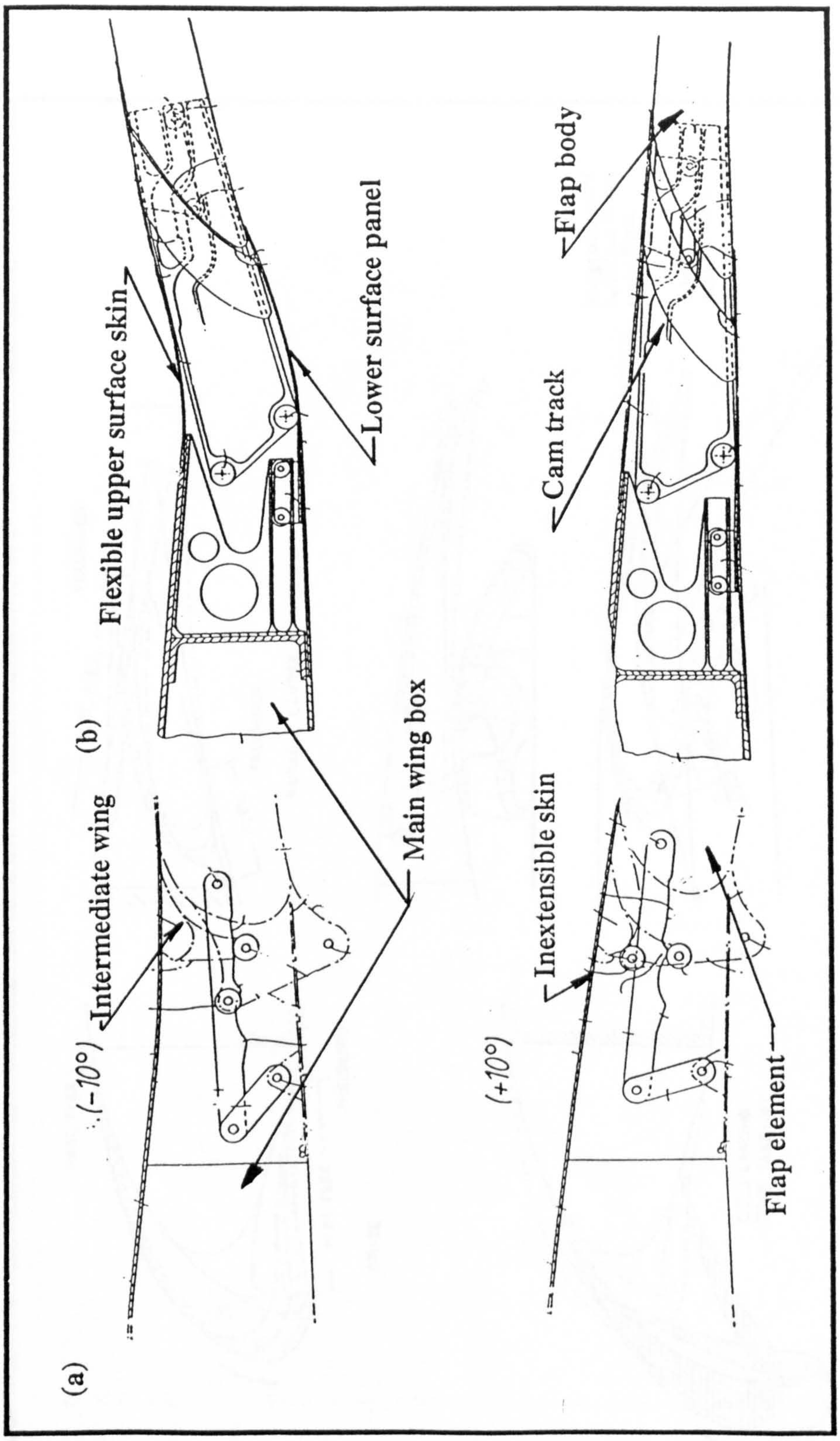

Figure 1.8: Patents of aft camber variation by chordal extension

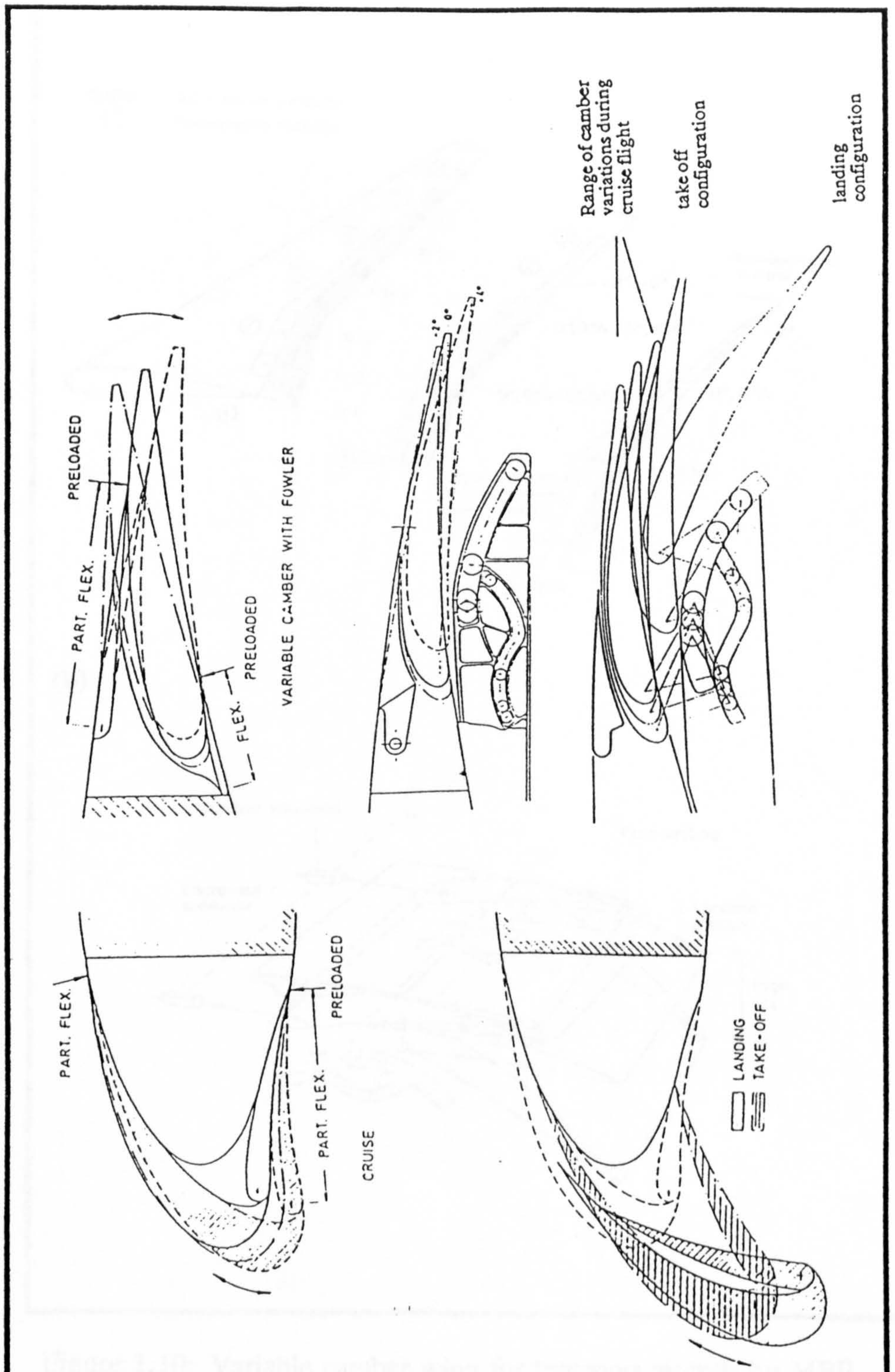

Figure 1.9: Two dimensional variable camber concept developed at MBB

(a)

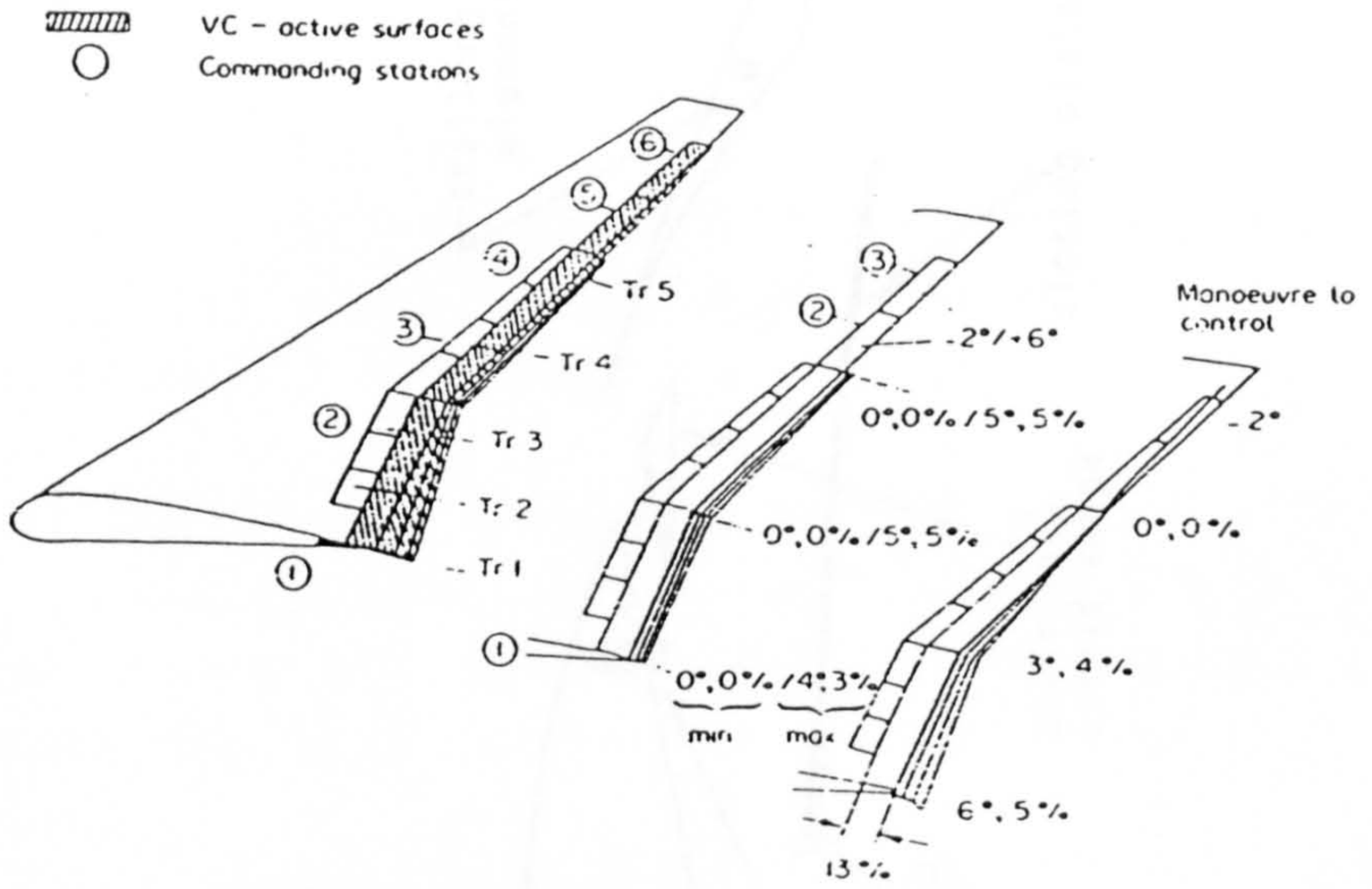

(b)

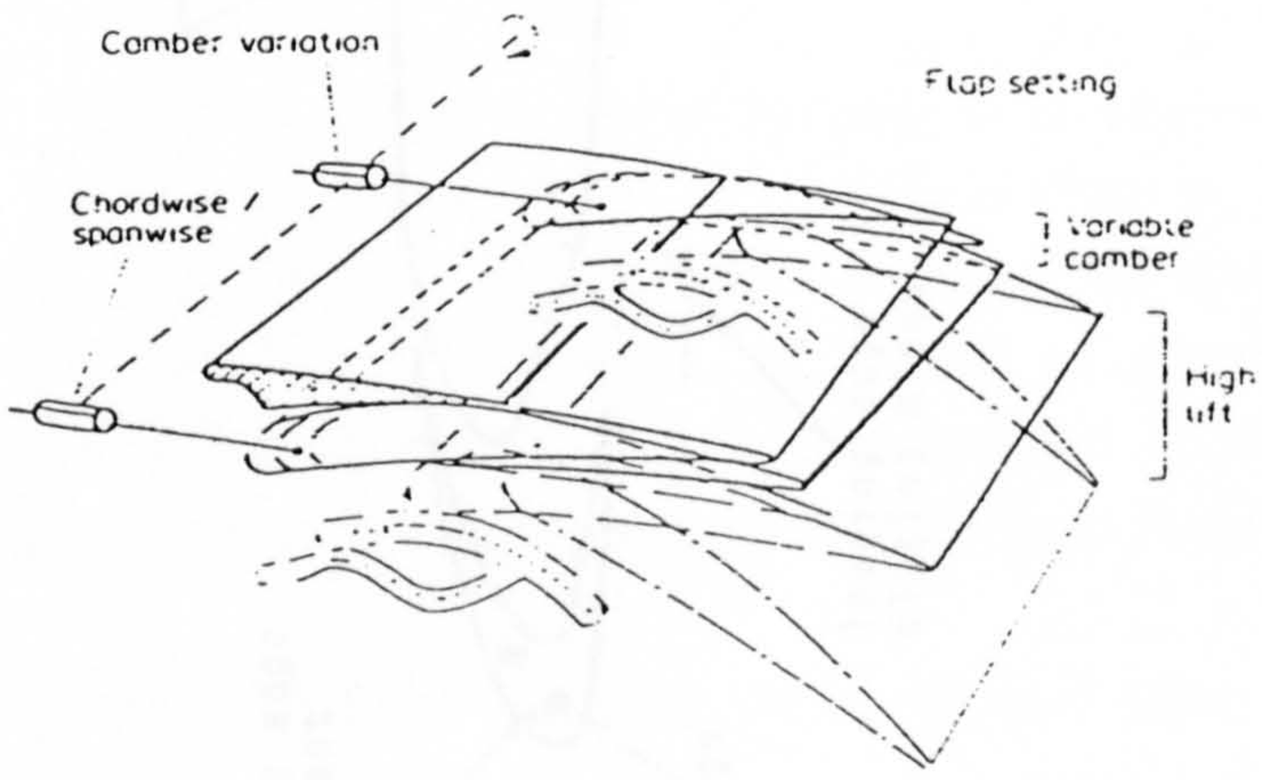

Figure 1.10: Variable camber wing for transport aircraft by MBB

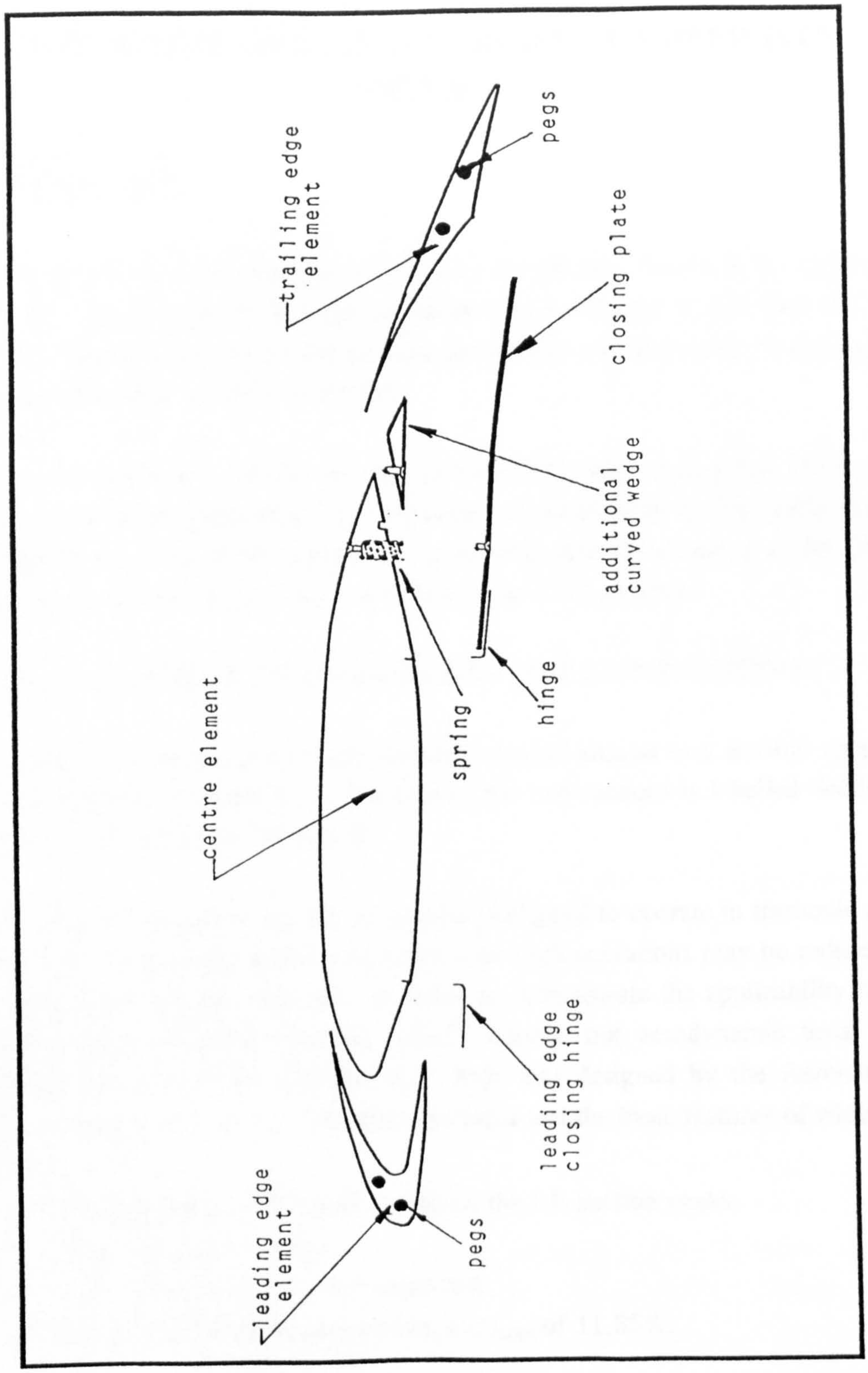

Figure 1.11: Two dimensional wing tunnel model for low speed testing in reference [24]

CHAPTER TWO

TWO DIMENSIONAL (2-D) VARIABLE CAMBER (VC) SYSTEMS

2.1 INTRODUCTION

The prime objective of this research was to study the practical feasibility of varying the wing camber for the type of deployment geometries developed in reference [24] and [27]. This chapter gives the details of these geometries and describes the appropriate aerofoil sections used by the two authors.

To justify the application of the variable camber (VC) system to a real aircraft the design must be suitably practical, light in structural weight and mechanically simple. This chapter discusses these aspects by examining two dimensional (2-D) design schemes for the leading edge (LE) and trailing edge (TE) regions.

2.2 VARIABLE CAMBER (VC) GEOMETRIES AND DESIGN SCHEMES

The investigations carried out in this research centred around two aerofoil sections. These are depicted in Figure 2.1. The first of the two sections is labelled Section A while the second is labelled Section B.

Modern transport aircraft wings are, in general, designed to operate in transonic flight regimes. The wing sweep angles associated with such operations may be reduced by using supercritical aerofoil sections. In order to demonstrate the applicability of the (VC) principles to transport aircraft, Rao[24] carried out aerodynamic tests on a supercritical aerofoil section (Section A). This was designed by the Aeronautical Research Association (A.R.A). The characteristics and the basic features of which are as follows:-

- A fairly generous LE radius to reduce the LE suction peaks,
- A flattened upper surface,
- A blunt TE with a small TE angle and
- maximum thickness to chord ratio, $(t/c)_{MAX}$ of 11.85%.

Mackinnon[27] appreciated the requirement to have a supercritical aerofoil for a transport aircraft wing. He developed a section specifically to accept the VC principles adapted in reference [24]. This section, (Section B) was designed with the assistance of British Aerospace (Commercial Aircraft) using their aerodynamic computer codes. The basic

features of the section are given bellow:-

- A larger radius than Section A,
- A flat top surface, (the emphases was to have a section with very little initial camber which could be increased to suite a particular condition),
- maximum thickness to chord ration, $(t/c)_{MAX,}$ of 14 %,
- A TE thickness of 1 % and
- A TE angle of 5°.

Further details of the above two aerofoils can be found in the appropriate references. The VC geometries and the design schemes developed around these aerofoil are all labelled in accordance with the system described in the notation at the beginning of this thesis.

The variation in aerofoil camber was applied[24][27]beyond the unchanged wing structural box, therefore the change in profile was limited to the LE and TE regions only. These regions (the LE and TE elements) were rotated and translated on circular arcs to give increments in chord. Such variations give continuity in curvature at the junctions between the moving elements and the wing centre section. The VC geometry for Section A is depicted in Figure 2.2a, while Figure 2.2b shows the same principle applied to Section B.

2.2.1 Leading Edge (LE) Camber Variation

In order to reduce the LE velocity (suction) peaks caused by the variation in TE camber, it is necessary to introduce a 'droop' at the nose of the aerofoil (reference [1], [24], [27] and [28]). Aerodynamic investigations suggest that the transition from one camber setting to the next must be smooth and continuous. This continuity helps to maintain the desired upper surface roof-top pressure distribution and so helps to delay the wave drag.

2.2.1.1 Variable camber (VC) on Section A

Figure 2.3a (LESA1) describes the deployment programme which gives the required camber variation on Section A. Point A marks the junction between the LE element and the wing centre section. This point is rotated on a circular arc and has sufficiently large local curvature to eliminate any localised suction peaks during LE deployment (reference [24]). The LE element is therefore separated from the main wing body by an arc (A-B) drawn forward from point A, which lies within the original aerofoil section. It strikes the lower surface at point B. This arc represents the defection profile for the LE element. The radius of curvature for A-B is considered to be small

enough to give a large droop at the nose (which is necessary for high TE camber settings).

In order to retain continuity on the under side, the LE nose extends to point C on the lower surface, as depicted in Figures 2.3b (LESA2) and 2.3c (LESA3). The continuity on the under side is maintained by clamping a flexible plate at the front spar position. This plate runs in a rail by means of a set of roller and link arrangement. The rail is part of the deploying LE device which is so shaped in order to allow the under surface plate to slide above it.

The deployment of the LE element is by means of track roller system, shown in Figure 2.3c (LESA3). This has a similar profile to the arc A-B. The track being part of the LE element and the rollers fixed to the solid body.

2.2.1.2 Variable camber (VC) on Section B

The point of rotation on the upper surface for Section B was initially taken at 17% chord. This is shown as Point A in Figure 2.4a (LESB1). Problems associated with this centred around the position of the axis of rotation for the LE and the length of the radius, R. As depicted in Figure 2.4a, the centre of rotation and therefore the radius required to keep the necessary continuity on the upper surface is notably higher than that for LESA1. Such a large radius gives an insignificant droop of only 4° of rotation (arc A-A'). This setting proved to be insufficient to relieve the LE suction pressures associated with the large TE camber settings (reference [27]). Furthermore, arc A-A' projects outside the profile of the main aerofoil section and caused such design difficulties that no solution was possible for this geometry.

In order to achieve a reasonable degree of droop, Point A was moved further forward in steps from 17% to 6% chord, as shown in Figure 2.4b (LESB2). Continuity is maintained when A is rotated through, say 15° to A'. In comparison with LESB1, greater degree of rotation and larger droop is possible. Although the arc A-A' lies outside the original contours of the aerofoil there is a possibility of maintaining smooth profile with flexible skins for the upper and lower surfaces. Figure 2.5 (LESB3) and 2.6 (LESB4) display two alternative solutions.

The flexible upper surface skin for scheme LESB3 (Figure 2.5) is stretched between two solid LE pieces (forward and aft). It is similar in principle to a roller top desk. One end of the skin is fixed to the main wing body (at 6 % chord) while the other end is pulled toward the front spar by a compression spring. The aft LE device is curved on the upper side such that during camber variation it drags the upper surface skin on

to it self, which helps to control the continuity.

With scheme LESB4 (Figure 2.6), the flexible upper surface skin is fixed to the nose piece at A. The skin sits on top of a support structure and extends up to 17% chord. This support structure is part of the wing box section. A series of compression springs provide the necessary load to hold the skin down, first on to the support structure and then on to the nose piece (during VC operation). The nose piece pulls the skin out while extending and therefore helps to maintain the continuity of curvature at A. The profile changes and the deployment of the LE device is by means of a track roller system.

The under surface is kept continuous by a flexible plate which can be controlled with a link roller arrangement similar to the design presented for LESA2 (Figure 2.3b).

2.2.2 Trailing Edge (TE) Camber Variation

Ideally the change in section profile aft of the rear spar should not cause separation of airflow, which would otherwise give rise to the profile drag[24]. To overcome the problem of separation, the radii of local curvature must be greater than half the chord[28]. A smooth profile is achieved by sliding the TE backwards and downwards, which effectively extends the basic chord. To obtain favourable pressure characteristics behind the 50% chord position and to operate at high subsonic cruise speeds, the aft camber must be varied by keeping the curvature constant, continuous and matching at the junctions between the TE element and the main wing section.

An illustration of the TE camber variation by this method is given in Figure 2.7a for Section A (TESA1) and in Figure 2.7b for Section B (TESB1). The requirement is to achieve a maximum positive rotation of A to A' and a negative rotation of A to A''. The local radius at A for both the sections is considered to be very large giving a significant extension of the aerofoil chord during the deflection of the TE element. This would help towards meeting the take off lift requirements. Negative camber, or chord reduction is desired for roll control and manoeuvre load control. The degree of rotation and the extension and reduction for the two sections is as follows:

Geometric variation	Section A	Section B
A-A' (Deg)	15.0	10.0
A-A'' (Deg)	- 5.0	- 3.5
Chord reduction (% x/c)	6.3	9.28
Chord extension (% x/c)	16.4	26.73
Radius (% x/c)	77.08	164.49
Origin of Rotation	(0.5, -0.7008)	(0.5006, -1.57783)

Comparison of the two VC geometries indicates that TESB1 has a greater radius of local curvature than TESA1. The former therefore experiences more extension for a smaller degree of rotation than the latter. This is due to the flatter nature of the upper surface on Section B.

The first scheme that was devised for the aft camber variation explores the design of the wind tunnel model used in reference [24]. The system is depicted in Figure 2.8a (TESA2) for Section A. The TE element comprises of a solid rear section which slides backward on a ridged body on a rail let in-to the fixed wing structure. The radius of arc A-B keeps Point A continuously attached to the ridged body during the deflection of the TE device.

The transitional motion detaches the TE element from the underside at large camber settings. In order to keep the lower surface continuous, a hinged (closing) plate is introduced. The rotation with a single plate is limited to only 10°. Rotation of up to 15° requires an additional plate which can slide backwards with the TE element. This feature is illustrated in Figure 2.8b, which shows a photograph of a demonstration model built around Section A.

Figure 2.8c (TESB2) features this scheme for Section B. The TE sliding element and the under surface plates are seen to have very little stiffness. Furthermore the sharpness of the TE element at Point A suggests very little contact region (attachment area). This scheme therefore appears to be unsuitable for aerofoil sections which are relatively flat on the upper surface.

Investigations to eliminate the possibility of using extending plates and to seek a solution which could be applicable generally to any aerofoil section led to a simple scheme designed by Lunn[25], who estimated the possible weight savings by applying the VC system to a transport aircraft wing. Lunn[25] suggested a scheme that would vary the TE camber by the method developed in reference [24]. Illustration of this scheme

is given in Figure 2.9. A shroud on the upper surface keeps the continuity between a conventional flap and the main wing box. This shroud is assumed to be designed such that it exerts a constant downward pressure on the TE flap.

Examination of the concept suggests that it is highly unsatisfactory from both the structural and the aerodynamic points of view. The flexible shroud skin is assumed to be restrained only at the rear spar position. Apart from which there are no physical or mechanical restraints to hold its shape or control the flexibility during VC operations. The latter is only dependent on the characteristics of the skin material. Such an arrangement cannot be practical, since the long unsupported skin panels will simply warp and lift due to aerodynamic loading.

An initial modification to this idea resulted in the scheme shown in Figure 2.10a (TESA3). The upper surface skin is held in a track through a roller system at one end while the other end is clamped at the wing rear spar: the track being part of the TE device. Figure 2.10b shows a photograph of a model made to demonstrate the system. It is obvious that the stiffness of the flexible upper surface plate would not be sufficient for it to hold shape when subjected to aerodynamic pressure loads. A way around this problem is to support the length of the plate through a series of rollers holding it continuously in a track. Figures 2.11a and 2.11b show the essential features of the idea for aerofoil Section B (TESB3). The scheme comprises of the following elements:-

1) a solid T E piece,
2) a flexible upper surface,
3) a hinged and spring loaded lower flap,
4) an extending track
5) a support track
6) a set of rolling elements for the conforming of the upper surface, and
7) a conforming track.

Curvature to the TE flap is provided by attaching it to a curved extending track which slides inside a support track of similar profile. The shape of these tracks is in keeping with the profile of the deployment arc A-B. Sliding between the two tracks is possible by placing rollers or low friction sliding material between them. Continuity between the TE element and the wing structure is maintained by a flexible skin on the upper surface and a hinged flap panel on the lower surface.

The flexible upper skin is clamped at the rear spar position and sits in a conforming track through a set of rolling pins. The conforming track is part of the TE device and the extending track, and therefore matches the upper surface of the un-deflected TE device from Point C to the TE tip and curves from Point C forward to match the shape

of the extending track. The upper surface thus slides within this conforming track during the transition of the TE device.

On the lower surface a hinged plate is provided which is spring loaded so that it automatically deflects to follow the movement of the TE device. It can be seen in both the scheme TESA3 and TESB3 that the under side is reduced along the chord of the TE device (C_{TE} in Figure 2.11a). The under side of the TE device is so shaped such that the transition from one camber setting to the next is smooth on the lower surface of the aerofoil. With this geometry the lower surface remains continuously attached to the TE device. Table 2.1 contains the coordinates of the reduced TE device of Section B. Computational investigations[27] showed no aerodynamic effects due the slight kink appearing at the hinge point of the lower surface of TESB3 (Figure 2.11a).

2.3 VARIABLE CAMBER WITH HIGH LIFT DEVICES

Reference [24] and [27] suggest that the high lift requirement necessary for low speed approach and landing conditions for a transport aircraft can not be achieved with full VC settings. Maximum VC for aerofoil Section A and Section B gives maximum 2-D C_L in the range of 1.6 to 1.8. C_{Lmax} for transport aircraft is generally in the range of 2.5 to 3.0. To ensure that such high lift demands are satisfied, it is necessary to add high lift devices to aerofoil as part of the VC control system.

Unfortunately in both reference [24] and [27] the investigations were limited to VC only with no aerodynamic suggestion as to the type and size of the high lift device necessary for low speed conditions. For sake of completeness it was decided to look at some methods of incorporating geometries of such devices with the VC geometries described above. The intention was to investigate only the possibilities without carrying out a detailed design study. Thus high lift devices were simply positioned inside the schemed profiles of the LE and TE cambering elements. No attempt was made to aerodynamically optimise the proposed geometries.

2.3.1 Leading Edge High Lift Devices

A conventional slat as an extension to the VC device is suggested for providing extra lift for scheme LEAS2. The original LE nose is divided in to two sections, a slat body and a LE aft body (LE device), as shown in Figure 2.12 (LESA4). The variation in camber is possible by actuating the LE device and sliding it in the track roller system previously described. The slat is actuated independently and it travels on a separate tracking system which is of the same profile as the VC track. On full VC setting the LE device comes to a stop. Thus further actuation simply detaches the LE device from

the slat which starts performing as a high lift device.

The size of the LE nose piece for schemes LESB3 and LESB4 eliminated the possibility of including an extra high lift device. Thus the maximum C_L is limited to what is achieved with full VC leading edge settings.

2.3.2 Trailing Edge High Lift Devices

With scheme TESA2 it is possible to install an auxiliary flap of approximately 10% chord, as depicted in Figure 2.8a. Flap operation would be on full VC setting with a separate drive system for which a screw jack or a linear actuator could be used. The actuation system together with the tracking system for the flap can be carried within the TE device.

With scheme TESA3, an auxiliary flap or a hinged (drop) flap of up to 30% chord could be installed to satisfy the high lift requirement. Figure 2.13 illustrates a photograph of a model made to demonstrate the former feature with a 10 % chord flap. The operation of the flap would be on full VC setting. The system can be carried within the VC aerofoil between the upper and lower surface skins aft of the rear spar.

2.4 DISCUSSIONS AND DESIGN EVALUATION

The selection of any of the combination of schemes depends on whether the:-
1) aerodynamic requirements are satisfied and
2) the design is structurally, mechanically and practically feasible.
A preliminary assessment and an evaluation was therefore necessary in order to select the best possible solution.

2.4.1 General Mechanical and Practical Design Considerations

In an attempt to judge the practicality of the designs an initial consideration was given to the following guide-lines:-

1) Safety and structural integrity,
The basic philosophy governing the design of the VC system was to develop mechanisms and structural components with adequate safety margins.
Since the system will be operating continuously throughout the entire flight of the aircraft, the load environment will involve many load factors such as flight manoeuvring loads, atmospheric gust loads, take off and landing loads, repeated loads, high and low temperature conditions, etc. The moving components will be susceptible to wear and

tear, and structural components i.e skins, will be susceptible to environmental degradation, i.e humidity/temperature variation, contamination. The likelihood of parts jamming and binding will be considerable high.

2) Mechanical reliability,

The proposed system had to be mechanically reliable without parts failure. Knowledge of reliability in terms of analysis is necessary in order to quantify and make comparison of different designs. The systems would have to have development tests for a considerable period before the initial analysis can be confirmed. However, a certain degree of confidence could be gained if conventionality is retained within the design.

3) Reduced complexity and weight,

Mechanical reliability could be guaranteed or improved if only few components are used to make up the system. Traditional flap/slat designs have shown that in order to reduce the design complexities aerodynamic sacrifices must be made. If however, the aerodynamic constraints are satisfied then the design becomes very complex. The use of VC on the Mission Adaptive Wing (MAW)[12] is a good example of a complex link arrangement designed so that aerodynamic characteristics could be maintained. Complex structural components and mechanical systems invariably mean extra weight. Reducing the number of moving components, would effectively keep the weight down.

4) Maintainability and inspection

This is an important aspect from the overall structural design point of view of the aircraft. The design philosophy of all modern aircraft cover the aspect of maintenance and inspection. It is necessary to design a system whereby the components are easily accessed to check and/or modify in case of failure.

5) Fuel Storage and Spar Position

The bulk of the fuel on transport aircraft is stored within the wing structural box. It is therefore crucial to design a system that will minimise the invasion of the fuel space and reduce fuel capacity owing to the size of system components, such as actuators, links and tracks.

The relative position of the front and rear spars is governed by fuel and torsional stiffness criteria. Observations of transport aircraft suggest that the front and rear spar are usually positioned at approximately 20% and 65% chord respectively. These positions provide sufficient fuel storage within the wing box. Preliminary stiffness calculations suggest that the structural box width with these spar settings is also adequate.

2.4.2 Advantages and Disadvantages of the Proposed Schemes

In view of the aerodynamic requirements and the general practical considerations outlined above, the relative merits and the probable disadvantages of all the schemes are discussed.

2.4.2.1 Leading edge design schemes

Initial observations of the three schemes presented in Section 2.2.1 (above) suggest that LESA2 (Figure 2.3b) is by far the best way of changing the LE camber. However, this idea can only be used on fairly well cambered aerofoil sections (Section A) and not on flatter aerofoils such as Section B. Unless the deployment programme for the latter type of aerofoils shifts away from giving a constant upper surface curvature, which would obviously be aerodynamically unsatisfactory.

Owing to the large deployment radius for Section B, the designs of both LESB3 (Figure 2.5) and LESB4 (Figure 2.6) require a flexible skin for the upper surface. Closer observations of the two ideas suggest that the former scheme is not satisfactory since the skin can only be supported at the two ends. When subjected to pressure loading the skin will be susceptible to warping.

The track length required for all three schemes has to be partially positioned inside the wing box. Thus, the front spar web will have to be cut locally to accommodate this intrusion into the fuel space.

The positive aspects of LESA2 are that it has a solid LE body and support structure. There is a possibility of including a high lift device with a positive drive mechanism. These features can not be implemented on either the LESB3 or the LESB4.

The problem with LESA2 arises when trying to blend the under surface between the LE and the main wing body. It is apparent from Figure 2.3c that there is slight mismatch at point C on maximum deployment (15°). For the wind tunnel model[24] simple curved plates were placed to close the gap occuring between the LE nose piece and the main wing box. In reality it is not possible to do this. Furthermore, owing to its physical size, the step near the aft region of the upper surface of the LE device (Figure 2.3b) will be difficult to hold during high pressure loads. Scheme LESB4 suffers from a similar basic disadvantage. Steps created near the aft region of the flexible upper surface and near the front spar position will cause disruption to the airflow.

Accepting all the problems associated with the three schemes it was concluded that VC by rotating the LE to increase the chord is not a feasible proposition. In view of this an attempt was made to derive an alternative geometry which simply drooped the LE without increasing the basic chord.

VC by drooping the LE is not a new concept. In Chapter One several designs are presented which achieved camber variation without any chordal extension. Investigations with regards to deployment by this method were made on Section B. From the two available aerofoils it seemed appropriate to use this section since it was designed with very little initial camber and had a flatter upper surface than Section A. The LE therefore required a greater degree of droop to meet the aerodynamic needs, thus presenting a greater design challenge.

The deployment geometry was determined by a trial and error basis using a Computer Aided Design (CAD) system. Figure 2.14a (LESB5) shows the geometric details of the LE in its un-deflected and deflected position. The nose is fixed between 4% chord (Point A) on the upper side and 6% chord (Point B) on the lower side. The length between A and 17% chord (Point D) on the upper surface and between B and 12% chord (Point C) on the lower surface is assumed to be flexible.

The method used to droop the LE geometry is described as follows:-
The region between A and D is isolated and subdivided into 15 points. Starting at point 1 (on the upper side) as the pivot, all the points greater than point 1 (2-15), and the nose piece are rotated about point 1 through an angle of 1.5°. Moving to point 2 (as the pivot) the procedure is repeated ie, all the points greater than point 2 and the nose piece are rotated through 1.5° about 2. After repeating the procedure for the rest of the points, the final position of each point is joined by a cubic spline. Resulting in a smooth curve from nose to 4.5% (A') and subsequently to 17% (D). Where A' is the deflected position of A. Point B become B' as the nose and the upper surface are deflected. Point C is fixed without any rotation.

Detailed design investigations with this arrangement were not made but preliminary investigations suggested that the upper side of the aerofoil (forward of 17% Spar position) can be made to simply bend down without changing its length. The under surface must push down as well but will experience a reduction in length, thus the design must incorporate sliding members (slip joints) to compensate for that. As shown in Figures 2.14a and 2.14b, the essential features of this scheme are likely to be:-
1) a flexible upper surface, from point A to D,
2) rigid nose piece from A to B,
3) a flexible lower surface between points B and C,

4) a solid lower surface body between D and forward spar E,
5) a system of three to four linkages to control the conformation of the upper surface (not shown),
6) a deployment track for the nose piece (not shown), and
7) a lower surface support track

The flexible upper surface would be attached at point A to the nose piece and at D to the wing structural box (near the forward spar position). The link system should hold the upper surface skin and conform it to the required shape during the actuation of the nose. The deployment of the LE nose piece can be made through a linear or a rotary actuator (power hinge type).

Figure 2.14b (LESB6) shows the lower flexible surface being held by a series of rolling elements in a track on one end and is fixed to the LE nose at the other end. Any rearward movement of the LE would therefore slide the lower surface skin backwards towards the rear spar.

A Krueger flap is suggested for high lift purpose. Detailed designing of the mechanism has not been carried out, but the operation and the control would be through links and rotary drive system similar to the one shown in Figure 1.2 of Chapter One. Flap operation is likely to be separate from VC operation and its deflection will only be possible on full VC setting.

This scheme does not suffer from the disadvantages related to the other three LE schemes discussed above. It also realises the following advantages:-
1) It has a generous droop to suite the TE camber,
2) It gives a roof top pressure distribution[27],
3) There is no aerodynamic interference,
4) It is easy to incorporate a high lift device with the VC system,
5) All moving parts can be confined within the LE (forward of front spar), but this will require detail design work, and
6) The system can be applicable to any aerofoil section.

The main drawback of this design is that it is likely to have too many moving parts and therefore its reliability could be questionable. There is also a question of access to the system, which appears not to be easy. Therefore inspection and maintenance will be difficult. This problem is shared by the designs of the other three LE schemes.

2.4.2.2 Trailing edge design schemes

From an aerodynamic point of view both scheme TESA2 (Figure 2.8) and TESB3 (Figure 2.11) satisfy the deployment constraints placed on the aerofoil sections[24][27]. Closer inspection of the two ideas suggests TESB3 is decisively better than TESA2. The latter suffers from a forward facing step and it also has a double kink on the lower surface (sliding plates), which will probably cause flow separation particularly at high speed conditions.

On a real wing the exposure of the tracking system to the airflow in scheme TESA2 means that large cover fairings will be required which will undoubtedly increase the overall drag. Scheme TESB3 on the other hand gives a much smoother profile without any breakup of surface continuity, except for the presence of a slight kink on the lower surface (hinged plate) which is not considered to be very significant. The tracking system for this design is all within the main body of the aerofoil therefore there is no reason for cover fairings. This is an obviouse advantage for keeping the drag down.

From structural point of view the positive features of scheme TESA2 are:-
1) The TE system components are all aft of the rear spar therefore the centre section remains intact.
2) It has a ridged support structure which can be used for fuel storage,
3) It has a positive motion,
4) It has a conventional tracking system,
5) An auxiliary flap can be installed to meet the high lift and roll control requirements, and
6) The system can easily be inspected and maintained.

The practical disadvantages of this scheme is that it can only be used on aerofoil sections with a high degree of initial camber. Even with such aerofoils, sliding plates have to be used on the under side to give the required deflections. These plates must be controlled and supported.

As well as the aforementioned aerodynamic advantages, TESB3 realises the following practical benefits:-
1) The system has no links and very few moving parts,
2) Both positive and negative deflections are possible to give the required profile changes,
3) Inspection and maintenance are not envisaged to be a problem,
4) It can be applied to any aerofoil section, and
5) The TE device can be installed with a high lift device that has up to 30 % local flap

chord.

The disadvantages of this design are:-
1) Wear between rolling elements and the tracking system, interchangeability and contamination problems if not protected and sealed properly from the environment could cause clogging and eventual jamming of the rolling pins, leading to binding and wrinkling of the upper surface skin,
2) Tracks have to be attached to the wing side ribs, thus reducing the fuel volume, and
3) Interruption of the wing rear spar web will reduce the structural efficiency.

It is apparent from the advantages and disadvantages of the designs discussed above that TESB3 is more attractive than TESA2 and is therefore considered to be a better solution to provide aft camber variation on a supercritical aerofoil section.

Table 2.1: Lower surface coordinates of the TE device of Section B

Coordinates along x-axis (x/c)	Coordinates along y-axis (y/c)
0.645142	0.061130
0.645142	-0.015494
0.668445	-0.014815
0.691342	-0.014598
0.713778	-0.014231
0.735698	-0.013723
0.757051	-0.013090
0.777785	-0.012353
0.797850	-0.011538
0.817197	-0.010674
0.835779	-0.009792
0.853553	-0.008924
0.870476	-0.008099
0.886505	-0.007342
0.901604	-0.006673
0.915735	-0.006101
0.928864	-0.005634
0.940961	-0.005269
0.951992	-0.004999
0.961940	-0.004812
0.970772	-0.004702
0.978470	-0.004661
0.985061	-0.004668
0.990393	-0.004704
0.994588	-0.004757
0.997592	-0.004825
0.999398	-0.004906
1.000000	-0.004999

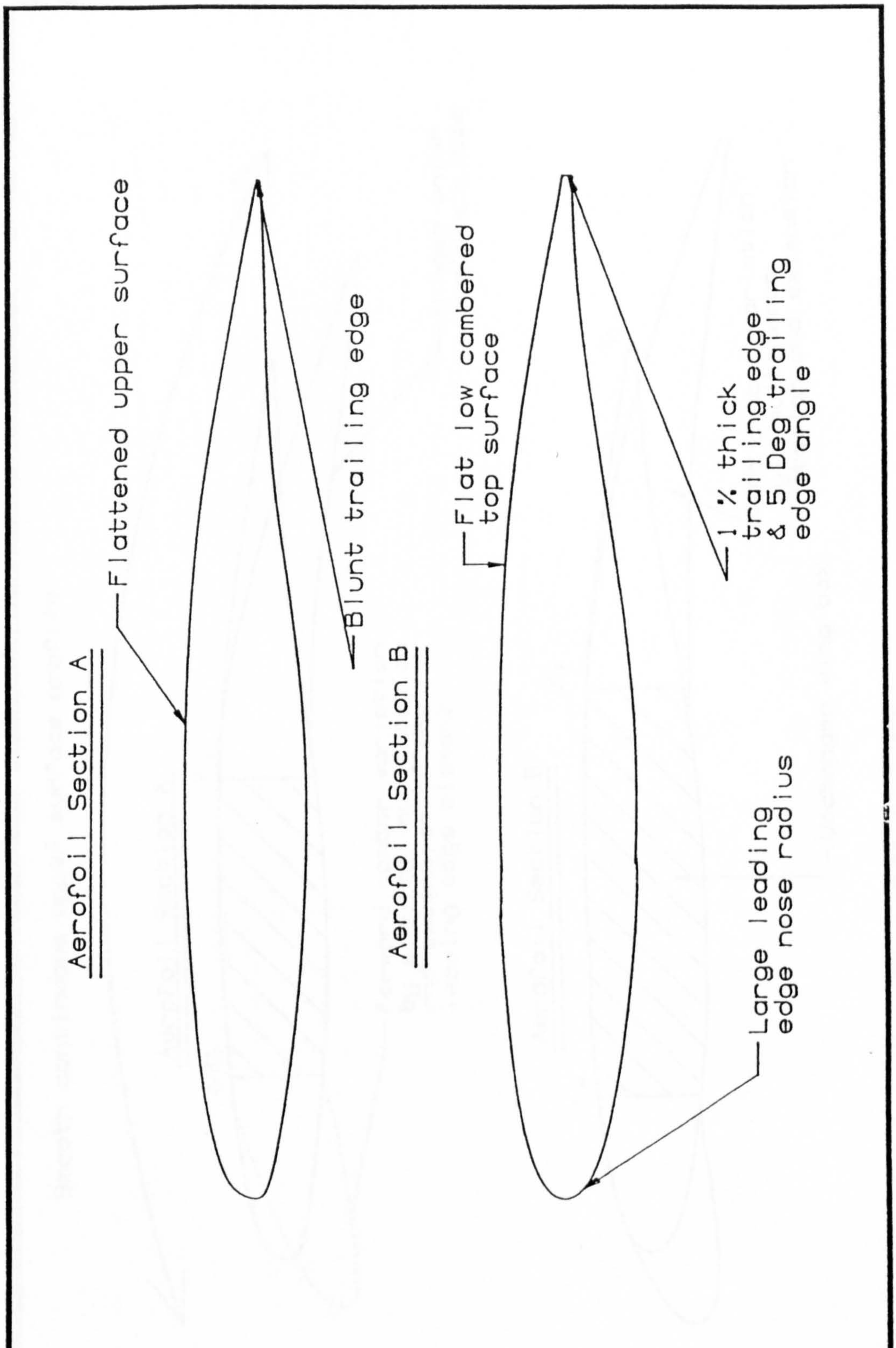

Figure 2.1: Details of the two aerofoil sections used in this research

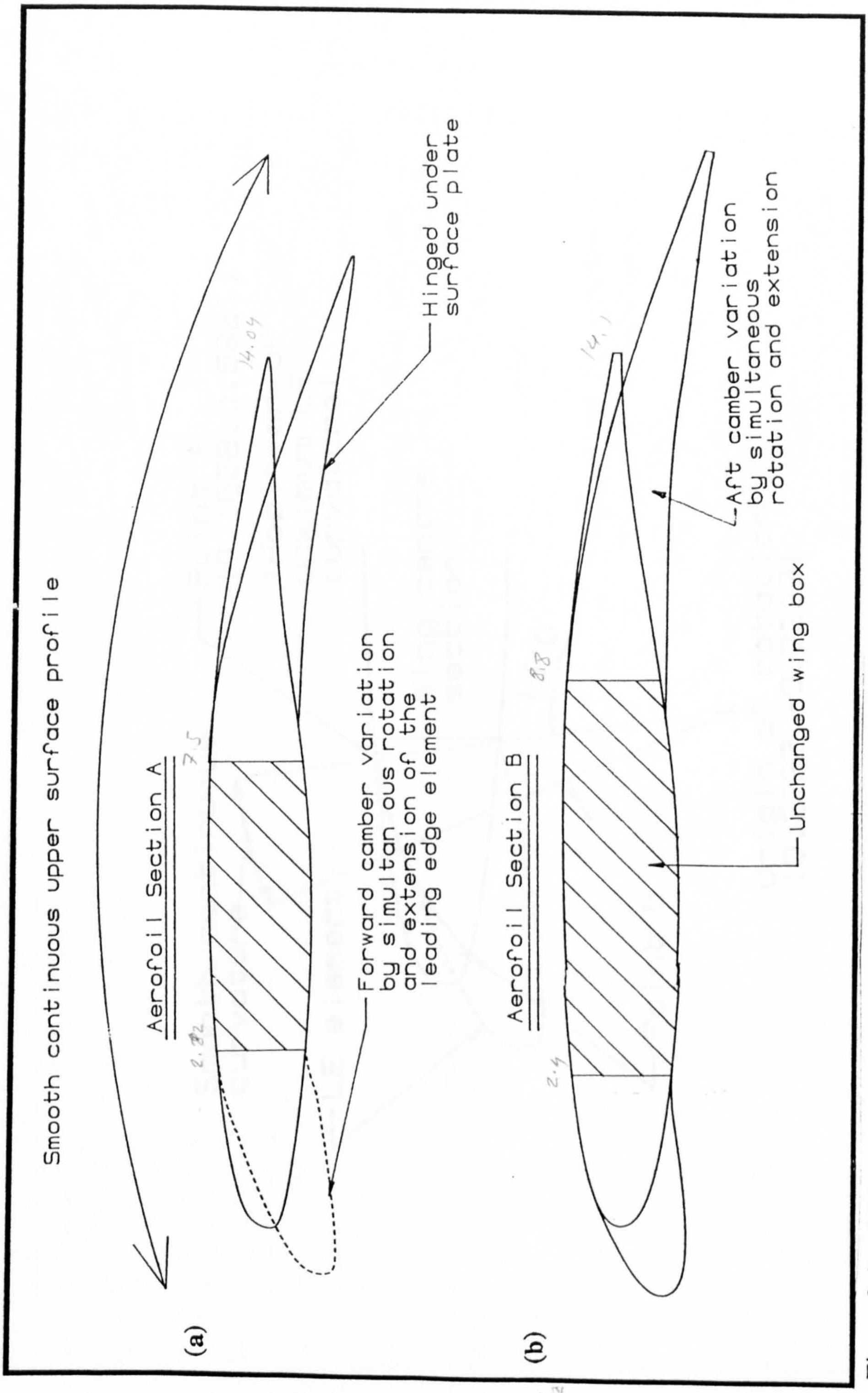

Figure 2.2a: 2-D variable camber geometry proposed for Section A

Figure 2.2b: Ideal 2-D variable camber profile for Section B

RSA = 7.5/14.04 = 53.4 %
FSA = 2.82/14.04 = 20.08 %
RSB = 8.8/14.1 = 62.41 %
FSB = 2.4/14.1 = 17.02 %

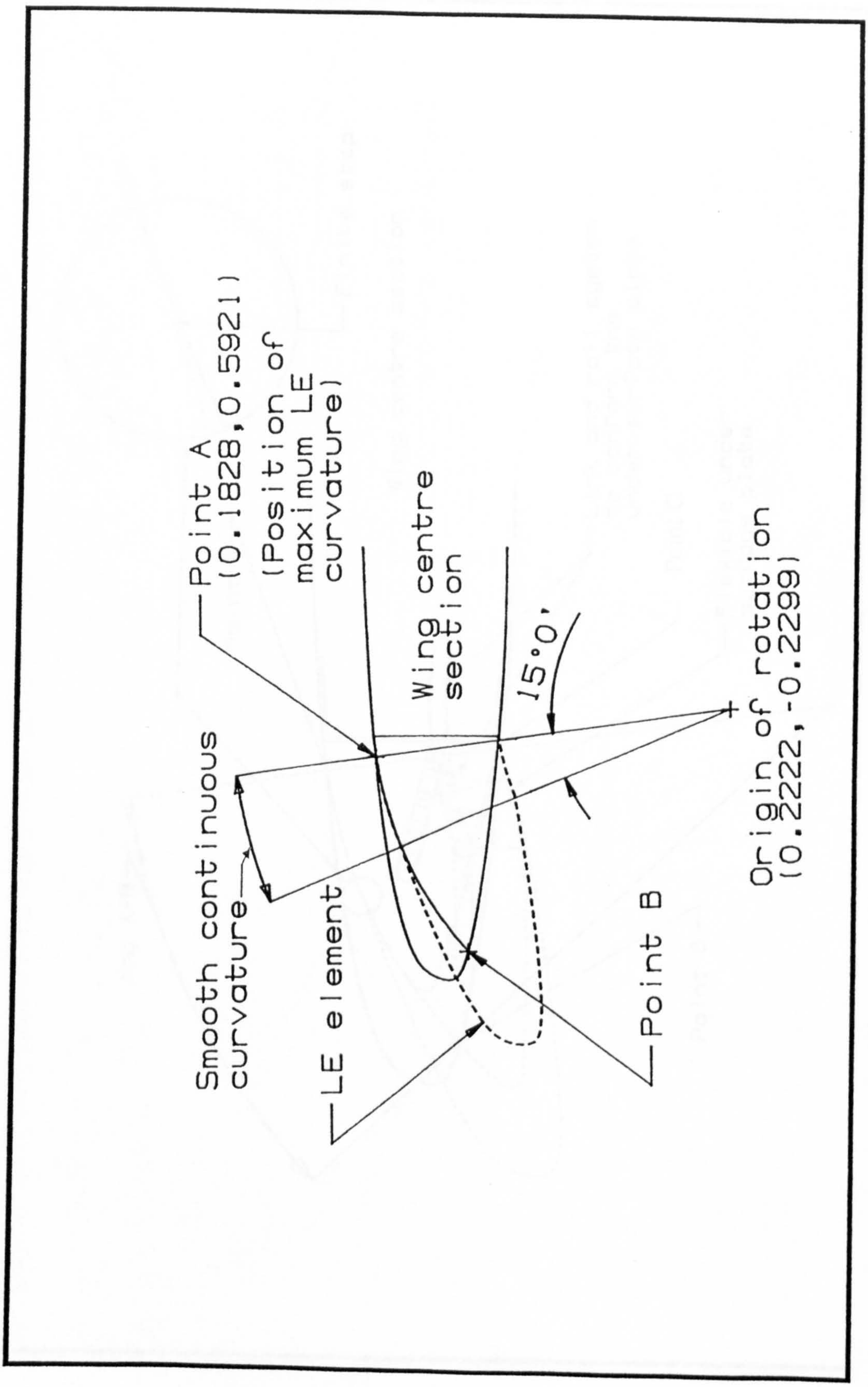

Figure 2.3a: Leading edge variable camber profile for Section A - LESA1

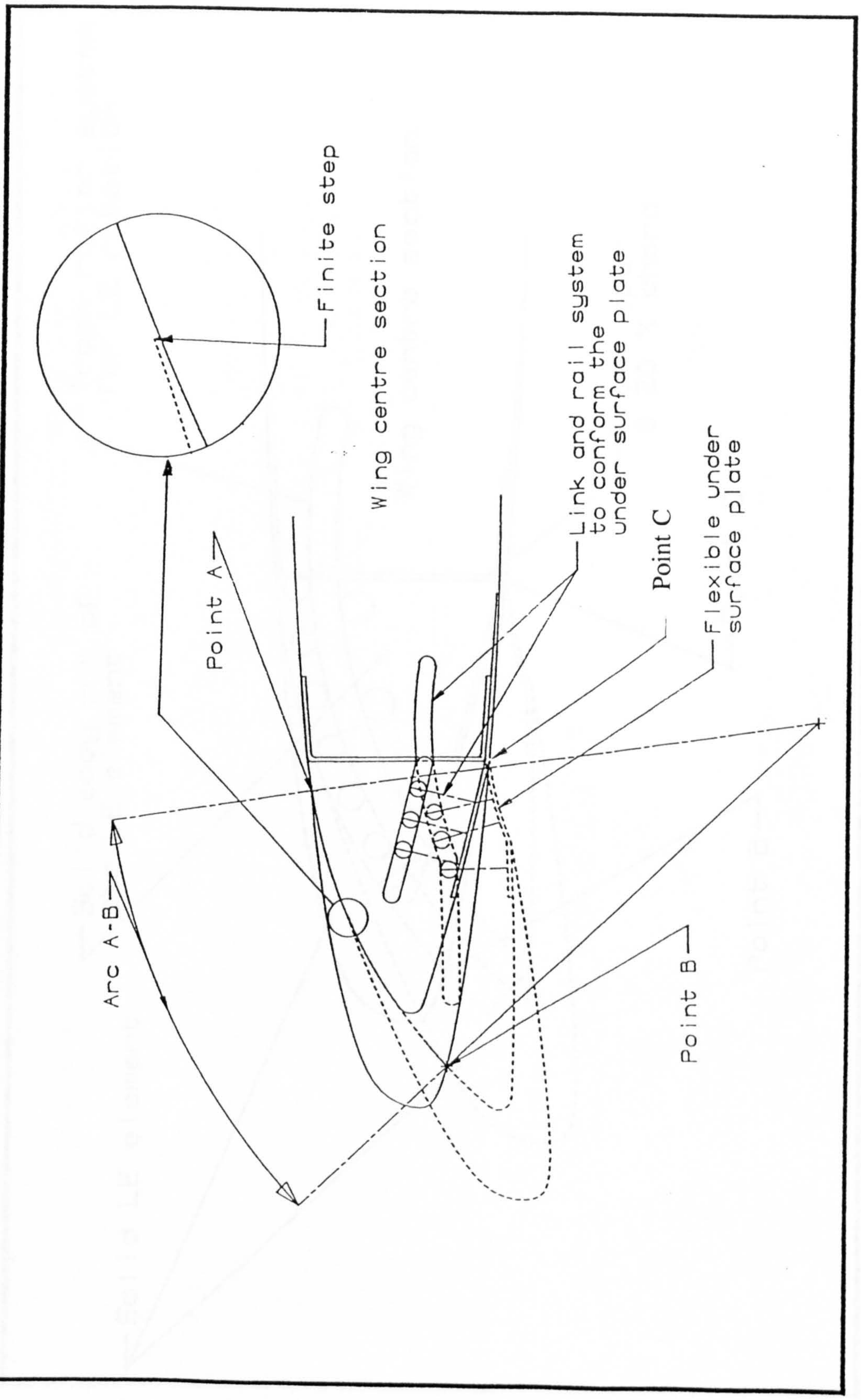

Figure 2.3b: Design scheme for LESA1 - LESA2

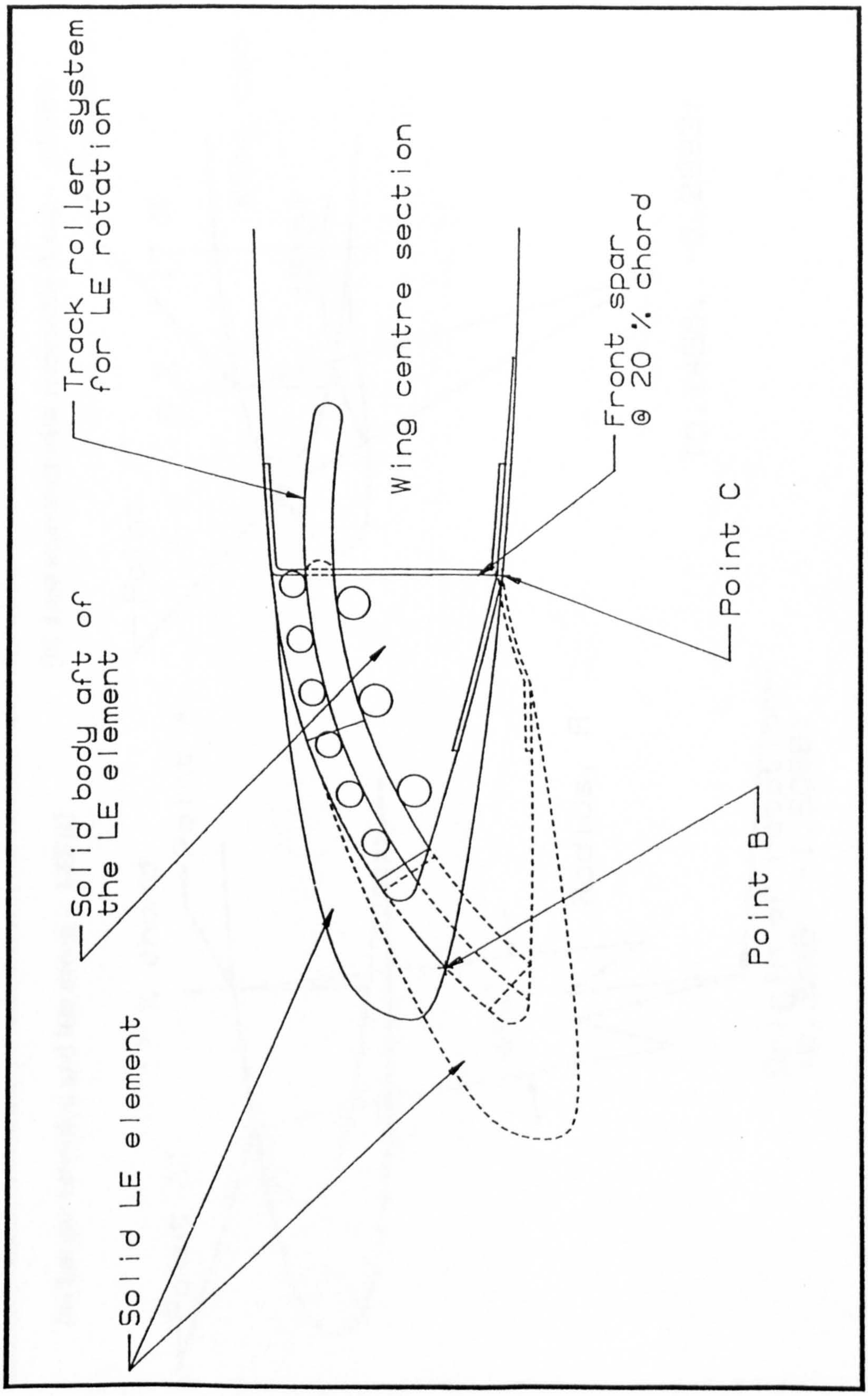

Figure 2.3c: Track details for LESA1 - LESA3

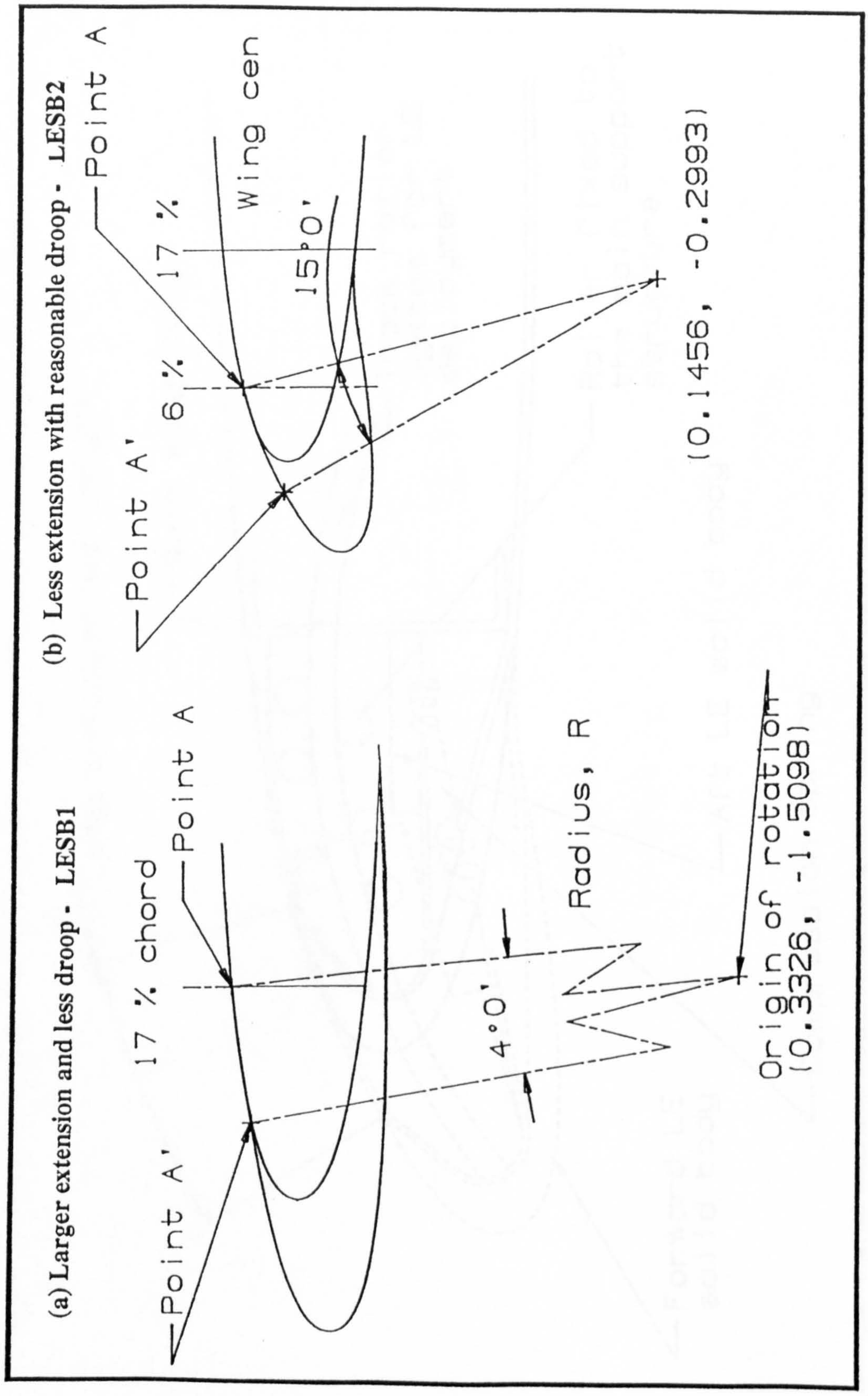

Figure 2.4: Leading edge variable camber profiles for Section B:

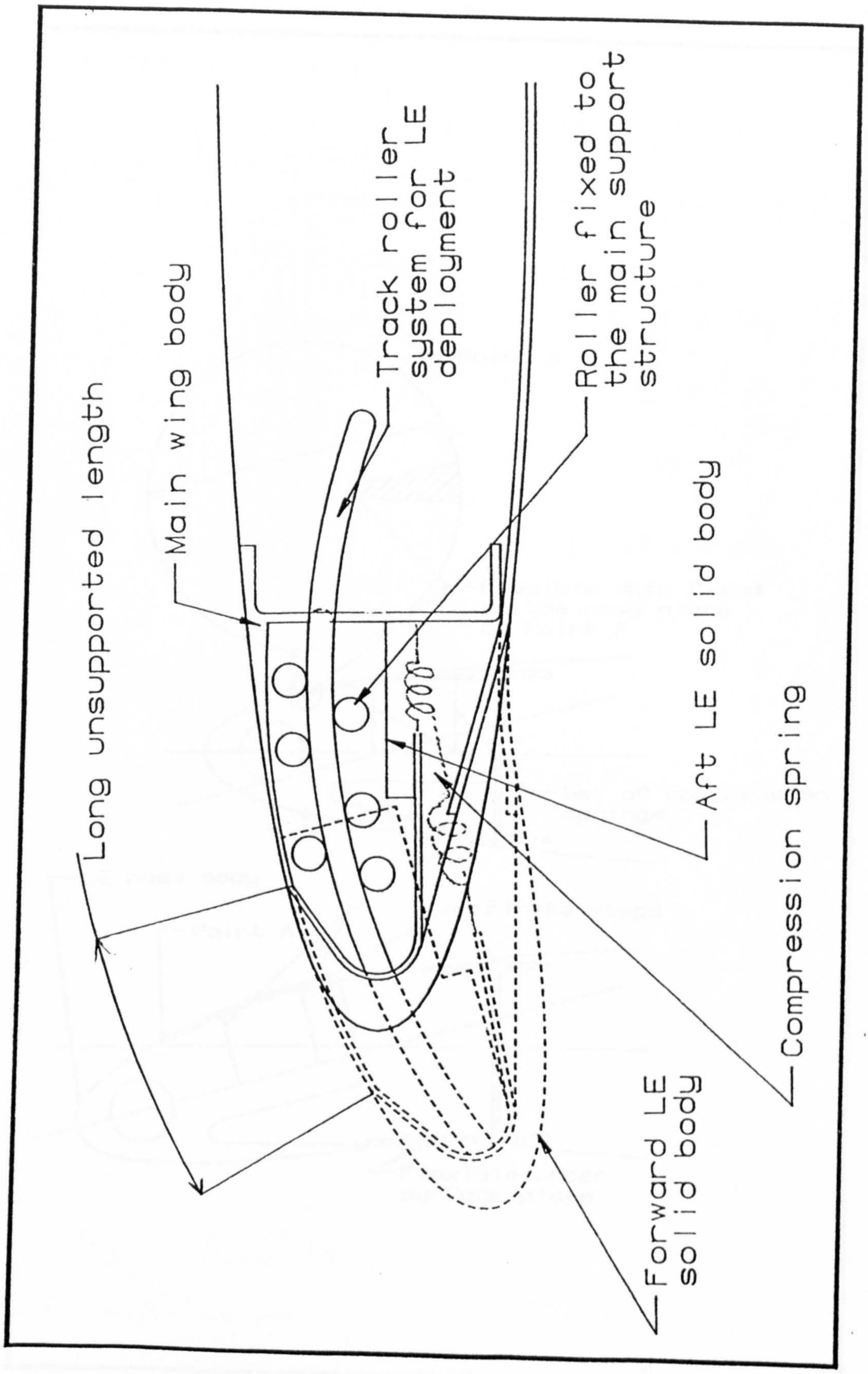

Figure 2.5: Variable camber design scheme one for LESB2 - LESB3

Figure 2.6: Variable camber design scheme two for LESB2 - LESB4

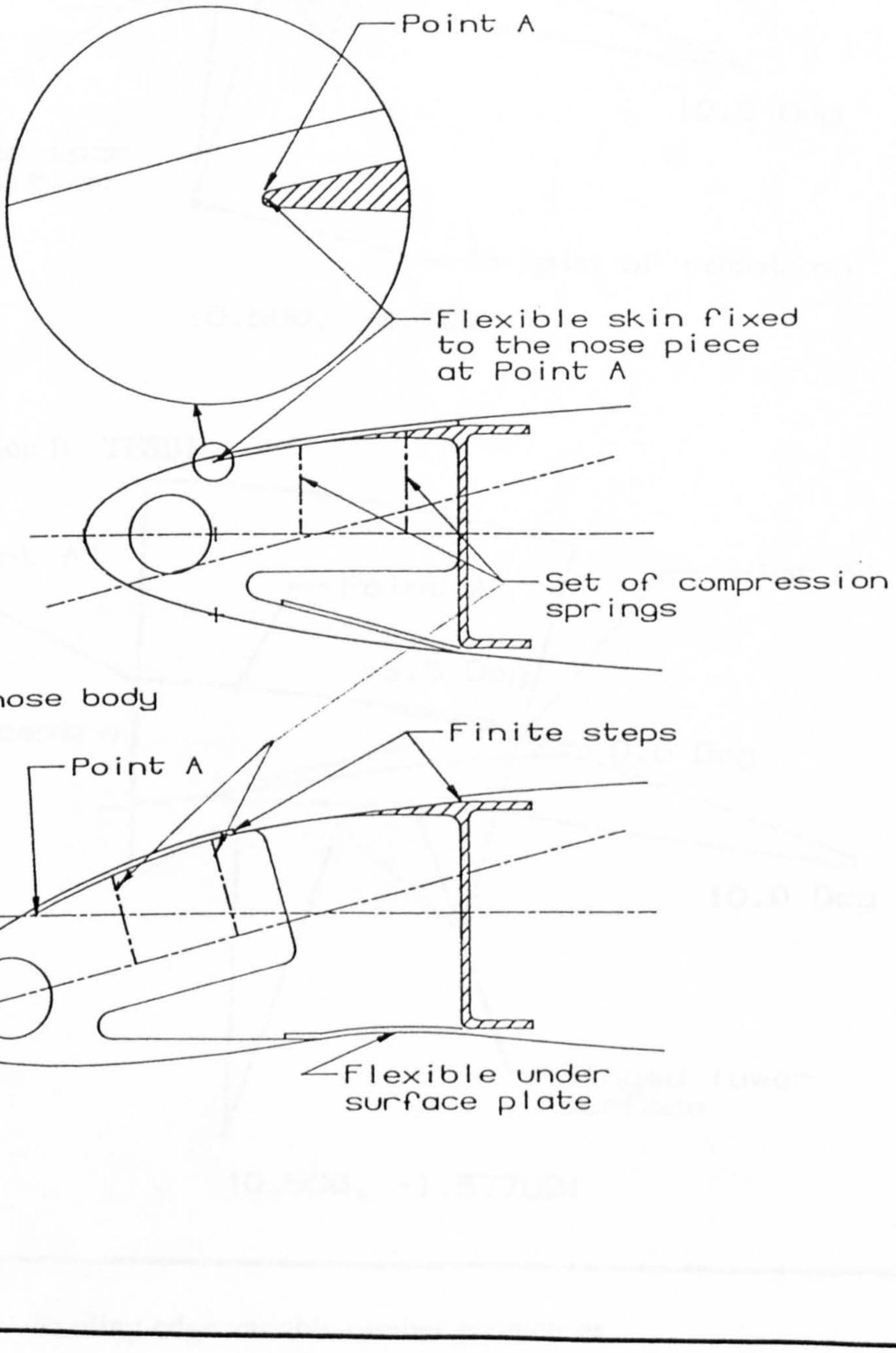

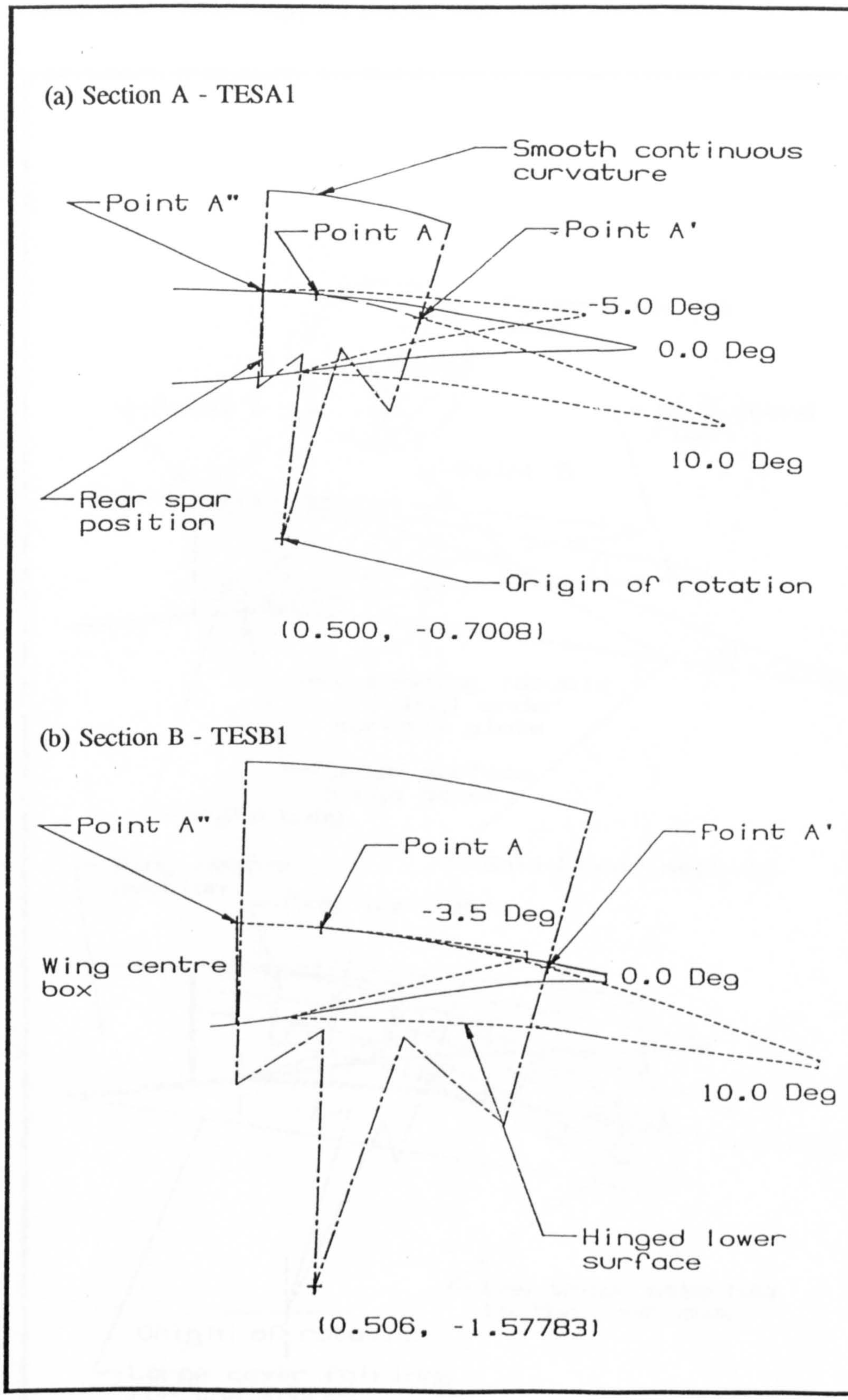

Figure 2.7: Trailing edge variable camber geometries

Figure 2.8a: Variable camber trailing edge design scheme one for TESA1 - TESA2

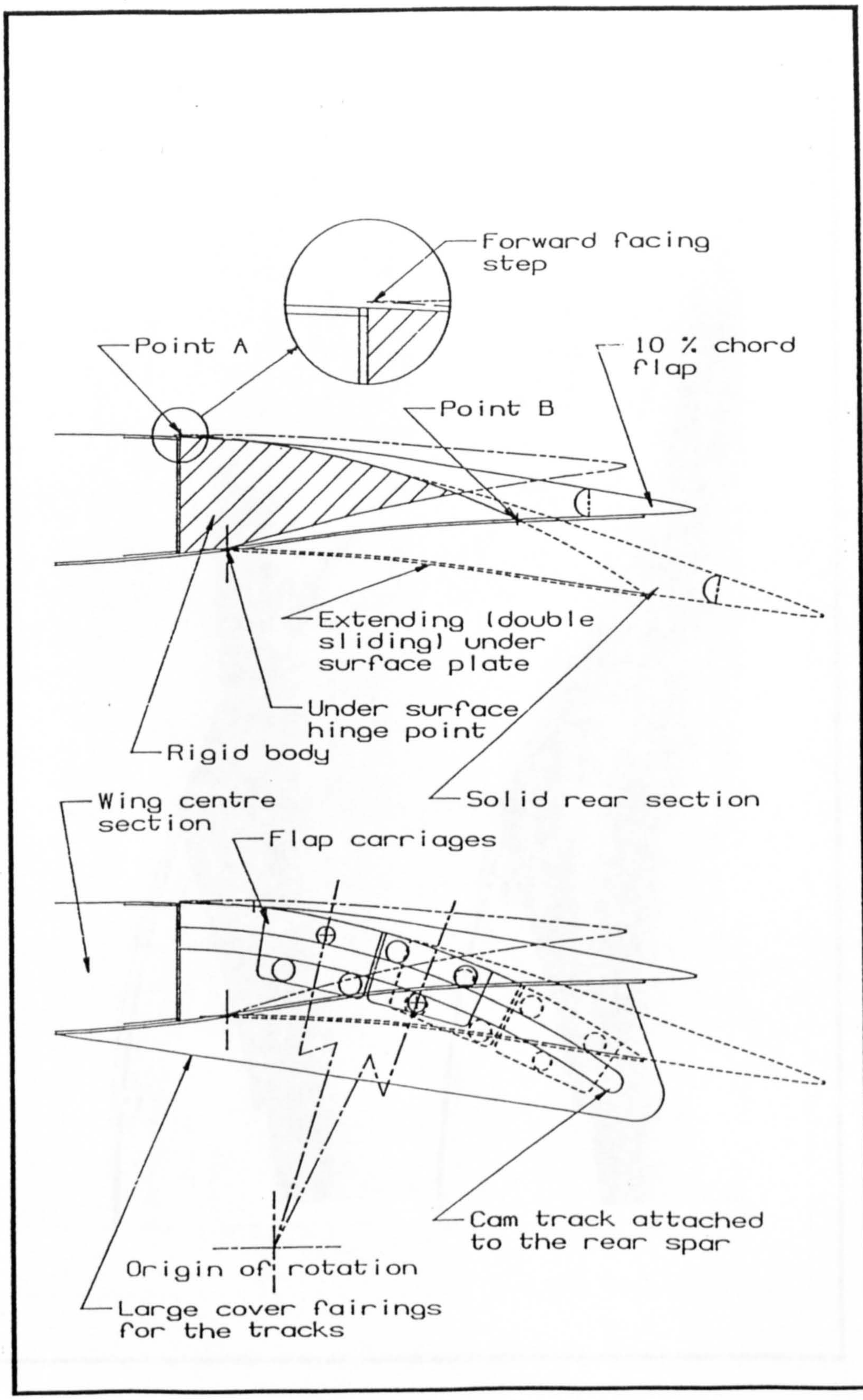

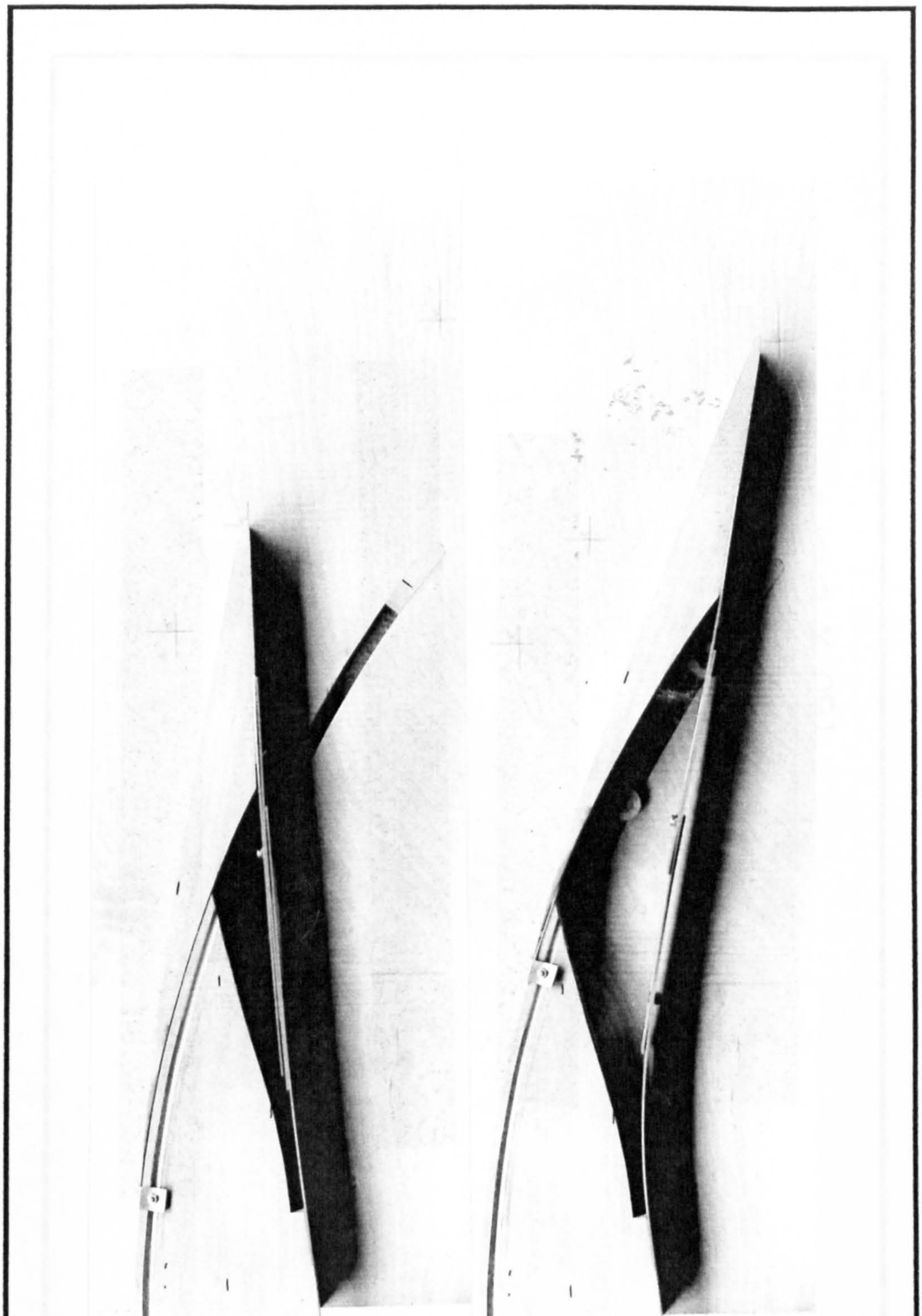

Figure 2.8b: Demonstration model of TESA2

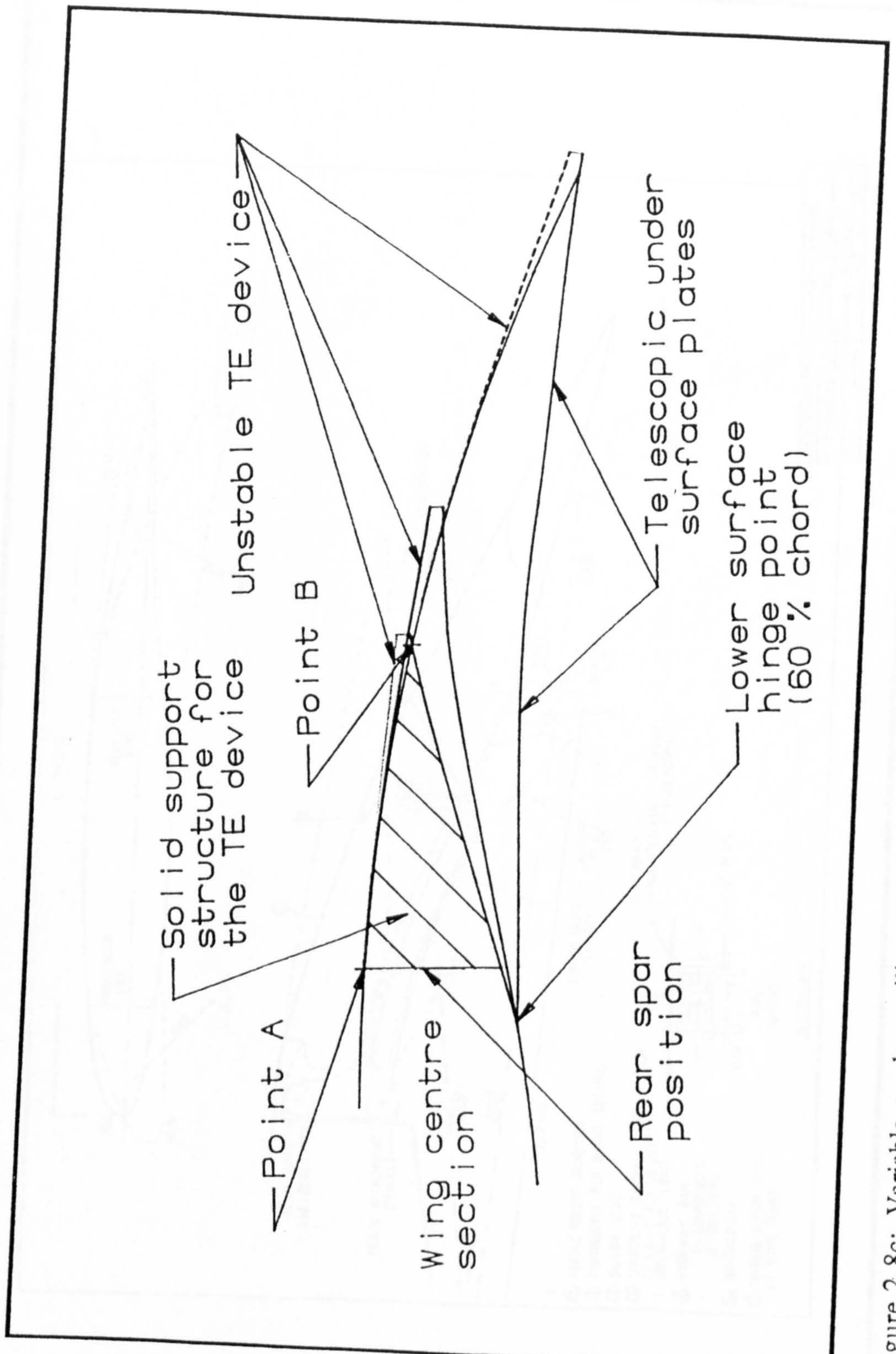

Figure 2.8c: Variable camber trailing edge design scheme one for TESB1 - TESB2

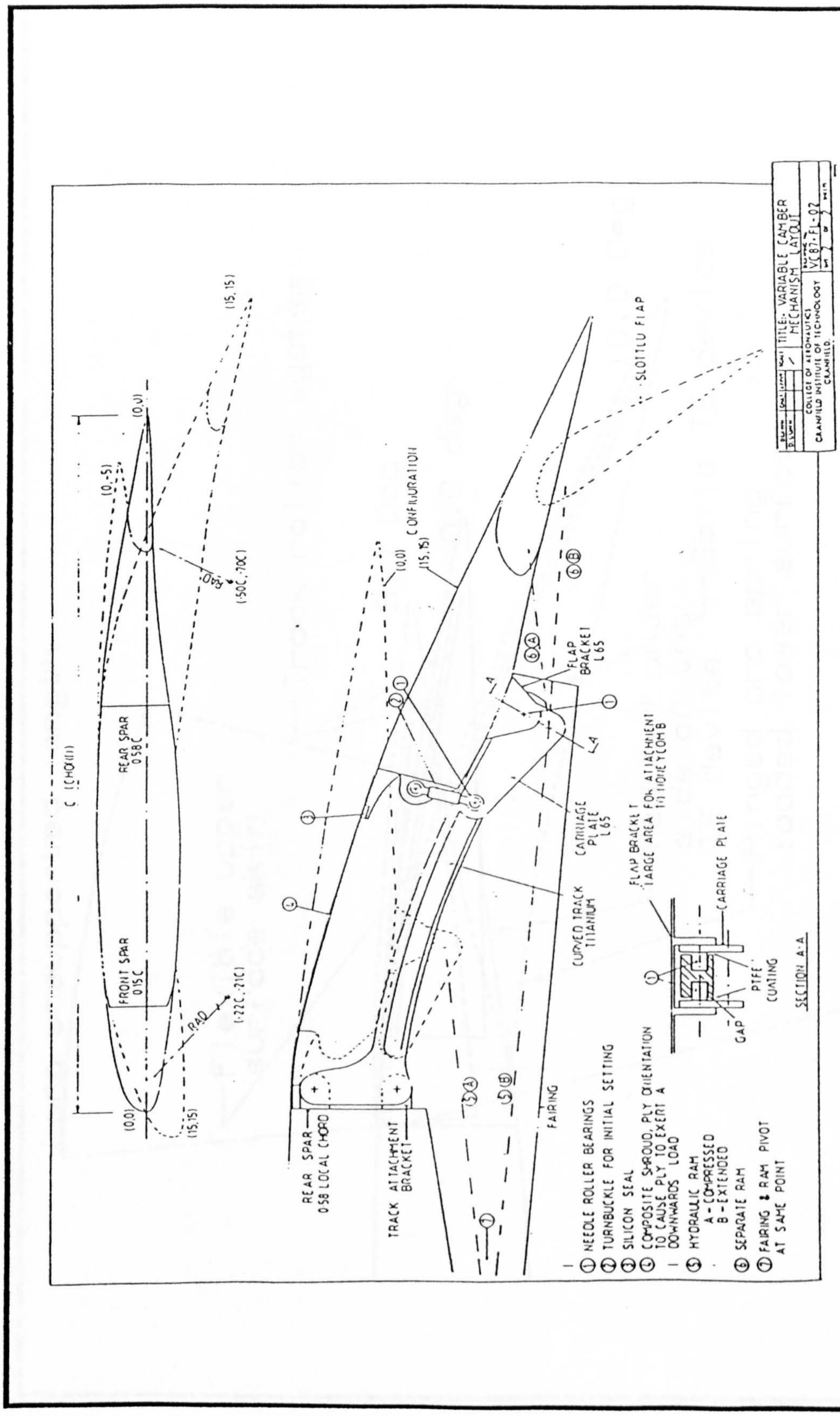

Figure 2.9: Trailing edge design scheme proposed in reference [25]

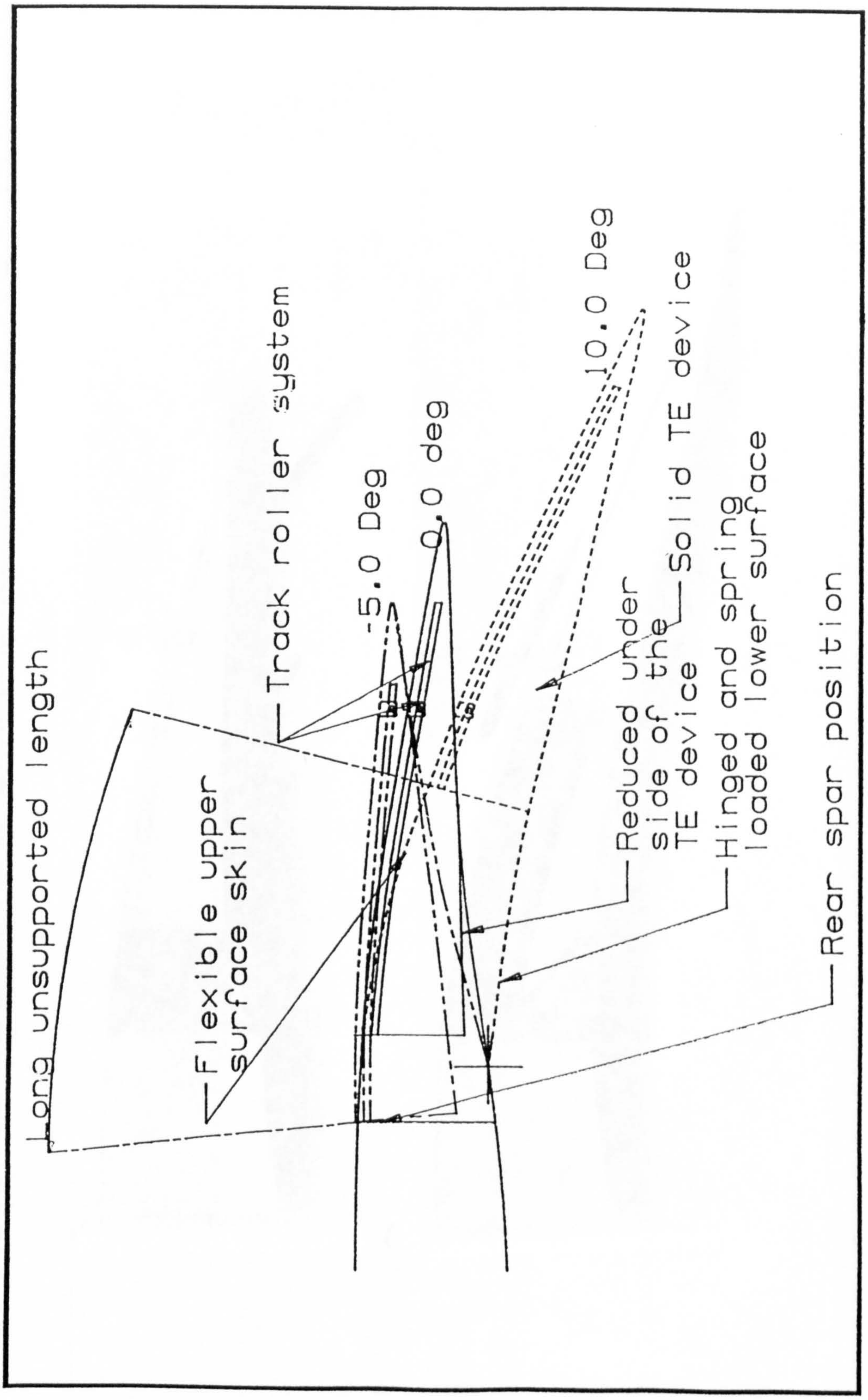

Figure 2.10a: Variable camber trailing edge design scheme two for TESA1 - TESA3

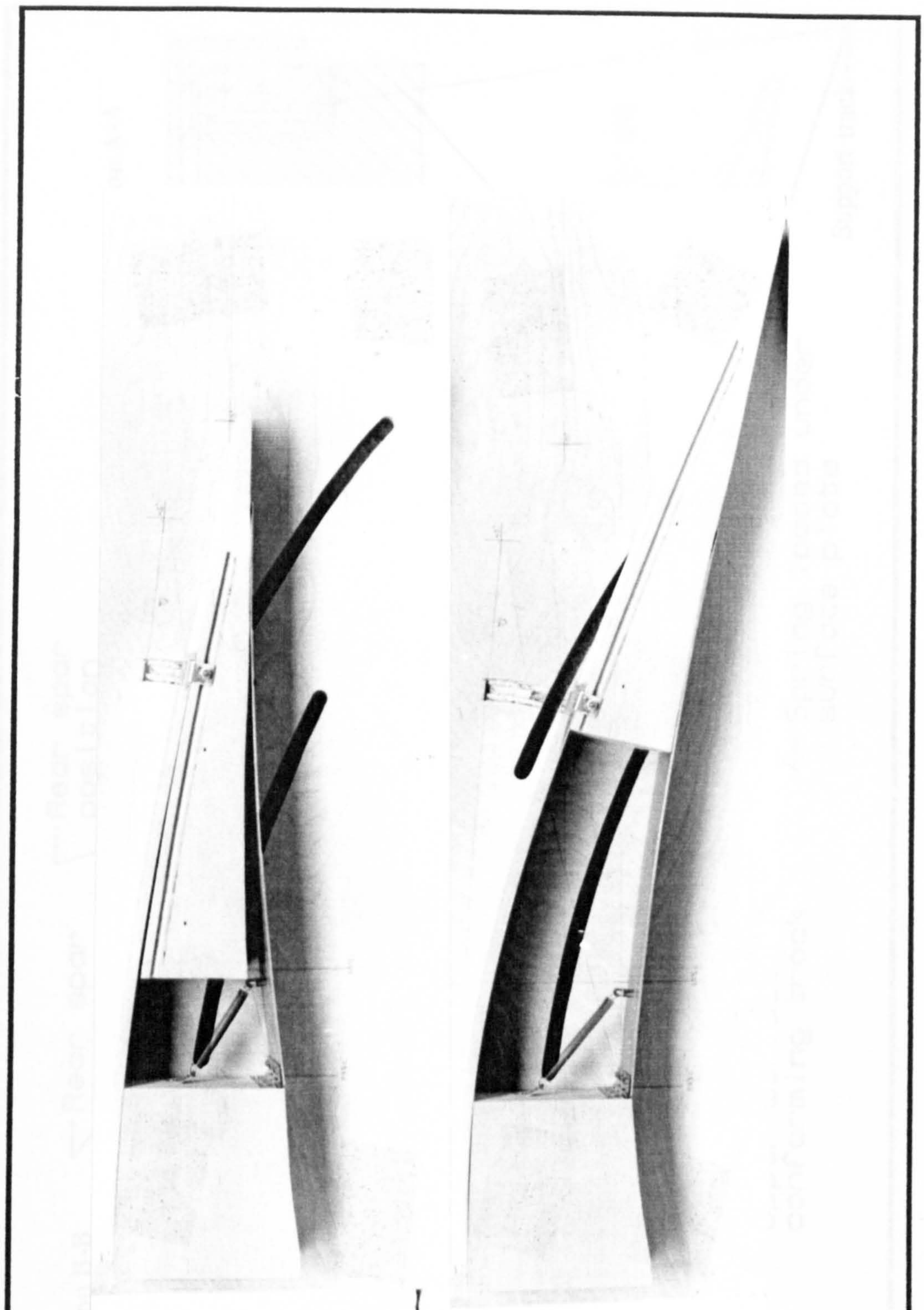

Figure 2.10b: Demonstration model of TESA3

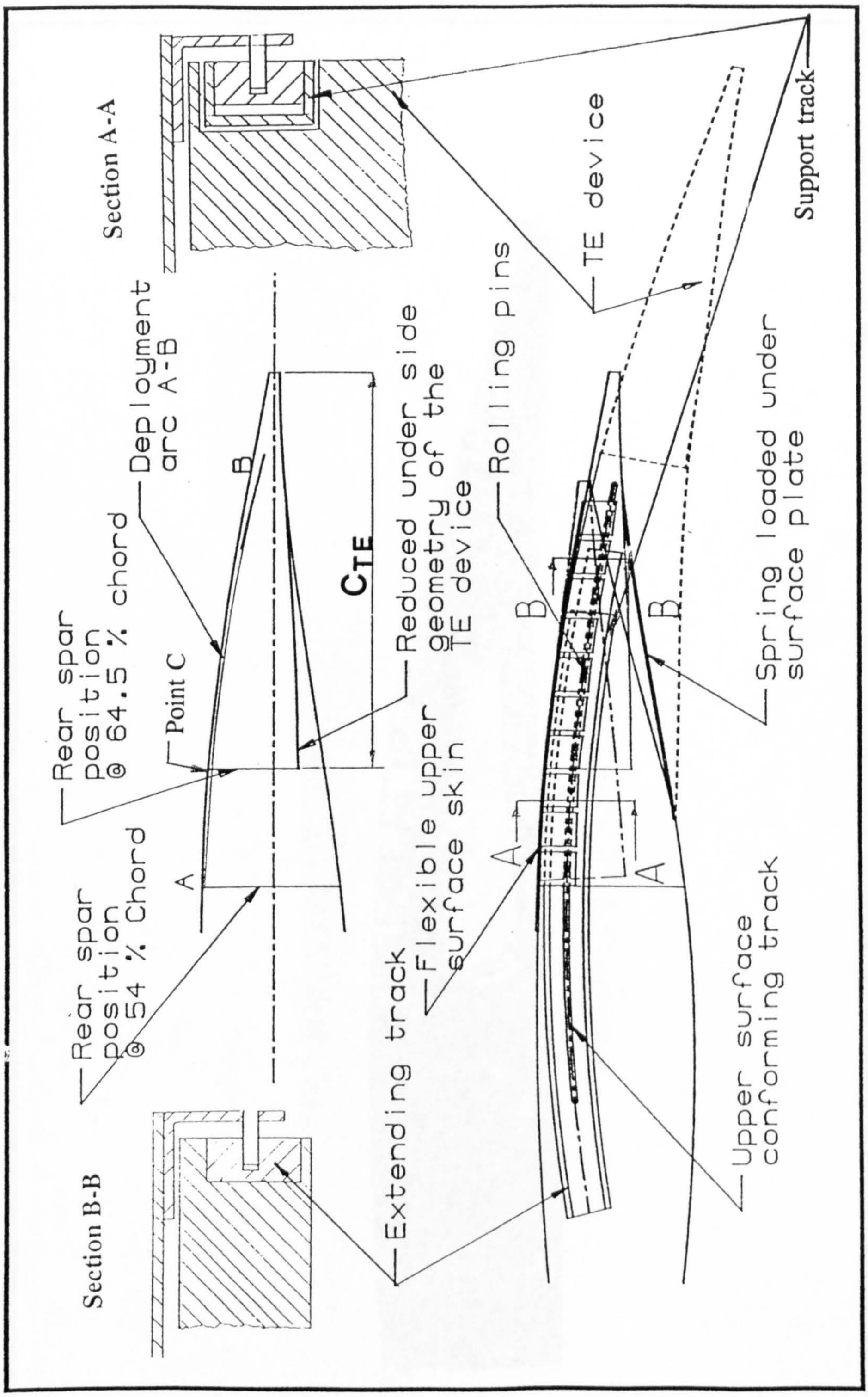

Figure 2.11a: Variable camber trailing edge design scheme three for TESB1 - TESB3

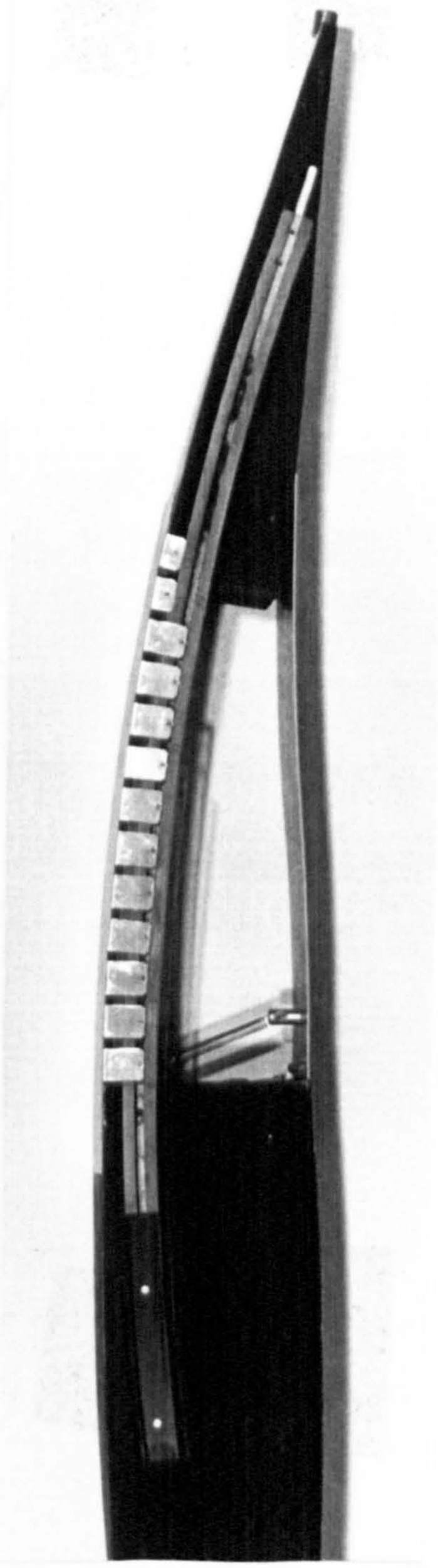

Figure 2.11b: Demonstration model of TESB3

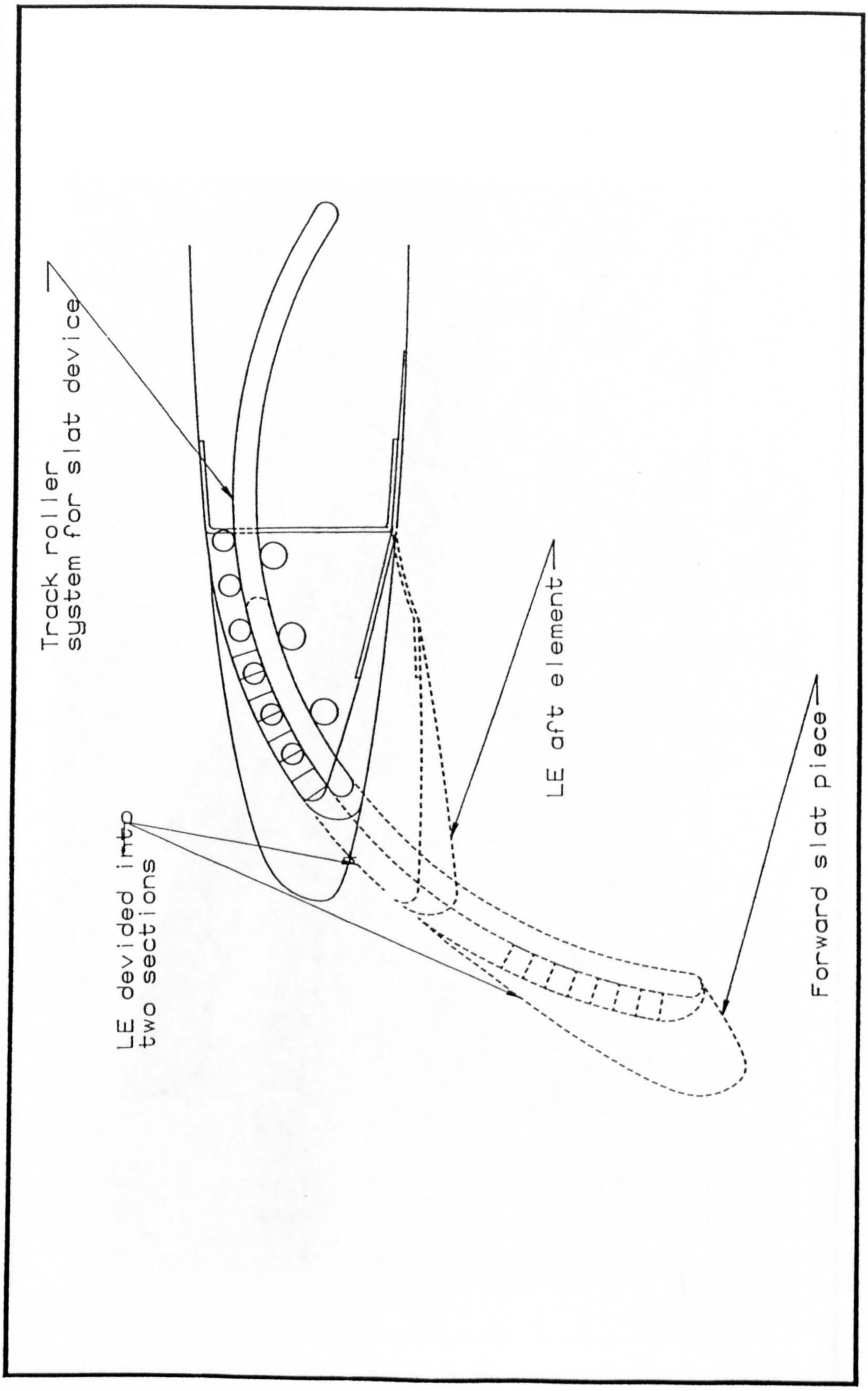

Figure 2.12: Leading edge slat combined with scheme LESA2 and LESA3 - LESA4

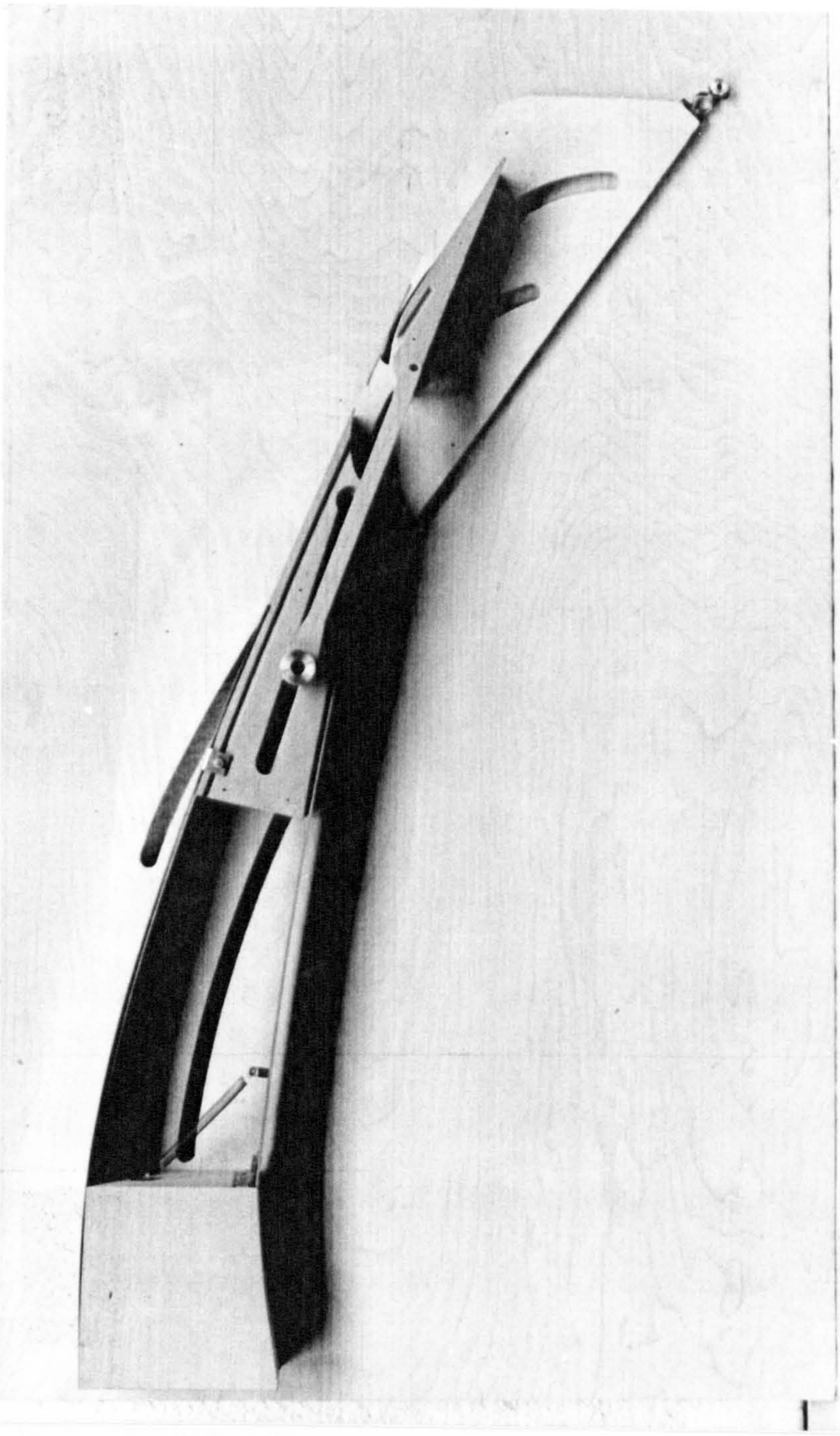

Figure 2.13: Demonstration model of the trailing edge design scheme TESA3 installed with a 10 % extending flap - TESA4

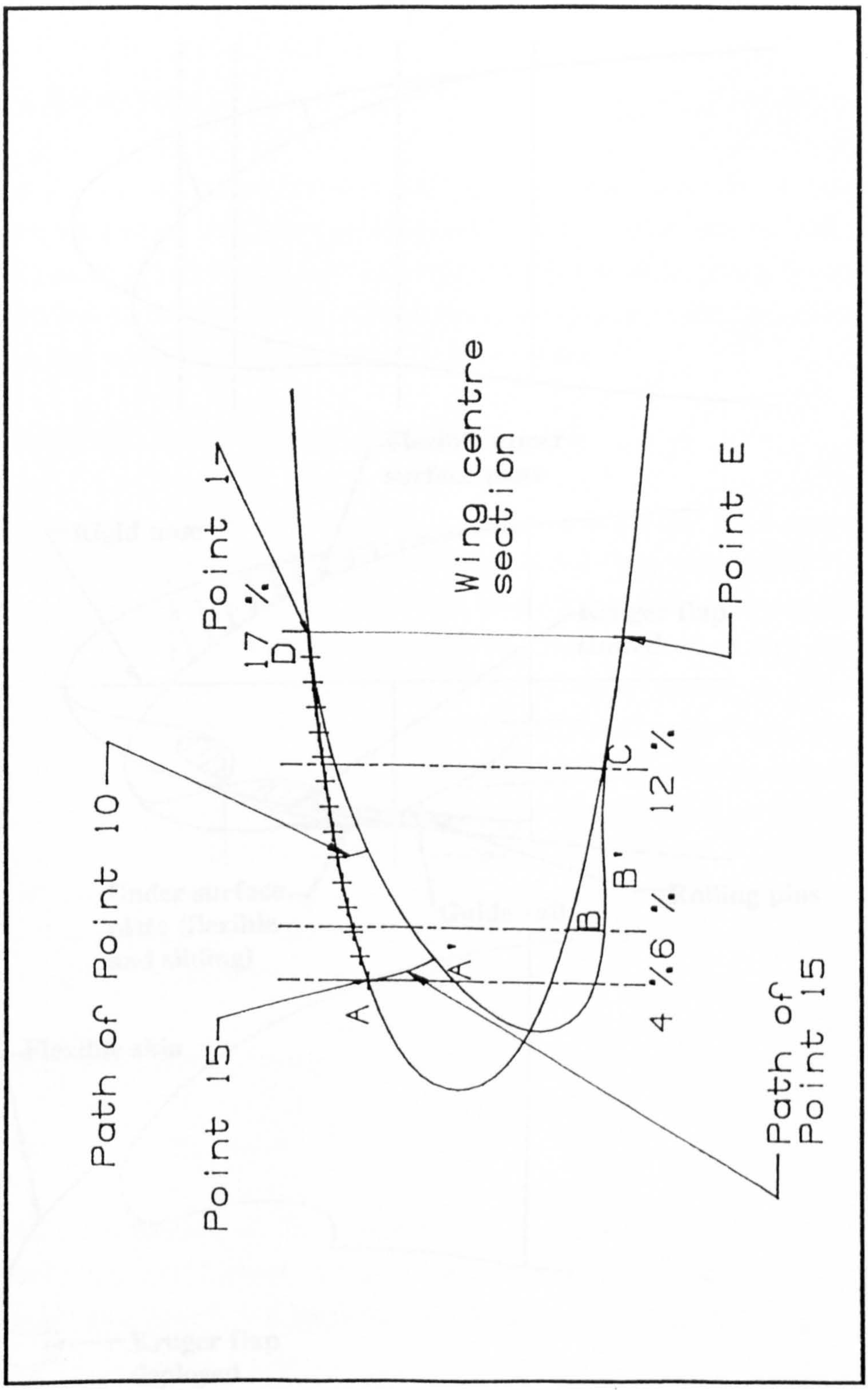

Figure 2.14a: Variable camber leading edge geometry for drooping the nose of Section B - LESB5

Figure 2.14b: Variable camber scheme LESB5 installed with a Kruger flap - LESB6

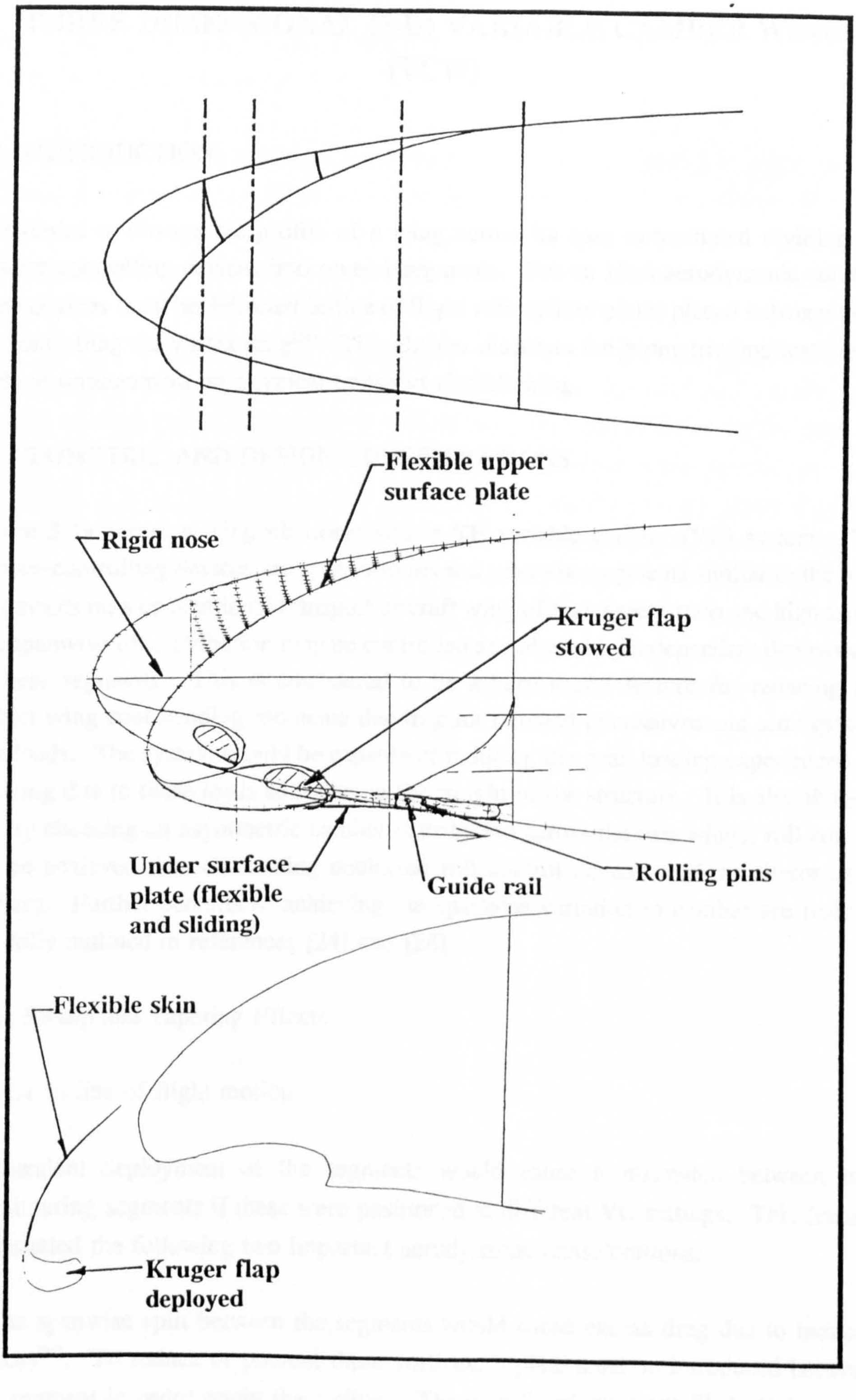

CHAPTER THREE

THREE DIMENSIONAL (3-D) VARIABLE CAMBER WING (VCW)

3.1 INTRODUCTION

The desire to change the profile of a wing across its span necessitated dividing the camber controlling devices into several segments. For an ideal aerodynamic solution these devices must be deflected in-line of flight with splitter plates placed between them for controlling the vortex drag[24]. This chapter discusses the geometric implications of such an arrangement on a typical transport aircraft wing.

3.2 GEOMETRIC AND DESIGN CONSIDERATIONS

Figure 3.1a shows a wing planform with a TE variable camber (VC) system. The camber-controlling devices are split in-to several spanwise segments similar to the high lift devices on a conventional transport aircraft wing of high aspect ratio and high taper. The spanwise lift distribution may be controlled and altered by independent deployment of these segments. This is considered to be a very useful feature for reducing the overall wing root bending moments due to pilot initiated manoeuvre and atmospheric gust loads. The system should be capable of reducing the peak loading experienced by the wing due to these loads so reducing the weight of the structure. It is also thought that by choosing an asymmetric camber distribution across the two wings, roll control can be achieved thus eliminating dedicated roll control devices such as ailerons and spoilers. Further benefits of achieving the spanwise variation in camber are realised and fully outlined in references [24] and [28].

3.2.1 Sweep and Tapering Effects

3.2.1.1 In-line of flight motion

Independent deployment of the segments would cause a mismatch between two neighbouring segments if these were positioned at different VC settings. This feature necessitated the following two important aerodynamic considerations:-

1) The spanwise split between the segments would cause excess drag due to induced vortices[24]. To reduce or prevent these vortices, a plate must be introduced between each segment in order retain the airflow. These 'splitter' plate are likely to be twice

the depth of the aerofoil in order to cover the full VC deflection range.

2) All the segments must ideally be deployed in-line of flight. Deployment on any angle from this would obviously increase profile drag of the splitter plates and therefore reduce the overall efficiency of the VC system.

The required planform geometry is similar to the layout of Figure 3.2, which satisfies the requirements for spanwise variation in camber with the chordwise VC from rotational and translational motion of the TE elements. In reality such a geometry is impossible to achieve on a swept and tapered wing, for the following reasons:-

Consider the 2-D geometry of the TE shown in Figure 2.7b of Chapter Two (sub-section 2.2) where the origin of rotation is (0.506, -1.57783)x/c of the local chord. If several of these points (origins) were joined along the span of the wing for each real chord, the constructed imaginary hinge-line (H/L) will be swept and tapered, as shown in Figure 3.3a. The local radius of curvature therefore varies along the span, decreasing from root to tip. The deploying point A (Figure 2.7b) thus lies on a frustum of a cone, the centre line of which is the imaginary hinge-line (H/L). Figure 3.3b shows the wing plan of the streamwise TE segments of Figure 3.1 being deployed perpendicular to this H/L. Quite clearly this geometry is unsatisfactory in both spanwise and chordwise planes, since all the segments shift laterally across the span from the inboard (I/B) to the outboard (O/B). If the segments are to move backwards in a streamwise direction with their edges streamwise, and at the same time rotate to give an angular deflection, the axes of rotation must be unswept. Figure 3.4a shows an untapered and unswept H/L, fixed such that the radius of curvature (R) matches at the centre of each segment. Thus, the local curvature only matches at one point along the span of the segment. The 2-D deployed profile shown in Figure 3.4b, of the centre, inboard and outboard part of a segment indicates that there is a miss-match in curvature along the span of the segment. Aerodynamically this will give undesirable flow characteristics, with the certainty of separation near the I/B end due to sharp changes in TE curvature. To avoid this problem and retain the in-line of flight motion, the forward and aft ends of the TE device must be unswept. Figure 3.5 illustrate how this would effect the planform of the wing of the same aspect ratio as Figure 3.1. R matches the O/B ends of the segments. With this arrangement the chord of the TE device (C_{TE}) decreases rapidly as the span of the segment increases, thus reducing the effectiveness of the VC system by practically restricting the degree of deflection, particularly at the IB end of the segment. To overcome this, the size of the segments must be reduced and therefore the number of segments across the span must be increased. That would introduce undesirable complexities and increase the overall weight of the system (further details are covered in Chapter Four).

3.2.2.2 Conical deployment

From the above arguments it can be assumed that it is unlikely, if not impossible to keep the profile smooth along the chord and at the same time retain the streamwise translation of the segments. It would appear that a VC profile can only be maintained if the moving elements were kept perpendicular to the conical H/L. The rotation of these elements would be on a frustum of a cone, as shown in Figure 3.6. A 'true' conical motion shifts the segments across the span. If splitter plates were to be used they would be skewed to the line of flight and therefore will require substantial cover fairings which undoubtedly will increase the profile drag of the wing. From a structural point of view the design complexities would be considerable and structural efficiency will be highly reduced in order to have a practical solution with 'true' conical motion. For example, to achieve this motion with the proposed TE design, the support tracks must be mounted at an angle equivalent to the sweep angle of the axis of rotation, shown as dotted lines in Figure 3.7. To improve the efficiency, these tracks must obviously be mounted directly to the wing side ribs, depicted by the full lines in Figure 3.7. Such an arrangement implies that the motion no longer remains 'truly' conical but slightly diverges. A compromise must therefore be made to obtain a 'near' conical deployment. This is possible by placing the segments parallel to the main wing box and deploying them perpendicular to the conical H/L. Simplistic illustration of this method is given in Figure 3.8. Structural constraints must be applied to keep the segments parallel to the wing box during translational motion. For example the TE structural box must be made to flex and twist or it must be attached to the extending tracks through pin jointed arrangement. Details of these possibilities are covered in Chapter Four, Six and Seven. With the arrangement shown in Figure 3.8, it is still disadvantageous to include splitter plates, since the segments are skewed with respect to the line of flight. It is therefore recommended not to have these plates.

From the above discussions it can be assumed that Figure 3.8 is a better representation of a spanwise geometry than Figure 3.2 (the required planform).

3.2.2 Negative Deployment

With the proposed design for the aft camber variation, it is apparent (from Figure 2.11 of Chapter Two) that in order to have a negative deployment the rear spar must be positioned at 54 % chord for Section B. Therefore if some of the segments were to have both negative and positive deployment while the rest only, the positive deployment the rear spar must be staggered. This is an obvious drawback since the structural efficiency of the system will be much lower than say the continuous spar arrangement.

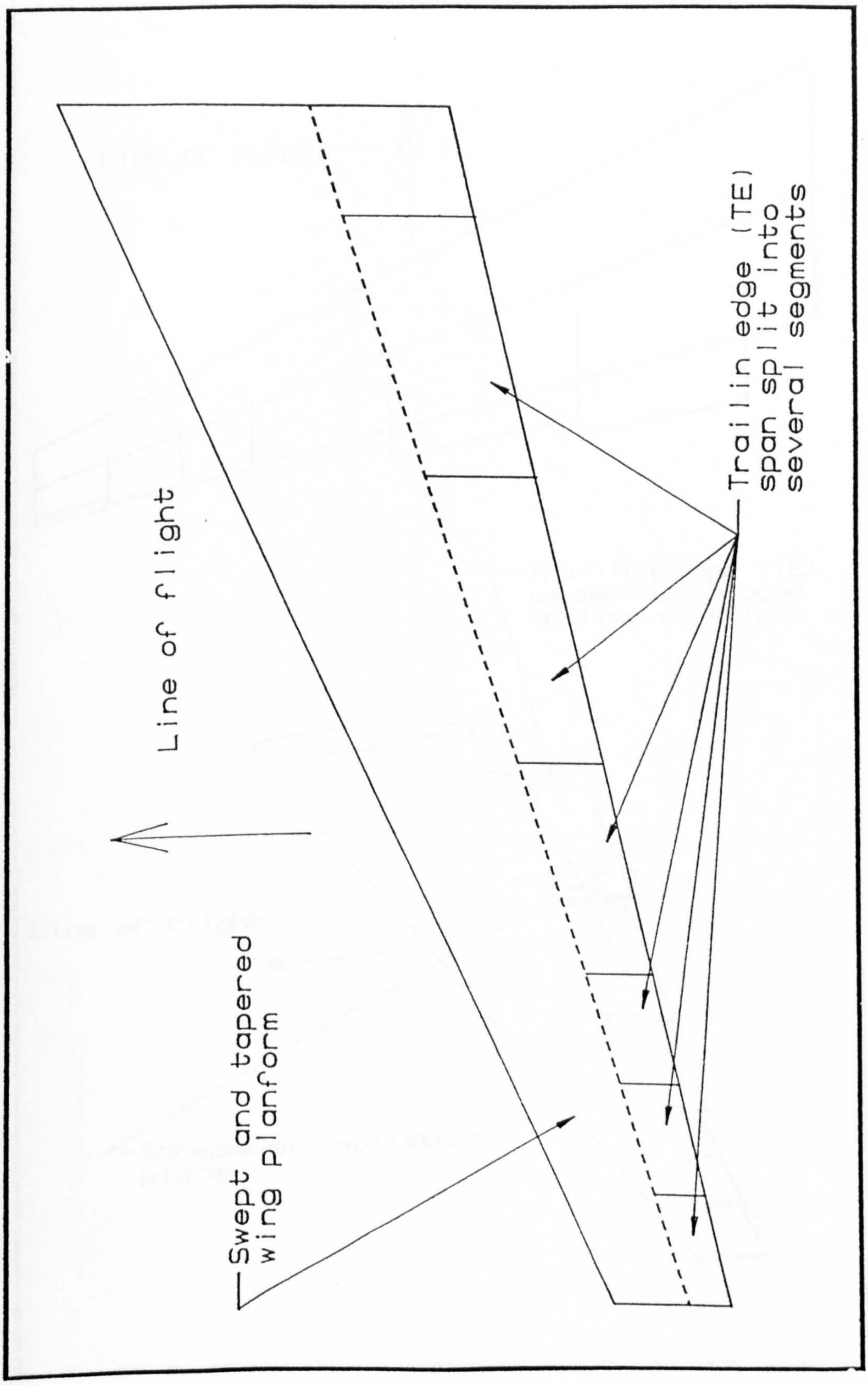

Figure 3.1: Swept and tapered wing planform with trailing edge span split into several segments

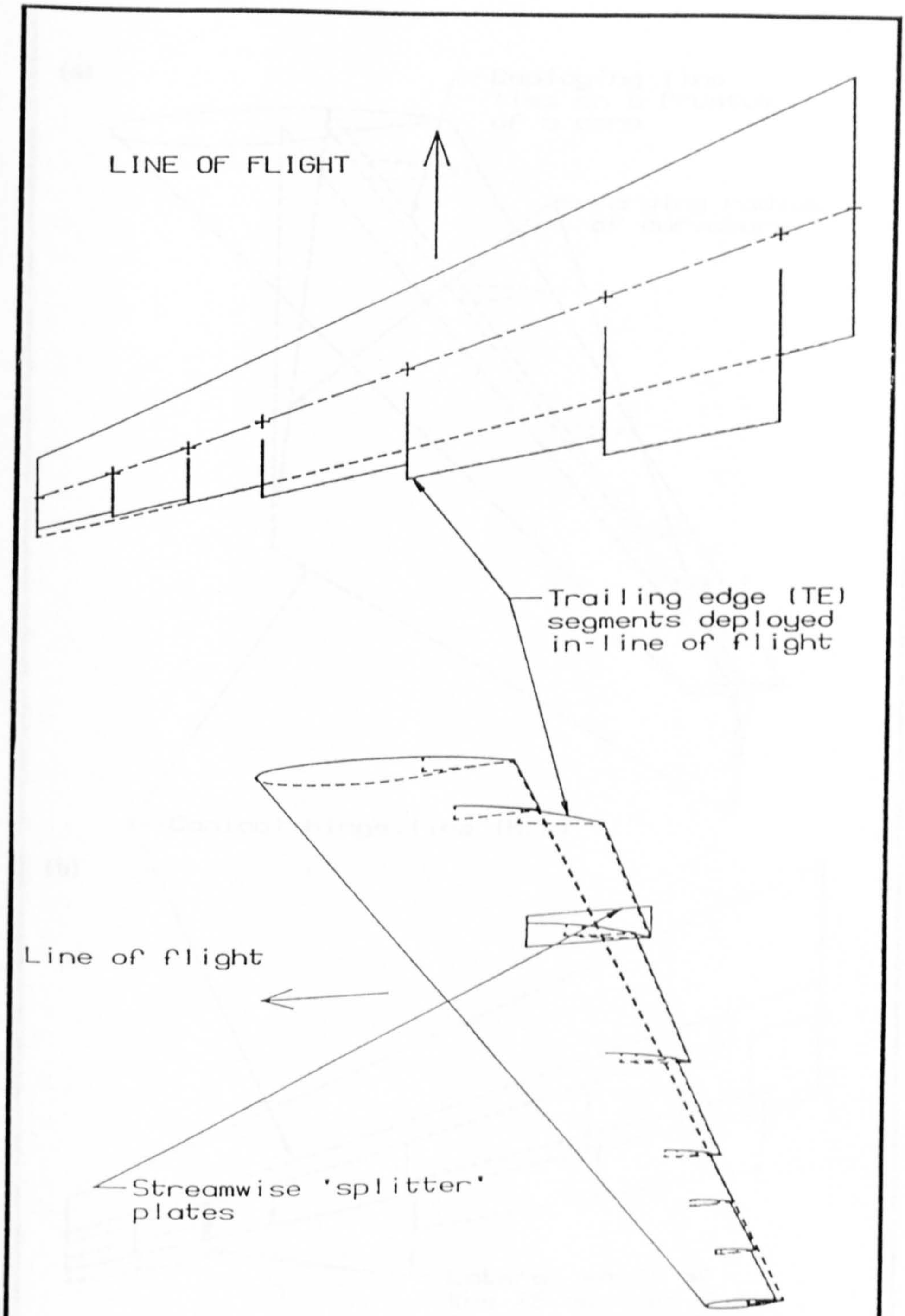

Figure 3.2: Ideal in-line of flight deployment of the trailing edge segments

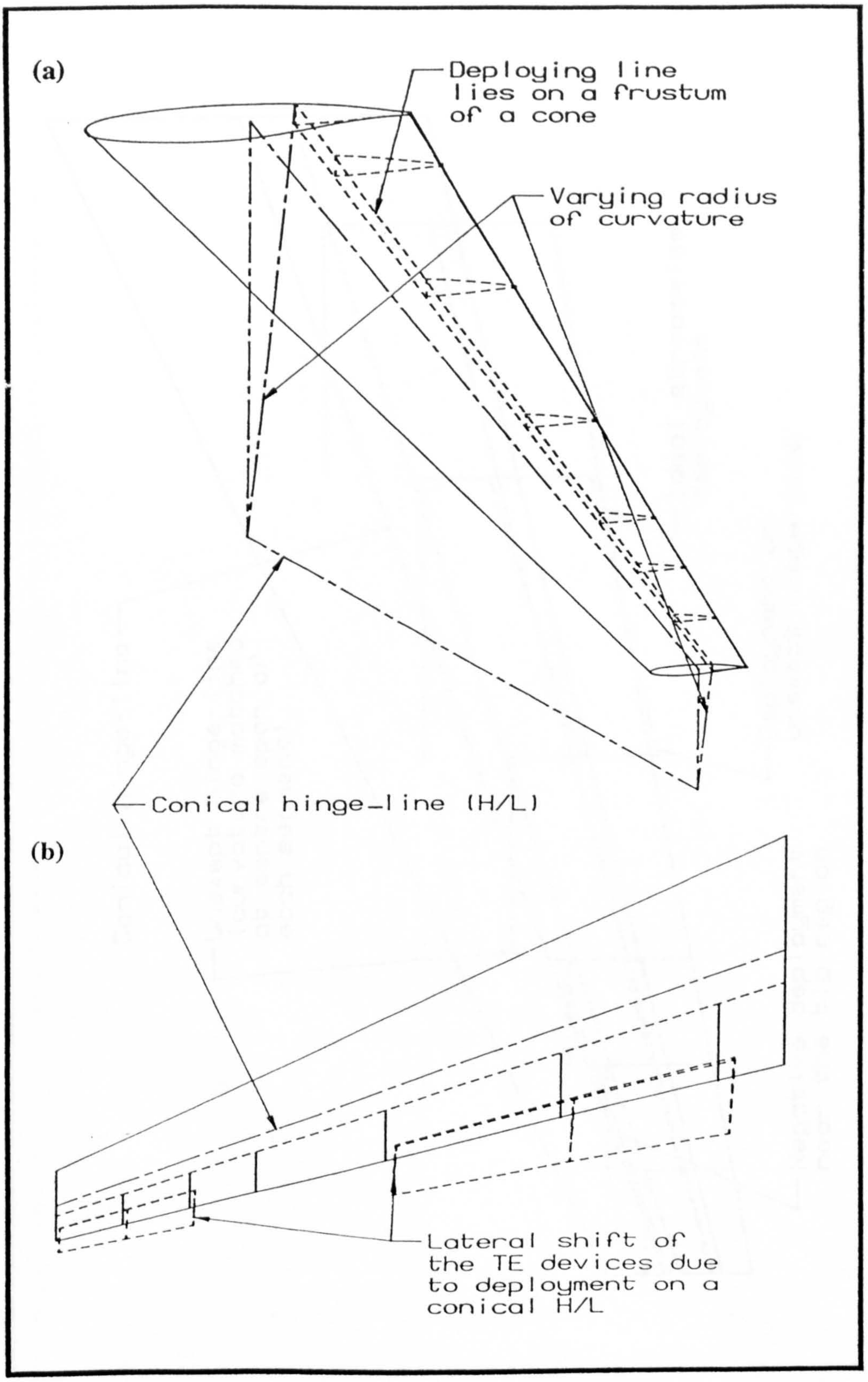

Figure 3.3a&b: Deployment of the streamwise segments on a conical hinge-line

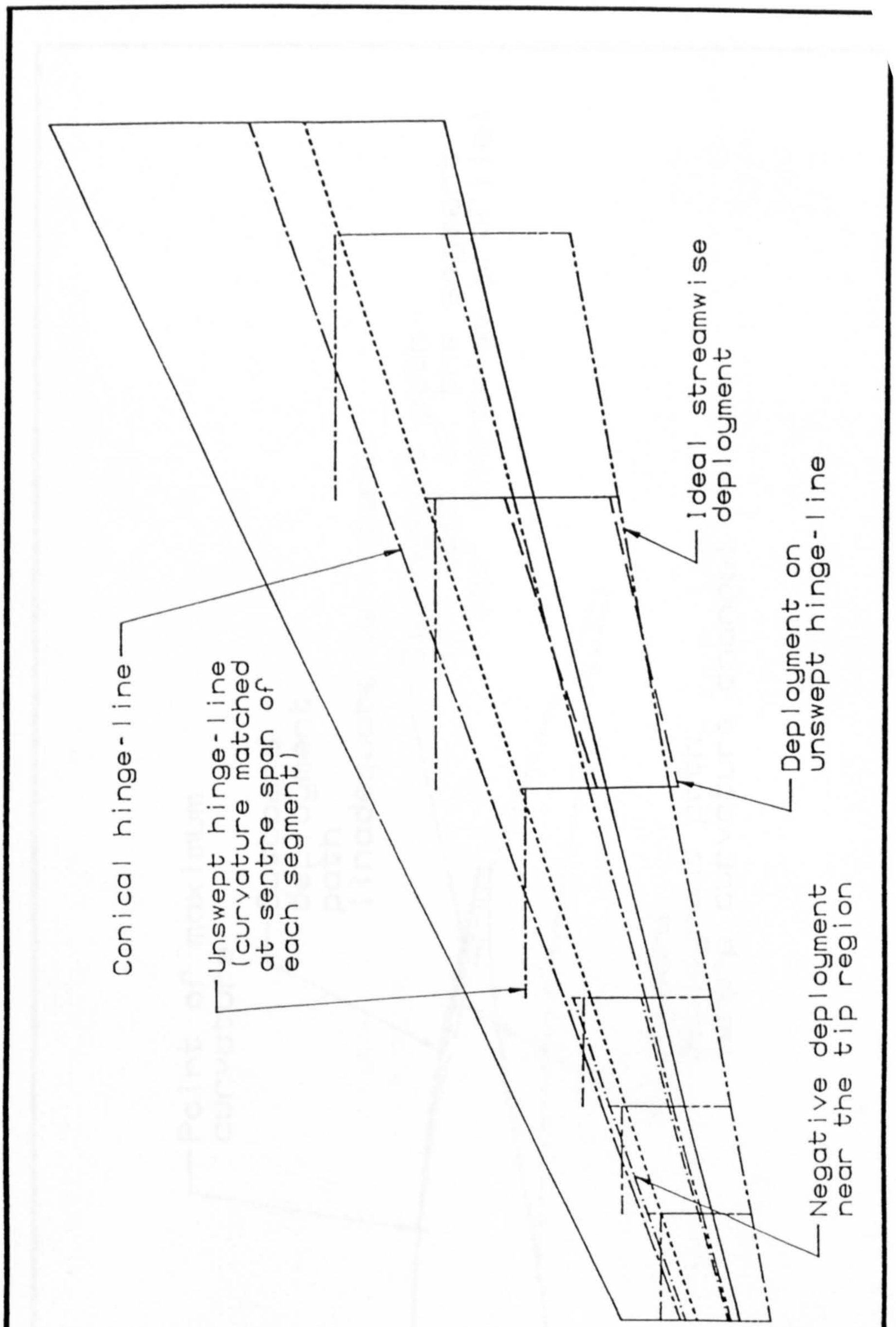

Figure 3.4a: Streamwise segments deployed on an un-swept hinge-line

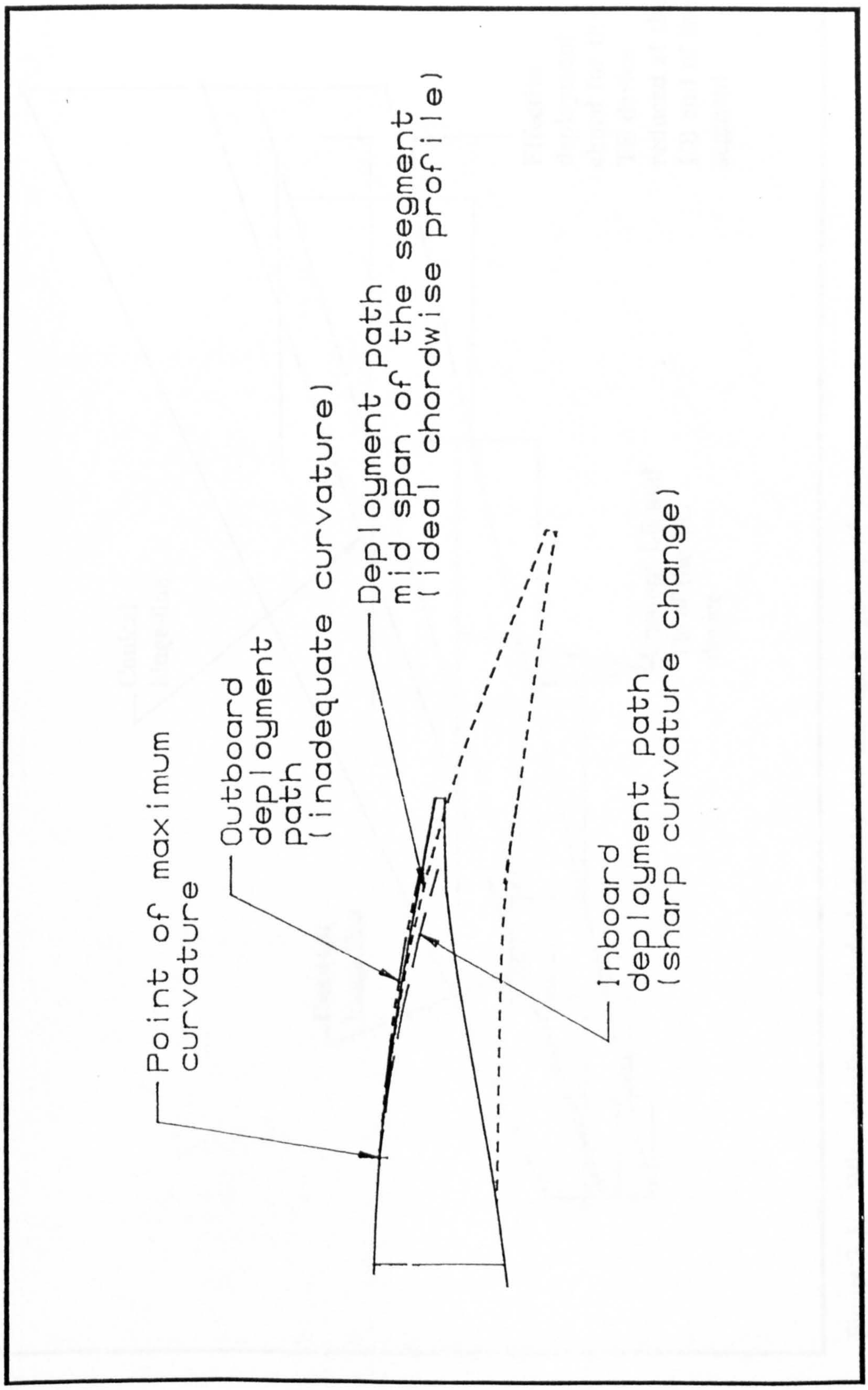

Figure 3.4b: Chordwise profiles at the inboard, mid-span and outboard stations of a segment deployed on an unswept hinge-line

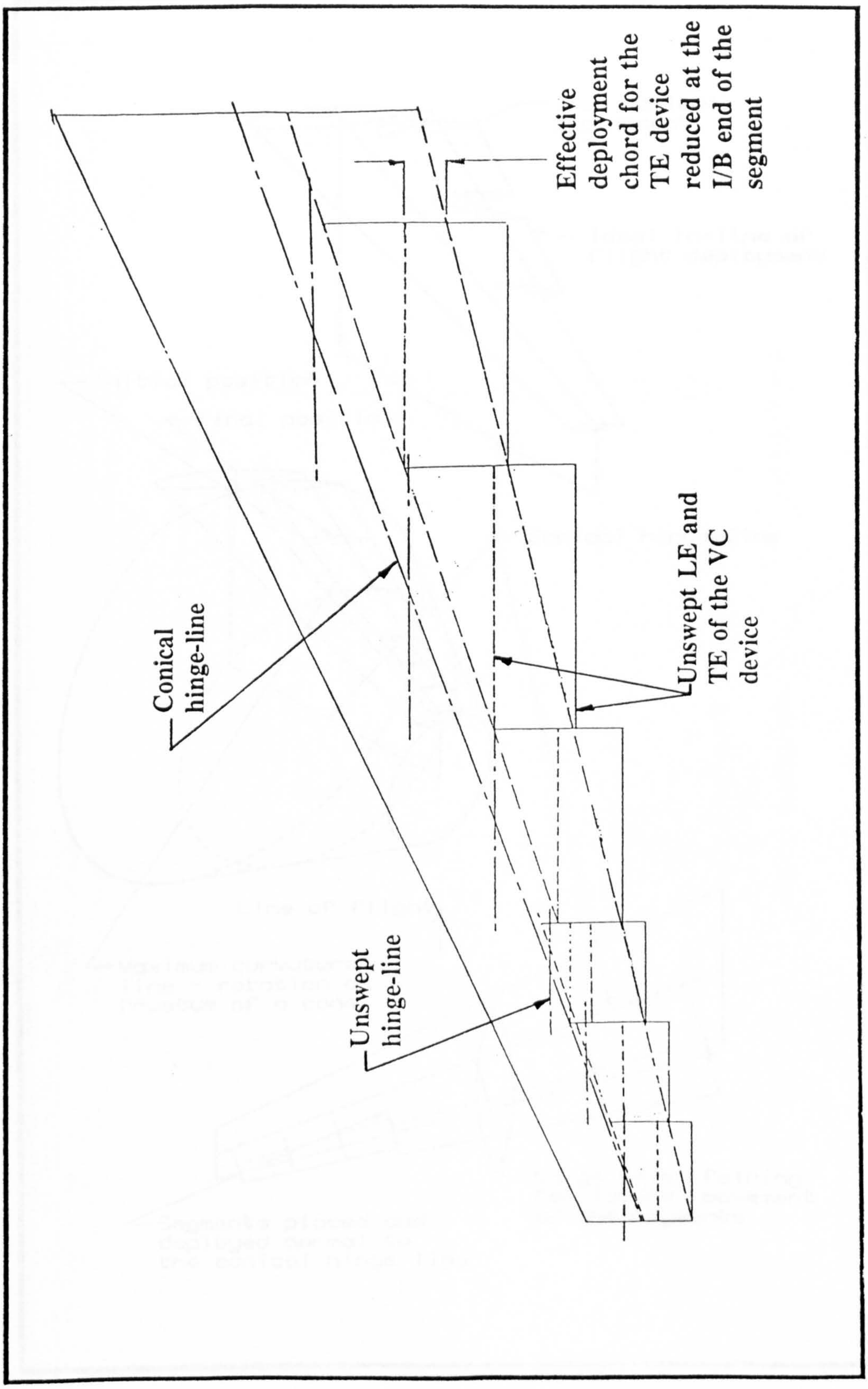

Figure 3.5: Wing planform with deployment on an unswept hinge-line of trailing edge segments that have unswept leading and trailing edges

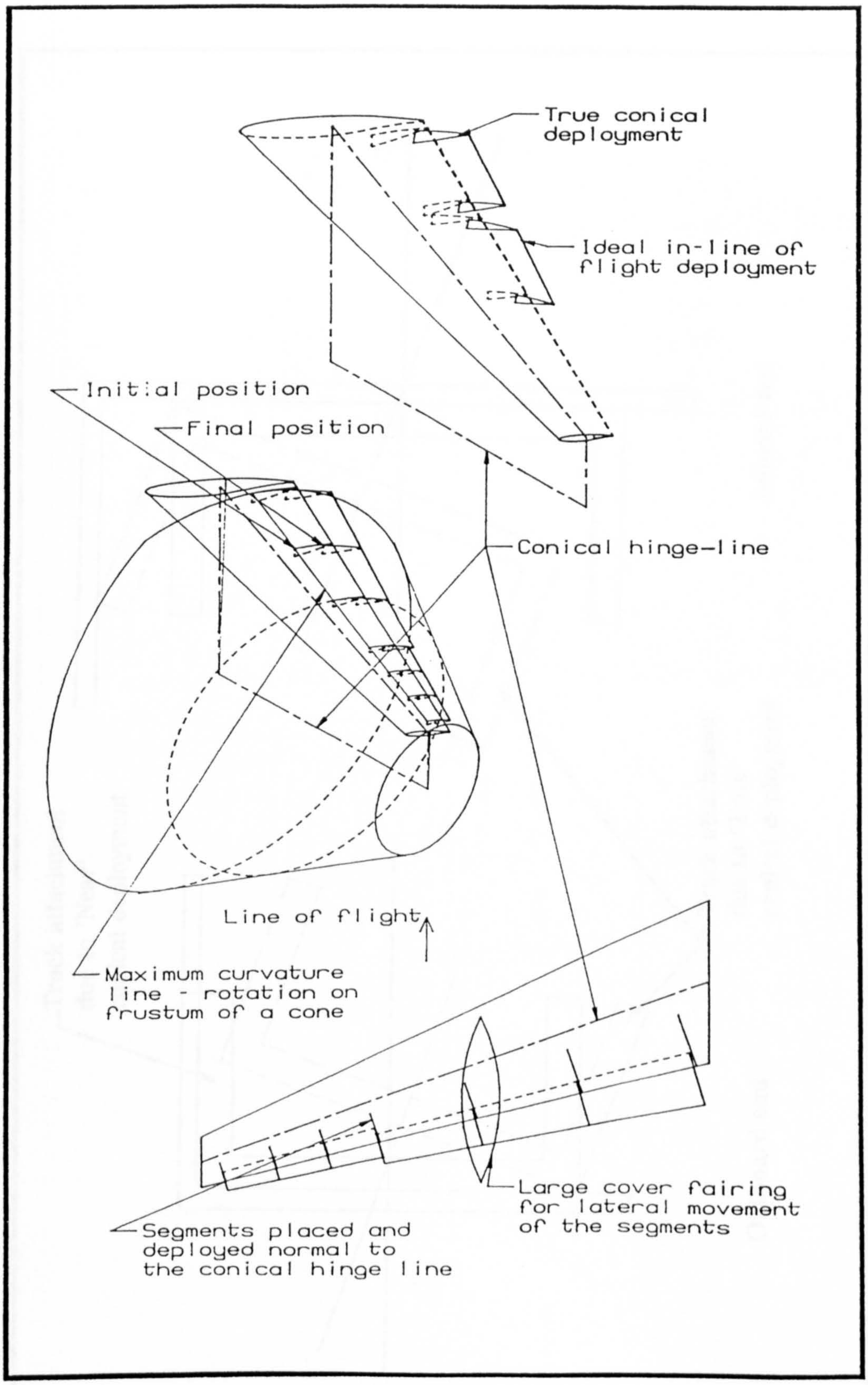

Figure 3.6: Trailing edge segments skewed to the line of flight and deployed on a conical hinge-line

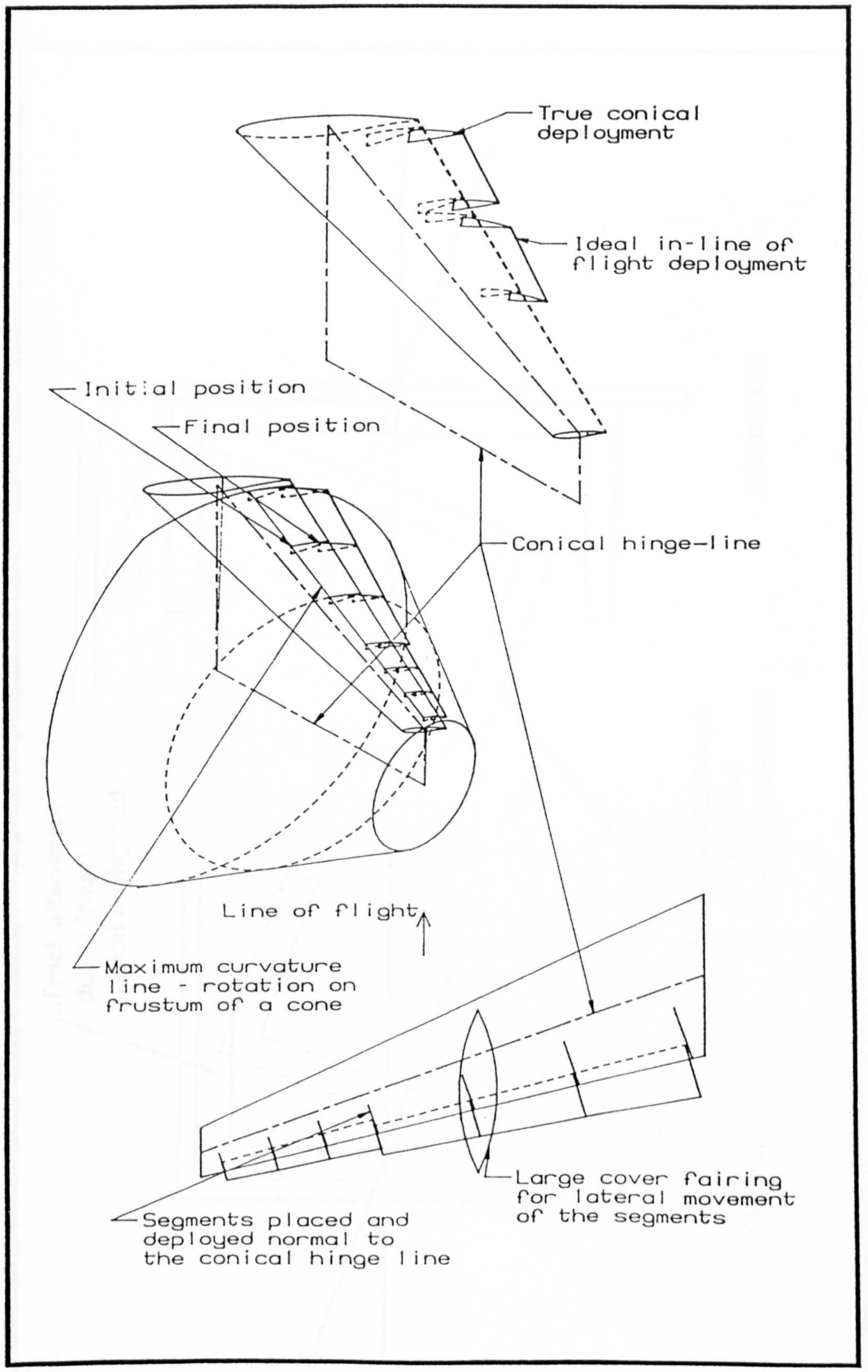

Figure 3.6: Trailing edge segments skewed to the line of flight and deployed on a conical hinge-line

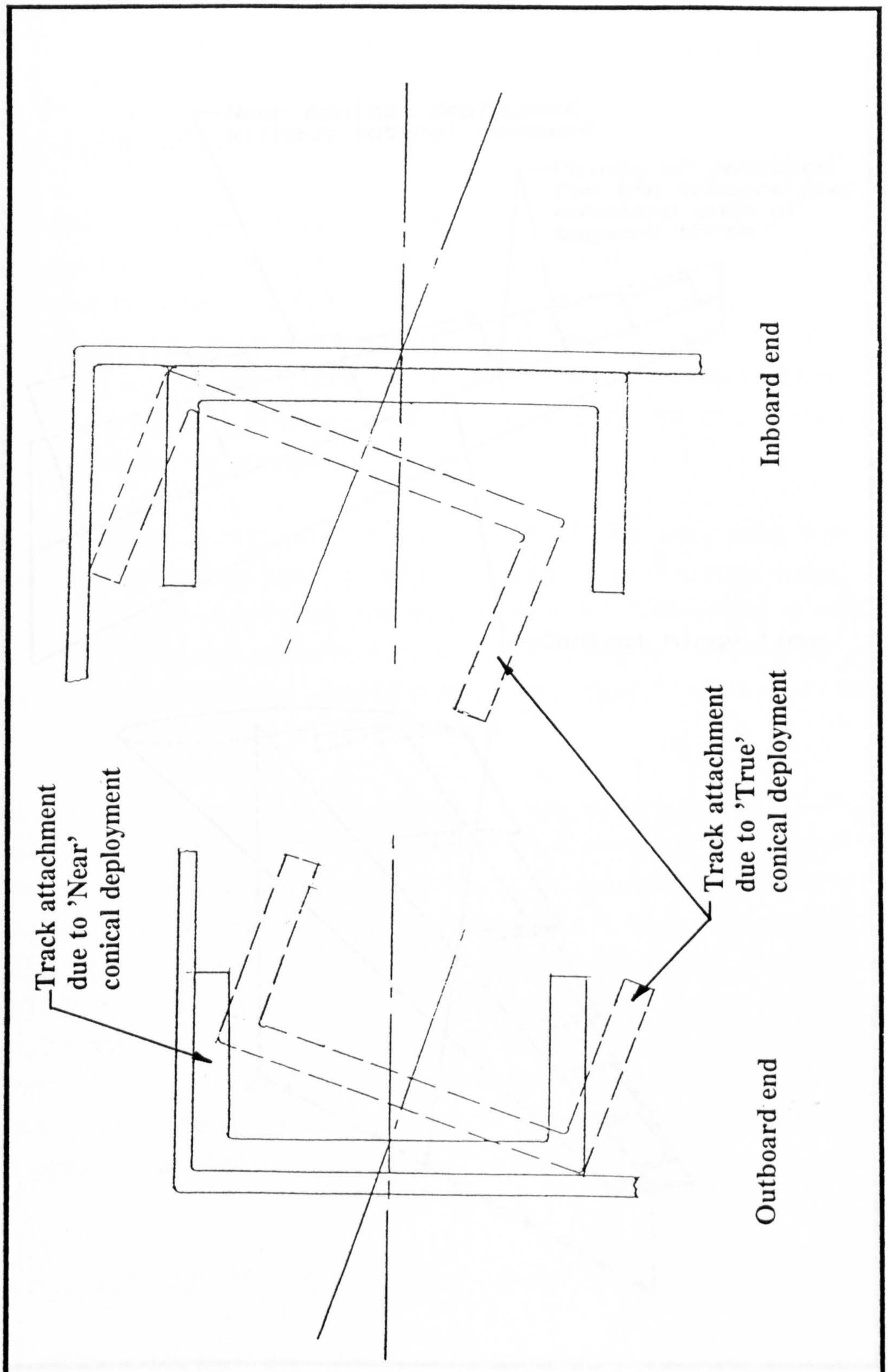

Figure 3.7: Track attachment due to 'True' and 'Near' conical deployment

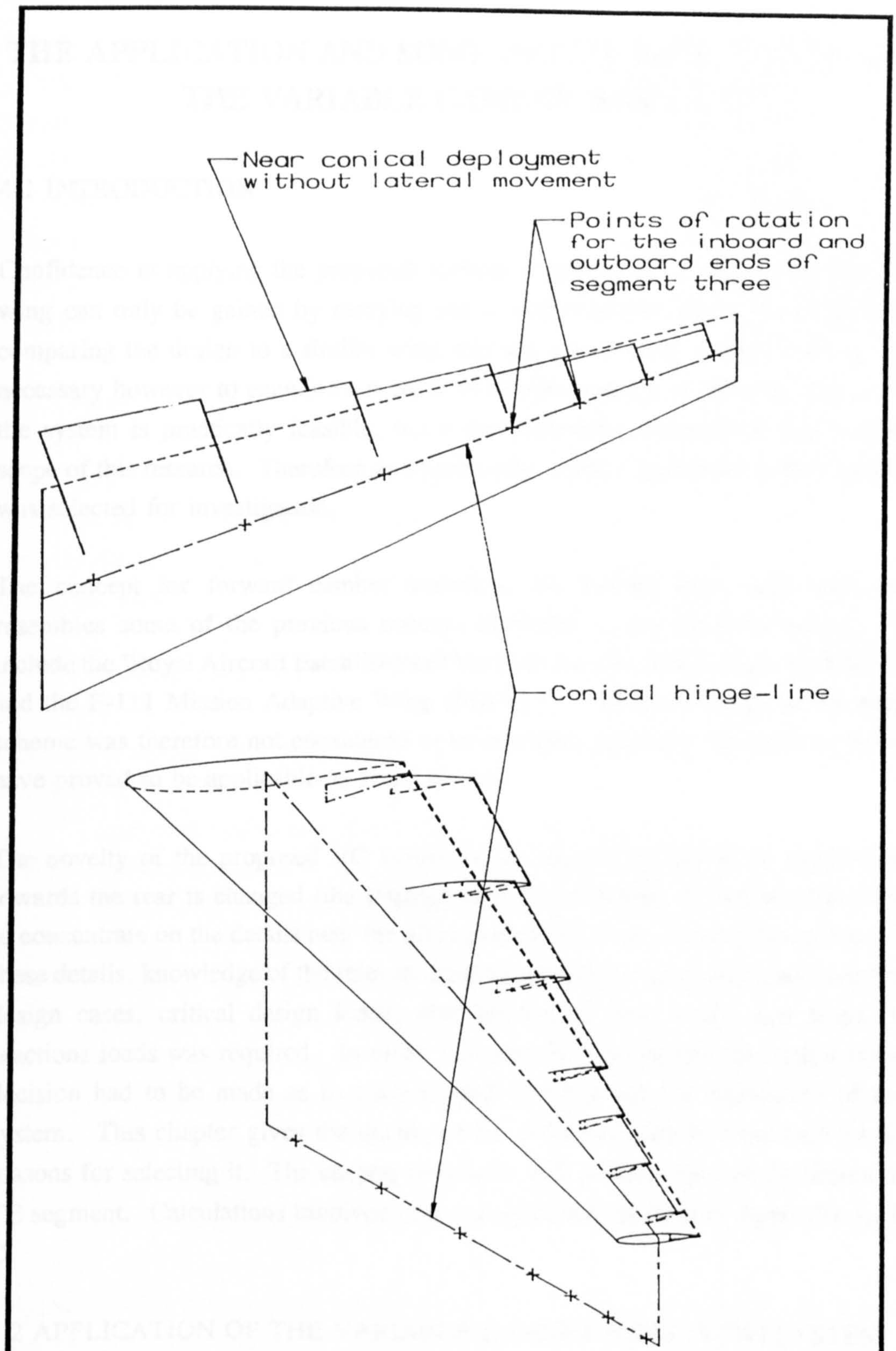

Figure 3.8: Skewed trailing edge segments deployed on a conical hinge-line without lateral movement

CHAPTER FOUR

THE APPLICATION AND SOME DETAIL DESIGN ASPECTS OF THE VARIABLE CAMBER WING (VCW)

4.1 INTRODUCTION

Confidence in applying the proposed variable camber (VC) concept to a real aircraft wing can only be gained by carrying out a comprehensive design investigation, and comparing the design to a similar wing that has conventional control devices. It was necessary however to examine a number of detailed aspects in ordēr to justify whether the system is practically feasible, but a comprehensive comparison was beyond the scope of this research. Therefore as a preliminary study a particular aircraft application was selected for investigation.

The concept for forward camber variation, the leading edge (LE) nose scheme resembles some of the previous concept disclosed in the literature search. These include the 'Royal Aircraft Establishment Variable Aerofoil Mechanism' or RAEVAM[4] and the F-111 Mission Adaptive Wing (MAW) [12]. Detailed design of the proposed scheme was therefore not considered to be essential, since the idea such as the MAW have proved to be applicable to a real aircraft.

The novelty of the proposed VC system is the manner in which the aerofoil profile towards the rear is changed (the trailing edge, TE scheme). It was therefore decided to concentrate on the details near the aft region of the wing. Before attempting to study these details, knowledge of the relevant loading conditions, operating load environment, design cases, critical design loads, distributions of these loads, and hinge (track) reactions loads was required. In order to assess the loading and the design aspects, a decision had to be made as to what aircraft to select for the application of the VC system. This chapter gives the details of the chosen aircraft and outlines briefly the reasons for selecting it. The chapter concludes with a description of the design of one TE segment. Calculations involved in the analysis are included in Appendix A, B and C.

4.2 APPLICATION OF THE VARIABLE CAMBER WING (VCW) SYSTEM

The VCW concept lends itself to both civil passenger aircraft from small executive jets to large commercial aircraft such as the 400 seat 747-400, and military aircraft used for airlifts, aerial drops, transportation of troops and cargo. The success of both categories

of aircraft depends on a wide and varied range of flight operations. For instance, the varying mission requirements for military airlifters call for the aircraft to have long range strategic and short range tactical airlift capabilities. In the case of passenger aircraft, the continuous change in market requirements with respect to payload, and range, suggests that it is necessary to look for technologies that provide commonality in wing design. This should therefore reduce the development of an increased number of variants, and hence prove to be an economical solution. The design of a common wing on the Airbus Industries A330/340 is a classic example of two aircraft with differing range requirements. One is a twin engine aircraft while the other has four engines.

4.2.1 Design Philosophies

The design of aircraft in both the civil and military transport category is based on an initial set of requirements which form a guide-line for a preliminary design work. As well as these a set of 'specific' requirements are established in order to meet a particular need.

4.2.1.1 General requirement

For civil passenger aircraft, current trends and key features for the overall wing design are to:-

- save fuel and reduce direct operating cost (DOC),
- achieve minimum weight design through structurally optimising the wing, i.e by reducing wing root bending moment (WRBM) through gust load alleviation (GLA) and manoeuvre load control (MLC),
- reduce initial development and eventual maintenance costs by designing common wings to satisfy the long term market requirements (reference [23]),
- Design safe and reliable systems that meet the airworthiness requirements,
- reduce sensitivity of aircraft to atmospheric turbulence for improved passenger comfort
- provide sufficient volume within the wing for fuel storage, and
- have provision for control devices to meet the roll and high lift requirements.

Simplicity in the design of the military aircraft wing is of prime importance to meet the stringent reliability and maintainability targets. Favourable designs with regards to control systems therefore usually incorporate fewer components which may be easily replaceable and modified at low cost. Wing aerofoils for these aircraft are generally designed with deeper sections to meet the aerodynamic needs and fuel requirements,

thus further reducing the design complexities. Other features which govern the overall design of the military aircraft are:-

- Survivability in a hostile environment and the ability to sustain battle damage,
- Alleviating 'bulking-out' problem due to shift in centre of gravity (cofg) position,
- Reduce the demands in fuel stocks in tactical operations during wartime and give operating economy in peacetime,
- Low production procurement and operating costs.

4.2.1.2 Specific requirements

To realise the full potential of the VCW system, the chosen aircraft must be designed to meet the following set of specific requirements:-

- Varying range of flight operations and mission requirement,
- Aircraft designed for short and long range operation,
- Operation through varying range of optimum C_L (good field and cruise performance),
- Longitudinal stability control to trim the aircraft due to changes in the cofg position.
- Passenger comfort by reducing sensitivity to atmospheric turbulence.

4.2.2 Aircraft Selection

It was recognised that the VC system could be applied to a very large number of aircraft in current operation. It was decided that in order to fully justify the concept, the ideal candidate must be of current interest for near-term development. The ideal process would be that two alternative wings could be designed. One installed with a conventional control system arrangement while the other installed with the new VC control system. This would eventually allow for a comprehensive performance analysis and a comparison between the two options.

One such aircraft was the FLA (Future Large Aircraft) which is still at its preliminary design stage. The FLA is an airlifter design involving several European aircraft manufacturing organisations. It is to replace current versions of the Hercules C-130. A brief history and the details of the aircraft are given in Appendix A. It was decided to select the FLA for further investigations of the VC concept for the following reasons:-

(1) Considerable fuel savings were envisaged by operating the aircraft at the optimum cruise conditions.
(2) Being a medium to large transport airlifter, it was thought the aircraft is likely to have sufficient wing depth to allow for the instalment of VC mechanisms and system, thus avoiding the need to use large external fairings and shrouds and therefore adding to the overall aerodynamic efficiency.
(3) As shown in Figure 4.1, Common to this type of aircraft is a wide variation in C_L range, ie, critical design conditions include take-off, climb, airdrops at different altitudes, various cruise conditions, landing, gust loading, etc. It was thought that optimum C_L by operating at these conditions could best be achieved by varying the wing camber.

4.2.3 Conceptual Design Study and the Base Line Wing Configuration

Being a new and a joint pursuit, the specification of the FLA and details with regards to its configuration and layout could not be obtained. Limited information was available in several journals and publications, but this was not adequate to give a clear picture of the aircraft and its intended role. In order to identify the required details, i.e wing planform arrangement, weights and loading, design conditions (to establish a base line configuration), it was necessary to carry out conceptual and preliminary design investigations. Prior to that a parametric study was carried out to collect data on relevant aircraft. Full details of these studies are given in Appendix A.

Much emphasis was placed upon the geometric details and layout of the wing, because of the thrust of the current research. The overall layout of the aircraft was based on comparison with current aircraft in the same category (details of the layout are given in Figure A.3 of Appendix A).

A general arrangement drawing of the wing for the derived FLA is shown in Figure 4.2. It has a moderate sweep back combined with thick and relatively low cambered aerofoil section (description of which is given in Chapter 2) to enable a cruise Mach number of up to 0.75. The principle geometric features of the wing are;

Gross area, S = 193.73 m^2
Aspect Ratio, A = 9.5
Span, b = 42.9 m
Sweep of 0.25c line = 22.5°
Leading edge sweep = 25.22°
Taper Ratio = 0.3

Wing mean aerodynamic chord (M A C) = 4.952 m @ 41% semi-span
Wing geometric mean chord (G M C) = 4.5158 m
Root Chord = 6.947 m
Tip Chord = 2.084 m

4.3 THE FLA WING INSTALLED WITH THE PROPOSED VC CONCEPT

The concept of varying the wing profile changes the whole philosophy behind the operational requirements of a transport aircraft. In principal, improvements in performance, increase in payload and range, reduction in overall drag by maintaining cruise lift coefficient, and stability and load control are the major goals of the proposed variable camber concept. Implementation of such a system in order to achieve these benefits could alter the overall configuration of the aircraft [28]. For example, wing span could be increased and its position arranged to reduce the vortex drag. The system can also enhance the control characteristics and handling qualities.

Unfortunately it was beyond the boundaries of this research to consider major changes and modifications necessary for an optimum solution. For the FLA it was therefore considered acceptable to retain the external geometry of the wing, and simply replace the conventional control devices with the suitable VC design schemes described in Chapter Two.

4.3.1 Segment Sizes and Track Positions

To control the load distribution across the span of the wing, the VC control surfaces must be split in to several segments. The size of these segments depends on a number of criteria which include:-
1) Optimum load distribution characteristics with minimum structural and mechanical component weight.
2) Loss of lift and therefore increased rolling moment due to loss of a segment.
3) Flap bending moment and track positions (or hinge reaction points).
4) Practical restrictions, ie fuel space, engine positions, main wing pick up rib position,

Small segments of equal span are ideal for controlling the load distribution across the wing. Such an arrangement is to give a continuous variation from root to tip in order to alter the shape of the wing during high 'g' manoeuvres and gusty conditions. The smaller the size the greater the number will be to cover the flap span. This is an advantage in that in case of damage or loss of a segment, a major catastrophe is avoided. Rolling moments are not too adverse due to the loss of a segment. Loss of

lift due to reduced flap area on one wing can be compensated by up deflection of the tip region on the other wing.

The weight of the segment is in proportion to its spanwise size. Therefore small segments invariably are lighter. Stiffness in bending becomes less critical as the unsupported span between hinges is relatively small.

With small size and large number of segments however the multiplicity of the parts (tracks, side support ribs, etc) means higher manufacturing and maintenance costs, substantial reduction in fuel volume, and possibly a heavier over all wing structure.

The design of large segments requires a considerable degree of system redundancy in order to avoid catastrophic failure. Additional redundancy undoubtedly increases the weight of the overall structure. In case of loss of a segment, large rolling moments will develop due to substantial losses in lift.

The numbers and positions of the tracks depends on the aeroelasticity of the flap TE structural box (deflection of the segment across the span), and side support ribs and their position in the wing box. An inadequate number of support tracks may lead to flutter and excess vibration resulting in loss of the whole flap. If the number of support tracks is high, then just as many side ribs will be needed which will obviously reduce the fuel storage space.

For a practical system (taking account of the above considerations) the FLA wing was split into six segments. Three relatively small outboard segments of approximately equal span and three larger segments on the inboard section. The size of the inboard three segments was primarily governed by the position chosen for the engines on the wing (see Appendix A). It was envisaged that the three outboard segments will be required to assist towards adequately distributing the spanwise load. Figure 4.3a exhibits the planform geometry of the wing showing the type of arrangement implemented.

For high lift requirements initial calculations were made using the method given in reference [29]. These suggested that the take off C_L of 1.875 was possible with a full VC setting. To meet the landing C_L requirement of 2.5, it was necessary to include (along with full VC setting) 30 % chord nested flaps (Figure 4.3b) on the inboard part of the wing (three inboard TE segments).

Roll control performance for the aircraft with the VC system was not checked, but it is envisaged that by appropriately distributing the camber across the wings, asymmetric load distribution should provide adequate roll. To achieve this, the tip region (outboard three segments) caters for negative deflection, i.e rotation of up to -3.5°, while the root region (inboard end) gives maximum positive camber setting, i.e rotation between 0.0° and 10.0°.

The shear force (SF) and bending moment (BM) distributions, deflection curves, and hinge reaction loads are all dependent on the position and the number of the hinges. It was decided to use the planform geometry of Figure 4.3 and support each TE device segments on two tracks placed at the inboard and outboard ends. The fairly substantial BM across the large segments and high reaction loads on the tracks were assumed to be acceptable, since the only way to reduce them was by placing extra support tracks at intermediate span position of the segments. With extra structure within the wing box an immediate penalty is paid by reducing the available fuel volume. Furthermore, by having only the two tracks per segment the number of cutouts in the wing rear spar web is kept to a bare minimum. Additional tracks would otherwise reduce the structural efficiency of the spar. This problem becomes much more severe if the number of small segments is increased. The proposed arrangement has an added advantage in that the tracks on the adjacent segments can be supported on a single rib (inside the structural box), thus further reducing the complexity and the weight of the system. By placing the tracks at the ends of the segments the task of inspection and maintenance becomes easier.

4.3.2 Detailed Design Considerations

The SF, BM and hinge reaction loads were calculated from the spanwise load distribution curves presented in Appendix B, using 'STRUCT' Structural Analysis program [30] available on the College of Aeronautics Personal Computers. These showed that the maximum load was concentrated near the inboard end of the wing and in particular over the fifth segment (see Figure 4.3a). This had been expected since it is the largest of the six segments. It was therefore decided to use this segment for further studies. Principle dimensions for the segment are given in Figure 4.4.

The main components considered in detail were the track roller system, conforming tracks and the upper surface skin. Stress calculations were made to size the track roller system and the upper surface skin, details of which are given in Appendix C. Figures 4.5 to 4.7 show the main features of theses components. Figure 4.6 shows the inboard

(I/B) track arrangement which is fixed to the TE device and designed as a 'C' channel in titanium to transfer high bending loads through to the main wing structure. These loads are accepted by the side support ribs which are designed as 'I' beams (see Figure 4.5) in titanium and stressed to check flange instability and shearing of the web. To retain conventionality within the system the sliding motion is provided by a series of cam rollers, as depicted in Figure 4.5. These are attached through carriages to side support structure of the wing ('I' beam side rib).

The upper surface is made to flex by placing it within a set of conforming tracks through a series of rollers and link arrangements. Details of the design for the I/B station of the segment are given in Figures 4.7a. The conforming tracks are part of the extending track and the TE device. The design for the roller/link arrangement at the intermediate span positions is shown in Figure 4.7b.

A stiffness criterion was used to ensure that the upper surface skin deflections due to aerodynamic loads remained within 2 % of the local maximum depth of the aerofoil[31]. This criterion must however be substantially checked for acceptance. Estimation of the deflections were made using SDRC Ideas™ finite element analysis (FEA)[32] system by representing the loads as face pressures on thin shell elements. Details of the finite element (FE) model are given in Appendix C. This system proved to be a useful tool for iterating between the material type, skin thickness and the position/number of the intermediate conforming tracks. Figure 4.8 shows the details of the notation used for ply orientation and the position of the conforming tracks. After many iterations it was found that a 4 mm carbon fibre reinforced plastic (CFRP) skin with the ply arrangement of $\{([0/90]_2/0/\pm 45)_2/0/90\}_s$ that is restrained at seven intermediate spanwise stations gave adequate deflections across the surface. The elastic modulus in 'x' (0° plies) and 'y' (90° plies) directions (E_x and E_y) is equal to 0.73×10^5 N/mm^2 and 0.537×10^5 N/mm^2 respectively. The modulus of rigidity for the laminate is 0.15×10^5 N/mm^2. Carbon fibre was chosen because it has the advantage of fibre orientation in that the upper surface skin could be tailored to meet the stiffness requirement. Carbon also has better strength characteristics than any other fibre reinforced plastic (FRP) materials. For an optimum solution the skin can be tailored such that it tapers along the chord (decreasing from rear spar position to the upper surface TE tip).

The under side between the TE device and the main wing box can be kept continuous by a hinged under surface flap. This could be held in position by a track at either end of the segment and deflects down as the TE device is actuated. Structural design details of this flap were not considered, but it is assumed that the flap can be made as a

sandwich box with composite face skins and honeycomb core.

The track radius varies across the span, decreasing from root to tip. Thus if the TE segment is made rigid and supported on say two tracks (inboard and outboard of a segment), on actuation the segment will either be reluctant to move or it will tend to ride more on the larger (inboard) track. The later will give an undesirable lateral movement. In order to eliminate this effect the TE element must be made to flex both across the span and chord. This way the TE segment will effectively have to deploy independently on the two tracks. Design details of the TE device (flap piece) have not been considered, but it is assumed that it can take the form of a conventional flap design, i.e a composite FRP box. This may require a linkage system (scissor type arrangement), the independent actuation of which would assist in flexing and twisting the composite box. Examples of such an arrangement can be seen in reference [11].

With a flexible TE box the system could quite simply be driven by a pair of linear hydraulic actuators placed at the ends of each segment. One end mounted to the wing structure while the other end attached to the extending track. Independent input to these actuators would ensure adequate deployment with twisting of the segment across the span for parallel motion.

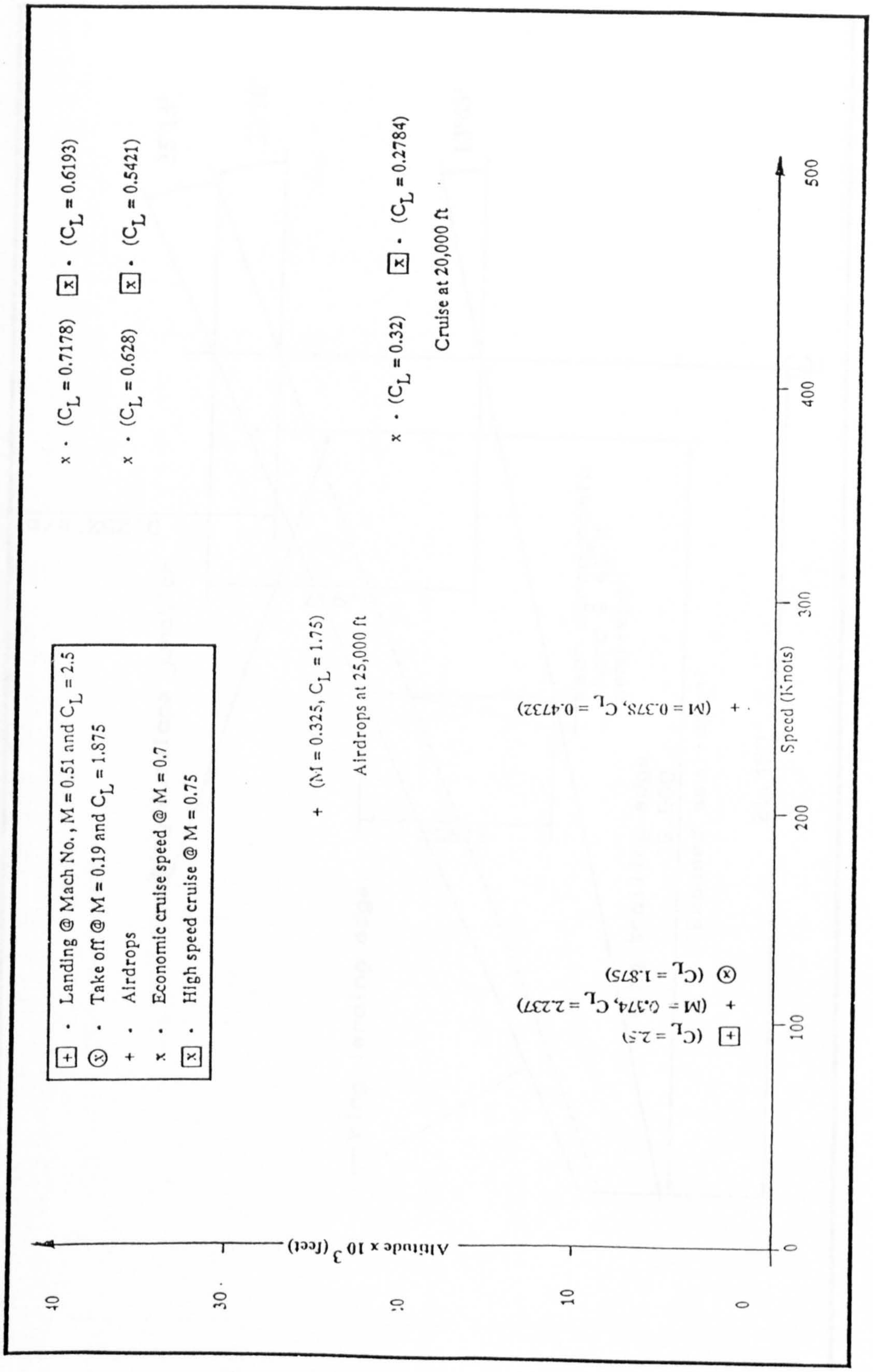

Figure 4.1: Varying C_L requirement for the FLA

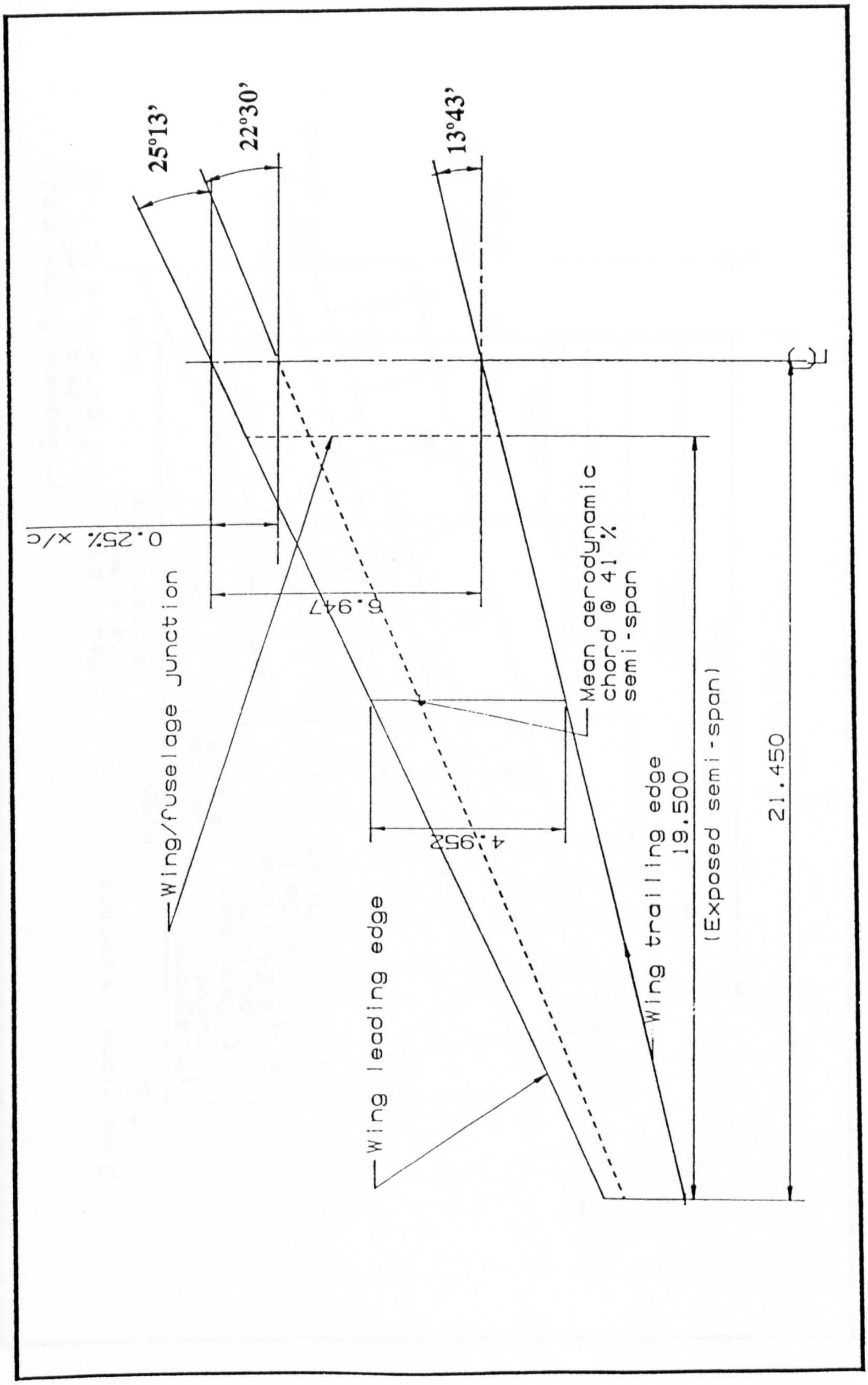

Figure 4.2: Planform geometry of the FLA wing

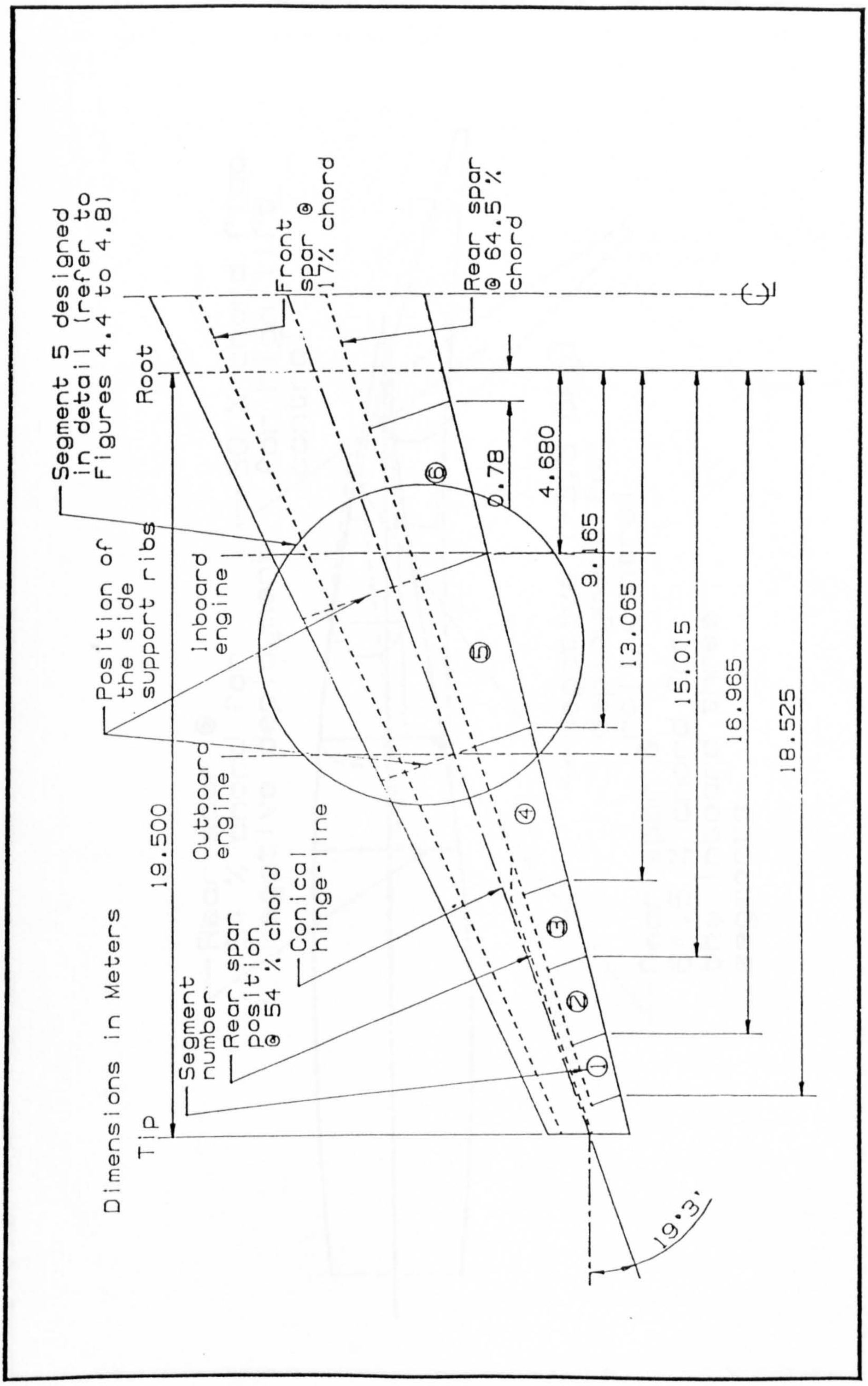

Figure 4.3a: Wing planform split into six trailing edge segments

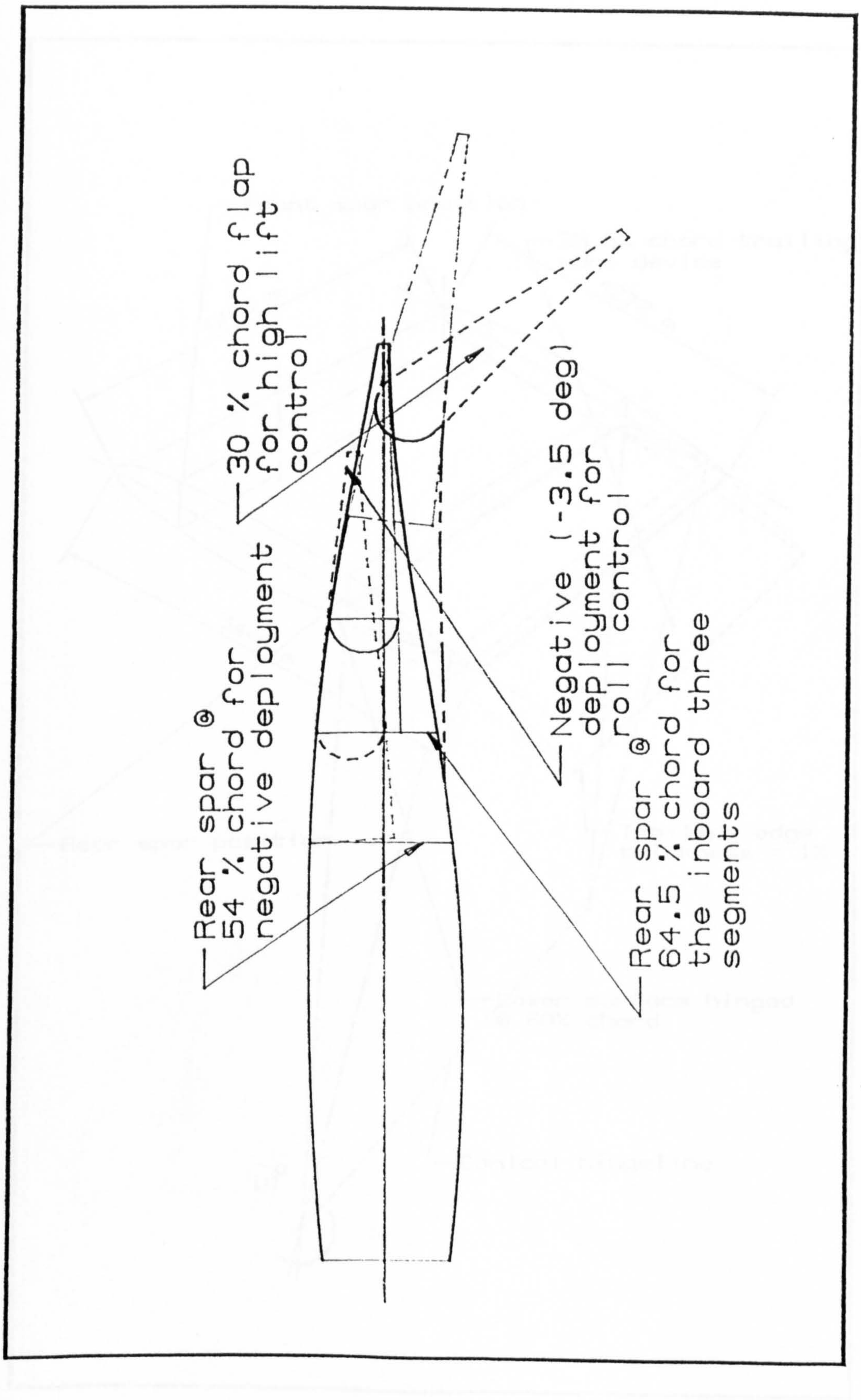

Figure 4.3b: Chordwise profile of the aft region of the aerofoil

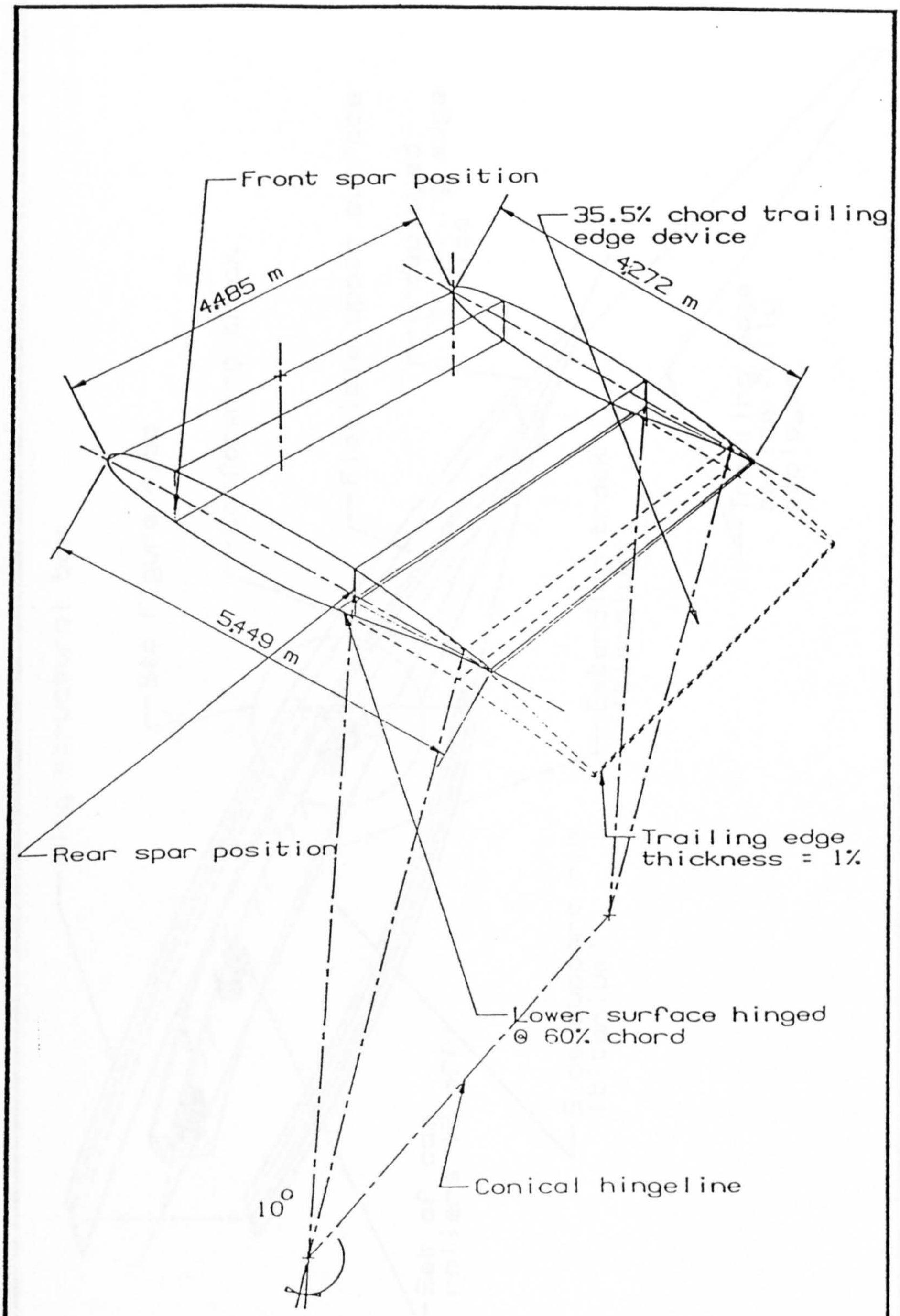

Figure 4.4: External dimensions of segment five

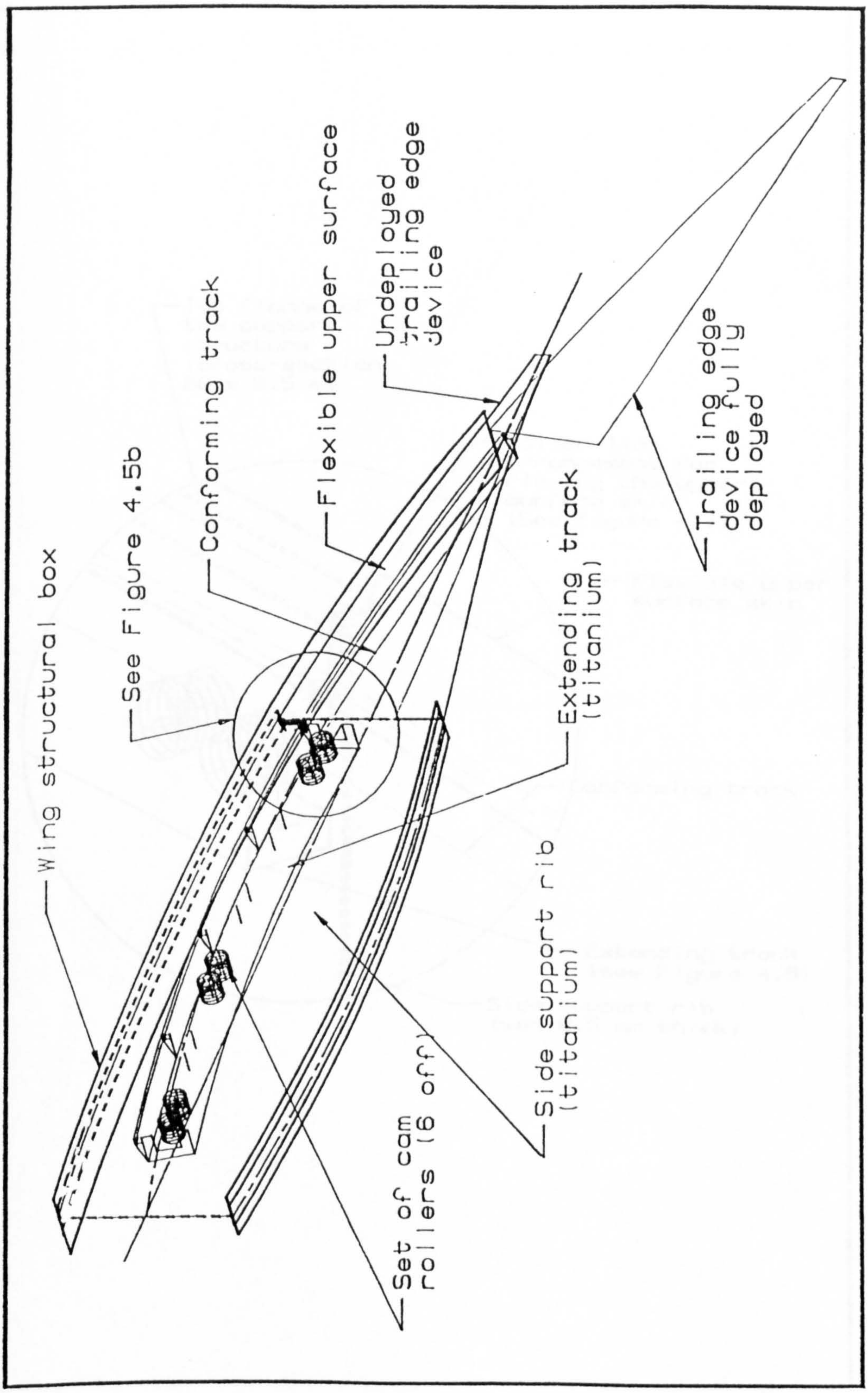

Figure 4.5a: Overall design of the inboard rib, extending track, upper surface skin conforming track and roller arrangement

Figure 4.5b: Details of the inboard rib, extending track and conforming track/roller arrangement

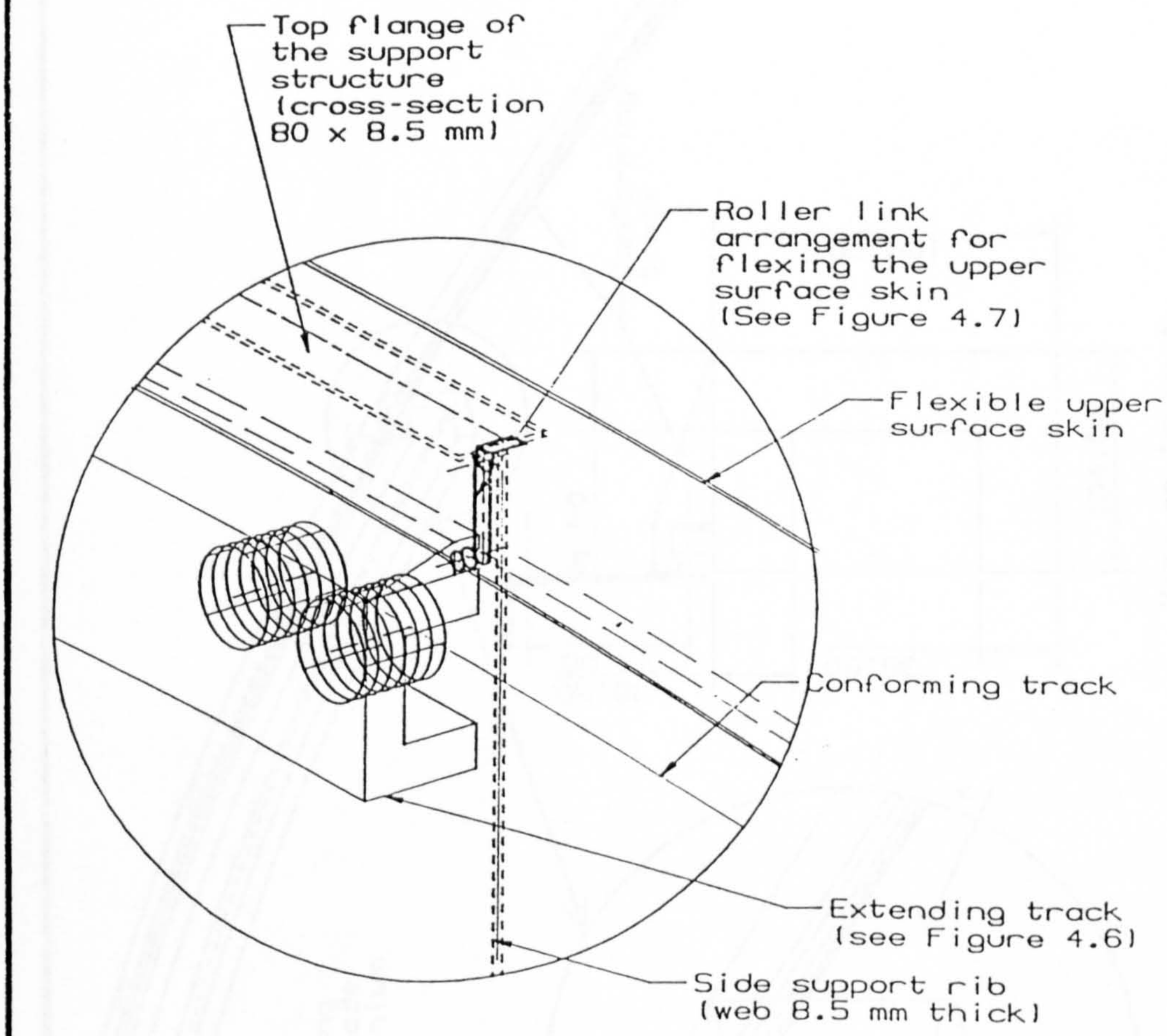

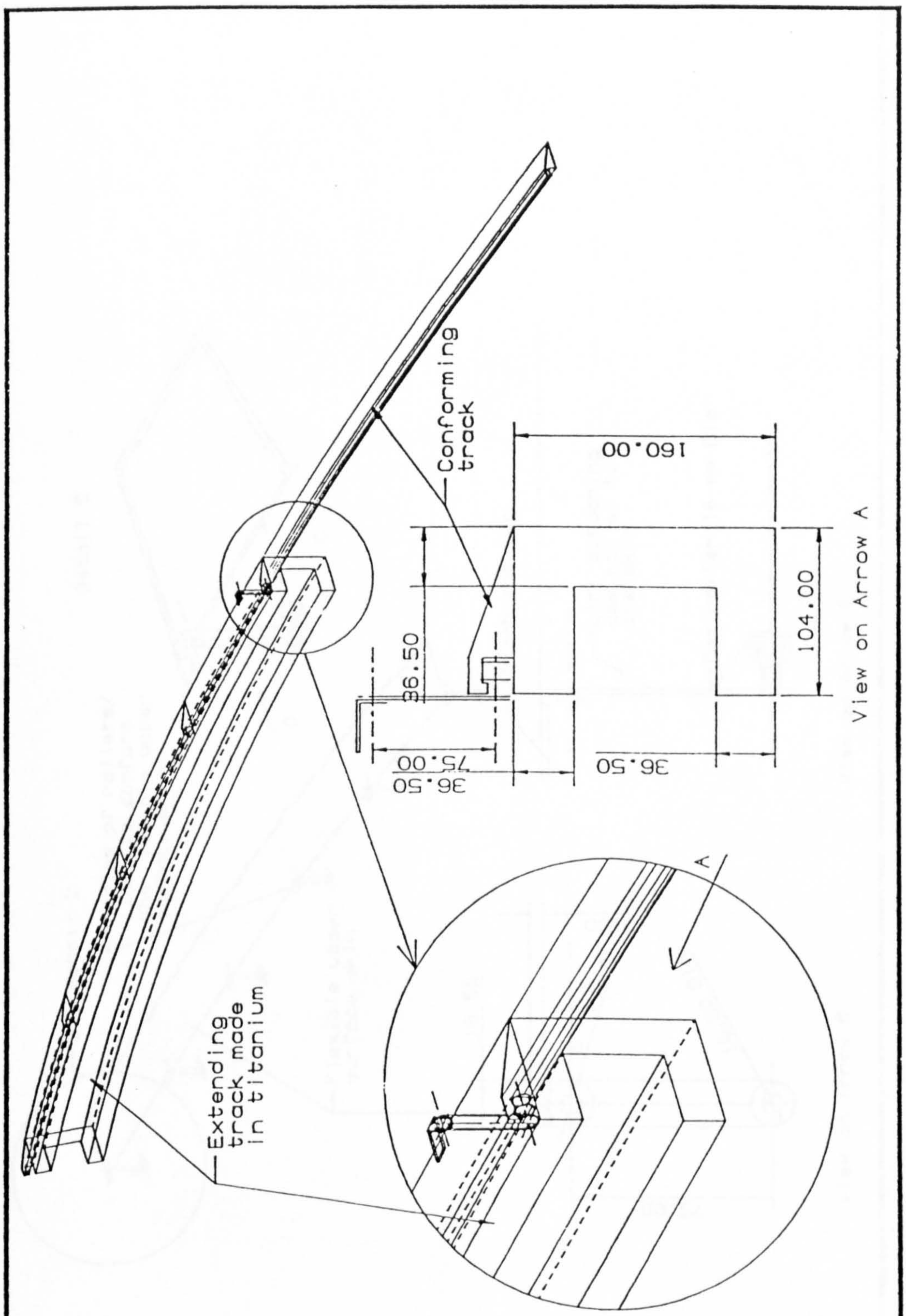

Figure 4.6: Details of the extending track and the upper surface conforming track

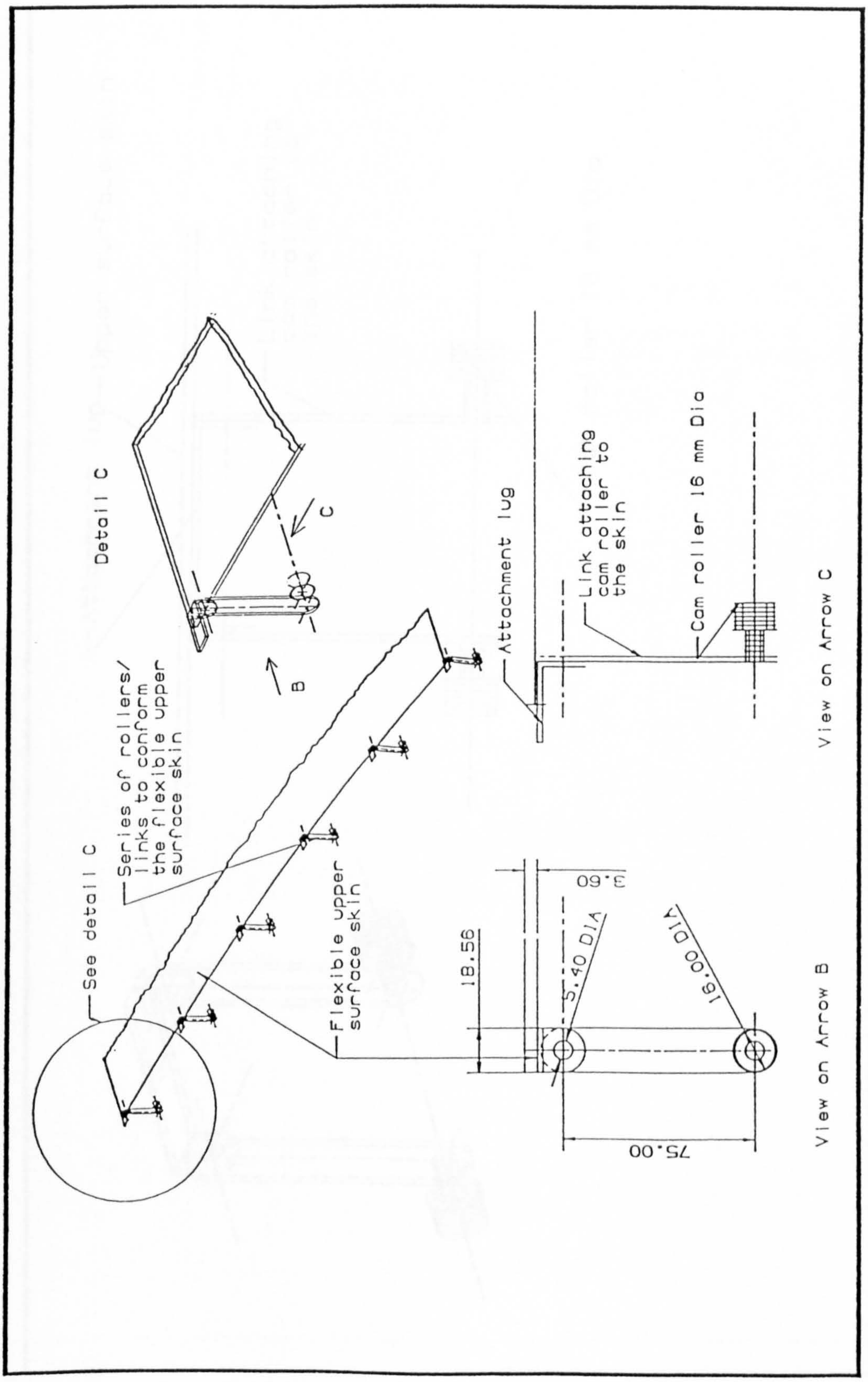

Figure 4.7a: Details of the outboard roller link arrangement to conform the upper surface skin

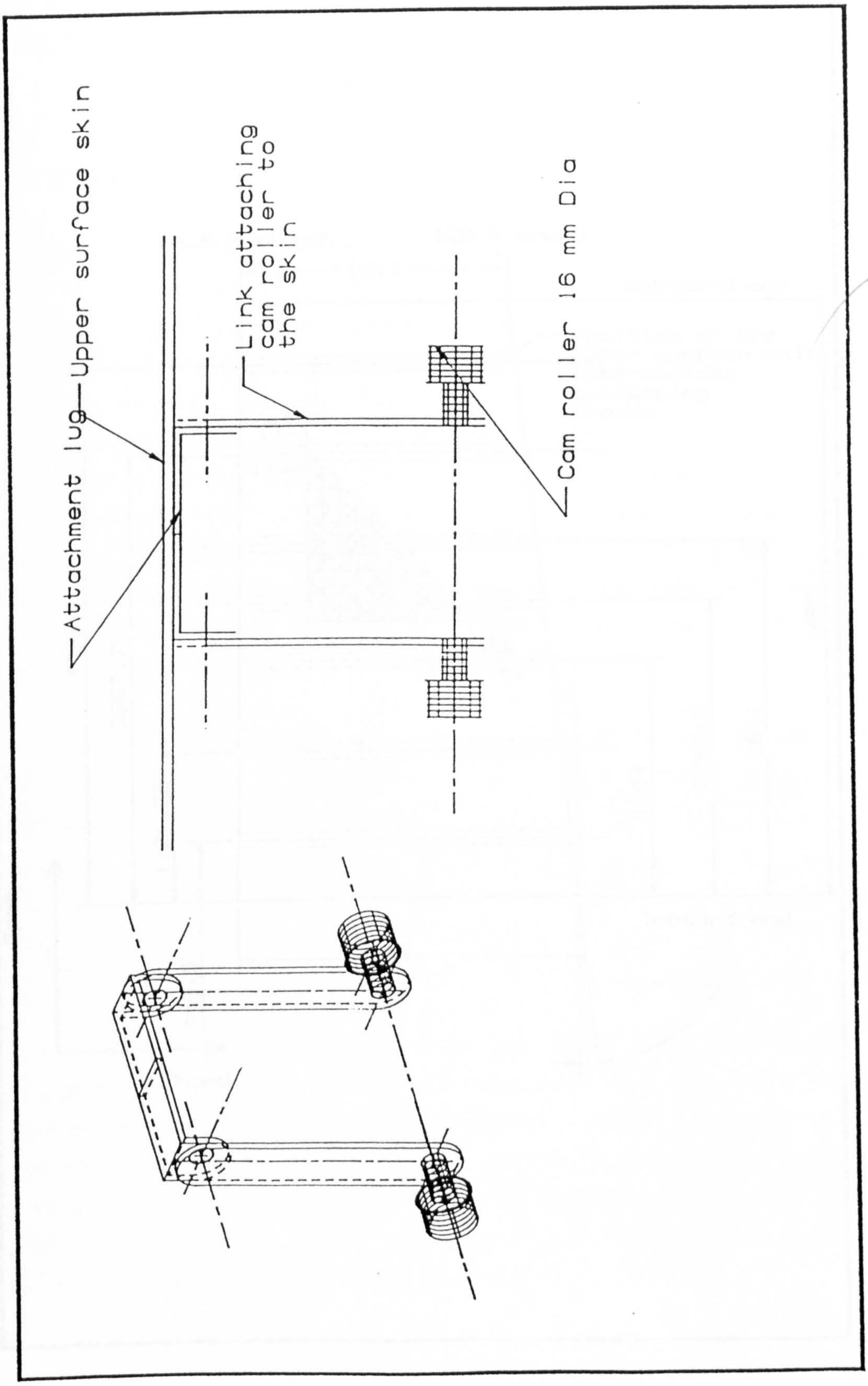

Figure 4.7b: Possible solution for roller link arrangement to conform the upper surface skin at the intermediate span position

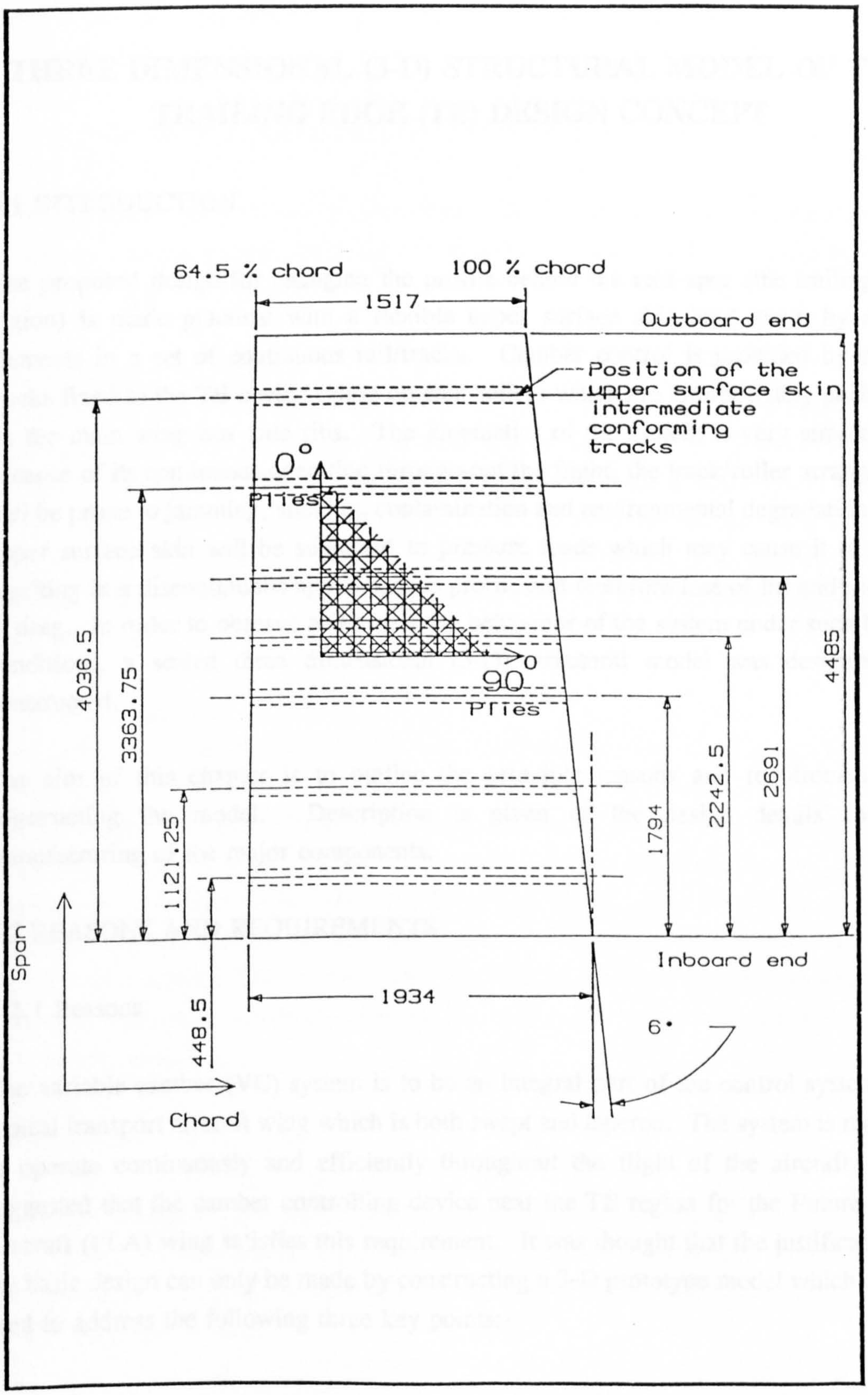

Figure 4.8: Details of the upper surface flexible carbon skin

CHAPTER FIVE

THREE DIMENSIONAL (3-D) STRUCTURAL MODEL OF THE TRAILING EDGE (TE) DESIGN CONCEPT

5.1 INTRODUCTION

The proposed design for changing the profile behind the rear spar (the trailing edge region) is made practical with a flexible upper surface skin held down by rolling elements in a set of continuous rail/tracks. Camber control is provided by curved tracks fixed to the TE device riding on cam rollers which are appropriately positioned on the main wing box side ribs. The kinematics of the system is very simple, but, because of its continuous operation through-out the flight, the track/roller arrangement will be prone to jamming, sticking, contamination and environmental degradation. The upper surface skin will be subjected to pressure loads which may cause it to warp, resulting in a discontinuous upper surface profile and therefore loss of lift and increase in drag. In order to observe and assess the behaviour of the system under such loaded conditions, a scaled three dimensional (3-D) structural model was designed and constructed.

The aim of this chapter is to outline the principle reasons and requirements for constructing the model. Description is given of the design details and the manufacturing of the major components.

5.2 REASONS AND REQUIREMENTS

5.2.1 Reasons

The variable camber (VC) system is to be an integral part of the control system of a typical transport aircraft wing which is both swept and tapered. The system is required to operate continuously and efficiently throughout the flight of the aircraft. It is suggested that the camber controlling device near the TE region for the Future Large Aircraft (FLA) wing satisfies this requirement. It was thought that the justification of the basic design can only be made by constructing a 3-D prototype model which can be used to address the following three key points:-

1) Jamming mechanisms

Jamming of the mechanism is one of the main reasons for flap failure. Lack of free movement can cause it to stick in one position, implying that the flap can become ineffective, which would obviously be catastrophic. The continuous use of the VC devices adds further complications in terms of wear and service life.

Although the track roller idea is in its infancy, the design is very simple, neat and tidy. However, history suggests that even the simplest mechanisms for flaps can fail under adverse loading conditions.

2) Upper surface stiffness

The upper surface skin is the critical feature of the concept. The most important aspect being requirements of spanwise stiffness and chordwise flexibility. The skin must have sufficient stiffness in order to hold its shape when subjected to aerodynamic loading. At the same instance, flexibility across the chord is desired for it to conform with ease. Hence, for the FLA wing the use of carbon composite material is suggested where the ply orientation in a laminate is arranged to give the required stiffness and flexibility characteristics.

3) Deflection geometry

It is quite clear from the findings of the 3-D geometric work in Chapters Three and Four that the desired conical deployment will not be possible with a rigid trailing edge (TE) element. For the FLA wing it is recommended that the TE box warps as it is deployed in order to achieve a near conical (parallel) motion. Furthermore, the under surface flap is required to be hinged at fixed 60% chord. This provides a reasonable continuity on the underside between the deployed TE device and the under surface flap. Given these geometric constraints it was questionable whether the proposed system will operate successfully. It was therefore necessary to build a working model to assess the system behaviour.

5.2.2 Requirement and Aims

To design and construct a model the size of the FLA wing was beyond the scope of this research. Limited manufacturing and testing capabilities within the department and restricted research funds available for the project were factors which governed the scale of the model to be made.

After much deliberation it was decided to confine the design to one TE device segment to half scale. The external geometry of this, showing the key dimensions, is displayed in Figure 5.1. This is representative of segment 3 on the FLA wing (see Figure 4.3).

It was required that the model should adapt a conical and parallel deployment motion such that the inboard (I/B) and outboard (O/B) tracks are arranged at two different radii of curvatures. Rotations of up to maximum VC setting condition was to be considered (ie take off). Therefore provision for incorporating an auxiliary flap (for landing purpose) was not necessary. The VC range being + 7° down and -3.5° up.

The basic aim was to design the tracking system and the upper surface in detail such that they could be tested with representative loads. It was also required to adhere to the given 3-D geometry for the TE device and the under surface flap so that the system could be used for dynamically demonstrating the 3-D variable camber wing (VCW) technology.

5.3 DESIGN APPROACH

5.3.1 General

In keeping with the design of the variable camber system for the FLA, the model had to comprise the following elements:-

1) A track/roller system which had adequate stiffness such that it would not deform and stick when deployed under a load,
2) A representative TE device, which must not restrict the overall deployment of the system,
3) An upper surface skin, which must be flexible to conform, yet stiff enough to hold its shape,
4) A lower surface, which had to be hinged at 60% chord and attached to the TE device,
5) A structural box with side ribs for track/roller support,
6) An actuation and control system

5.3.2 Design Criteria

In view of the above requirements, stiffness checks and stressing calculations were limited to the upper surface, the tracking system and the support structure only, since these were to be the loaded elements. Furthermore, since the model was to be a

technology demonstrator, use of aerospace standard materials was not necessary.

5.3.2.1 Upper surface skin

The design of the upper surface skin was based on the following three criteria:-
1) Maximum deflection at any point was restricted to 2% of the maximum depth of the aerofoil. This is a general 'rule of thumb' criterion which has been used for a number of years for project work at the College of Aeronautics, and is considered to be adequate for preliminary design work[31].

Maximum aerofoil thickness to chord ratio is 14%. Therefore maximum allowable deflections at the I/B and O/B ends of the model were limited to 4.46 mm and 3.91 mm respectively.

2) The skin had to be manufactured in one piece in order to retain it's flexibility in chord, because several pieces bonded or fastened together would prevent this.

3) Constant contact had to be provided between the lower part of the upper surface skin and the upper side of the TE device across the segment span. This was to help retain the continuity on the top side of the aerofoil.

5.3.2.2 Tracking system

The tracking system and support structure of the chosen TE configuration will be subjected to a high level of bending loads due to the large extensions in chord. Inadequate design will be prone to excess deformation and eventual jamming. Therefore the track sections had to be designed such that they do not become unstable due to bending loads. Details of these calculations are given in Appendix D.

5.3.3 Loading

5.3.3.1 Upper surface

The upper surface skin will deflect and warp under aerodynamic pressure loads. Where,

$$\text{Pressure, } P = \tfrac{1}{2}\rho V^2 C_P$$

C_P is the 2-D pressure coefficient, obtained from reference [27], and V is the EAS for take off condition case, Thus V = 103.3m/s (see Appendix B) and ρ is the air density = 1.225 Kg/m^3.

The upper surface skin extends from the rear spar position (54 % chord) to 90 % chord. The variation in C_p and pressure loading across its chord is given in Table 5.1.

It must be noted that the upper surface skin should ideally be tested under high speed or high gust level since these give the highest loads (refer sub section B.4.1.3 of Appendix B). However owing to the magnitude of the load due to these cases, the testing of the skin through a medium such as sand (refer sub section 6.3.1.1 of Chapter Six) became highly impractical. Therefore a lower speed case was used instead.

5.3.3.2 Tracking system

The purpose of the tracking system was to transfer the aerodynamic loads aft of the rear spar position in to the main structural box of the wing. Theoretically these loads arise from the TE device, the upper surface skin, and the lower surface panel.

It was assumed that a wing half the size of the FLA wing will be used on an aircraft which will fly at same take off conditions. Therefore total lift on half the wing will be approximately = 0.93 x 10^6/ 4 = 23.25 KN, with the design operating velocity being 103.3 m/s (see Appendix B).

From the spanwise load distribution (Appendix B), the load between 70 % and 79 % span (span of segment No. 3 on the FLA wing) is approximately 8.2% of the total for a full span take off VC setting.

For the aerofoil section with the deployment of 0° at the LE and 7° near the TE, the load across the chord aft of 54% (rear spar) is 38.8%. This was estimated from the 2-D theoretical pressure distribution calculations made in reference [27]. The load was proportioned between the flexible upper surface skin, the lower surface, the TE device under side and the TE upper side. The portion of load on these components is as follows:-

Component	Length (% Chord)		Load (%)	Position (% Chord)
	From	To		
1	54	90	13.74	-
2	60	90	10.75	-
3	90	119	6.61	105.9
4	90	119	7.70	98.7

1 - Upper surface
2 - Lower surface
3 - Under side of the TE device
4 - Upper side of the TE device

For initial design work the component loads were simply estimated by factoring the total half wing load by the chordwise pressure and spanwise distributions. Thus, the magnitude of the loads is as follows:

Component	Load (N)	Load (Kg)
Upper surface	2620	267
Lower surface	2050	209
TE under side	1261	129
TE upper side	1468	150

5.3.4 Structural and Finite Element Analysis (FEA)

5.3.4.1 Structural analysis of the tracking system

The design of the tracks depended on their ability to withstand shear and bending loads. The shear loads governed the stiffness, while the bending loads dictated the stability. Estimation of these loads together with stiffness calculations were first made manually by balancing the moments, and then checked with the College of Aeronautics structural analysis package, 'STRUCT'[30]. Stress calculations were made using design data sheets. Details of these calculations are given in Appendix D.

5.3.4.2 Finite element analysis

Accurate assessment of the stiffness of the upper surface skin could only be possible with a FEA system. Simple finite element (FE) models were developed on SDRC IDEAS Finite Element Analysis™ system[32], the selection of which was thought to be suitable because it has the capability of applying face pressures as loads on thin shell elements, avoiding the necessity to calculate the exact elemental or nodal loads.

Illustration of the loaded and restrained FE model is given in Figure 5.2. A flat plate was assumed using thin shell quadrilateral elements. The pessimistic approach of modelling the upper surface skin as a flat plate was considered to be acceptable since the aerofoil section required little change in profile during camber variation. The width of each element was governed by the size of the elemental pressure loading from the

chordwise pressure distribution obtained for the aerofoil (see Table 5.1). The thickness of the upper surface depended on the levels of deflections due to the applied pressures, as given in Table 5.1.

The model was restrained in six direction (translation and rotation in X, Y and Z axis) at face 'A' (rear spar position, 54% chord), and in the vertical direction (Z axis) at the inboard and outboard ends and at three intermediate spanwise stations (representing the position of the conforming tracks). The vertical restraints along the chord at the five spanwise stations of the segment were necessary to predict the loads experienced by the tracking system. These loads were then combined with the applied aerodynamic loads due to the TE device and used to design the tracks.

A number of material types were considered (see Section 5.4.1.1). The set of properties for the material being used were declared interactively. For fibre reinforced plastic (FRP) composite laminates the stiffness matrix (A and D) were obtained from the College of Aeronautics Laminate Analysis program (COALA)[33].

5.4 DESIGN DEVELOPMENT

5.4.1 Upper Surface Skin Design

The design of the upper surface skin centred around:-
1) the requirement to have variable stiffness in span and chord, and
2) the possibilities of positioning it in rails (or tracks) by means of a set of rolling elements.

5.4.1.1 Material selection

The SDRC IDEAS™ FE system[31] became a useful tool for trying to find a solution in terms of design and material selection. It was assumed that the top surface skin will be continuously held at the five spanwise restraint (or track) positions previously referred.

The upper surface skin material was selected from either aluminium, aluminium lithium, or carbon fibre reinforced plastic (CFRP) composites. These being the three basic materials used for the skin construction of the modern transport aircraft wings. As well as satisfying the stiffness criterion mentioned previously, the material choice depended on the stiffness to weight ratio. Table 5.2 contains the basic characteristics

and properties of the selected materials. Both aluminium and aluminium lithium have similar density but the latter has higher elastic modulus and therefore higher stiffness. CFRP composite appears to be superior in terms of reduced weight than its isotropic counterparts: however, its stiffness is very much dependent on fibre orientation. The figures for elastic modulus appearing in Table 5.2 are those for a laminate with 0° plies only (see also Figure 5.2). It is quite clear that the stiffness along the x - axis is much higher than the stiffness along the y - axis. With a balanced lay-up the laminate could be tailored such that the stiffness in the two directions is approximately equal. A typical elastic modulus with such an arrangement is 0.6×10^5 N/mm^2. With the density of 1.6×10^{-6} kg/mm^3 the stiffness to weight ratio is 3.75×10^{10}. This is shown to be better than the value for either the aluminium or aluminium lithium (see Table 5.2).

Before attempting to find an appropriate lay-up solution with a composite material, it was decide to use aluminium lithium as a base line material to estimate the required thickness. As a result of many iterations of restraint positions and skin thicknesses, it was found that a 2 mm Lital A[34] with five restraint positions (fixed equidistant apart) gave deflections that were within the required level. In terms of flexibility it was not certain that this gauge thickness would conform adequately. A solution was to reduce the thickness and introduce spanwise stiffeners as shown in Figure 5.3. This however did not provide a continuous attachment between the upper surface skin and the TE device.

Fatigue behaviour of the flexible skin have not been assessed, but it is felt that repeated loads due to continuous flexing and deforming of the skin material could be the critical case for design.

Comparison of the material and manufacturing cost of the above materials were not made. It is known[35] that isotropic materials in general cost less than FRP, and are much easier to manufacture. However it was felt that the design of the upper surface skin should be governed by the stiffness and flexibility criteria rather than the cost or ease of manufacturing.

As a result of the above considerations it was decided to seek a solution using carbon composites. The laminate had to have the spanwise stiffness of the same order as the base line material to give a controlled deflection.

5.4.1.2 Conformation

The purpose of the conforming tracks/roller system is to:-

1) Keep the upper surface skin continuously attached to the TE device, which would otherwise tend to lift due to aerodynamic loading and
2) Alter the upper surface shape during TE camber variation.

Initial intention was to design the system for conforming the upper surface skin such that it could be loaded when assembled as part of the structural model. Ideally this system should be similar to the design suggested in Chapter Four (Figure 4.7a and b). Complications with regards to the conically warped TE box suggested that the manufacture of such suitable roller fittings would be expensive. The end conclusion was to eliminate the idea of applying representative loads on the upper surface skin (see Chapter Six Section 6.3.3). It was necessary however to make sure that the skin was adequately held such that it remained attached to the TE device and that smooth profile was achieved during VC operation.

5.4.2 Under Surface

The design of the lower surface simply depended on maintaining the given lower surface geometry of the aerofoil. Sufficient depth between the lower side of the TE device and the lower side of the aerofoil suggested inclusion of stiffening members or foam filling to increase the stiffness.

5.4.3 Trailing Edge (TE) Device

The whole concept of varying the camber conically and parallel to the wing side ribs hinged on the design of the TE device. Parallel actuating tracking system with a single piece TE device giving a percentage extension in chord could be possible by warping the TE box as it is deployed. Such an idea could be achieved by designing the TE box in composite FRP material and appropriately tailoring the fibres to provide the required flexibility. Construction of a FRP warping TE box was too costly and time consuming to produce a feasible design, so solid laminated wood device was used.

5.4.4 Actuating Track System

The extending track to deploy the TE device had 'of course' to be curved and located in a manner so as to allow the TE device to deploy on a continuous curvature. On a real design these would either be made in titanium or high grade steel such as S96[34]. For the purpose of the model these materials were considered far too expensive to purchase and machine. It was therefore accepted that low grade commercial steel such as E8M[36] would adequately serve the purpose.

An initial suggestion was to have a low friction bearing material such as PTFE (PolyTetro Floro Ethylene) or Nylon coating between a two track system. One track would act as a support track while the other would be the deployment track which extends the TE device. The cross-section of the system is illustrated in Figure 5.4. The advantages of such an arrangement are:-

- very simple design and therefore reduced complexity,
- reduced weight,
- easy to manufacture,
- no rollers therefore less probability of jamming, and
- continuous sliding contact.

This design had to be rejected because it was unconventional and it suffered from the following disadvantages:-

- the bearing material would be prone to contamination,
- it will be subjected to varying environmental and loading conditions and therefore wear away steadily.

In order to retain conventionally, it was decided to introduce rollers to provide low friction sliding and transfer of the bending loads to the wing support structure.

5.5 DESCRIPTION OF THE FINAL DESIGN

Displayed in Figures 5.5a is a photograph of the structural model made to satisfy the above mentioned requirements. Figure 5.5b gives sectional details of the model at the I/B end of the segment. Detailed drawings made to manufacture the major components are contained in Appendix E. The design comprises of:-

a) A flexible upper surface skin, with tags as sliding elements and conforming rails,
b) A set of two tracks situated at either end of the segment,
c) A load bearing support structure used for attaching the TE components,

d) A single TE device which is assumed to twist during deployment,
e) A hinged under surface flap - foam filled for increased stiffness, and
f) A hydraulic actuator system for providing deployment.

Detailed description of these items is given in the next few paragraphs.

Upper Surface and Conforming Rails

The upper surface is made as a single piece from CFRP material. The laminate thickness is 2.00 mm, made from 8 plies of thickness 0.25 mm and the fibre orientation of $[(0^2/90/\pm45)_s]$. 0° plies run along the span while the 90° plies run parallel to the chord (Figure 5.2). Details of the laminate and stiffness matrix along with the material properties are contained in Table 5.3.

Figure 5.6 shows the deflection geometry obtained from the FEA for the above skin material and previously described loading and restraint conditions (Figure 5.2). It can be seen that the deflection due to these conditions is 1.41 mm. This is well below the required value of 3.91 mm.

It was agreed that the designs suggested for the conforming tracks and rollers for the FLA wing would lead to manufacturing difficulties. In order to avoid these a very simple solution was sought. Details of this solution are given in Figure 5.7. 'C' channel rails were made from strips of steel. At the I/B and the O/B ends of the segment these rails are fixed to the extending track and the TE device, while in the intermediate span positions they are fixed to the TE device only. Tags as apposed to rollers are used to ensure upper surface camber variation.

Trailing Edge (TE) Device

It was necessary to ensure that the design of the TE device gave the desired motion without the system jamming. The simplest way of achieving the requisite geometry was by manufacturing the TE device from Jelutong (a high grain wood)[37]. This decision was justified since there were no torsional loads to be carried by the TE component and therefore it was not necessary to design the structural box in detail. Because of the soft nature of the wood material, it was thought that by having a direct attachment between it and the extending tracks adequate twist will result. Deflection tests (details of which are fully outlined in the Chapter Six) proved that this arrangement is satisfactory.

Track Roller System and Support Structure and under surface flap

The most striking feature of the proposed design is the deployment of the TE device by means of the extending tracks (Figure 5.8a). A two track system has been designed with one track fixed to the support structure and the other track attached to the TE device. An initial suggestion was to have only track rollers to take the bearing loads and provide continuous contact rolling motion. Owing to the conical nature of the system there appeared to be an appreciable degree of lateral movement of the TE device (see Chapter Six). The required free movement of the system was also observed to be unsatisfactory. To overcome this, a set of needle rollers were introduced between the two track system (Figure 5.8b).

The support structure is made from mild steel and comprises of the front and rear spar and the side ribs. The rear spar provides the attachment for the upper and the lower TE surfaces. A hydraulic actuator is mounted mid span of the front spar. The side ribs support the tracking system and are designed to react bending and shear loads.
The design of the conforming rails and sliding elements shown in Figure 5.7 was kept simple in order to reduce the manufacturing cost. Their simple design meant that these had to be placed very close to the upper surface skin. As is shown in Figure 5.8b, such an arrangement requires cut outs in the top flange of the spar in order to allow free movement of the rails.

A foam filled aluminium sandwich panel was designed for the under surface flap. This is fixed to the support structure (Figure 5.8c) by means of a longitudinal piano hinge. Two spring loaded 'L' section channels an the I/B and O/B ends of the segment provide a continuous attachment of the under surface to the TE device.

Hydraulic Actuator and the System

The deployment of the TE device is by means of a single linear hydraulic actuator placed in the mid-span position of the segment (Figure 5.9). The system to deploy the TE device comprising essentially of, a power pack, a throttle (control) valve which can be adjusted to change the flow hence the deflection rate, a linear hydraulic actuator, a flow direction valve and a control switch.

The stroke of the actuator is in keeping with the maximum deployment range of +7° to -3.5°. It is pin mounted to the front spar such that it pivots vertically and laterally.

5.6 MANUFACTURING

The desired motion meant that close tolerance manufacture was required for the track roller system, the conforming rails and the sliding tags, the TE device, and the upper surface skin. The manufacture of the two sets of tracks was simply a matter of machining from a solid billet of steel and stress relieving them. The assembly of the conforming strips was also a simple process. These were made from three sets of steel strips and spot welded along their length.

Initial intention was to use a wooden plug shown in Figure 5.10a as the tool for manufacturing the upper surface skin. The material selected for the upper surface skin is a carbon epoxy in a pre preg form (Ciba Geigy 913C)[38]. Pre pregs normally require an elevated curing temperature. Likewise the associated tooling must be capable of working comfortably at this temperature. The laminated wooden plug therefore could not be used directly as a tool because of this heating. The tool matrix material had to be a room-curing wet epoxy system possessing a high heat deflection temperature. The system chosen was SPS 695 HDT and 5P5 S95 gel coat [39]. Figure 5.10b shows a photograph of the composite tooling made from the wooden plug.

Initially the upper surface was laid up and vacuum consolidated on a flat surface and later transferred to the tool for curing. The curing procedure carried out is shown in Figure 5.11. To stop the flap sticking to the tool surface, the surface was first sprayed with a release agent and then covered with a release film. Secondary bonding was required on the skin surface, a good bonding surface is produced by using peel plies on the outside pre preg faces. A thin piece of mild steel sheet plate controlled the thickness of the skin and was placed on top of the release film and exactly over the skin. A glass breather cloth was used as a bath to extract air and volatile. The complete breather stack and tool were placed in a nylon bag initially for vacuum and secondly for pressure consolidation in the autoclave. The cure cycle was as per manufactures specification[36][37]. Figure 5.12 shows the upper surface skin manufactured from carbon composite tooling.

The laminated wooden plug shown in Figure 5.10a was trimmed further and cleaned to the size of the TE device.

Table 5.1: Chordwise pressure distribution across the upper surface flexible skin

Elemental Strip No	Strip Width % Chord	C_{Pmean} (-ve) *	Pressure (-ve) N/mm^2 X 10^{-6}
1	3.56	0.7818	5080
2	3.87	0.7827	5086
3	3.81	0.7883	5122
4	3.72	0.8051	5232
5	3.65	0.8160	5302
6	3.55	0.8058	5236
7	3.44	0.7792	5063
8	3.30	0.7403	4810
9	3.16	0.6906	4488
10	3.03	0.6597	4287
Total width of the upper surface skin = 35 % Chord			

* - C_{Pmean} (mean coefficient of pressure) obtained from 2-D computational calculations carried-out in reference [27]

Average pressure = 4970 N/mm^2

Average chord = 523 mm

Segment span = 970 mm

Therefore average load on the upper surface skin = 2522 N. This compares well with the estimated applied load of 2620 N.

Table 5.2: Material properties

Material Type	Elastic Modulus, E x 10^5 (N/mm^2)		Density,ρ x 10^{-6} (kg/mm^3)	Stiffness to weight ratio (E/ρ) x 10^{10}
	E_x	E_y		
Aluminium Lithium	0.795	0.795	2.54	31.3
Aluminum	0.720	0.720	2.80	25.7
CFRP	1.400	0.100	1.60	-

LAMINATE CONSTITUTIVE EQUATION FOR THE ANALYSED CONFIGURATION

"A,B,D" STIFFNESS MATRIX

C.1681E+06	C.2166E+05	-C.1614E-04	0.2686E-02	0.3662E-03	0.1514E-04
C.2166E+05	C.1026E+06	-C.2896E-02	0.3662E-03	0.1953E-02	-0.7733E-04
-C.1614E-04	-C.2896E-02	C.2562E+05	0.1514E-04	-0.7733E-04	0.0000E+00
C.2686E-02	C.3662E-03	C.1514E-04	0.5264E+05	0.5998E+04	0.1022E+04
C.3662E-03	C.1953E-02	-0.7733E-04	0.5998E+04	0.4003E+05	0.1022E+04
0.1514E-04	-C.7733E-04	C.0000E+00	0.1022E+04	0.1022E+04	0.7319E+04

"a,b,d" COMPLIANCE MATRIX

0.6116E-05	-C.1290E-05	-0.1420E-12	-0.3093E-12	0.5310E-13	0.9497E-14
-C.1290E-05	C.1001E-04	0.1131E-11	0.4851E-13	-0.4884E-12	0.1699E-12
-0.1420E-12	C.1131E-11	0.3904E-04	-0.2002E-13	0.7862E-13	-0.8183E-14
-C.3093E-12	C.4851E-13	-C.2002E-13	0.1937E-04	-0.2843E-05	-0.2308E-05
C.5310E-13	-C.4884E-12	0.7862E-13	-0.2843E-05	0.2549E-04	-0.3162E-05
0.9497E-14	C.1699E-12	-0.8183E-14	-0.2308E-05	-0.3162E-05	0.1374E-03

LAMINATE EQUIVALENT ENGINEERING ELASTIC CONSTANTS

	Membrane Mode	Bending Mode
Ex	0.81748E+05	0.77459E+05
Ey	0.49927E+05	0.58358E+05
Gxy	0.12808E+05	0.10917E+05
NUxy	0.21098E+00	0.14679E+00
NUyx	0.12885E+00	0.11154E+00
mx	0.23221E-07	0.11917E+00
my	-0.11297E-06	0.12409E+00

Table 5.3: Material properties for the chosen carbon fibre reinforced plastic laminate

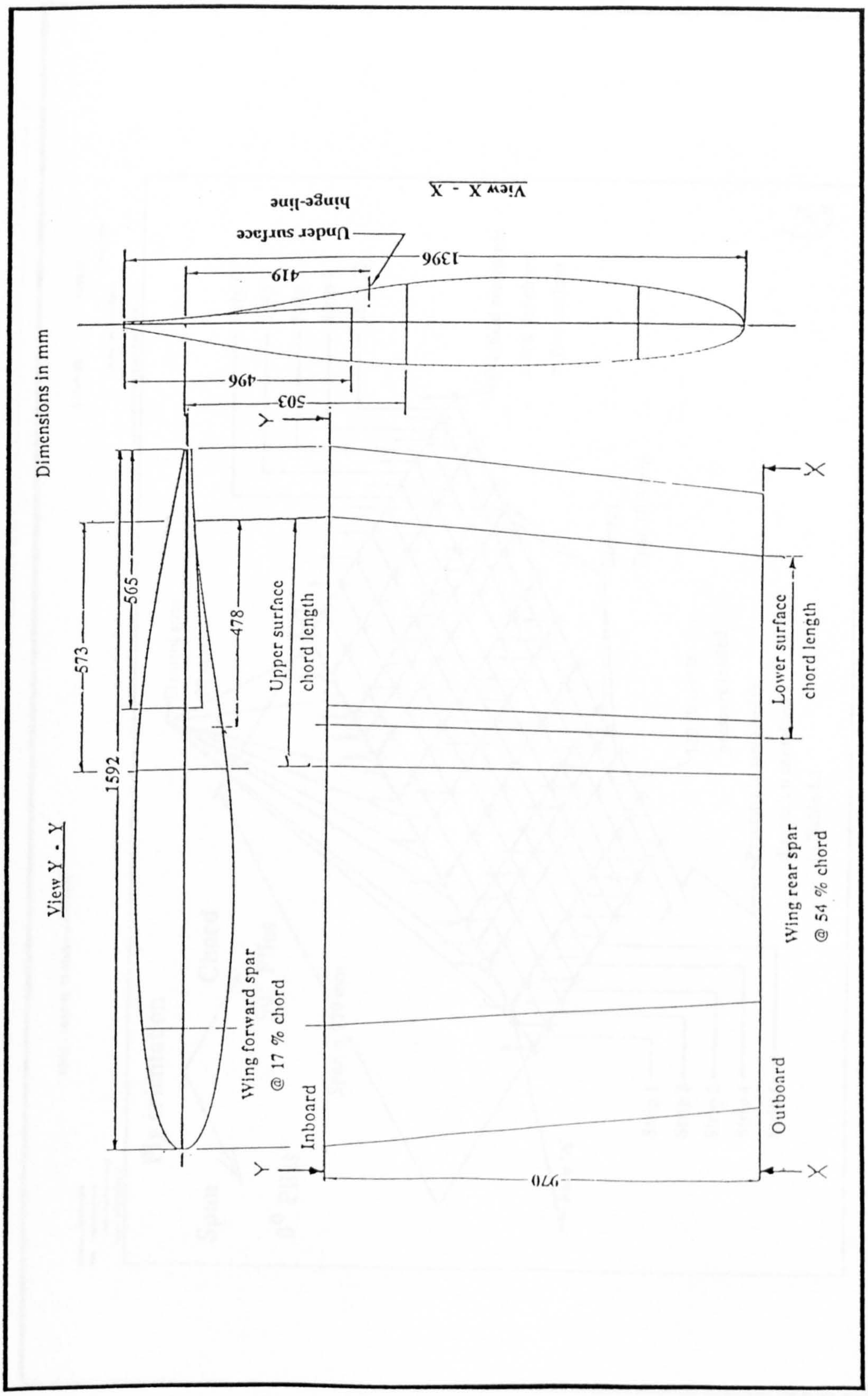

Figure 5.1: Overall dimensions of the structural model

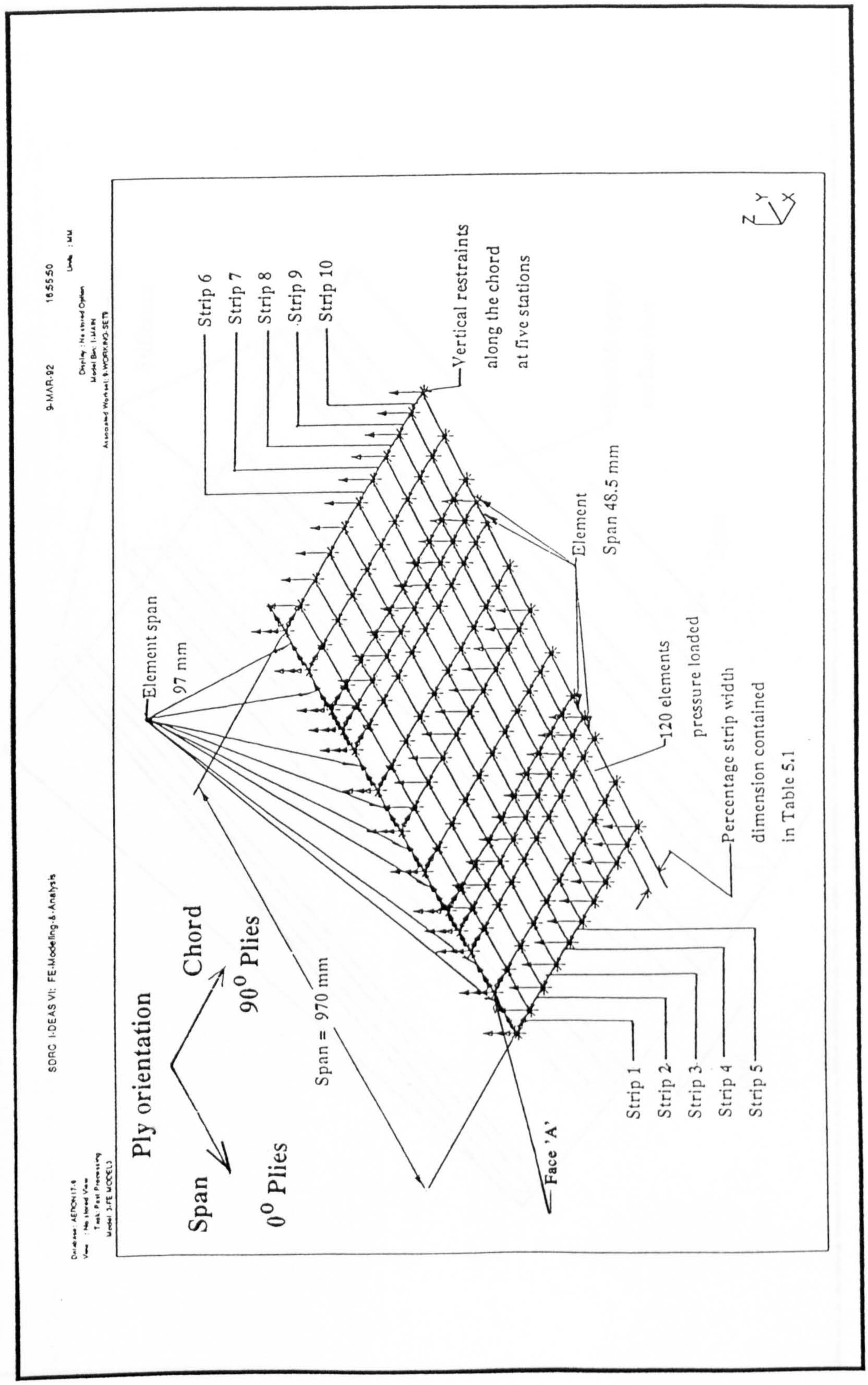

Figure 5.2: Finite element (FE) model of the upper surface flexible skin

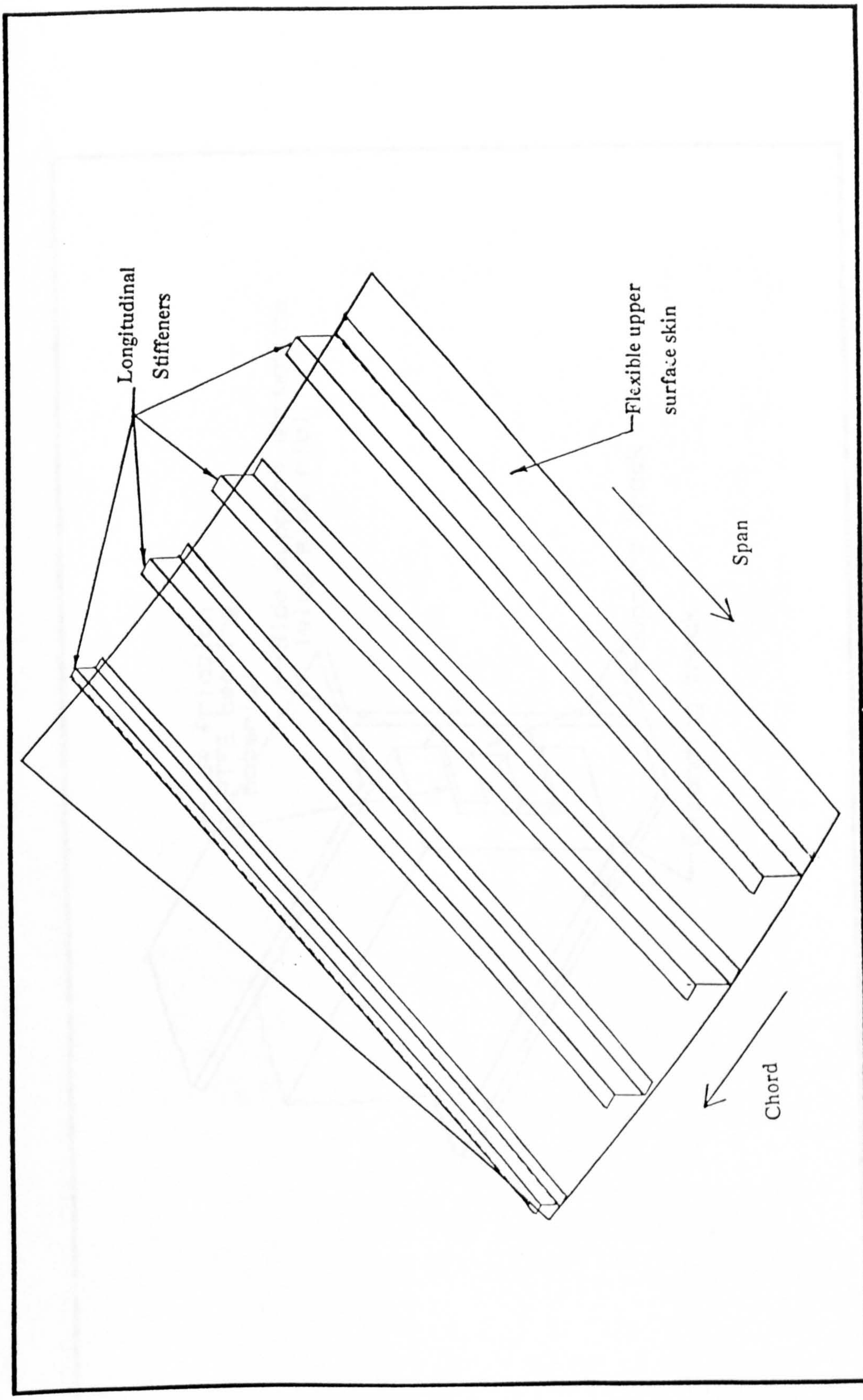

Figure 5.3: Upper surface skin stiffened along the span

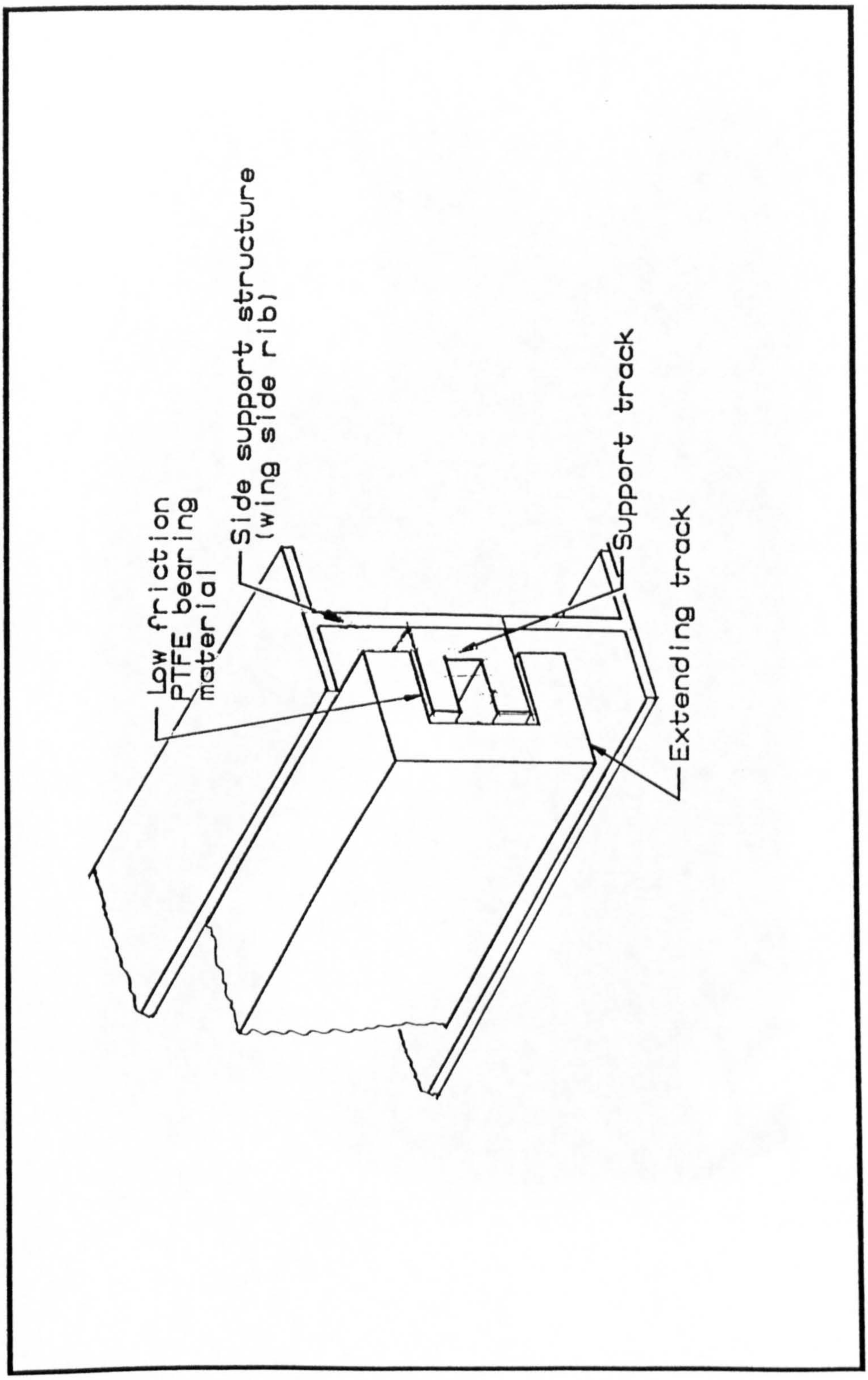

Figure 5.4: Track cross-section with PTFE providing the sliding and bearing properties

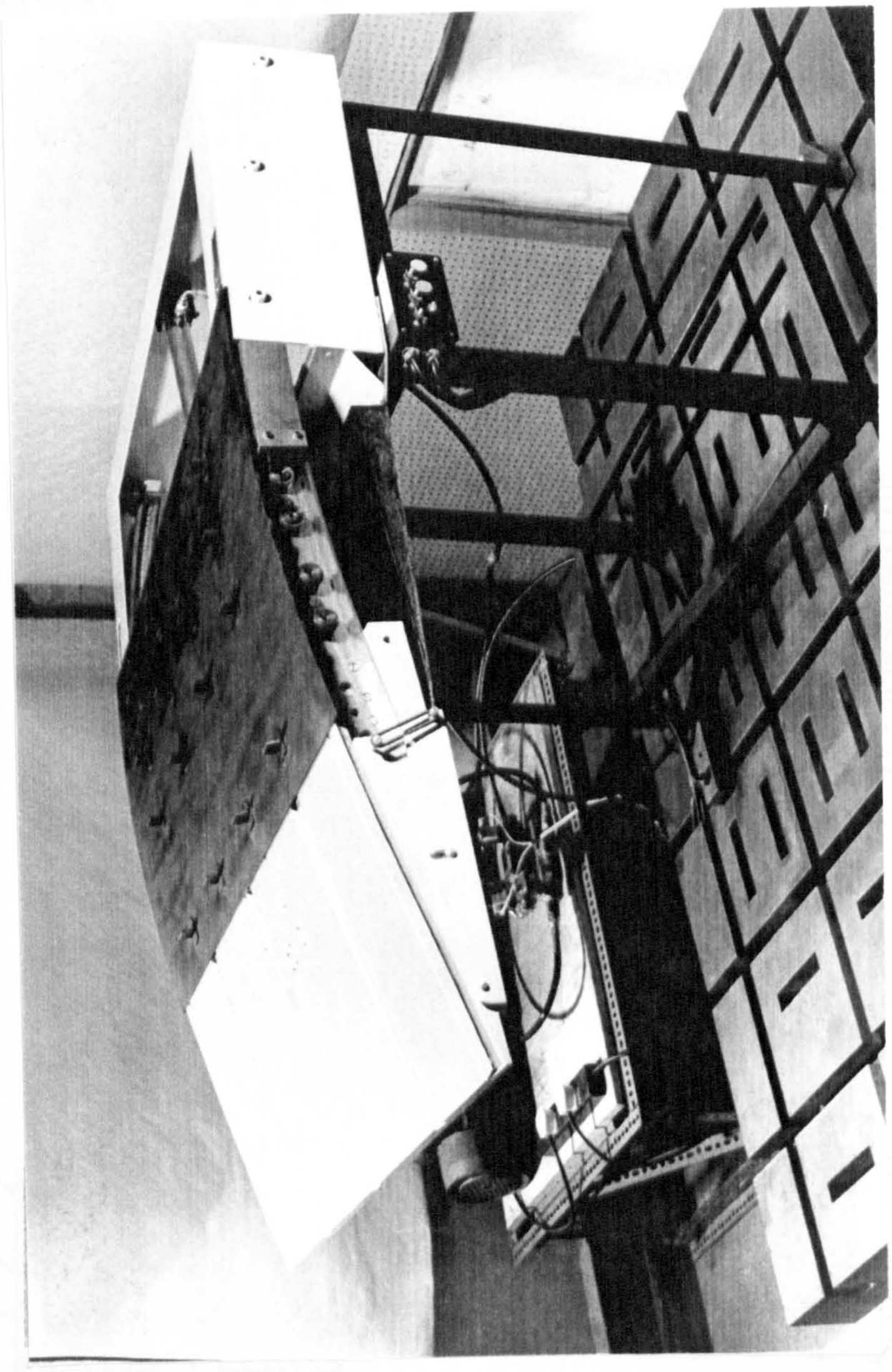

Figure 5.5a: Illustration of the structural model

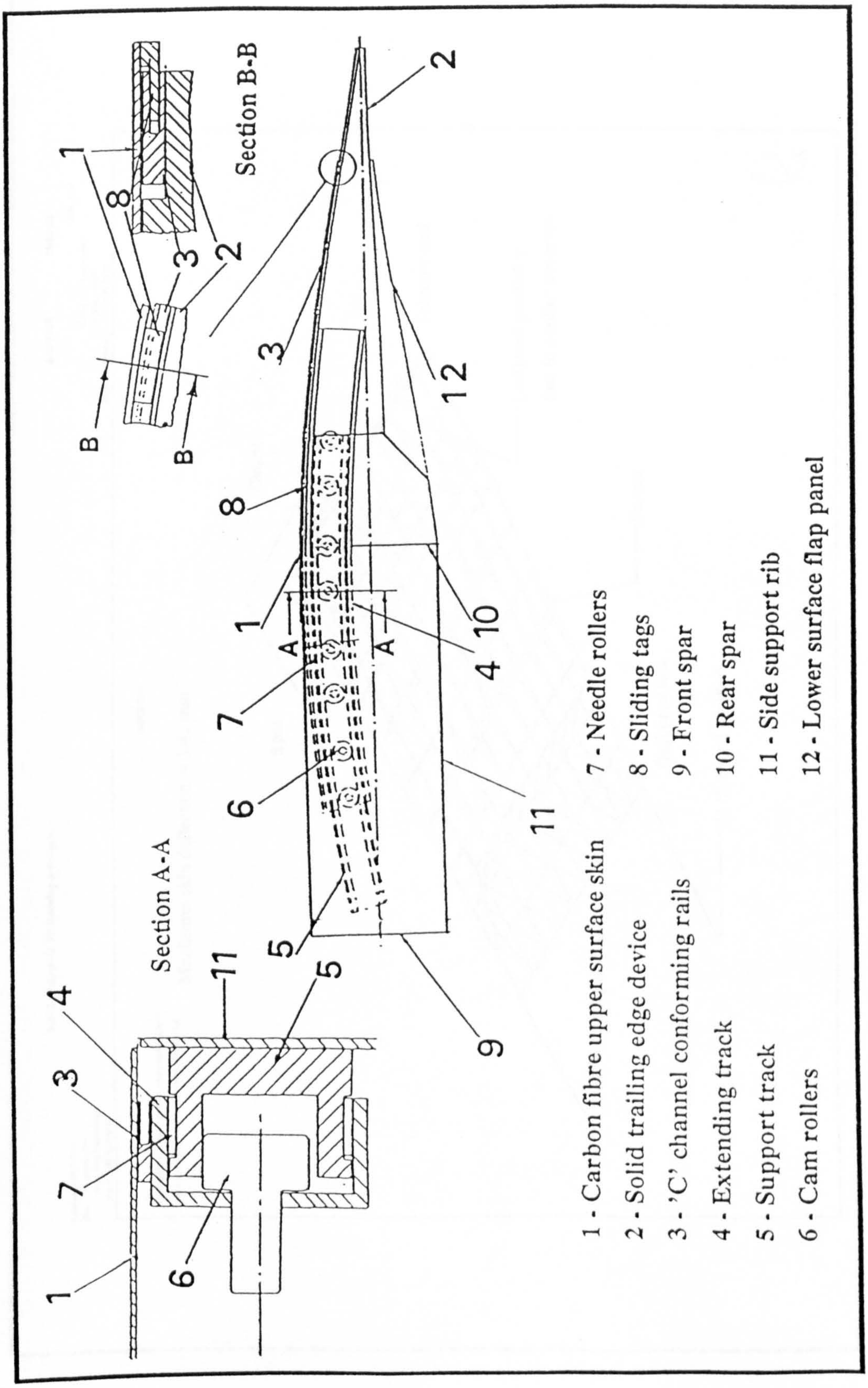

Figure 5.5b: Detailed arrangement of the components within the structural model

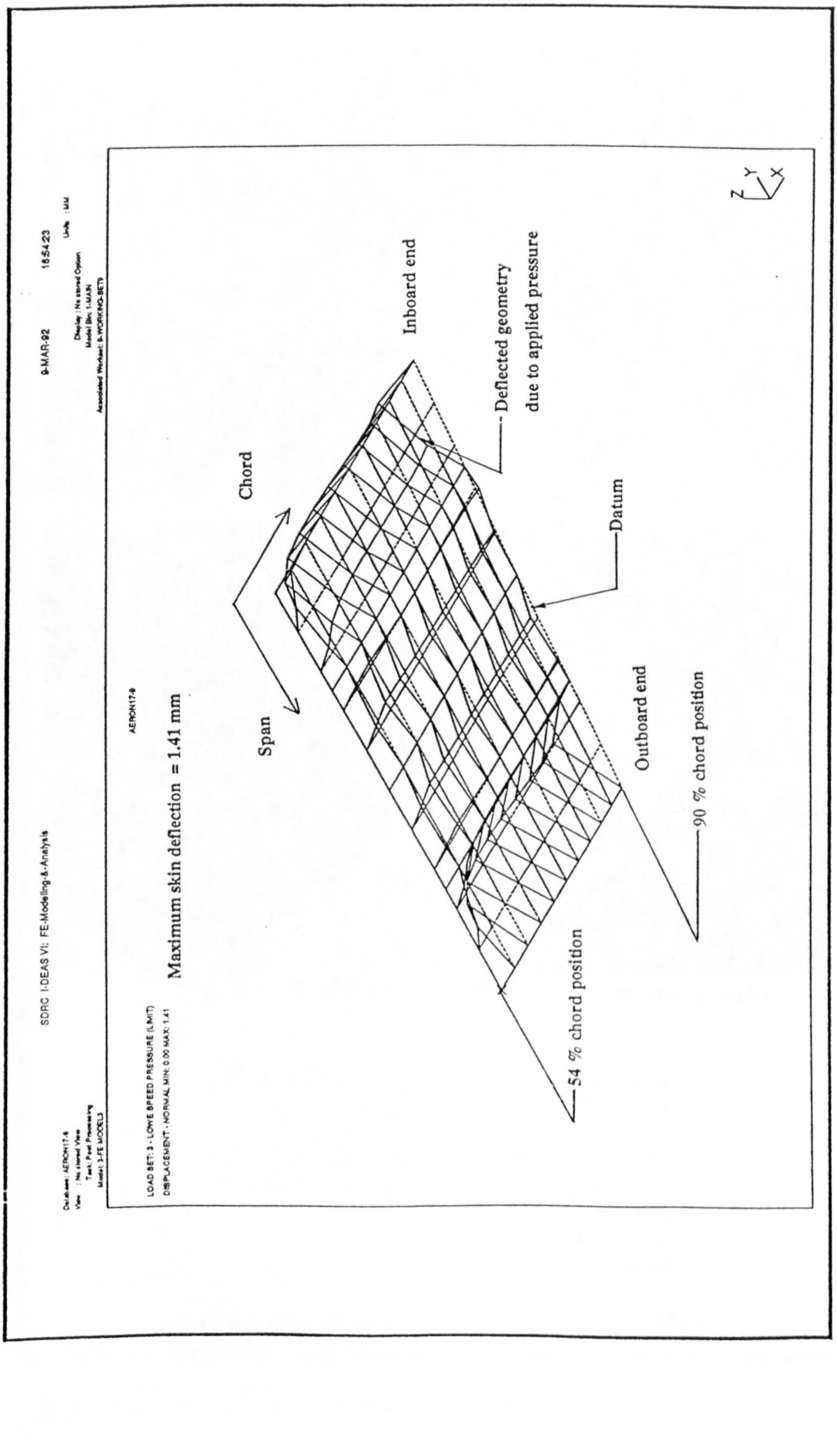

Figure 5.6: Deflection geometry of the upper surface carbon skin due to applied pressure

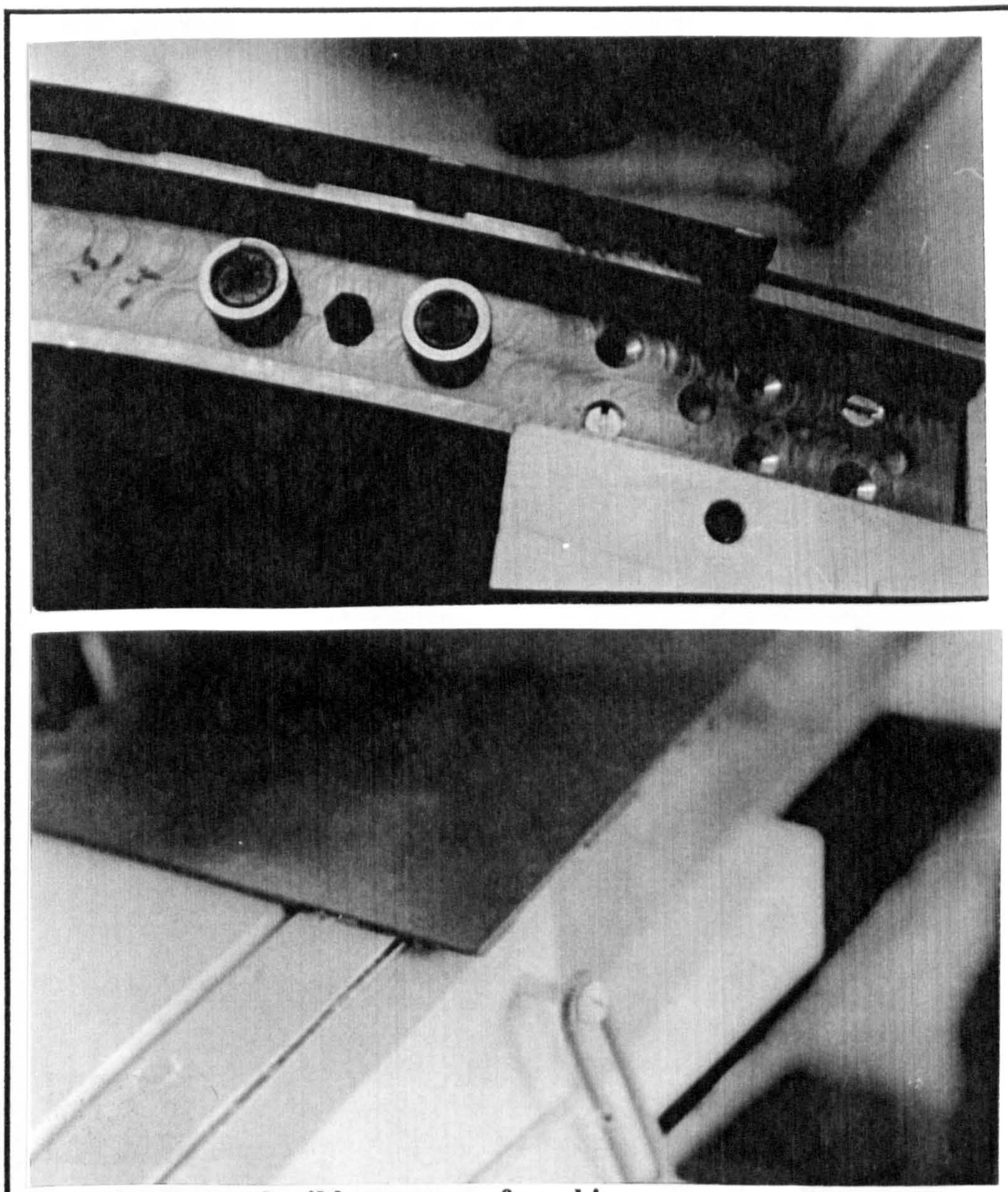

Figure 5.7: Solution for conforming the upper surface skin

(a)

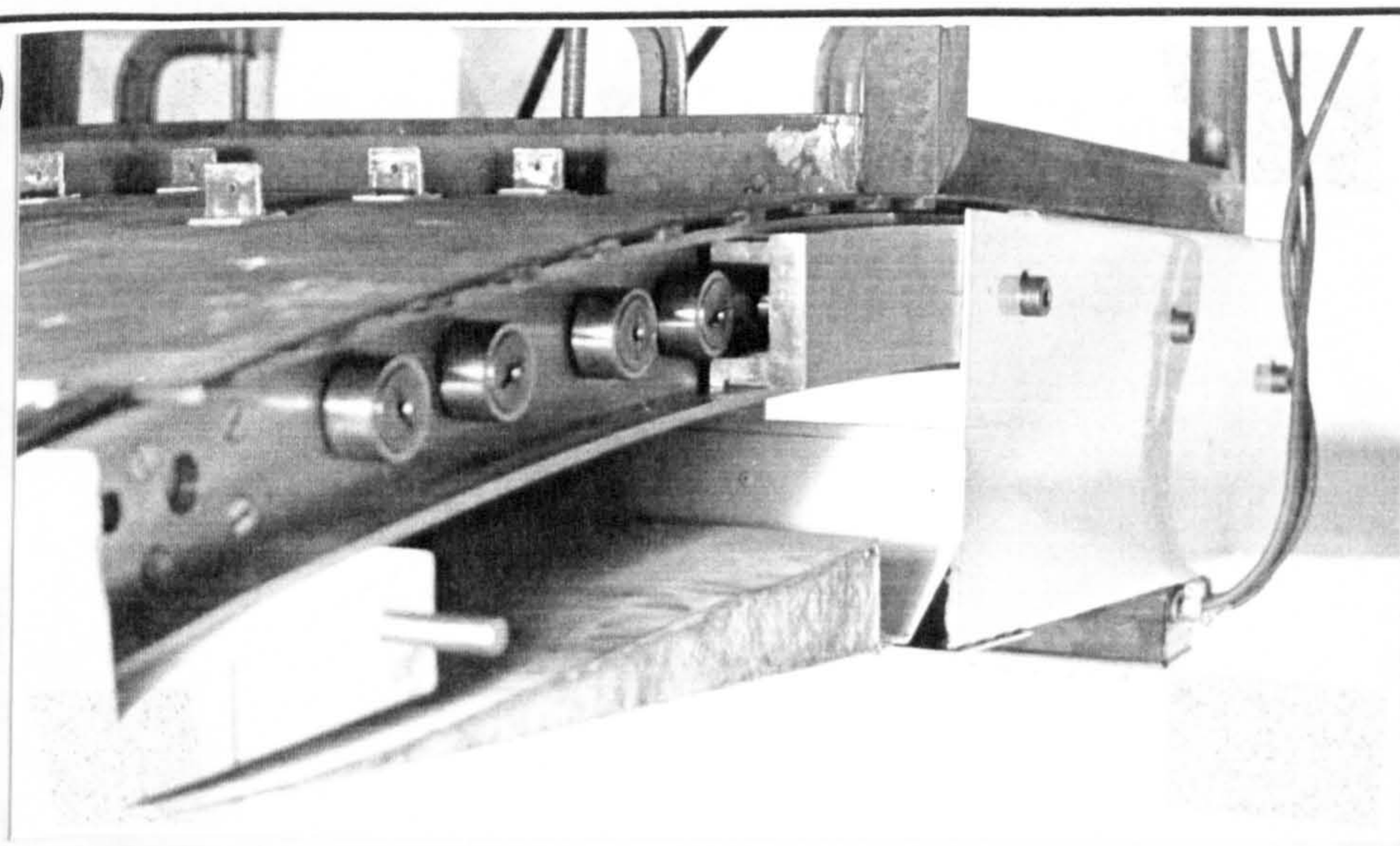

(b)

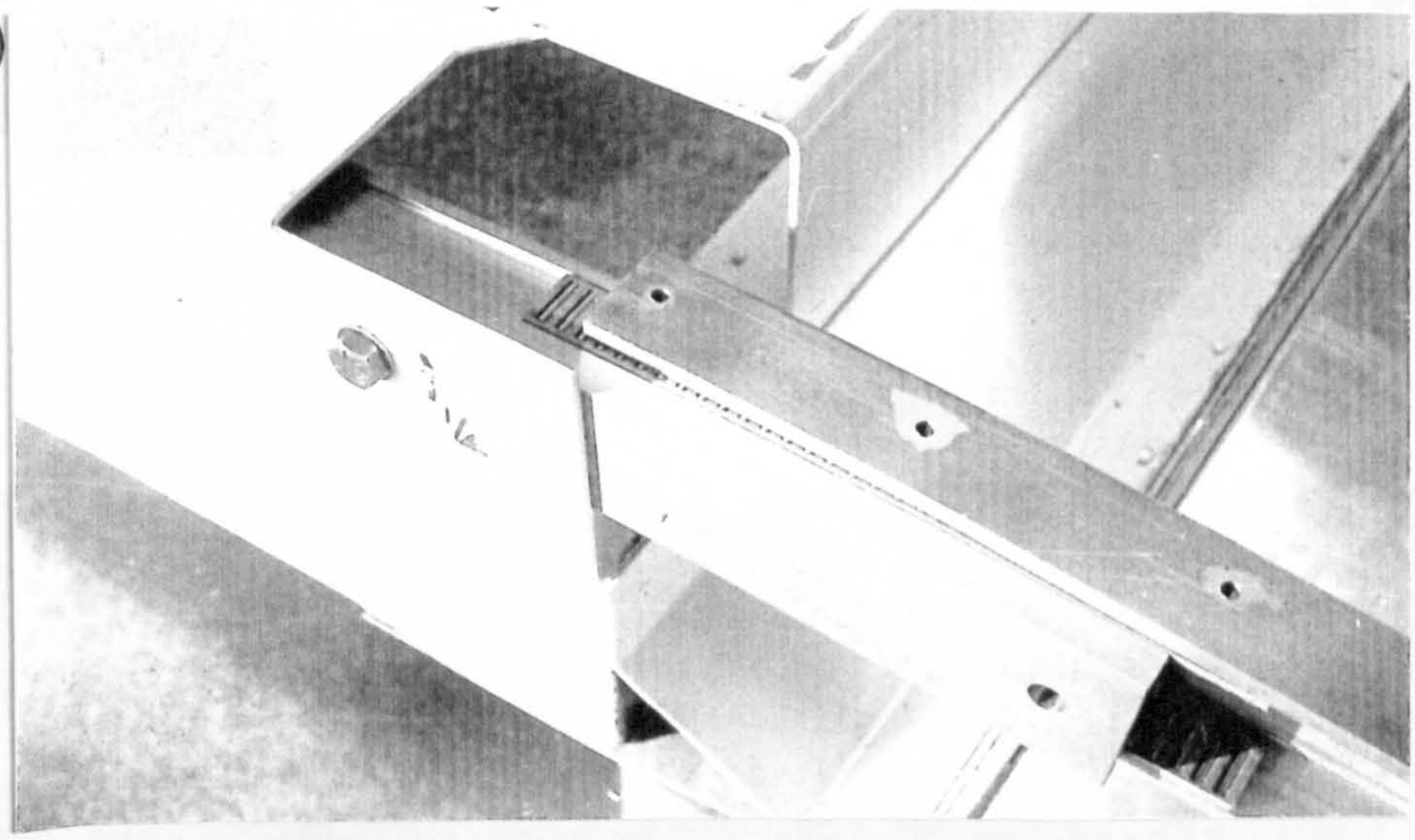

(c)

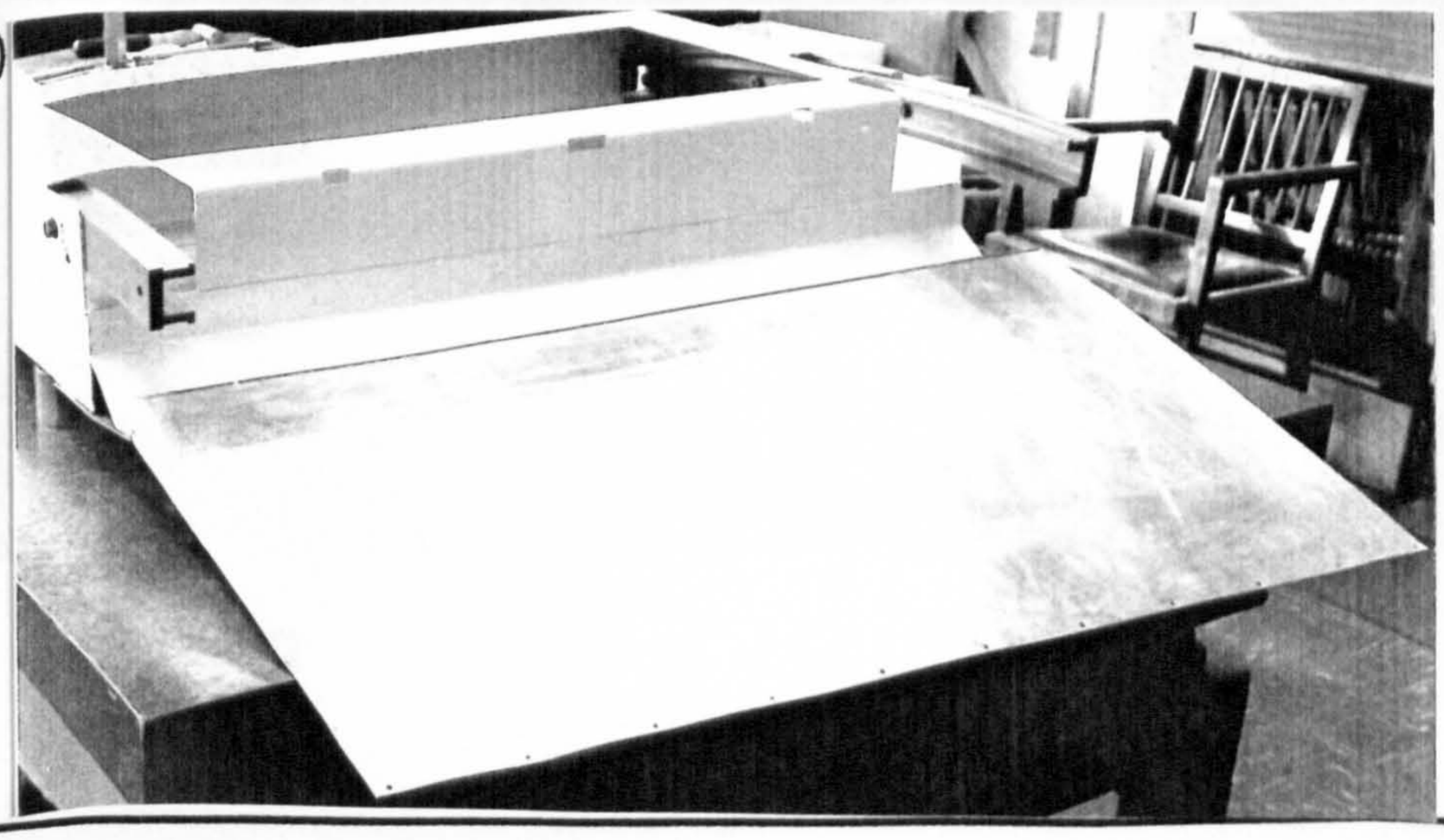

Figure 5.8a-c: Details of the track roller system, support structure and the under surface flap

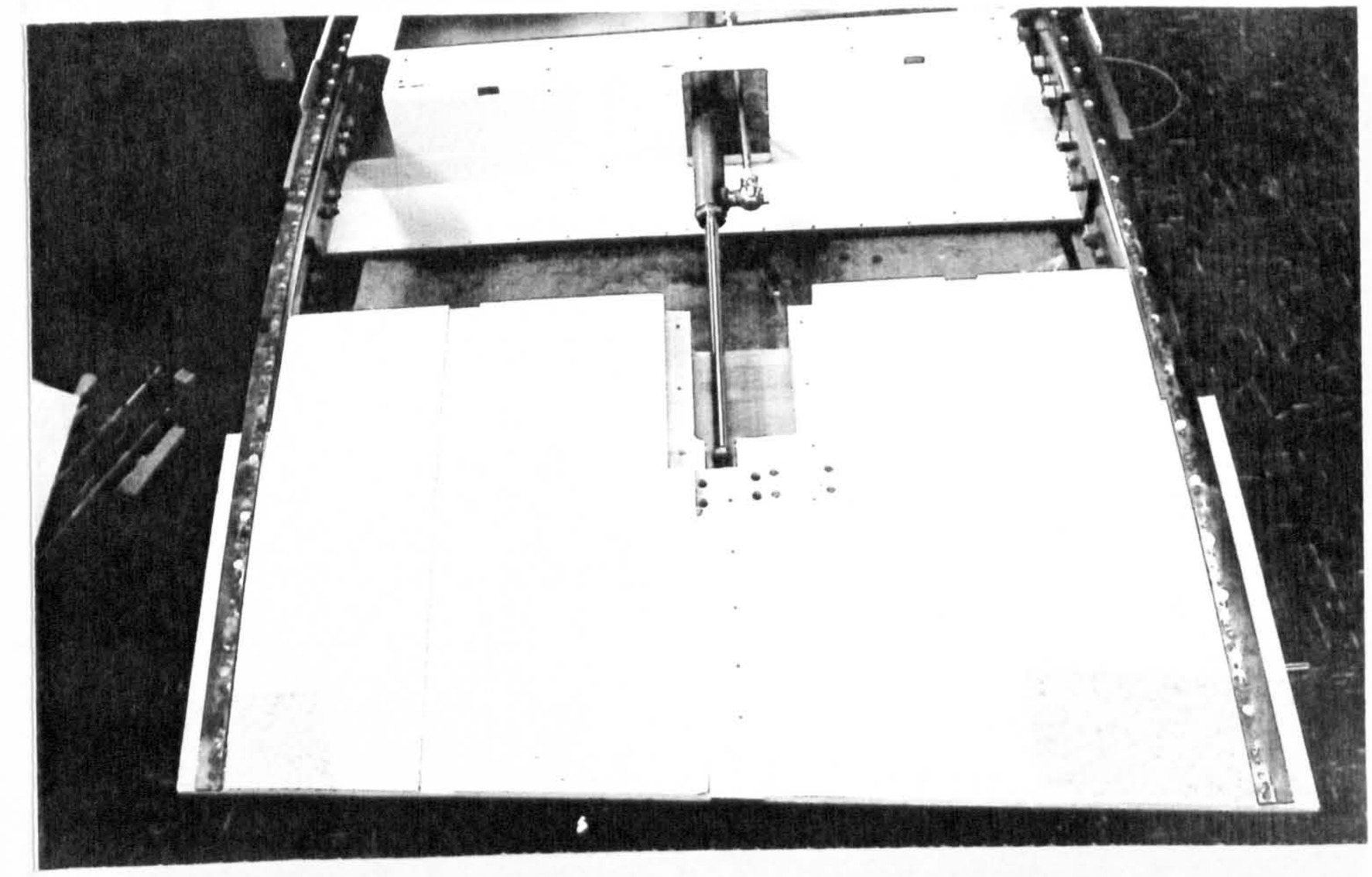

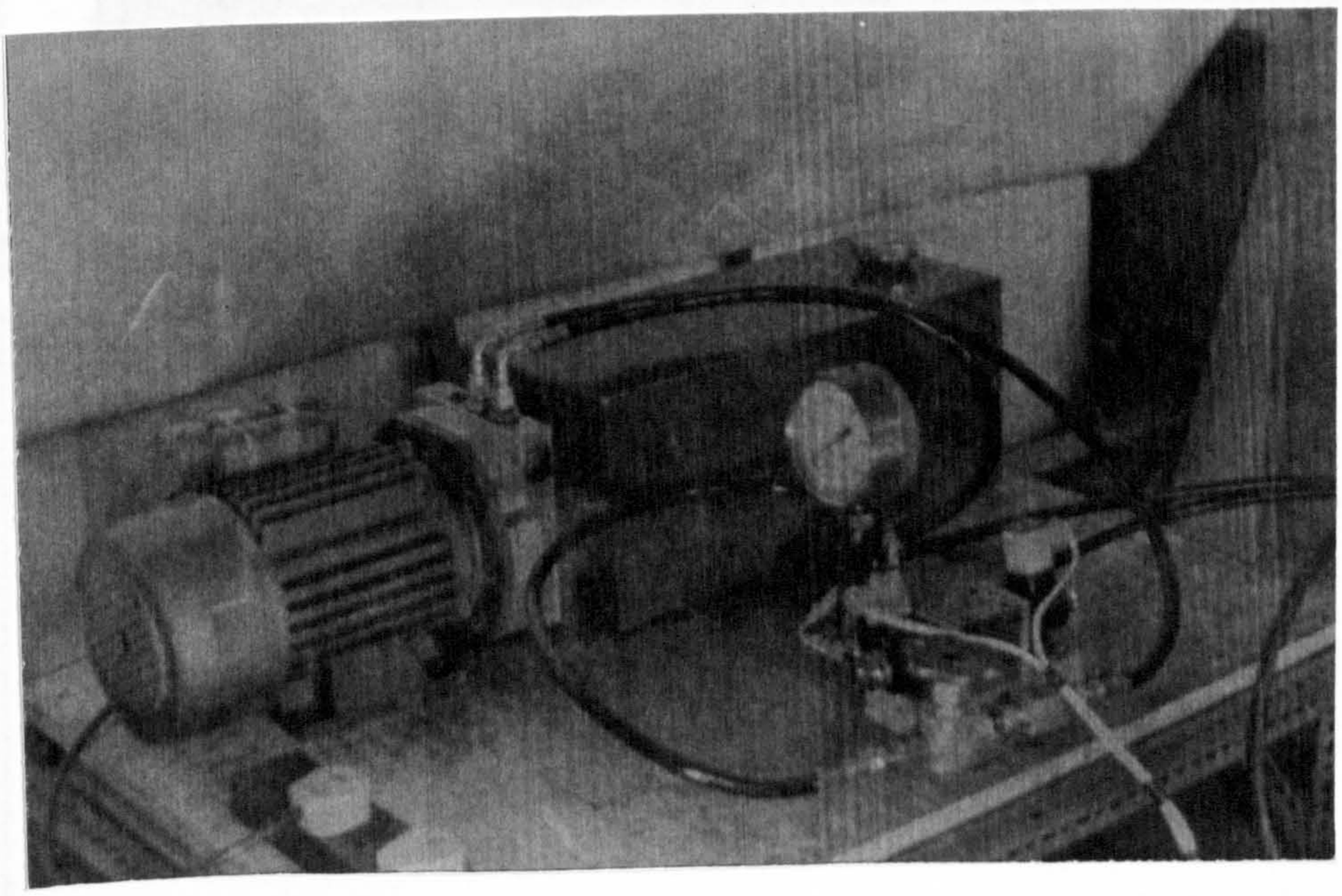

Figure 5.9: Hydraulic system and actuation

(a)

(b)

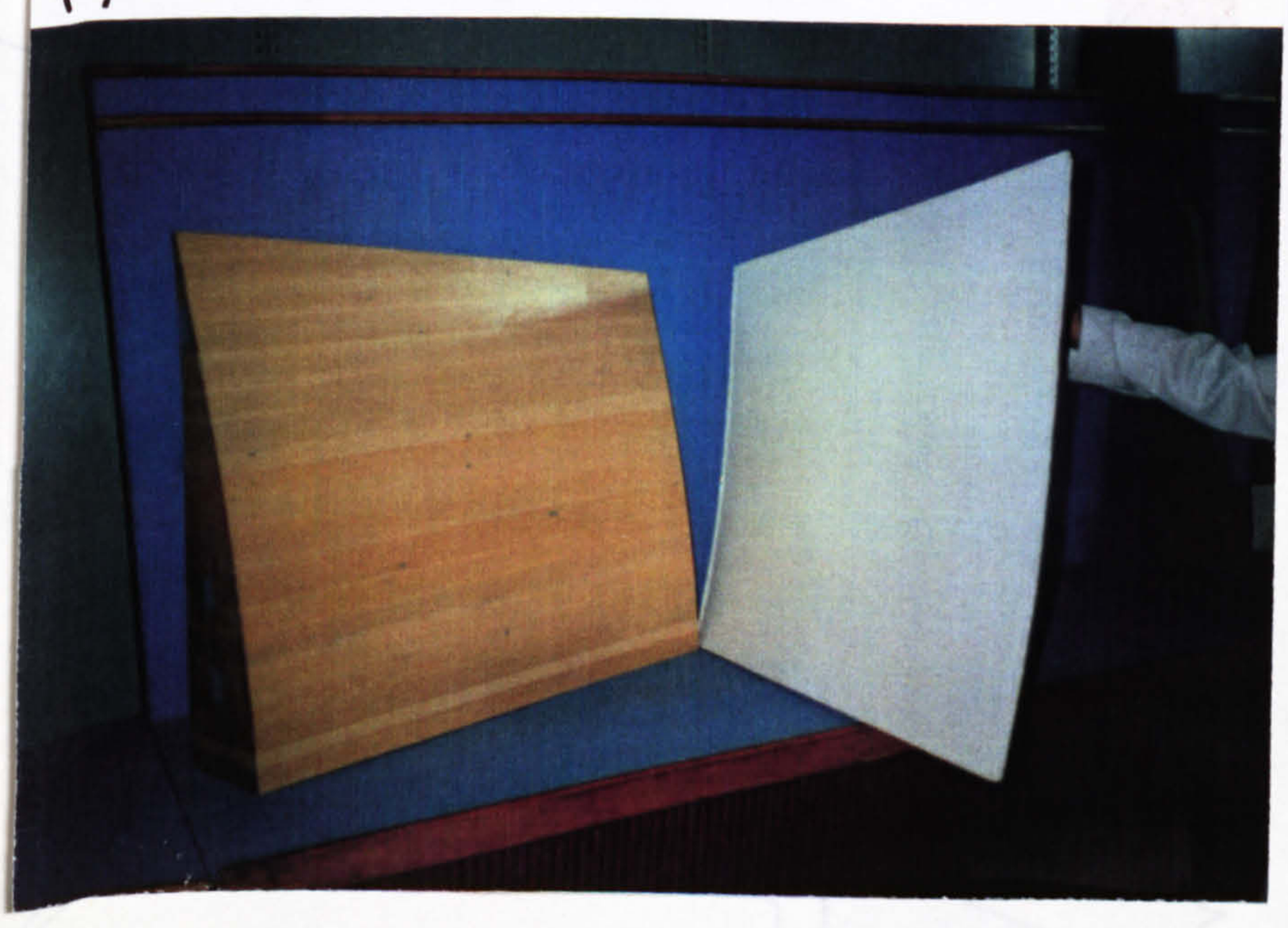

Figure 5.10a&b: Wooden plug used for manufacturing the composite tooling

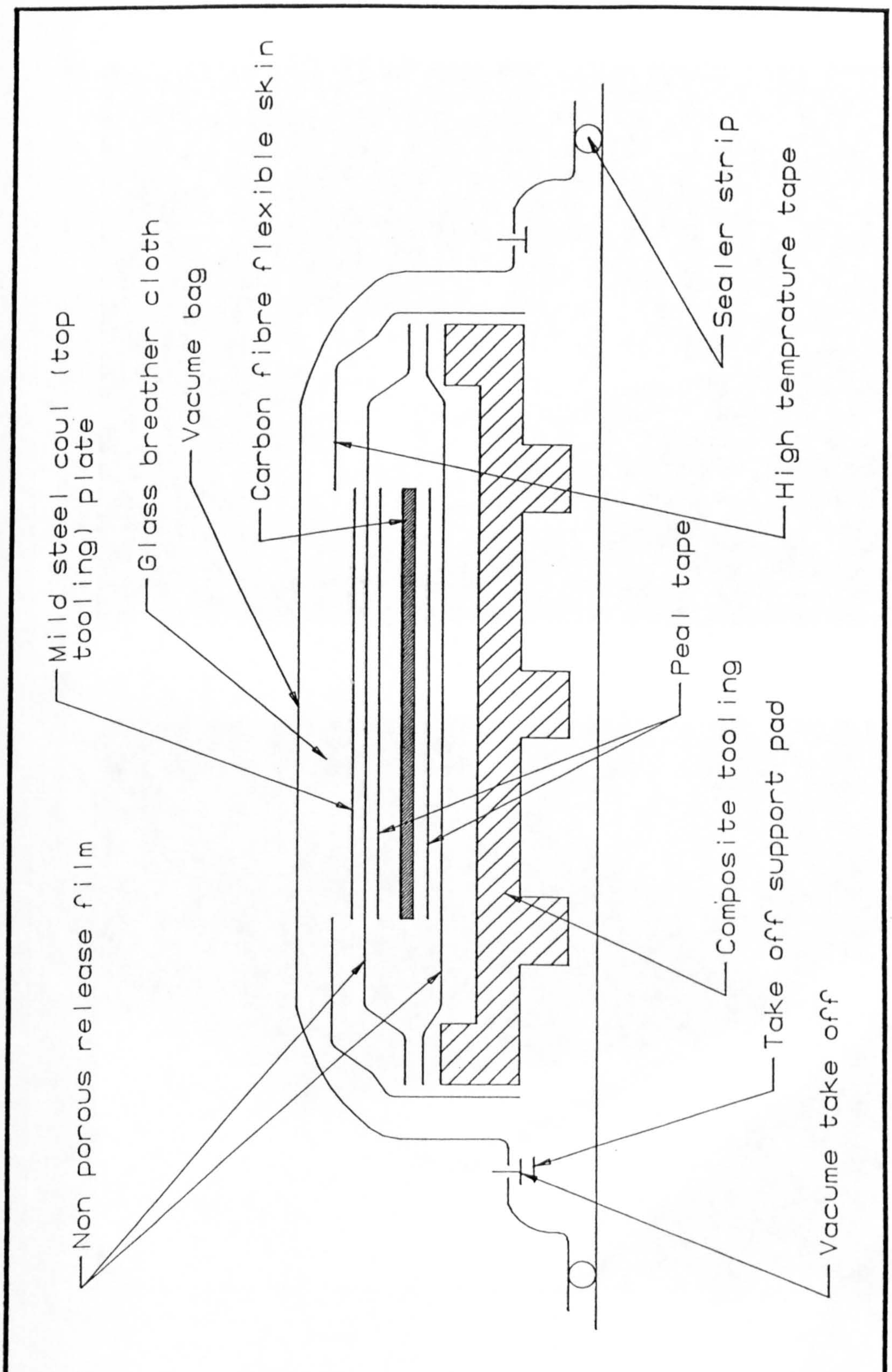

Figure 5.11: Curing procedure for the flexible upper surface skin

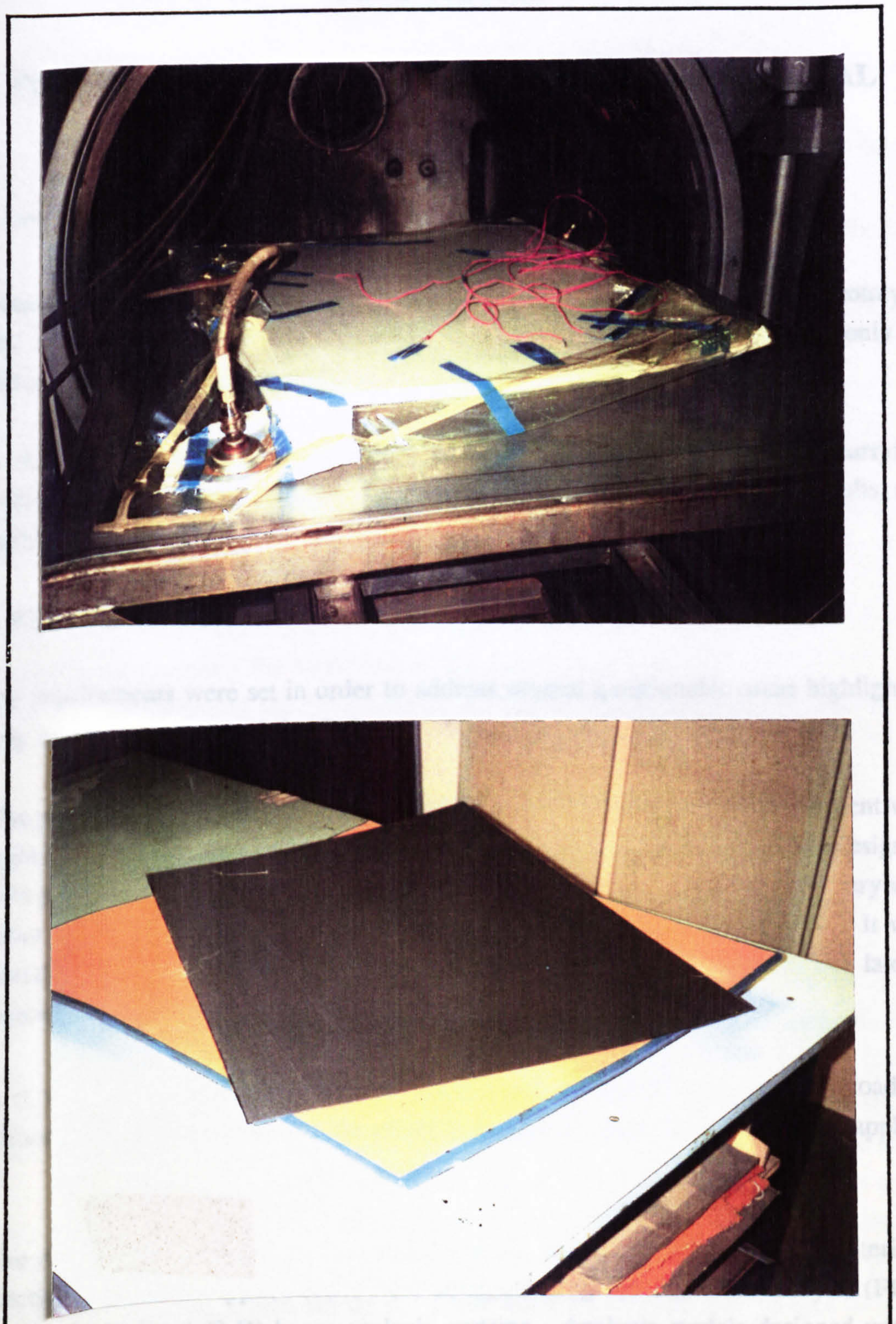

Figure 5.12: Carbon skin manufactured to the form of composite tooling

CHAPTER SIX

TESTING OF THE THREE DIMENSIONAL STRUCTURAL MODEL

6.1 INTRODUCTION

As stated in the last chapter, the purpose of designing and constructing a prototype model was to validate the proposed design concept. This verification could only be possible by virtue of testing under both unloaded and loaded conditions.

This chapter offers a brief outline of the reasons, requirements, and aims for carrying out these tests. Test methods and procedures are described and the results are discussed.

6.2. REASONS, REQUIREMENTS AND AIMS FOR TESTING

Three requirements were set in order to address several questionable areas highlighted during initial assessment of the design:-

1) The proposed design of the three dimensional (3-D) trailing edge (TE) segment was thought to be feasible practically, but this had to be proved. The model was designed to give parallel deployment with a solid wooden TE piece. The fundamental query was whether this type of deployment could be possible with a tapering segment. It was required therefore to assess the behaviour of the system and monitor the lateral movement of the tracking system.

2) It is vital for this system to operate continuously without binding under all loading conditions. A test was therefore necessary to ensure a smooth operation under applied load.

3) The designs for the upper surface and the tracks were based on a stiffness criterion. Deflections due to the applied loads were obtained using finite element analysis (FEA) and two dimensional (2-D) beam analysis systems. Analysis models designed within these systems were very simple and unrefined. Therefore very little confidence could be placed in the results. In order to check the validity of these results and to guarantee the stiffness, it was necessary to carry out some form of loading test for both the upper

surface skin and the tracks.

In view of these requirements the main objectives for carrying out the tests were to:-

1) Observe the deployment schedule and the expected lateral movement of the tracks at the inboard (I/B) and outboard (O/B) ends,
2) Statically load the upper surface and the tracks and measure the deflections, and compare the results with finite element (FE) predictions, and
3) Observe the behaviour of the assembled model while deploying it under simulated loads.

6.3 TEST SET UP, PROCEDURE AND RESULTS

The three objectives stated above suggested that the testing had to be divided into three distinct phases:-

(1) Phase I for testing the stiffness of the upper surface,
(2) Phase II for assessing the behaviour of the unloaded model, and
(3) Phase III for assessing the behaviour of the loaded model and statically testing the stiffness of the tracking systems.

6.3.1 Phase I (Stiffness testing of the upper surface skin)

6.3.1.1 Test apparatus

Details of the test set up are shown in Figures 6.1a and 6.1b. Where Figure 6.1a illustrates a set of photographs, while Figure 6.1b depicts schematic drawings giving dimensions and position of the various item. The upper surface is placed inverted on five sets of chordwise formers and one longitudinal former representing the rear spar. The three intermediate formers simulated the support and stiffness of the guide rails. 'G' clamps were used to hold the skin down at the I/B and O/B positions and at the rear spar. All the formers were nailed to a 3/4" plywood which rested on a 'Dexion' frame work and had 48 holes drilled across it. These holes allowed the dial gauges to reach the loaded skin. A set of eight dial gauges mounted (across the span) on a 'Dexion' frame work were used to make six sets of deflection measurements along the chord.

The required load across the upper surface was 267 Kg (see Chapter Five). Due to the width of the chordwise formers the effective area for loading the upper surface skin was reduced. The magnitude of the reduced load was worked out to be 238 Kg. To apply this load it was important to use a loading medium that could be distributed adequately and practically. Dry silver sand with a density in the range of 1500 - 1600 KG/m^3 (depending on the moisture content), packed in plastic bags was considered to meet this need. In order to maintain even load distribution the sand had to be as dry as possible. Moisture content was reduced by drying the sand in an autoclave. For the required distribution, the load was effectively split between eight cells, as depicted in Figure 6.1b. Table 6.1 contains the incremental load applied in five stages in these cells. Thus five deflection measurements were made at each of the dial gauge position. Owing to only eight dial gauges being used, the panel had to be loaded and unloaded six times.

6.3.1.3 Results

Measured deflections for the five load stages are contained in Table 6.2. Maximum deflection of 2.262 mm is seen to occur at gauge position 28. This is well within the allowable value of 3.91 mm (2 % of the maximum depth of the aerofoil at the outboard end of the segment). Figure 6.2 shows the deflection vs load curve for dial gauge positions 4, 6, 9, 14, 21, 32, 40 and 47. The purpose of plotting these set of curves was to check whether the measured deflections were accurate at various dial gauge positions. It is apparent from Figure 6.2 that the stiffness is very much similar across the surface. It is suggested that the slight variation is largely due to the inaccuracy of the dial gauges and also due to the uneven distribution of the sand. The later effect could not be controlled because the upper surface was curved and therefore the sand had the tendency to shift toward the rear spar position. This is justified by the relatively large deflections seen to occur at gauge positions 21 and 32.

6.3.1.4 Comparison with the finite element analysis (FEA)

The main purpose for carrying out the upper surface skin stiffness test was to check the validity of the predicted FE results. The FE model for the upper surface skin described in Chapter Five was modified slightly to take account of the chordwise formers. This was possible by including beam elements to represent the extra stiffness. Results of the FE analysis of the modified model and the test are contained in Table 6.3 and shown in Figure 6.3.

The correlation between the two sets of results is observed to be better at mid-chord stations than the ends. The measured deflections at mid-chord stations are slightly less than those obtained from the FE analysis. This had been expected and is due to the stiffness of the 3/4" wooden ply board, which is not included in the FE model. At the ends the measured deflections are higher than the FE values. This was due inadequate distribution of the loads near these regions. Particularly towards the rear spar position, where the concentration of loads was greater than what was required. This was due to the curvature of the skin which was tending to slide the dry sand towards that region. The uneven load distribution together with stickiness of the dial gauges has resulted in an irregular distribution curves of the measured deflections.

6.3.2 Phase II

The upper surface skin is shown to satisfy the stiffness requirement both analytically and practically. The next stage was to examine how its flexibility tied in with the deployment of the assembled model. Assessments were made purely by way of observing the movement of the parts.

Photographs of the model shown in Figure 6.4 for -3.5°, 0° and 7° deployment settings suggest that the system is operational and gives both positive and negative deflections. The design of the TE device in laminated wood is therefore justified.

The variation in deflection across the span suggested that the upper surface had to twist and warp as well as conform in chord. Owing to the large radius of deployment curvature the twisting was fairly subtle. This moderately changing profile of the upper surface along the span was observed to be smooth and controlled. The use of carbon composite material assisted in providing the desired flexibility in chord and the necessary continuity. Evidence of achieving this flexibility from maximum negative to maximum positive angles of rotation is apparent in Figure 6.4a and 6.4c. It can be seen that the upper surface skin conforms smoothly without wrinkling or binding inside the rails.

The maximum (7°) achieved extension of the TE device at the I/B and O/B ends were found to be approximately 270 mm and 261 mm respectively. In comparison the maximum extensions required at the two ends are 301 mm (I/B) and 264 mm (O/B) relative to the 64.5% chord. The maximum achieved extention at the I/B end is approximately equal to the expected value for 7° camber setting at the centre span position. Thus the total translational motion was limited by the stroke of the actuator.

Furthermore the magnitude of maximum extension is approximately equal to 6.5° of rotation of the I/B end. The required extension for 6.5° camber setting at the O/B end is 237 mm. It is apparent that the stiffness of the TE device is considerable for it to flex at large camber settings. It therefore tends to ride more on the larger (I/B track) radius. Figure 6.5 shows the position of the TE device at 0° and at full camber settings (at the O/B end) due to such a motion. It is apparent that the TE device experienced a degree of lateral movement during its deployment. The measured movement at the I/B and O/B ends was 2.65 mm and 3.05 mm respectively. The difference in these two measurements provides further evidence of the twisting action necessary for achieving a conical motion.

Due to the simplicity in the design of the upper surface conforming strips and the sliding tags, the aforementioned lateral movement caused some difficulties in supporting the upper surface skin at five spanwise stations. It was therefore decided to assess how the skin flexes while being supported at the two ends and at the mid span position. Such an arrangement was found to be adequate in providing the required flexibility to the upper surface, as is shown in the photographs displayed in Figure 6.4.

If the TE device were to be of a flexible nature (made from fibre reinforced plastic material) then ideally, the system requires two actuators placed at either end of the segment. These would adequately twist the segment resulting in a continuous spanwise and chordwise camber. The design of the TE device in solid material (which moved laterally) meant that only a single linear hydraulic actuator placed in the mid-span position could be implemented for this set-up. This position of the actuator meant that the spar web had to be cut locally.

The under surface in this design is simply held in position by a pair of spring loaded angled rails placed at the I/B and O/B ends. It is apparent from Figure 6.4 that these rails are quite adequate in keeping the under surface continuously attached to the TE device. There is no evidence of clashing between the rails and under surface owing to the previously mentioned lateral movement.

6.3.3 Phase III

The purpose of this exercise was simply to monitor the changes in deployment behaviour of the TE device and the tracks due to the applied loads. The distribution and application of the load was as shown in Figure 6.6. The model was mounted inverted. Sand bags totalling to 102 kg were used to load the TE device and dead

weights of 146.7 kg were suspended in pans were placed on the extending tracks. Additionally, mass of up to 16 kg was hung on the upper surface skin through a series of loading lugs. The initial intention had been to load the upper surface skin with 267 kg (the exact magnitude of load, calculated in Chapter Five). Unfortunately it was not possible to carry out this task because of the inadequate design of the conforming rails and the tags (used to locate the upper surface skin). The relatively small load of 16 Kg was applied only to provide friction between the conforming rail and the sliding tags. The total load was applied in gradual increments as contained in Table 6.4.

Observations during the operation of the system indicated no real difference in the deployment of the loaded model in comparison with the unloaded model. Except that the former system was much slower as proven by the increment in applied actuator load shown in Table 6.4. This had been expected and is primarily due to the increased friction between the needle rollers and the two sets of tracks. Figure 6.7 shows three photographs taken at zero degrees, intermediate and maximum camber settings while the system was operating under loaded conditions. The number appearing on the bottom right hand corner represents the time at which the picture was taken. This suggests that a successful deployment is achieved from zero to maximum camber setting. Further evidence of this is given in Figure 6.8.

The dial gauge shown in Figure 6.6 was used to measure the deflections of the O/B track system. The measured deflections due to loading and unloading of the system are contained in Table 6.4. A plot of load vs deflection shown in Figure 6.9 gives a predictable trend. The maximum deflection is 5.827 mm. It is felt that the measured deflection is due to the deformation of the whole of the structural model rather than simply the deformation of the tracks. If the tracks were to deflect to such a degree then the system would bind and eventually seize. This obviously is not the case, as is proven by the photographs in Figures 6.7 and 6.8.

6.4 CONCLUSION

It can be concluded from the above discussions that the combination of a conical and parallel deployment is possible if a warping TE flap box is used. This point is highlighted by designing the TE device of the structural model in laminated wood and operating under unloaded and loaded conditions. Deployment checks indicated no problems of achieving VC with continuous curvature tracks. The translational motions were observed to be smooth, and the upper surface skin flexed without wrinkling or binding.

FE analysis and initial static tests of the flexible upper skin surface suggest that it is possible to satisfy the stiffness requirements, provided that an appropriate number of chordwise rails are positioned along the span. The close proximity between the two sets of results indicates that much confidence can be placed in FE analysis. Thus future work may not require separate static stiffness checks for the upper surface.

The operation of the system was very quick with a simple linear hydraulic actuator. With high pressure power packs and modern systems control technology, it is envisaged that much faster operations, such as those required for load alleviation purpose, could be carried out.

Table 6.1: Applied laod to the upper surface skin in five increments

Cell No	Load (KG)				
1A	8	16	24	-	36
1B	4	8	12	16	19
2A	8	16	24	-	42
2B	4	8	12	16	22
3A	8	16	24	-	42
3B	4	8	12	16	22
4A	8	16	24	-	36
4B	4	8	12	16	19
Total	48	96	144	196	238

Table 6.2: Upper surface skin deflection measurements due to applied load increment

Cell No 1 A						
Deflection (mm)						
Dial Gauge Number						
Load (KG)	1	2	3	7	8	9
8	-	0.296	0.135	-	0.197	0.208
16	-	0.305	0.274	-	0.399	0.401
24	0.320	0.308	0.415	0.604	0.433	0.600
36	0.415	0.467	0.675	0.794	0.811	0.825
Cell No 1 B						
Dial Gauge Number						
	4	5	6	10	11	12
4	0.055	0.172	0.000	0.032	0.189	0.192
8	0.146	0.310	0.003	0.210	0.386	0.407
12	0.234	0.445	0.070	0.233	0.419	0.405
16	-	0.555	0.158	-	0.604	0.405
19	0.407	0.658	0.248	0.601	0.786	0.414

Table 6.2 (Cont.):

Cell No 2 A						
Dial Gauge Number						
	13	14	15	19	20	21
8	-	0.150	0.230	-	0.485	0.400
16	-	0.421	0.477	-	0.915	0.815
24	0.723	0.657	0.695	0.873	1.236	1.155
42	0.988	1.097	1.460	1.276	1.756	1.675

Cell No 2 B						
Dial Gauge Number						
	16	17	18	22	23	24
4	0.183	0.225	0.470	0.292	0.295	0.291
8	0.540	0.447	0.784	0.746	0.553	0.430
12	0.870	0.640	0.784	1.148	0.844	0.699
16	-	0.906	0.801	-	1.142	1.029
22	1.460	1.229	1.102	1.875	1.575	1.500

Table 6.2 (Cont.):

Cell No 3 A						
Deflection (mm)						
Dial Gauge Number						
Load (KG)	25	26	27	31	32	33
8	-	0.606	0.318	-	0.431	0.368
16	-	1.145	0.852	-	0.863	0.956
24	0.990	1.545	1.278	0.083	1.235	1.254
42	1.410	2.225	1.908	0.300	1.885	1.835
Cell No 3 B						
Dial Gauge Number						
Load (KG)	28	29	30	34	35	36
4	0.345	0.396	0.241	0.330	0.310	0.039
8	0.816	0.697	0.514	0.687	0.439	0.354
12	1.302	1.051	0.879	0.899	0.717	-
16	-	1.357	1.489	-	0.953	-
22	2.262	1.970	2.003	1.477	1.224	0.950

Table 6.2 (Cont.):

Cell No 4 A						
Dial Gauge Number						
Load (KG)	37	38	39	43	44	45
8	-	0.425	0.278	-	0.176	0.189
16	-	0.752	0.270	-	0.305	0.256
24	0.823	1.063	1.050	0.415	0.367	0.536
36	-	1.618	1.545	0.440	0.567	0.685

Cell No 4 B						
Dial Gauge Number						
Load (KG)	40	41	42	46	47	48
4	0.213	0.245	0.205	0.135	0.055	0.094
8	0.445	0.477	0.532	0.266	0.213	0.315
12	0.692	0.651	0.765	0.435	0.345	0.478
16	-	0.861	1.026	-	0.466	0.839
19	1.008	0.956	1.241	0.654	0.547	0.980

Table 6.3: Comparison of measured deflections with finite element (FE) predictions

Chordwise Station No.	Gauge Position	Measured Deflections (mm)	FE Predictions (mm)
One	1	0.415	0.213
	7	0.794	0.546
	13	0.988	0.695
	19	1.275	0.594
	25	1.410	0.599
	31	0.300	0.627
	37	-	0.492
	43	0.44	0.242
Two	2	0.467	0.484
	8	0.811	1.412
	14	1.097	1.781
	20	1.756	1.509
	26	2.255	1.468
	32	1.855	1.614
	38	1.618	1.292
	44	0.567	0.550
Three	3	0.675	0.560
	9	0.825	1.719
	15	1.46	2.201
	21	1.675	1.854
	27	1.908	1.781
	33	1.835	1.985
	39	1.545	1.594
	45	0.685	0.650

Table 6.3 (Cont.)

Chordwise Station No.	Gauge Position	Measured Deflections (mm)	FE Predictions (mm)
Four	4	0.407	0.491
	10	0.601	1.486
	16	1.460	1.200
	22	1.875	1.755
	28	2.262	1.670
	34	1.477	1.802
	40	1.008	1.425
	46	0.654	0.650
Five	5	0.658	0.339
	11	0.786	0.891
	17	1.229	1.387
	23	1.575	1.401
	29	1.970	1.318
	35	1.224	1.260
	41	0.956	0.936
	47	0.547	0.482
Six	6	0.248	0.257
	12	0.416	0.544
	18	1.102	1.010
	24	1.500	1.195
	30	2.003	1.125
	36	0.950	0.942
	42	1.241	0.633
	48	0.980	0.405

Table 6.4: Track deflections and actuator loads due to applied loads (Phase III testing)

Applied load	Outboard track deflections (mm)		Actuator load (N)
	Loading	Unloading	
0	0.000	0.000	0
+ 16 KG Sand (US)	0.341	0.214	157
+ 18 KG Sand (TE)	0.792	0.453	334
+ 14 KG Sand (TE)	1.232	0.697	412
+ 8 KG Sand (TE)	1.479	1.154	549
+ 6 KG Sand (TE)	1.667	1.228	687
+ 14 KG Sand (TE)	2.051	1.516	746
+ 14 KG Sand (TE)	2.475	1.796	883
+ 14 KG Sand (TE)	2.845	2.021	1020
+ 14 KG Sand (TE)	3.235	2.179	1096
+ 17 LB (Bar)	3.392	2.480	1213
+ 12 KG (Pans)	3.615	2.813	-
+ 40 LB (Weights)	3.884	3.234	1391
+ 40 LB (Weights)	4.328	3.642	1569
+ 40 LB (Weights)	4.605	3.811	1747
+ 40 LB (Weights)	5.023	4.070	1925
+ 40 LB (Weights)	5.477	4.563	2103
+ 40 LB (Weights)	5.549	5.096	2281
+ 40 LB (Weights)	5.827	5.827	2459
264.7 KG (Total)			

US - Upper surface
TE - Trailing edge device

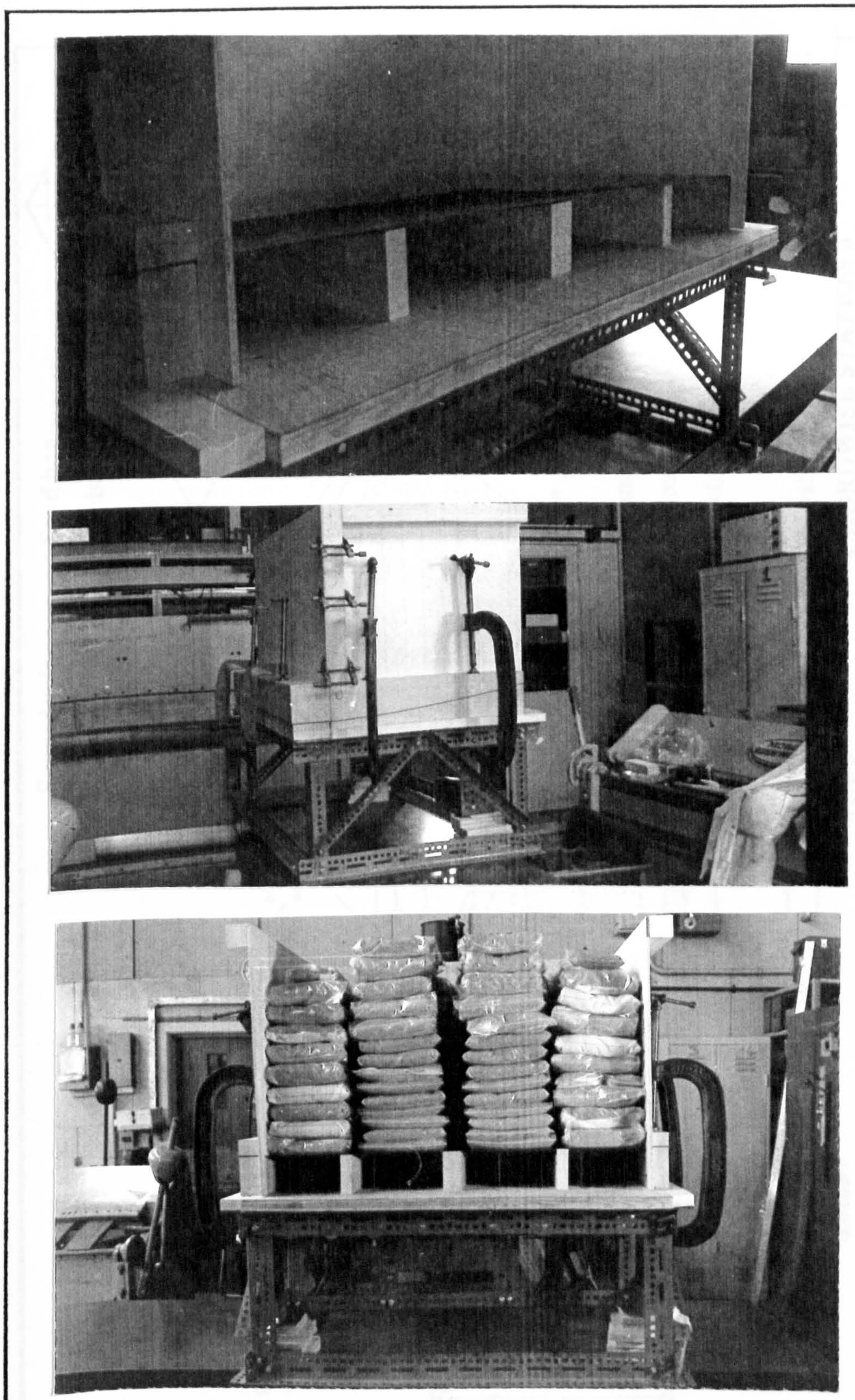

Figure 6.1a: Apparatus for Phase I testing

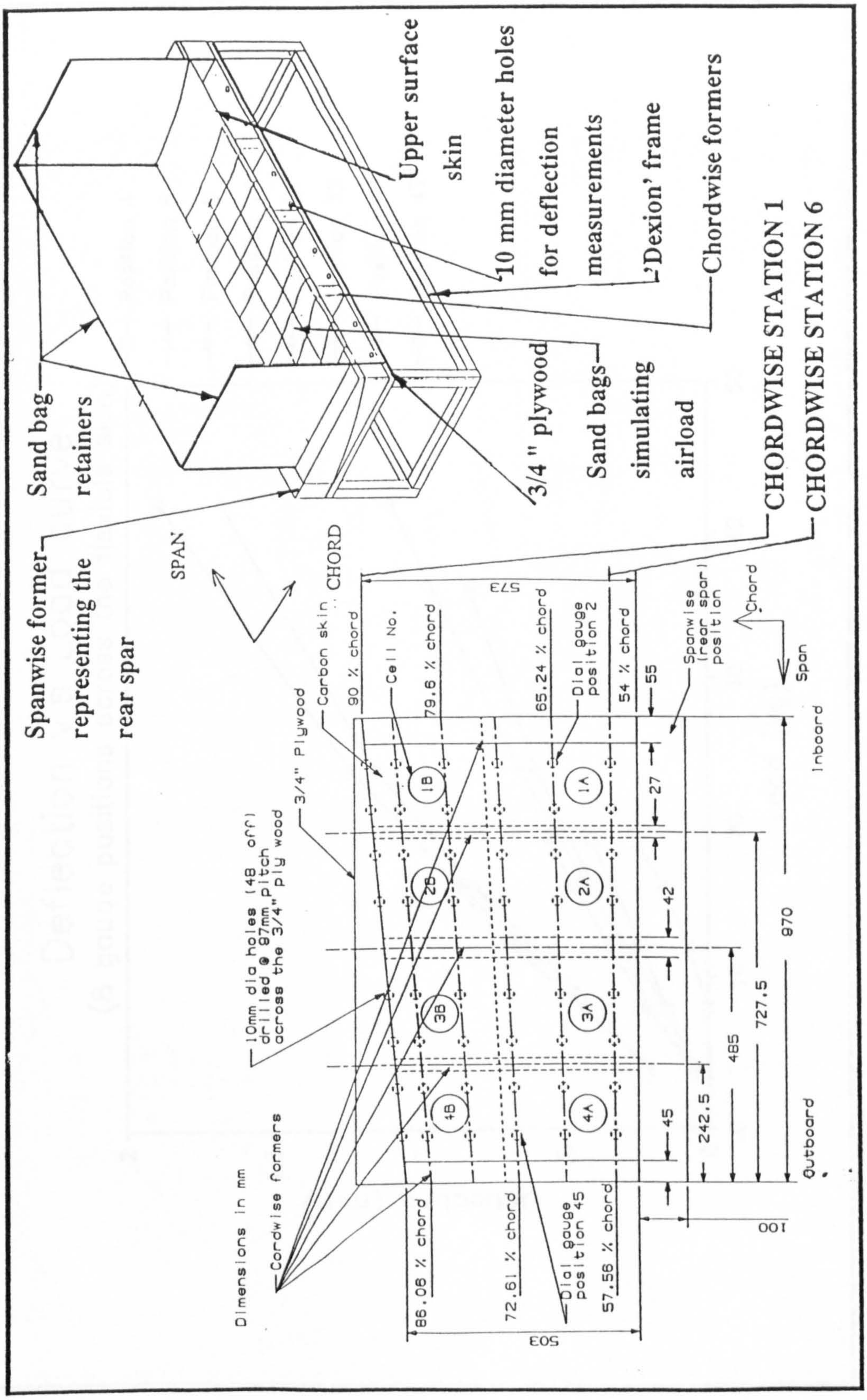

Figure 6.1b: Further details of the set-up for Phase I testing

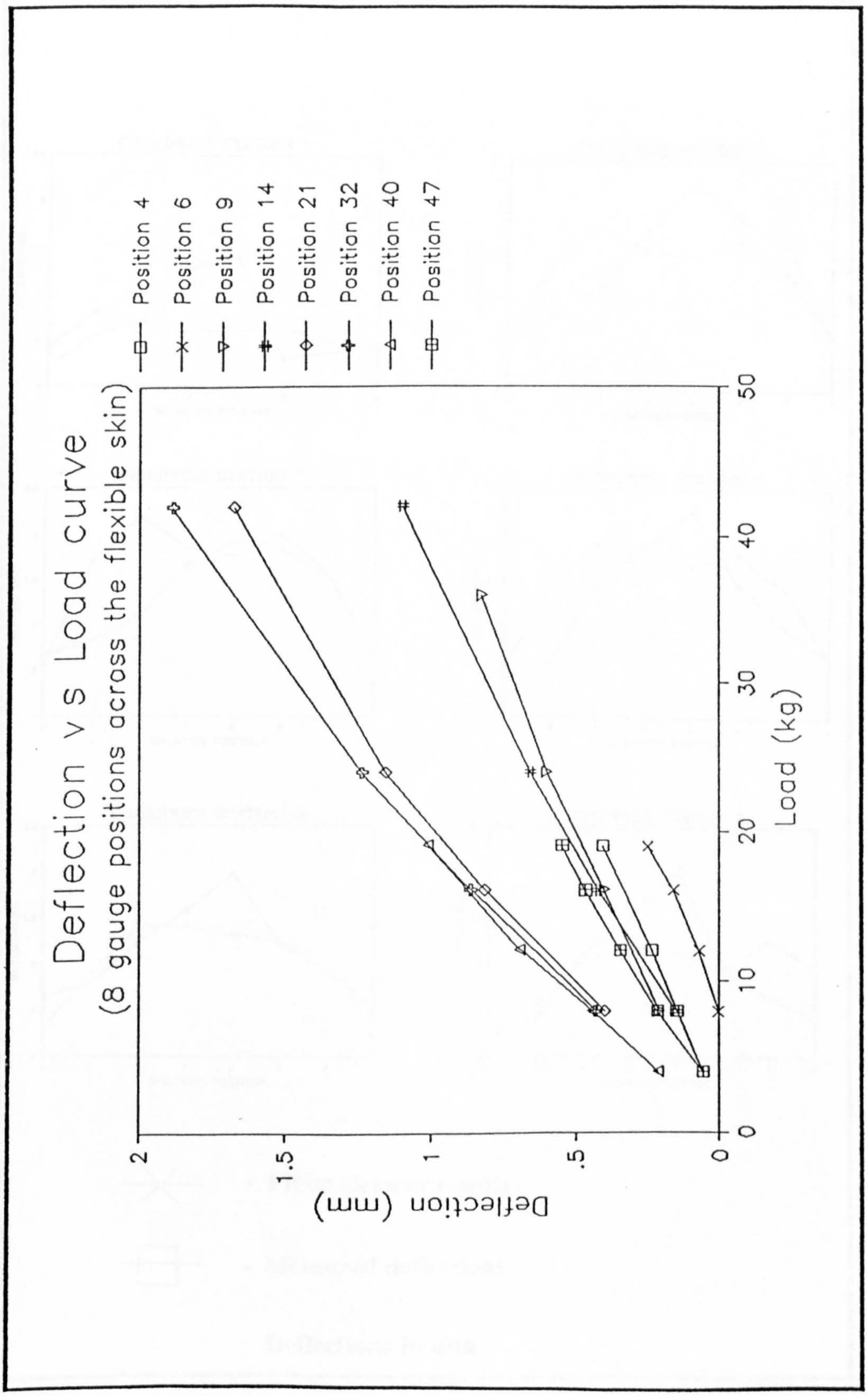

Figure 6.2: Deflection vs load curve for eight dial gauge positions

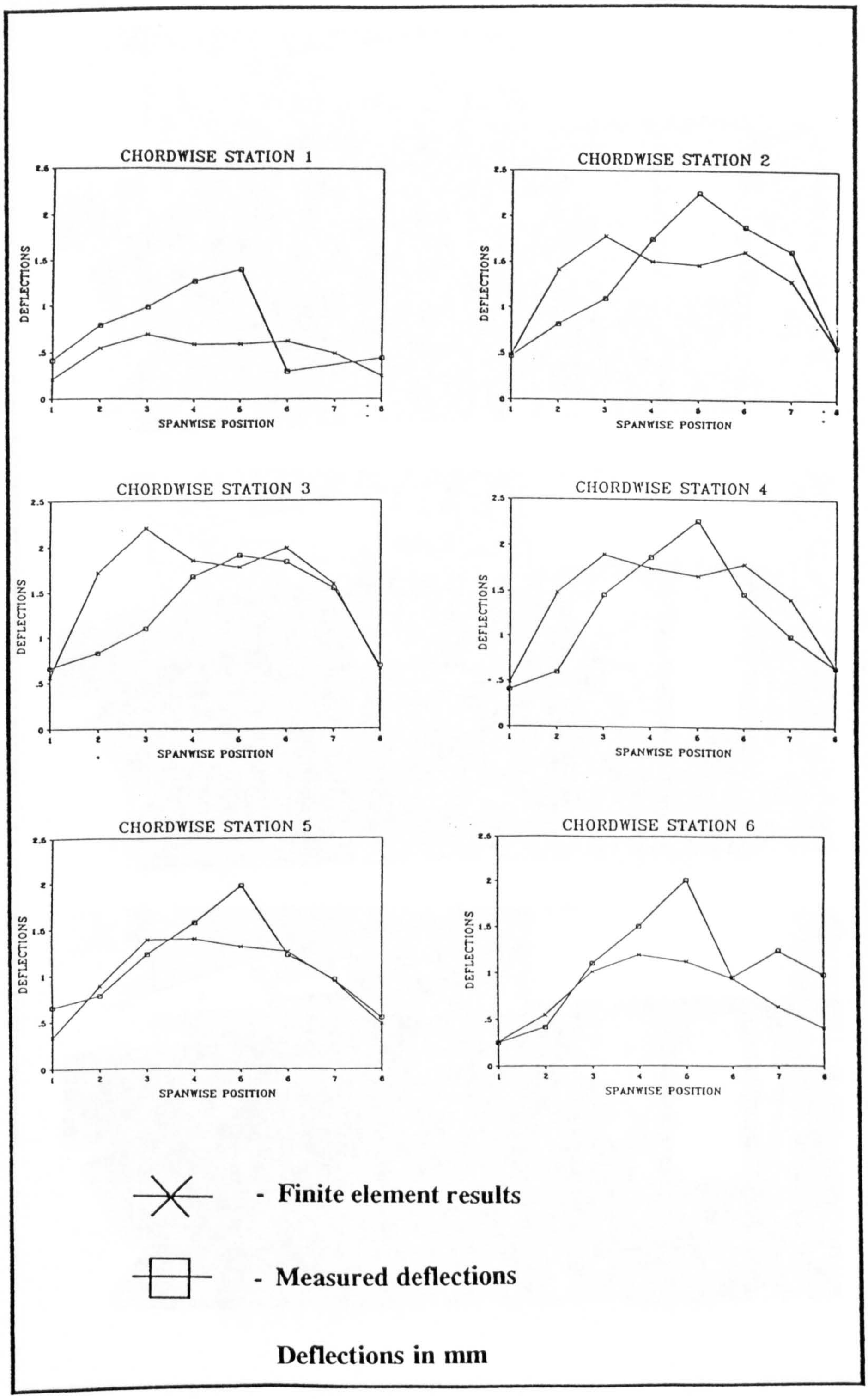

Figure 6.3: Comparison of measured deflection with the FE predictions

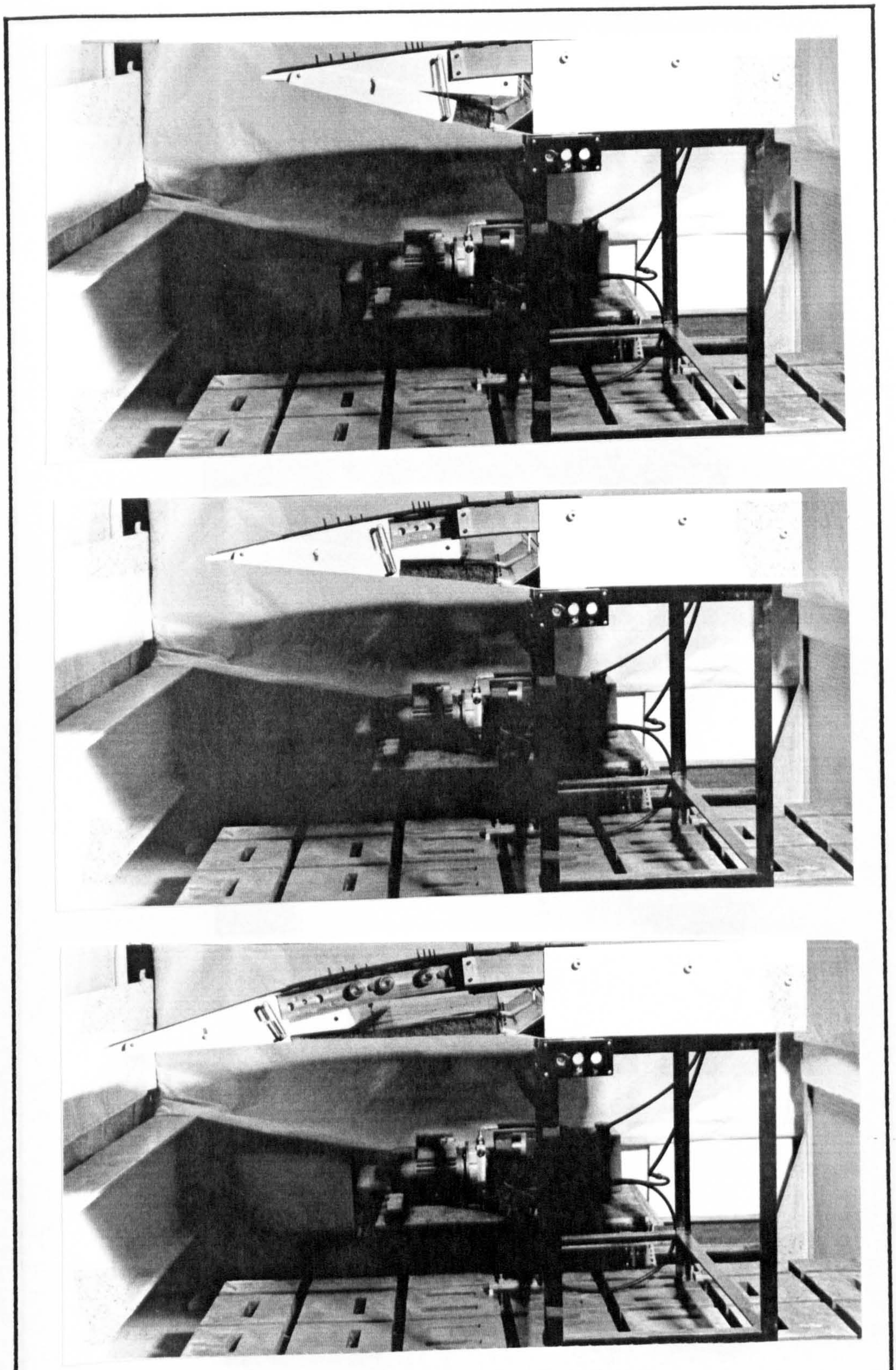

Figure 6.4: Structural model actuated without any loads (Phase II testing)

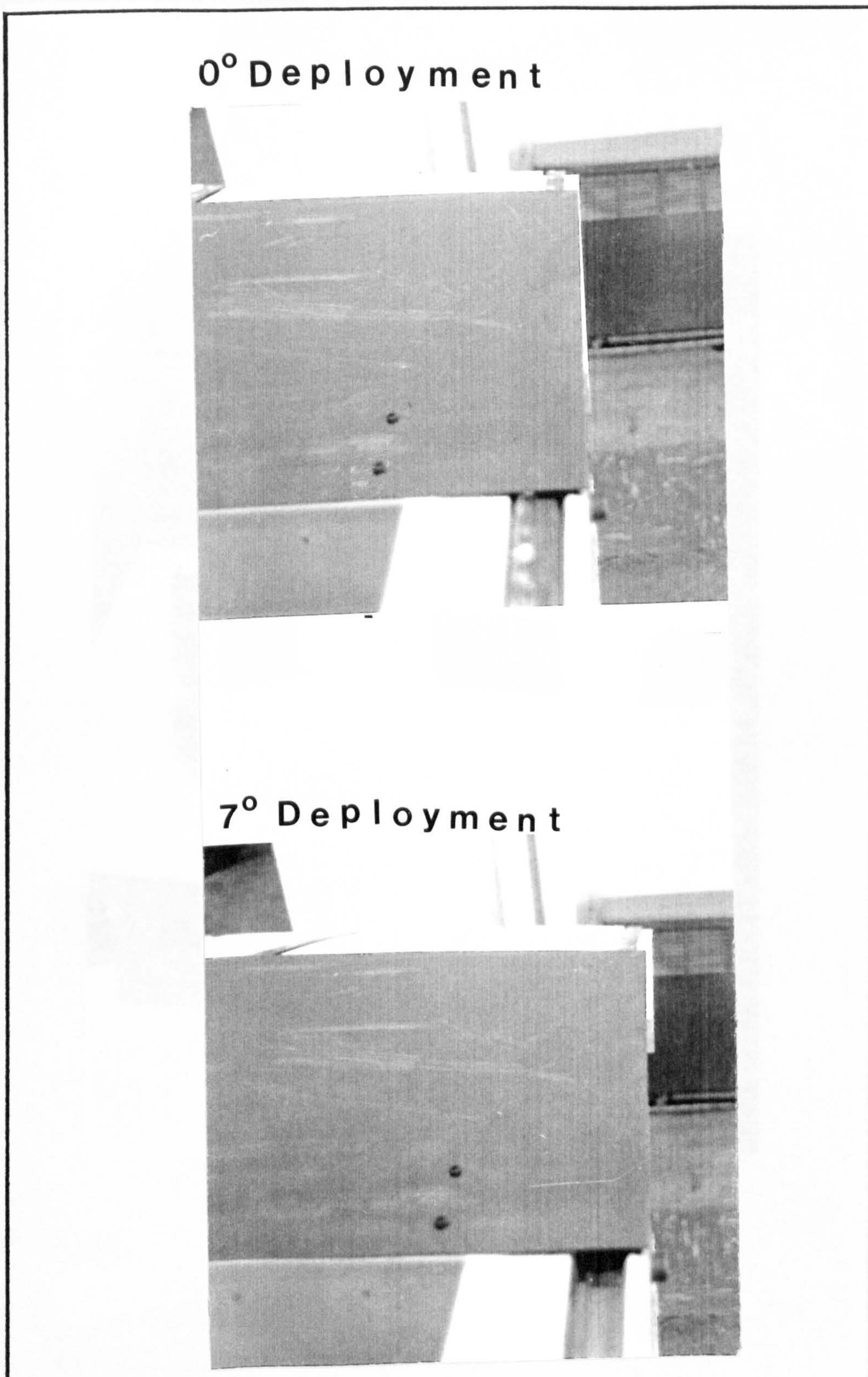

Figure 6.5: Lateral movement of the trailing edge device due to conical deployment

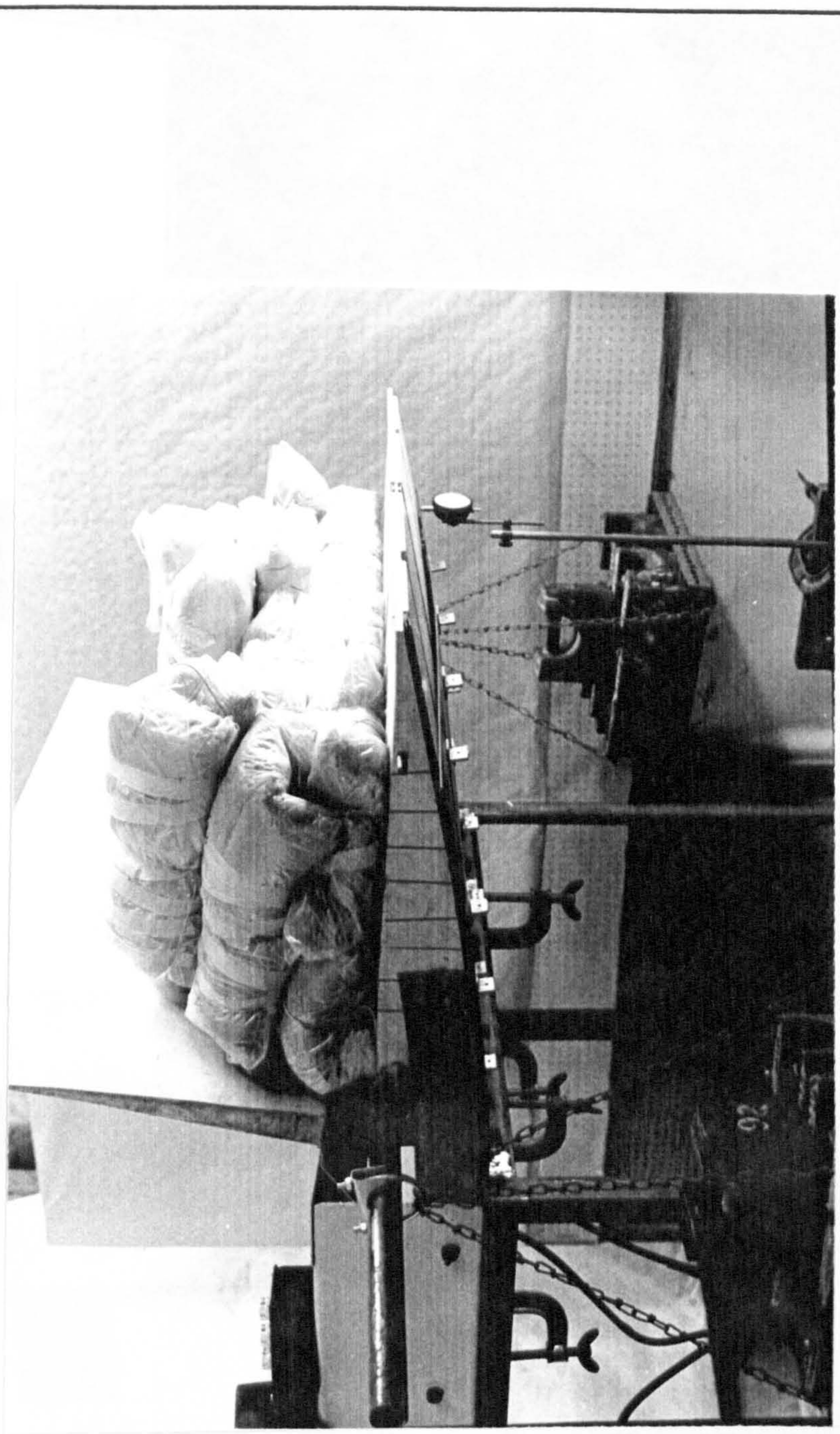

Figure 6.6: Set-up for Phase III testing

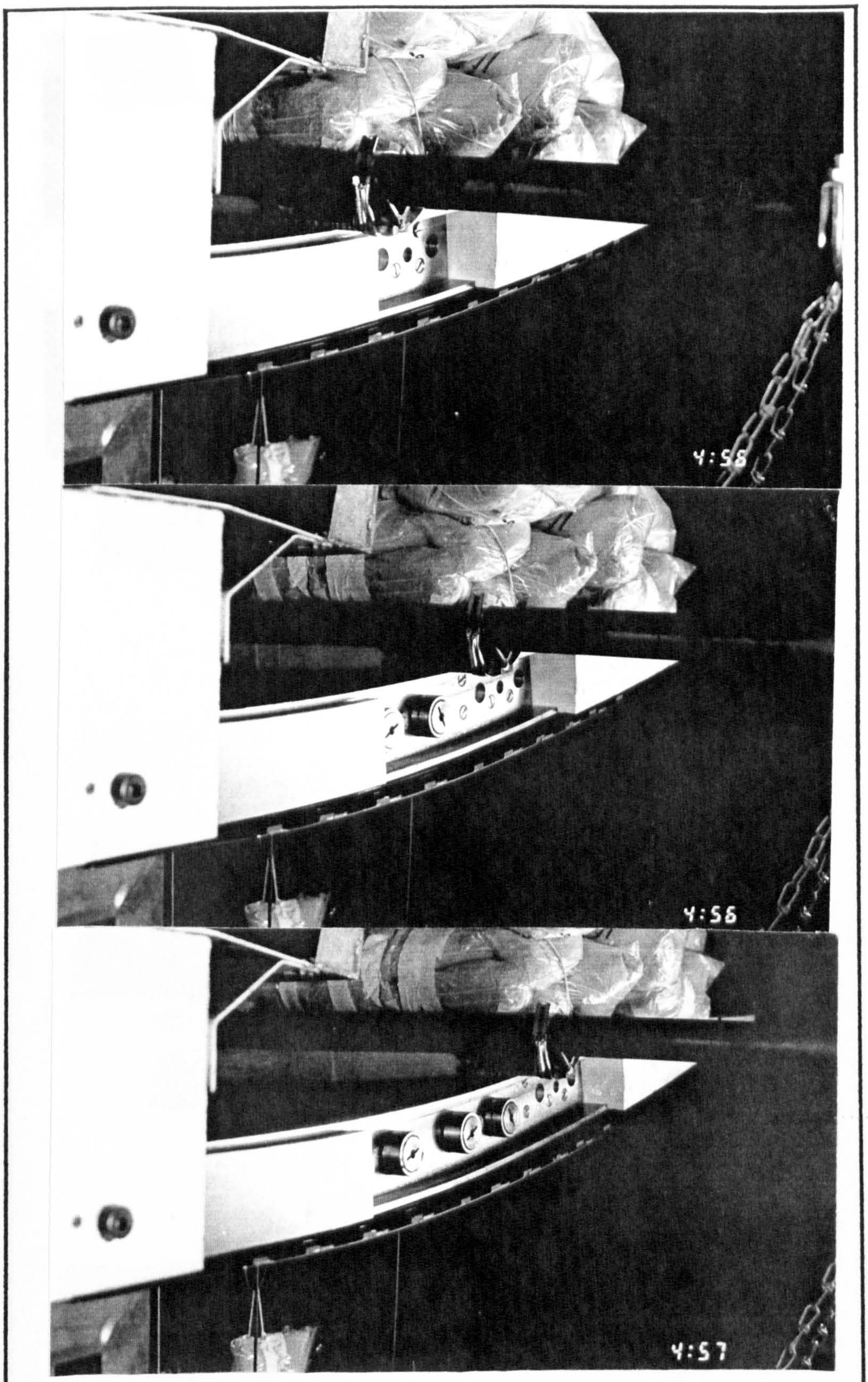

Figure 6.7: Structural model actuated with loads (Phase III testing)

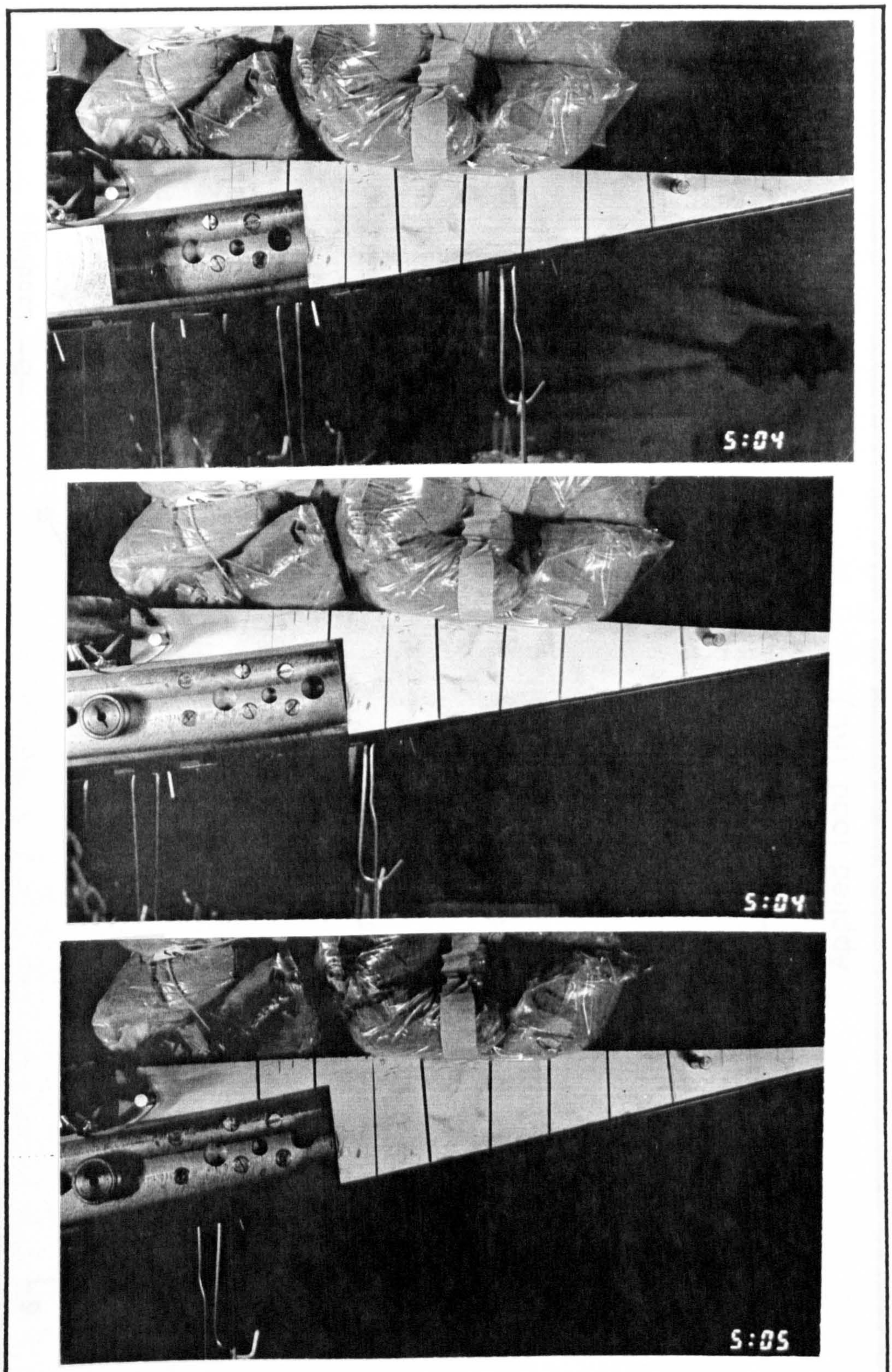

Figure 6.8: Further evidence of deployment under loaded conditions

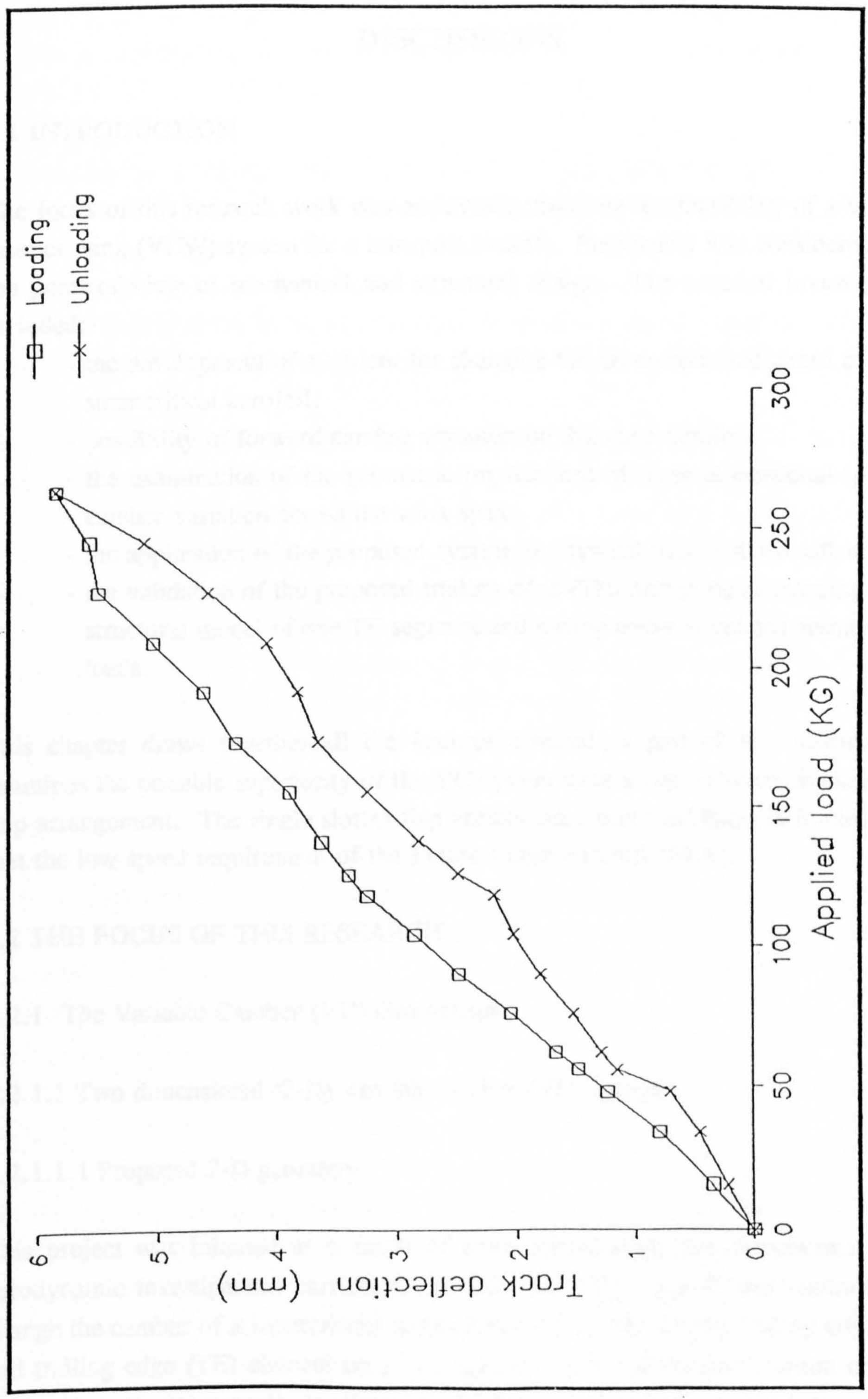

Figure 6.9: Outboard track deflections due to applied loads

CHAPTER SEVEN

DISCUSSIONS

7.1 INTRODUCTION

The focus of this research work was an investigation into the feasibility of a variable camber wing (VCW) system for a transport aircraft. Practicality was considered from the point of view of mechanical and structural design. The areas of investigations included:-

- the development of a system for changing the aft camber and chord of a supercritical aerofoil,
- possibility of forward camber variation on the same aerofoil,
- the examination of the geometric implications of three dimensional (3-D) camber variation across the wing span,
- the application of the proposed system to a typical transport aircraft wing,
- the validation of the proposed trailing edge (TE) design by developing a 3-D structural model of one TE segment and testing under simulated aerodynamic loads.

This chapter draws together all the features covered as part of this research and examines the possible superiority of the VC system over a conventional single slotted flap arrangement. The single slotted flap arrangement was used because it adequately met the low speed requirement of the Future Large Aircraft (FLA).

7.2 THE FOCUS OF THIS RESEARCH

7.2.1 The Variable Camber (VC) Geometries

7.2.1.1 Two dimensional (2-D) variable camber (VC) system

7.2.1.1.1 Proposed 2-D geometry

This project was initiated as a result of some encouraging two dimensional (2-D) aerodynamic investigations carried out in reference [24]. Rao[24] was committed to change the camber of a supercritical aerofoil section by rotating the leading edge (LE) and trailing edge (TE) element on a circular arc. The translational motion of these elements gave increments to the overall chord and thereby helped to provide considerable lift without paying a significant drag penalty. Accepting the arguments to

change the aerofoil profile by increasing the chord, Mackinnon[27] varied the profile of a thicker supercritical aerofoil section in a similar way. The essential requirement was to have a roof-top pressure distribution by maintaining the continuity on the upper surface.

A literature review on the subject suggested that such a form of profile variation has not been studied in the past. Most of the practical ideas that were disclosed accepted the change by simply drooping the forward and aft regions of the aerofoil. These required no chordal extension, but some systems did provide a translational motion to counteract the reduction in chord. An example of such a system is the Royal Aircraft Establishment Variable Aerofoil Mechanism (RAEVAM) concept[4].

The unique VC geometries developed in reference [24] and [27] suggested that for the concept to work practically on a transport aircraft wing the system would have to be radically different from those currently employed. Accepting this challenge, an assessment was made of the geometric and practical implications. This resulted in a design for aft camber variation which utilised the profile developed by the two aforementioned authors. A practical solution was not possible for the forward camber variation with rotational and translational motion of the leading edge (LE) element. It is recommended therefore that in order to relieve the LE suction peaks the LE element should only be drooped. A geometry is proposed which maintains a smooth profile on the upper surface. Initial computational (aerodynamic) investigations[27] suggested that this LE geometry along with the proposed aft geometry (for a supercritical aerofoil) proved to be suitable for providing an ideal roof top pressure distribution. The recommended method for changing the LE geometry is very much similar to a number of ideas that have been developed to-date. These include the RAEVAM[4] and the F-111 MAW[12][14]. In view of this and to give more time to develop the more important trailing edge configuration, further work on the development of a forward camber varying system was not carried-out in this project.

7.2.1.1.2 Alternative 2-D geometries for aft camber variation

The chordwise pressure distribution for the basic aerofoil section and the VC geometry showed that the aerofoil experiences considerable aft loading. The large extensions in chord observed during the aft VC operations induced high torsional stresses into the wing structural box due to the aerodynamic loads acting on the TE device. This is due to the large moment arm between the TE air-load and the centre of rigidity. The structural material required to accept these stresses can be considerable, resulting in

high structural weight and stiff design. This initial uncertainty of the proposed scheme resulted in considering alternative geometries with a reduced torsional arm.

The moment arm may be reduced by either decreasing the radius of curvature (R) or the camber should be varied without increasing the chord. An illustration of these geometries for Aerofoil Section B (see Chapter Two) is given in Figure 7.1 (TESB4) and 7.2 (TESB5).

Decreased chordal extension (TESB4)

For the first of the two methods the TE element is rotated on a circular arc. The position of the point of rotation on the upper surface (A) is set at 90 % chord and the radius to deploy this point is approximately half the value for TESB1. Deflection by this method indicates sharp changes in sectional curvature at A which will allow marked increase in lift at high subsonic speeds but usually with an increase in drag.

The TE element in this scheme is separated by an arc drawn from A to B (Figure 7.1a). A much sharper curvature cuts the rear spar near the wing centre-line, thus allowing a rigid structure on the top side. Deployment can be by means of guide rails fixed to this structure with roller carriages attached to the TE device. A flexible under surface clamped at the rear spar is necessary to keep the underside attached to the TE device. Discontinuities appearing on the underside are unavoidable and are considered to be insignificant.

The VC system shown in Figure 7.1a can be combined with a double slotted flap system. The mechanism for the VC/flap combination can be similar to a conventional double slotted flap arrangement. An example of such an arrangement is the B767, shown in Figure 7.1b.

The under surface can be spring loaded, such that during high lift operation it closes the gap formed between the top surface shroud and the lower side.

From a practical point of view this scheme can be considered to be an ideal solution with the following advantages:-

- A conventional slotted type of flap arrangement,
- Solid and positive drive system,
- Possibility of inclusion of a spoiler,
- Moving elements are all behind the wing rear spar, therefore there is no invasion of fuel space,

- Clamped under surface plate, therefore no kinks,
- The system is not too complex, and
- It is easy to inspect and maintain.

This VC geometry (TESB4) was proposed for the A-90[41], a short haul passenger aircraft with the wing quarter chord line swept at 25°. Pratical design were developed for both the inner wing[42] and the outer wing[43].

Aft camber variation without chordal extension

Elimination of chordal extension is possible by simply preventing any translational motion of the TE element. Figure 7.2 shows the necessary changes made to the VC profile of TESB1 (Figure 2.7b) which accepts zero chordal extension, and at the same time gives a relatively smooth curvature. The extended chord (C_B + C_B') is reduced to the basic chord (C_B) by shifting the deployed section ABC', such that C' lies on the same x/c co-ordinates as C (100 % chord). Point A (maximum curvature) moves across first to A' then to A'' (to match the upper surface at 54 % chord). In doing so, it reduces and changes the shape of the structural box. The centre of rotation for arc A'-A'' shifts from (0.506, -1.5778) to (0.3167, -1.5704). From the structural point of view, although the torque is reduced appreciable, the reduction in structural box area would increase the torsional stresses. Initial calculations suggest a possible increment of approximately 2%.

Continuity between the TE element and the wing box section is provided by flexible skins on both the upper and lower surfaces. Both the skins are fixed to the centre section at one end and at the other end the upper surface skin is attached to the TE device, while the lower surface skin simply sits under the TE device without being fixed.

Detailed design of the mechanism for this geometry has not been considered. It is envisaged that in order to actuate the TE device it would have to be pivoted through a crank arm about the point O. The upper surface skin can be held continuously between the two ends through a series of pivoting links. One end of each link must be attached to the crank arm while the other end can be fixed to the flexible upper surface skin. On actuating the TE device, the pivoting action of the crank arm would push the links accordingly, which would change the profile of the upper surface skin to the required degree. The lower surface can be pushed up or down depending on the movement of the TE device. For high lift a simple drop flap operated independently is

recommended.

Aerodynamically this scheme has the following advantages:-

- Clamped under surface skin, therefore no kinks on the under side, and
- It can be applied to any aerofoil section.

The major disadvantages of this system are:-

- That it requires complex link mechanisms, and
- It necessitates intrusion into the structural box for the support and deployment mechanism of the TE device.

7.2.1.1.3 Comparison of the proposed and alternative concepts

Schemes TESB4 appears to be both structurally and mechanically better than scheme TESB3 (Figure 2.11). Scheme TESB5 appears to be complex and could be unreliable.

The geometries of both the above schemes were designed to seek an alternative structural concept. Camber variation with either of these ideas is not smooth and continuous. Therefore higher camber settings will give higher suction peaks and probably increase the aerofoil drag. It is therefore recommended to test these profiles theoretically before proceeding with these designs.

7.2.1.2 Three dimensional (3-D) camber variation

This is possible by dividing the LE and TE control devices into several spanwise segments. It was found that the ideal in-line of flight deployment of these segments is not possible. This is due to the tapering and sweep effects of the wing. The resulting investigations proved that if the rotational and translational motion is combined then the deployment of the VC system must be on a conical hinge-line, i.e the segments must ride on a frustum of a cone. Both the structural and mechanical impracticality of achieving such a motion, and the aerodynamic drawbacks with possible increases in the overall drag, suggested that a slightly modified deployment programme is necessary. Hence the segments of the proposed aft VC scheme are deployed parallel to the wing ribs (see Chapter Four). These ribs are placed perpendicular to the angle of sweep of the hinge-line.

It is suggested that the TE devices for the proposed scheme should be made to twist and flex along the chord to allow for the differing track radii at the two ends of each

segment.

The suggested method of varying the camber along the span will of course suffer from aerodynamic disadvantages (increase in profile drag) since the segments are all skewed to the line of flight. This aspect must be investigated aerodynamically before attempting to pursue the proposed design. The system is satisfying if the adjacent segments are deployed at the same angle. The problem arises when two adjacent segments are at different VC settings.

The alternative geometries presented above in Section 7.2.1.2 must also allow for these 3-D effects. The extra link mechanisms required to flex the TE devices of the TESB5 (Figure 7.2) and conically warp the flexible surfaces of the TESB4 (Figure 7.1a) will most likely be complex and heavy. The flexible upper surface will require support along the intermediate span positions. This will further increase the complexities of this idea. The change in profile of the TE device support structure on the second scheme (due to flexing of the box across the span) will introduce manufacturing difficulties.

7.2.2 Application of the Variable Camber Wing (VCW)

Details are given in Chapter Four of an aircraft selected as a typical candidate for the application of the VCW concept. The chosen aircraft was the Future Large Aircraft (FLA), sponsored by EuroFLAG (see Appendix A). The detailed design of the proposed aft camber varying scheme suggests that the system is very simple provided that the TE device structural box can be made to twist without a complex link mechanism.

Three of the major benefits of installing such a system are:-
1) Improved performance and therefore reduced fuel consumption,
2) Operational flexibility, and
3) Load relief due to atmospheric gusts and high 'g' manoeuvres.
Further explanation of these is given below:-

<u>Improved performance and operational flexibility</u>

From an aerodynamic point of view it is expected that the cruise performance of the FLA will improve considerably by including the VC system (assuming that the skewness of the TE device segments does not increase the drag). Evidence of such an improvement is given in Figure 7.3 and 7.4. Where Figure 7.3 depicts the variation

in lift coefficient (C_L) against incidence and Figure 7.4 shows the lift to drag (L/D) ratio for VC settings of 0, 1 and 2 degrees at high speed Mach no of 0.74. These were derived by converting the 2-D computational information supplied by Mackinnon[27] using ESDU sheets[38]. It was assumed that the change in profile across the wing was made with all the six segments. It is apparent from Figure 7.4 that the L/D ratio increases with increase in aft camber. The maximum L/D ratio for the aircraft with the basic wing is 18.68 (see also Appendix A). With 1° camber setting across the wing span the L/D ratio rises to 21.8.

In Appendix A an estimation is made of the approximate fuel mass required by the FLA using the Braguet range equation. This equation shows how the range of a transport aircraft is very much dependent on the L/D ratio. Evaluation of the equation suggested that the ratio of aircraft mass at the start of cruise to the aircraft mass at the end of cruise (M_1/M_2) is 1.1546. By increasing the L/D ratio to 21.6, M_1/M_2 drops to 1.13. This results in 16% reduction in fuel consumption. With the improved performance it is therefore possible to increase either the payload mass or the cruise range if the maximum gross mass is to be maintained. Studies carried-out by Greff[22] suggest that camber variation through a fowler motion on a long-range aircraft configuration gives 4% improvement in L/D ratio. Even though the system shown suffers from a mild discontinuity on the upper surface.

A common practice in the design of a transport aircraft is to use the wing structural box for fuel storage. It is therefore suggested that the bulk of the fuel for the FLA should be stored in its wings. One of the main reasons for following this practice is that the inertial loads (particularly at high 'g' case) continuously help relieve the wing from excess bending moments caused by the aerodynamic loads. It is envisaged that by reducing the fuel mass due to improved performance, the inertia loads will also be reduced. This will result in increased structure mass which is required to carry the bending loads (particularly near the root regions of the wing). The extra bending moment must therefore be relieved by further utilising the VC system. Such a situation may result in a complex control law which will require a command input to optimise the L/D ratio and simultaneously optimise the load distribution across the wing span. These feature must be studied and quantified in order to justify the advantage offered by the VC system in improving the performance.

During its mission the weight of an aircraft decreases as it burns fuel. Thus for 1 'g' flight the aircraft lift reduces either by reducing the lift coefficient (C_L) or by reducing the dynamic pressure. For an optimum flight it is best to maintain a cruise C_L. In

order to achieve this it is often the case to increase the cruise altitude (decreasing density), i.e cruise climb. Drag decreases with decrease density so L/D ratio remains constant. Furthermore, engine power decreases with reduced air density and so Thrust/Drag balance is kept without changing engine setting. From air traffic control point of view it is believed that cruise climbing can be a source of concern. With the VC system the aircraft can operate at optimum L/D ratio and therefore no restrictions need be imposed on altitude, since it can slot into any air space.

Load distribution

Figure 7.5a represents a unit load distribution on the FLA wing in its basic uncambered configuration. Such a distribution is normally associated with a wing that is flying at an incidence without the deflection of control surfaces, such as the high 'g' gust conditions and pitching manoeuvres. Double integral of this distribution curve (which is elliptical) from tip to root gives a unit bending moment of 0.43 near the wing root region. This effectively represents the position of the spanwise centre of pressure (i.e bending moment /load).

One of the main assets of the VC system is that it can be used for manoeuvre load control (MLC) and gust load alleviation (GLA). To achieve these the centre of pressure must be shifted inwards. For example to relieve the maximum bending moment (BM) for a 2.5 g manoeuvre case such that it is equivalent to a 1.5 g case the spanwise centre of pressure (C of P) must shift to (1.5 x 0.43) / 2.5 = 0.258 semi-span. The load distribution associated with this shift in C of P will be similar to that depicted in Figure 7.5b. Such a distribution can only be possible by applying a low or negative camber near the tip region while nearer the root the camber must be increased. Figure 11 in Appendix F gives a concrete evidence of variation in spanwise camber attainable to suite the required C_L. It is assumed that the type of spanwise variation shown could certainly be possible on a wing the size of the FLA wing. Full justification of this requires translation of the experimental data[27] by virtue of considerable amount of calculations.

7.2.3 Comparison of the Proposed (VC) System to a Conventional Single Slotted Flap Arrangement

Preliminary calculations on high lift requirement suggested that the FLA will require a conventional single slotted TE flap and a LE slat (see Appendix A for details). The span of the TE flap system was assumed to be split in to three segments. The size of

these segments is the same as the span of the three inboard VC segments (discussed in Chapter Four). The outboard track design suggested for the intermediate TE flap is given in Figure 7.7 (this segment has the same span as segment five on the VCW of the FLA). Estimates were made of the loads experience by the flap. These together with a few stressing calculations resulted in the proposed scheme. The flap was assumed to be supported on three flap tracks made in Titanium along its span via rollers. Each flap track is mounted off the rear spar and roller carriages are fixed on chordwise flap ribs. All the tracks protrude outside the basic aerofoil and therefore require cover fairings.

Comparison of the flap system shown in Figure 7.7 with the proposed VC system suggests that the latter is much cleaner in the undeployed position and also when all the segments are set at the same deployed setting.

Estimated mass of the outboard track for the flap scheme is 63 kg while for the VC system it is 146 kg. Detailed design of the flap and the TE device structural box have not been carried out, but it is assumed that their masses are likely to be of the same order. It is also likely that the overall mass of the two system will be very much the same. The total flap span of the conventional slotted arrangement will include the mass of the cover fairings and nine track systems (three per flap segment). With the VC system the predominantly heavy structure will be the six tracking systems. A complete comparison of the two systems can only be made once the flap system has been designed in detail. It is recommended therefore to accurately assess the number of segments required for the total flap span and the number of tracks need per segment and their positions.

In terms of mechanical complexity the VC system suffers from the requirement to hold the upper surface skin down continuously. To achieve this a track roller arrangement is proposed. This system will obviously be prone to contamination and probable jamming if not protected. Furthermore the continuous operation of the system will require considerable attention and maintenance. Complexity will further increase if the TE device structural box includes link arrangements for providing adequate twist. As a result it is likely that the structural weight will also increase.

With the conventional flap design the apparent complexity is in the design of the tracking system. The tracks are shaped to allow the flap to take three positions. These being the nested (0°), deployed for take off (10°) and deployed for landing (30°). To have relatively small tracks the pitch between the front and rear roller has to be fairly small. The change in flap motion during deployment and the distance between the

rollers may lead to lack of free movement and probability of roller sticking. The track system of the VC design would not suffer from this since the roller pitch is fairly high and the motion is on a continuous arc.

The proposed design for the VCW also realises the following advantages over a conventional system:-

- It is a single control system across the span, therefore there is no requirement for an aileron, extra high lift units and spoilers for low speed roll control. Inclusion of these on a conventional wing will result in additional weight,
- The design can be made fairly conventional,
- The system can be used for gust load alleviation (GLA) and manoeuvre load control (MLC).

It is important to note however that roll control may be inadequate, even with the total asymmetric distribution of the VC system.

The proposed VC system requires tracking system which invades the fuel space. Initial estimation of the available fuel volume by taking into account 10% reduction due to this invasion suggest that there is sufficient space for the total fuel needed for maximum range.

7.2.4 Design and Testing of a Trailing Edge (TE) Variable Camber (VC) Structural Model

The development of the VC system into a structural model justifies the potential of the VC concept. Cost limitation resulted in several assumptions and 'shortcuts' for designing and manufacturing the model. These include:-

- The TE device which had to be made in laminated wood, and
- The design of the conforming rails.

Discussions with regard to conical deployment suggest that the spanwise variation in camber is possible by warping the TE segment. In order to have adequate flexibility in both the chordwise and spanwise directions, the TE device should be made from a carbon or equivalent composite fibres. Such a system requires considerable amount of detailed design study from the point of view of both stiffness, strength and fatigue aspects.

An alternative scheme for achieving conical deployment is by introducing pin jointed arrangement such as that shown in Figure 7.8. Double pin joint fittings are placed between the extending track and the TE device at the inboard (I/B) and outboard (O/B)

ends of the segment. The varying track radius at the two ends will cause the TE device to move laterally along the span (I/B to O/B). For the same reason the vertical deflection of the I/B end of the segment will be more than the O/B end. The vertical pins will allow the TE device to move laterally, while the horizontal pins should assist the vertical pitching movement. The rails required at the intermediate span positions (not shown) to conform the upper surface skin will be fixed to the laterally moving TE device. These rails must therefore be shaped such that they ride on a frustum of a cone. The system shown in Figure 7.8 is an idea that was briefly considered during the latter part of this project. Development of this scheme has therefore not been possible. It is thus recommended that this scheme along with the warping box idea previously discussed should be designed in detail to assess the potential of spanwise camber variation.

It can be argued that the static test set up for measuring the upper surface skin deflections is not a good representation of the actual situation. The purpose of this test however was not to simulate the actual loading and environmental conditions. It was necessary to devise a simple and cost effective way to measure the skin deflections which could then be compared with a similar finite element (FE) model. The intention was to gain confidence in the FE analysis such that, for future work the upper surface skin will not require further deflection tests. Indeed the results for the both the static tests with the sand bags and the FE analysis do show a good correlation. In any case the design of the conforming strips and the retaining elements (sliding tags) proved to be inadequate to fully load the upper surface skin while it was assembled as part of the structural model. Furthermore it was necessary to design the upper surface such that it had adequate stiffness. Of course the exercise would have no value if simply a thin sheet were to be used for the upper surface skin which flexed with ease. By choosing what is believed to be an appropriate material and lay-up (for the scale and size of the TE segment), a considerable effort was required to change the skin profile with the conforming strip and sliding tag arrangement. In comparison with the conforming track and link roller arrangement, proposed for the FLA wing, this system suffers from high friction due to large contact area.

For future work it is suggested that the upper surface skin should be appropriately loaded during the operation of the structural model. This will require a good design for the rollers and fittings that help maintain a curvature on the upper surface skin.

The success of the proposed concept of varying the camber depends heavily on the continuous attachment of the upper surface skin to the TE device. Ideally it is

necessary to monitor this by applying representative loads to the upper surface while operating the system continuously. Figure 7.9 illustrates one possibility of carrying out such a test. The model is mounted inverted with a set of compression springs pulling the upper surface skin. For appropriate load distribution, springs of different stiffness could be used. The tension in the springs will vary as the TE device is deployed. This could therefore be used to increase or decrease the loading on the upper surface skin as per requirement.

Also shown in Figure 7.9 is a technique to load the TE device with varying load along the chord. A set of rams are placed along the chord at several spanwise stations. These are fixed to a frame at one end while the other end pushes the TE device. The frame can be made to translate on a rail during camber variation. It therefore requires actuators (possibly two) which have the same stroke as the actuators used to deploy the TE device. Ram pressure to load the TE device could be varied to suit the chordwise pressure distribution associated with the change in camber.

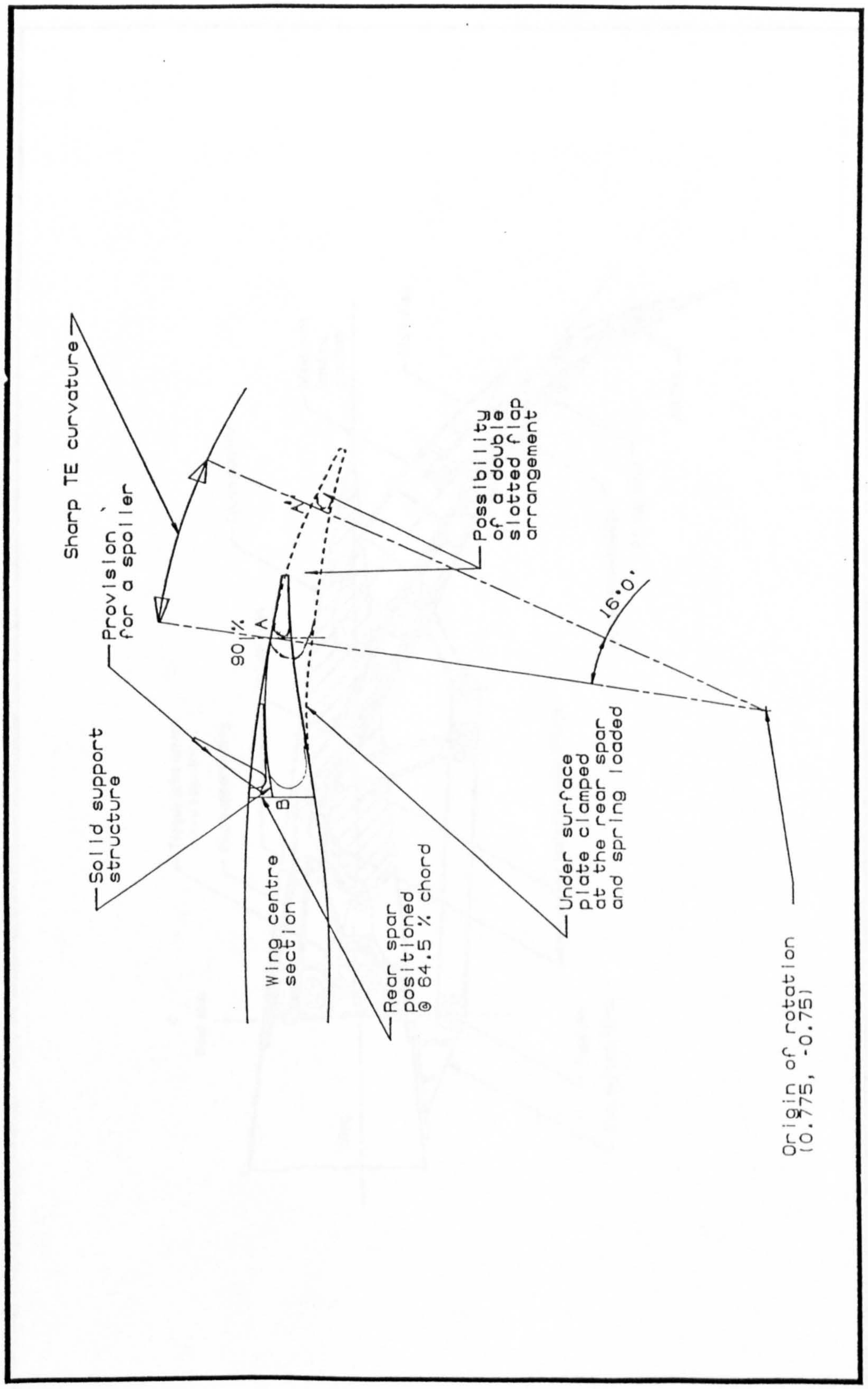

Figure 7.1a: Trailing edge variable camber geometry on Section B with reduced extension - TESB4

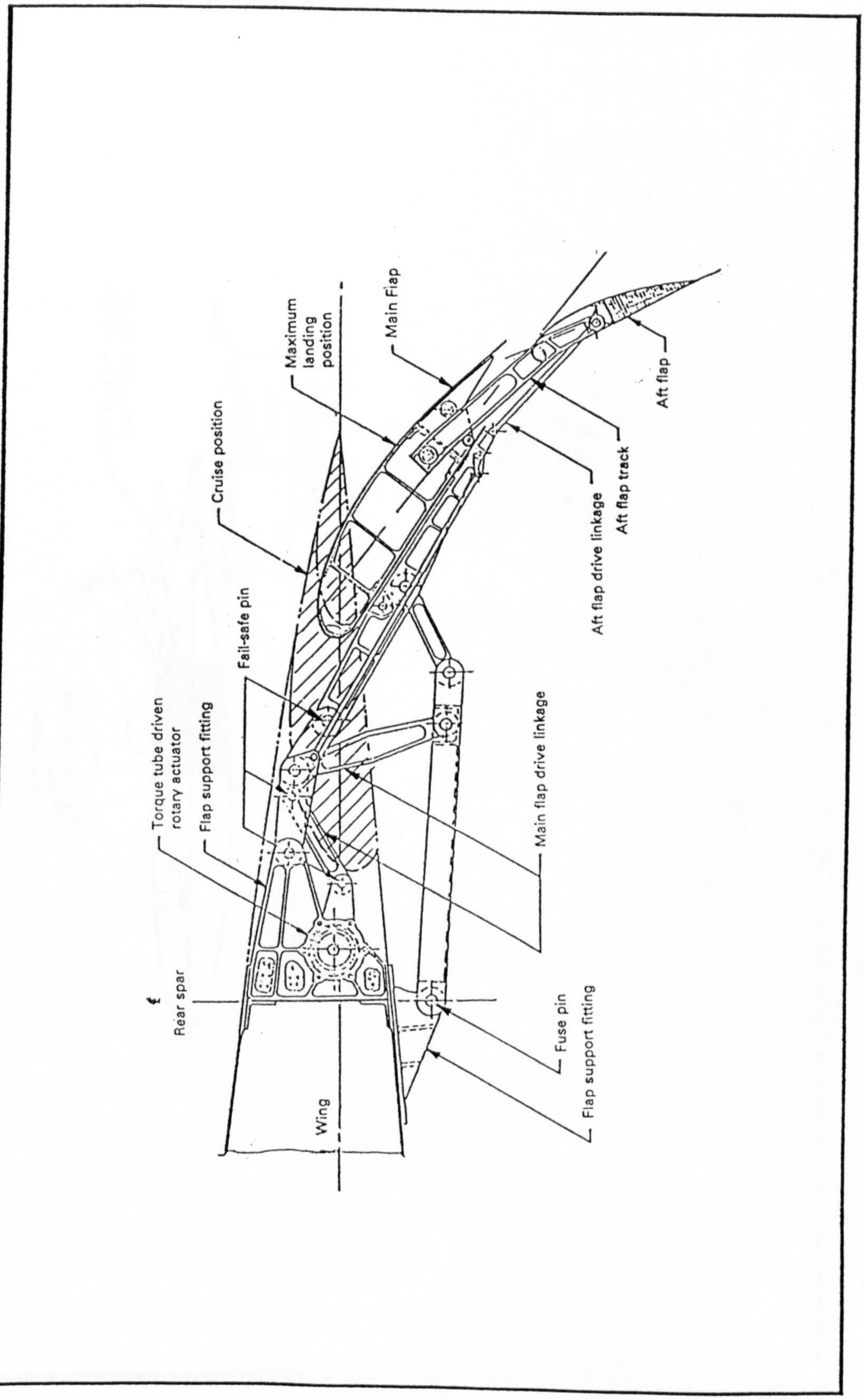

Figure 7.1b: Double slotted flap system for B767

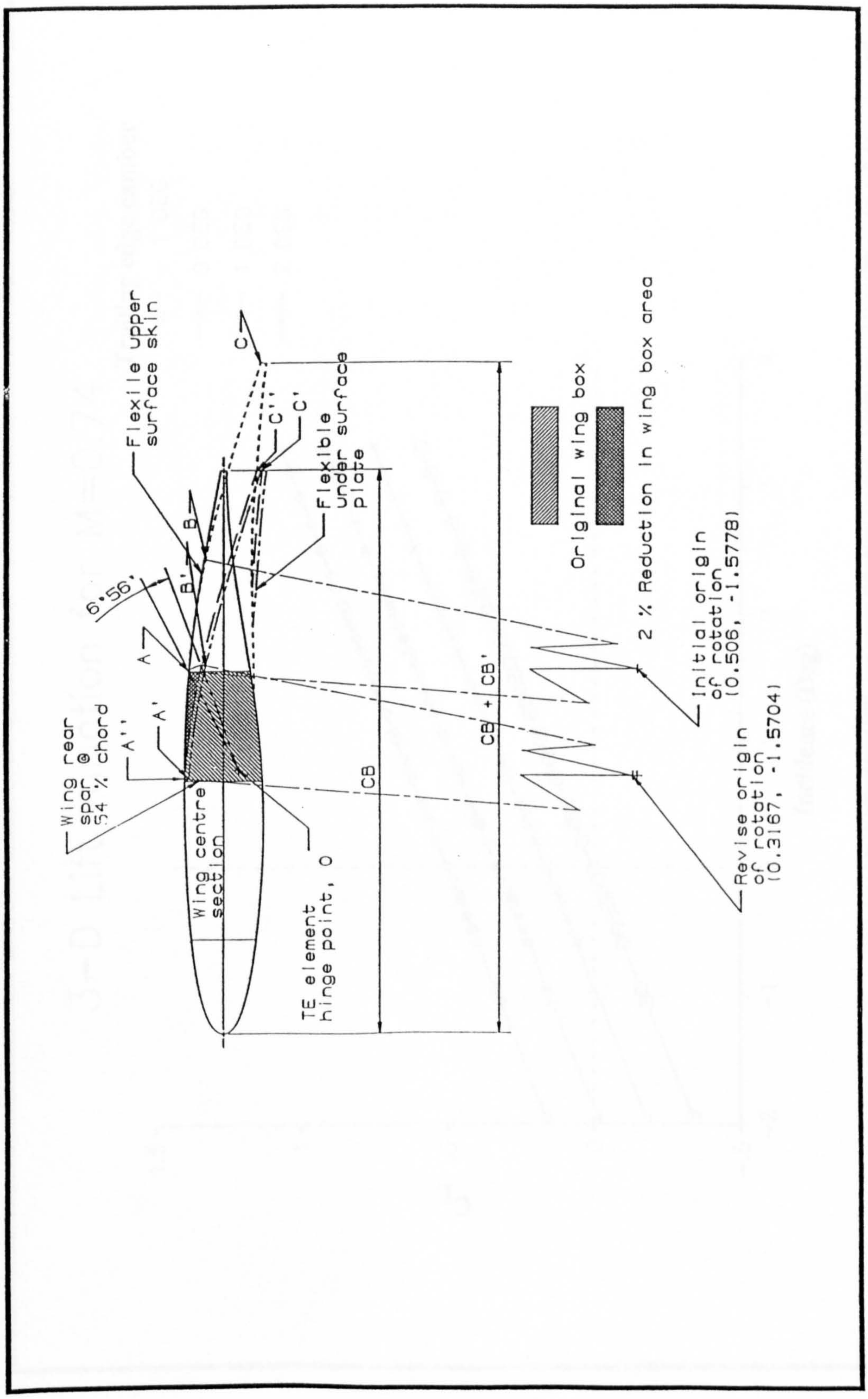

Figure 7.2: Trailing edge variable camber on Section B by drooping the aerofoil - TESB5

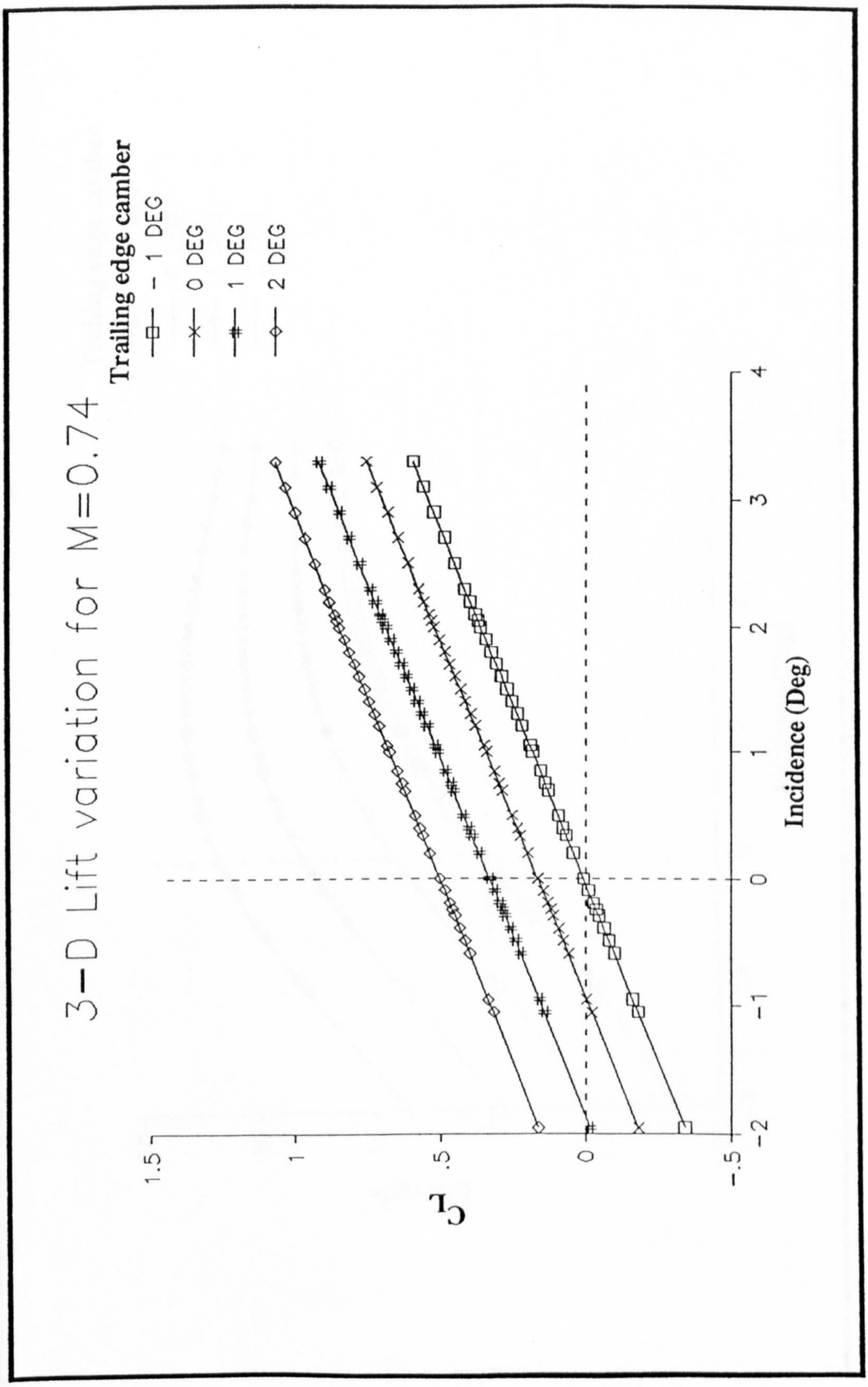

Figure 7.3: Variation of C_L with incidence for different camber settings at high speed cruise conditions

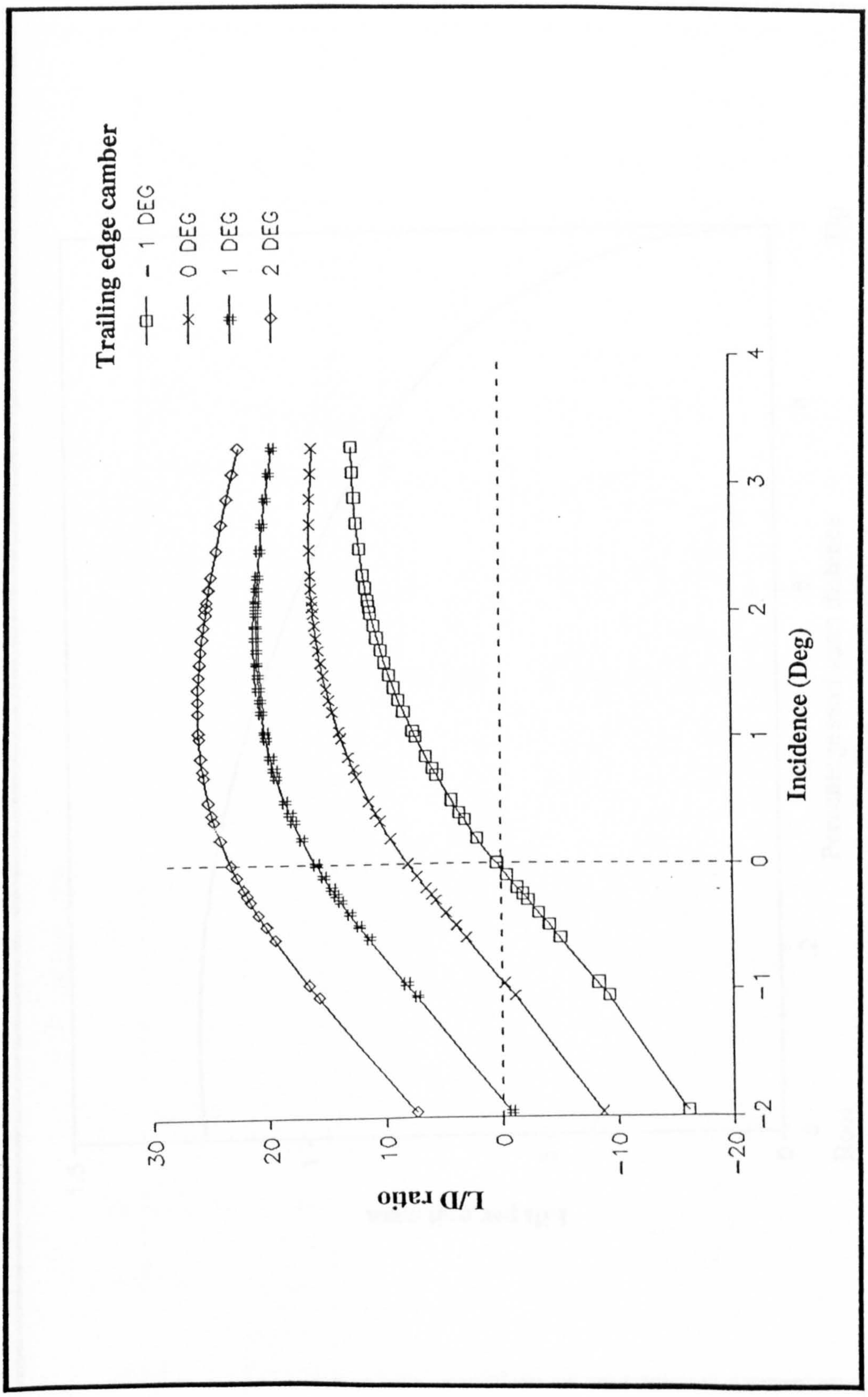

Figure 7.4: Variation of L/D ration with incidence for different camber settings at high speed cruise conditions

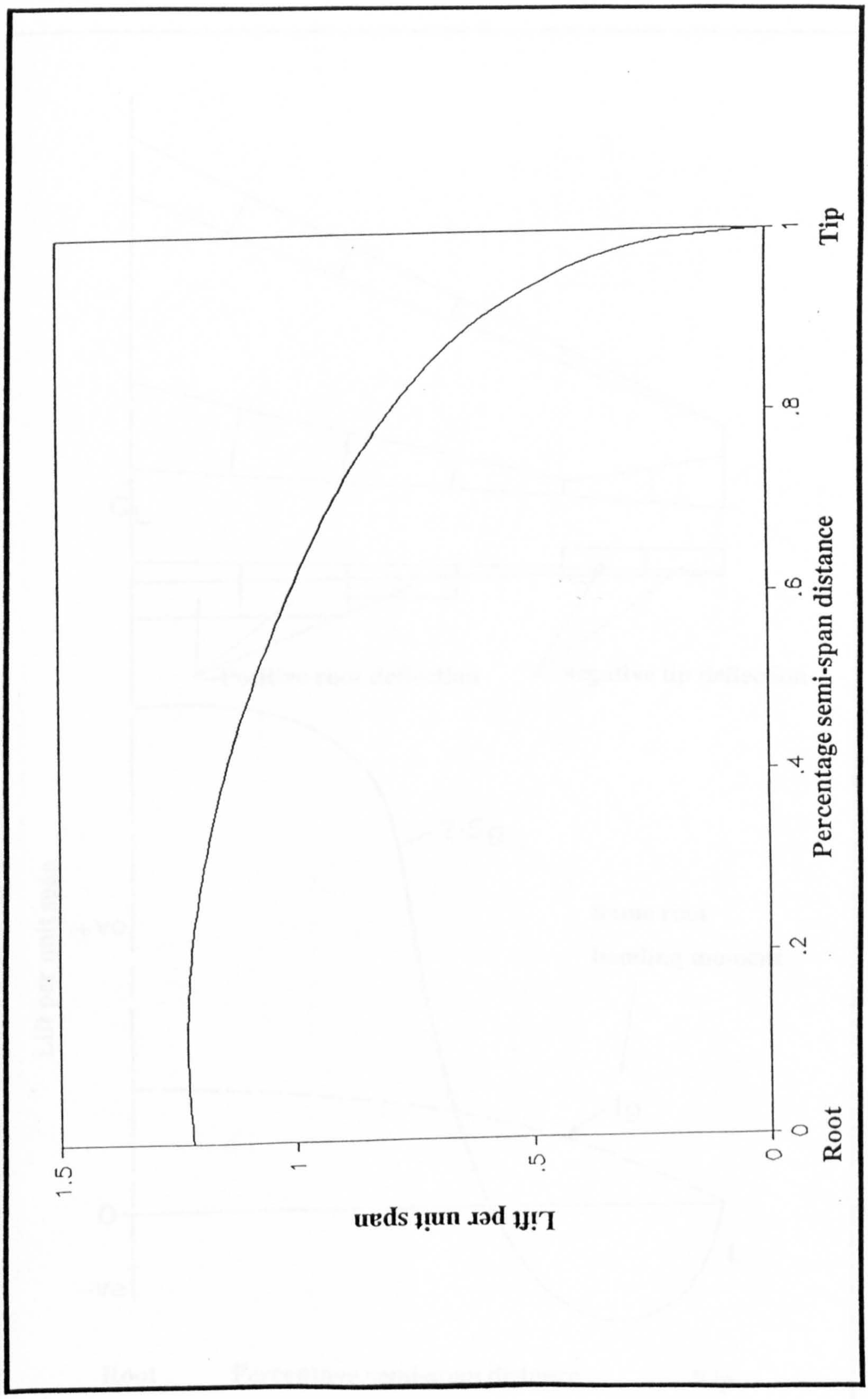

Figure 7.5: Unit airload distribution due to wing incidence

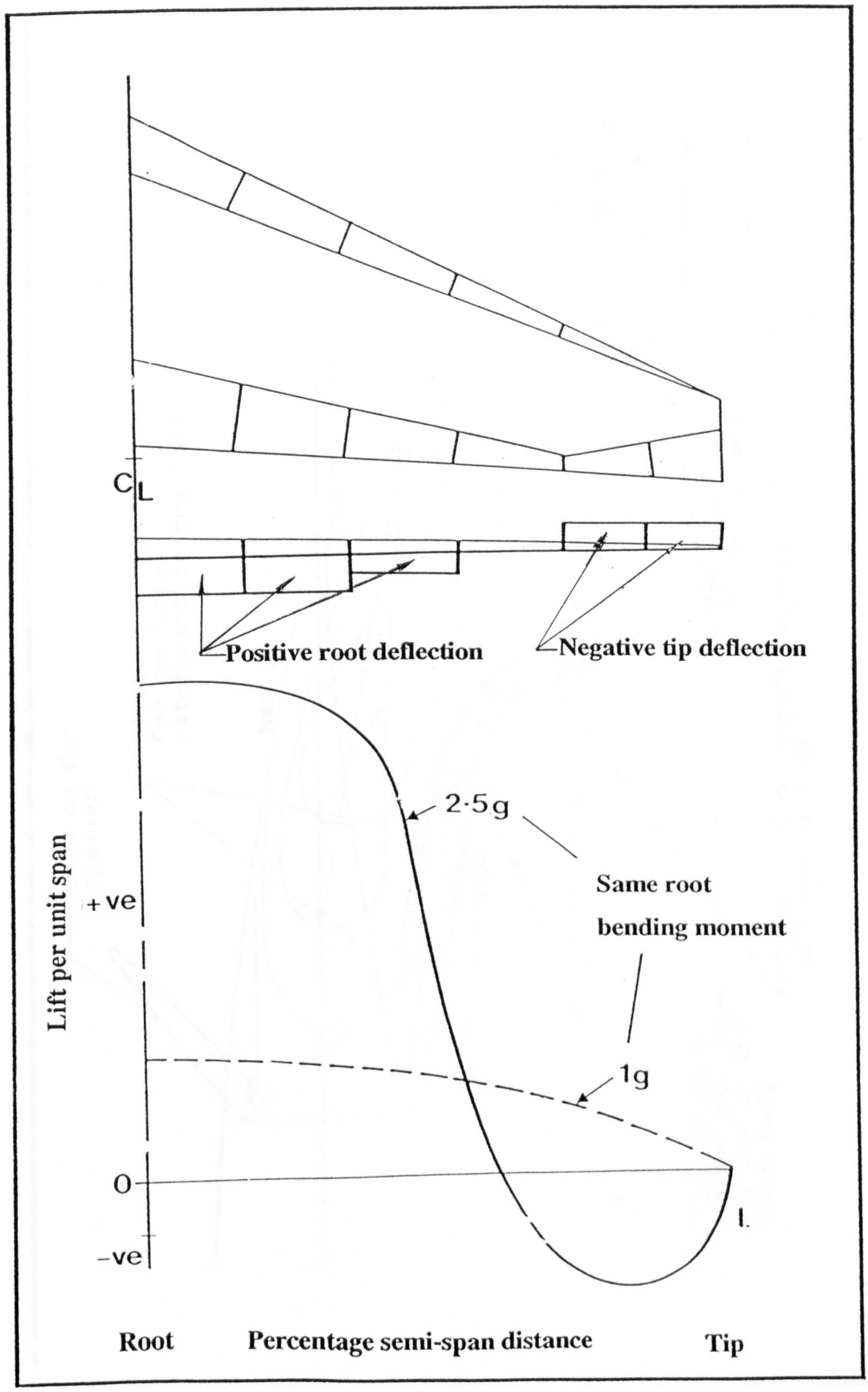

Figure 7.6: Unit airload distribution due to spanwise variation of camber

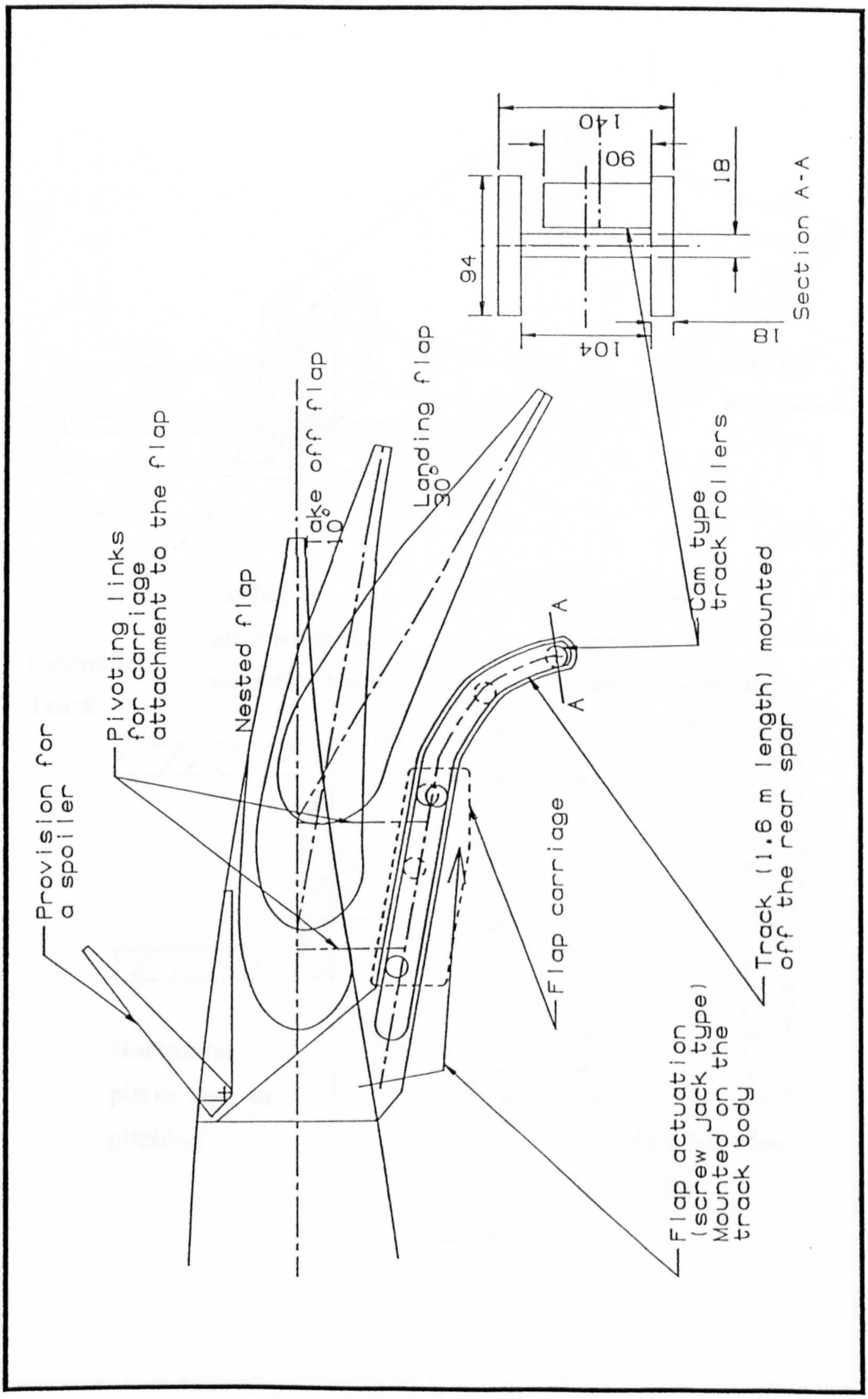

Figure 7.7: Track design for a conventional single slotted flap arrangement

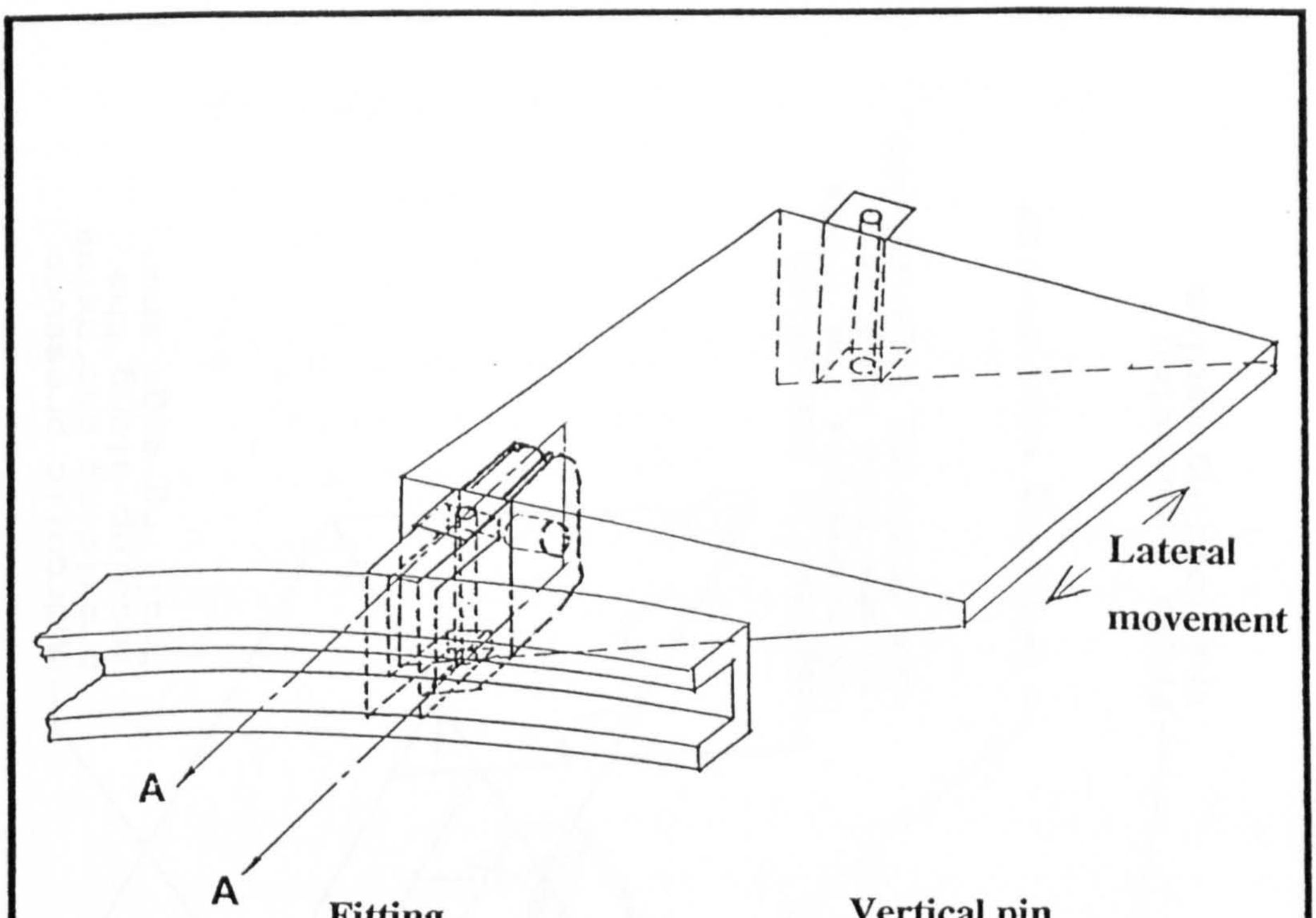

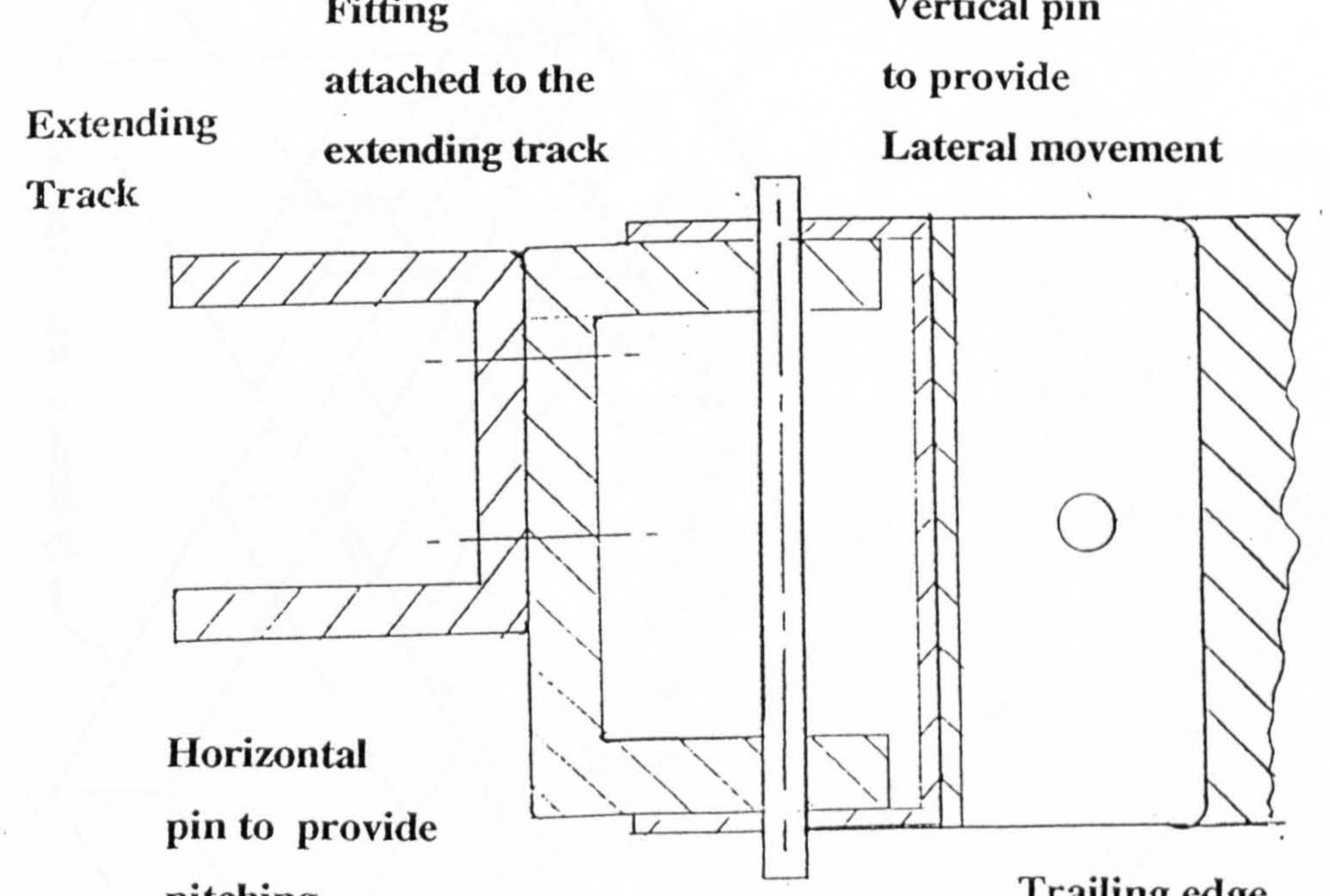

Figure 7.8: Conical deployment with pin jointed arrangement

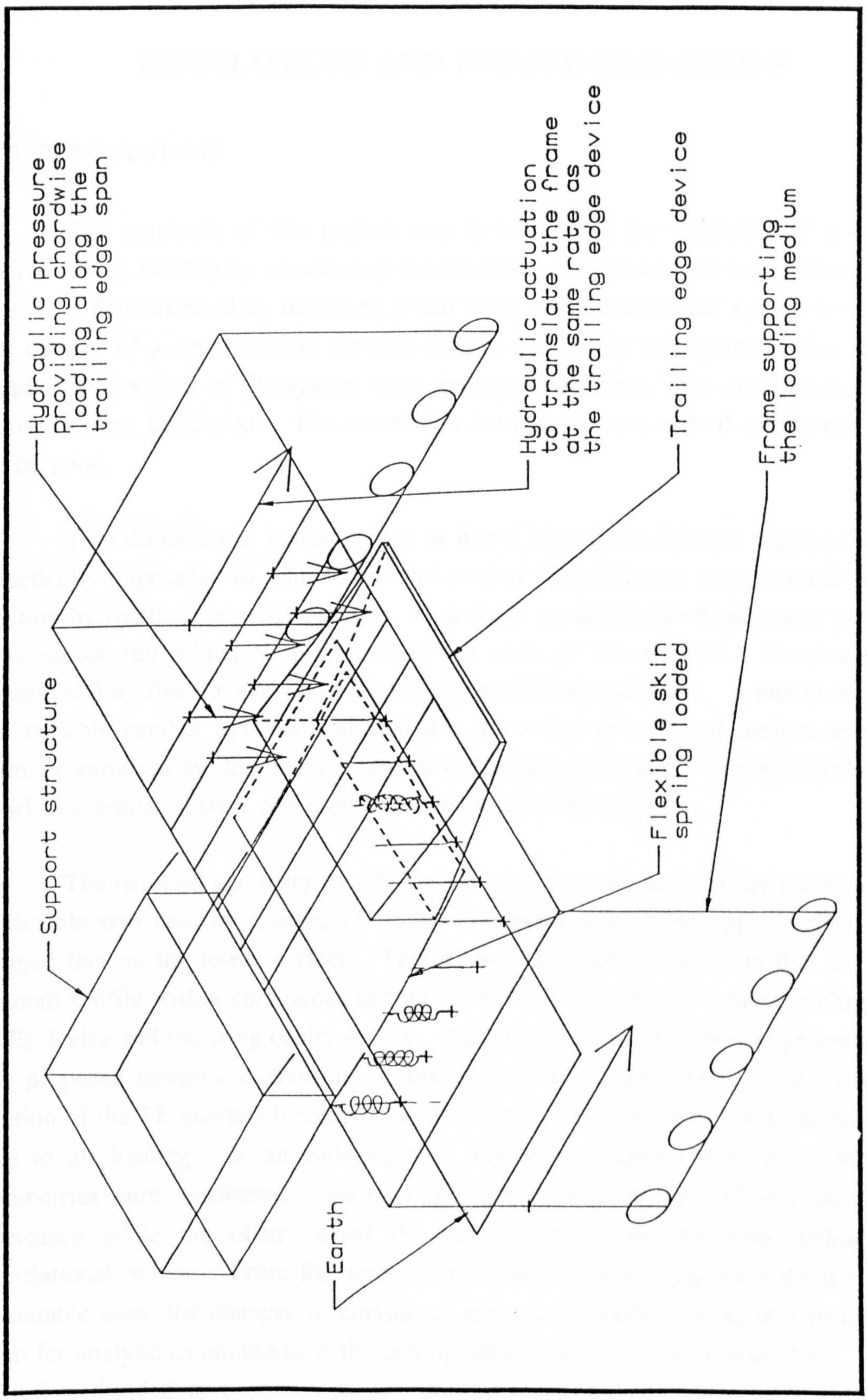

Figure 7.9: Method suggested for continuously applying loads to the structural model during its operation

CHAPTER EIGHT

CONCLUSIONS AND RECOMMENDATIONS

8.1 CONCLUSIONS

1) The emphasis of this project was to investigate the feasibility of a variable camber wing (VCW) by considering the structural and mechanical implications. This has been demonstrated by designing a half scale three dimensional system to vary the aft camber of a super critical aerofoil section and testing this system under realistic loads. Deflections of the system were measured and these were compared with the finite element predictions. The correlation between the two sets of results was found to be good.

2) Two dimensional investigations to find a kinematics solution suggest that it is practically impossible to achieve forward camber variation on a super critical aerofoil section by rotation on a circular arc. As a result an alternative deployment geometry was considered which simply drooped the nose of the aerofoil. Continuity was maintained by flexible skins on both the upper and lower surfaces. A literature survey on variable camber systems indicated that a number of practical designs accepting camber variation by this method have already been developed. Further development work for similar system was therefore not immediately necessary.

3) The required geometry for aft camber variation was successfully maintained by a flexible skin held by a series of rollers in a guide rail on the upper surface and a hinged flap on the lower surface. The method developed is novel in that it gives a smooth profile with a continuous curvature between the variable camber trailing edge (TE) device and the wing centre section. Full details of the deployment geometry and the proposed design are given in Section 2.2.1.2 of Chapter Two. The translating motion of the TE element increased the moment arm and therefore the torsional stress due to aft loading. In an endeavour to reduce the moment arm, two alternative geometries were considered. One provided camber variation through reduced radii of curvature while the other varied the camber by simply drooping without any translational motion. From the aerodynamic point of view these were thought to be unsuitable since the changes in curvatures were not smooth. There was insufficient time for analytic examination of the aerodynamic changes in the current study. It was therefore decided to postpone further development work on these ideas until such information was available.

4) Three dimensional geometric investigations showed that spanwise camber variation through ideal in-line of flight deployment of camber controlling devices was not possible on a typical transport aircraft wing that is swept and tapered. The required profile can only be obtained by conically deploying the aforementioned devices which must ride on a frustrum of a cone. The rotating elements must either be made to flex in both chordwise and spanwise directions or they must be supported on a pin jointed arrangement.

5) Comparison of the proposed VC system with a preliminary design of a conventional single slotted flap arrangement for the same aircraft suggests that the new VC system is mechanically simple. The mass of the two systems could be of the same order.

6) Estimates made of the possible performance improvements by applying the proposed variable camber system to this aircraft suggest a 16 % reduction in fuel consumption.

8.2 RECOMMENDATIONS FOR FUTURE WORK

Some further development areas which can be pursued as part of the continuing research effort towards the development of the variable camber wing (VCW) system, to ensure it's practical and economical viablity, are now discussed:-

1) The proposed geometry for varying the camber forward of the front spar requires a design scheme. The solution must be studied in detail and possibly manufactured for testing under loaded conditions.

2) The proposed concept for the aft (behind the rear spar) camber variation can only work with parallel deployment. In doing so the true conical profile across the wing span is not retained. Such motion is acceptable provided that the TE element is made to flex. The design of the TE device in laminated wood for the structural model accepts this to a certain degree. In order for the system to be practical it is recommended that the TE should be made in composite fibre reinforced plastic (FRP).

The scheme shown in Figure 7.8 suggests a possible alternative for conical deployment with pin joint arrangement. This scheme must be pursued further by considering the detail design aspects of the fittings.

Comparison of these two systems is necessary such that a lighter solution with minimum complexities is realised

3) Practical designs are required for the two alternative deployment geometries for aft camber variation.

4) The continuous operation of the system under loaded conditions needs further justification. This requires an appropriately designed track roller system for changing the upper surface skin profile (similar to the design suggested in Chapter Four).

5) Fatigue testing along with reliability analysis (systems assessment) is needed to quantify possible effects due to contamination and degradation of material properties (particularly the composite upper surface skin).

6) An optimisation program is required to size the VC segments by considering:

i) The aerodynamic requirement (from the point of view of ideal load distributions to suit all flight conditions), and

ii) The structural and practical aspects, i.e flexural deformation, redundancy and fail safe, engine position, etc (see also Chapter Four).

7) The advantages offered by the VCW in terms of operational flexibility suggests that aircraft can be designed with a common wing. However there can be marked differences in the number (and position), size and type of engines required for operating through varying range of flight missions. With the application of the VC concept a study needs to be conducted to assess the engine integration.

8) Kinematics of high lift devices combined with the VC system require detailed assessment, i.e the design possibilities of the control mechanism required to operate the VC system and an auxiliary flap.

9) Successful operation of the variable camber wing concept depends on automated computer controls. Assessment of the systems requirement (which must be fail safe with considerable redundancy) must be made to establish the practical possibility of continuously changing the wing profile.

10) Detailed comparison of the direct operating cost, mass and performance must be made with conventional control system if the variable camber system is to be justified.

REFERENCES

[1] **Spillman, J. J.** A New Approach to Wing Design. Aerogram, Vol 4 No. 1, Cranfield Institute of Technology, 1985

[2] **Gould, D. K.** Variable Camber Wings. Home Built Experimental Aircraft, Theory and Practice, Proceedings of the Symposium, 1975

[3] **Cole, J. B.** Airplane Wing Leading Edge Variable Camber Flap. Boeing Commercial Airplane Company

[4] **Pierce, D. Treadgold, D.** A Simple Mechanical System to Vary a Wing Section Shape to Suit Various Flight Conditions. RAE Technical Memorandum (TM) Aero 1149, 1969

[5] **Moss, G. F. Haines, A. B. Jordan, R.** The Effect of Leading Edge Geometry on High Speed Stalling. Conference proceedings on Fluid Dynamics of Aircraft Stalling, AGARD-CP-102, 1972

[6] **Rowarth, R.** Variable Camber Wing. United Kingdom Patent No. 20593684, 1980

[7] **Brown, S. T. Statkus, F. D.** Variable Camber Aircraft Wing Tip. United States Patent No. 4429844, 1984

[8] **Cole, J. B.** Variable Camber Leading Edge Assembly for an Aerofoil. United States Patent No. 4706913, 1987

[9] **Ishimitsu, K. K.** Mechanisation and Utilisation of Variable Camber in Fighter and Attack Airplanes. Boeing Airplane Company Report No. D180-15377-1, 1973

[10] **Gould, D. K.** Variable Camber Wing - Phase I-Final Report, Boeing Airplane Company Report No. D180-17606-1, 1973

[11] **Davice, D. F.** Development of Variable Camber System for a Supercritical Wing. AFFDL-TR-76-65, 1976

[12] Gilbert, W. W. Mission Adaptive Wing System for Tactical Aircraft. J Aircraft Vol 18 No. 7, 1981

[13] Moore, M. Frei, D. X-29 Forward Swept Wing Aerodynamic Overview. AIAA Applied Aerodynamic Conference, AIAA-83-1834, 1983

[14] Moxon, J. Mission Adaptive Wing. Flight International, Vol 128, 10th August 1985, pp 22-25.

[15] Boeing Commercial Airplane Company. Assessment of Variable Camber Wing for Application to Transport Aircraft. NASA CR 158430, 1980

[16] Hill, T. G. Variable Area, Variable Camber Wing for Aircraft. United States Patent No. 3904152, 1975

[17] Sharrock, B. Variable Camber Wing. United States Patent No. 4361299, 1982

[18] Sharrock, B. Halliday, D. P. Aircraft Wing and Flap Arrangement. United States Patent No. 4395008, 1983

[19] Hilbig, H. Wagner, H. Variable Wing Camber Control for Civil Transport Aircraft. International Council for Aerospace Science 1984, ICAS-84-5.2.1. pp 243-248.

[20] Renken, J. H. Mission Adaptive Wing Control System for Transport Aircraft. AIAA 3rd Applied Aerodynamic Conference, AIAA-85-5006, 1985

[21] Szodruch, J. Hilbig, R. Variable Wing Camber for transport Aircraft. Aerospace Science Vol 25 pp 297-329, 1988

[22] Greff, E. Aerodynamic Design and Integration of a Variable Camber Wing for a New Generation Long/Medium Range Aircraft. International Council for Aerospace Science 1988, ICAS-88-2.2.3

[23] Greff, E. The Development and Design Integration of a Variable Camber Wing for Long/Medium Range Aircraft. Aeronautical Journal Paper No. 1750, 1990

[24] Rao, A. Variable camber Wing for a Transport Aircraft. PhD Thesis, Cranfield Institute of Technology, 1989

[25] Lunn, J. D. Weight Effects of a Variable Camber Wing. Msc Thesis, Cranfield Institute of Technology. 1987

[26] Spillman, J. J. Stollery, J. L. A proposal for a Research on Variable Camber Wing for Transport Aircraft, 1989, Unpublished

[27] Mackinnon, A. V. An Experimental Study of a Variable Camber Wing. PhD Thesis, Cranfield Institute of Technology, 1992

[28] Spillman, J. J. The Use of Variable Camber to Reduce Drag, Weight and Cost of Transport Aircraft. Aeronautical Journal, Royal Aeronautical Society Paper No. 1844, January 1992

[29] Torenbeek, E. The Synthesis of Subsonic Airplane Design. Delft university Press, 1986

[30] Young J. B. 'STRUCT', College of Aeronautics Structural Analysis Computer Programme, Cranfield Institute of Technology

[31] Howe, D. College of Aeronautics Loading Analysis Notes, Cranfield Institute of Technology.

[32] Structural Dynamics Research Corpration. SDRC-IDEAS Finite Element Modelling™, Users Guide, 1990

[33] Young J.B. 'CoALA', College of Aeronautics Laminate Analysis Computer Code, Cranfield Institute of Technology

[34] Young, J. B. College of Aeronautics Material Properties and Design Data Sheets, Cranfield Institute of Technology

[35] Niu, M. C. Y. Airframe Structural Design, 1990

[36] Macreedys Glynwed Steels and Engineering Ltd. Engineering Properties of Free Cutting Steel

[37] James Lathem Limited. Material Properties of Jelutong. Wood Merchants, Simpson Road, Fenny Stratford, Bletchley, Milton Kynes, United Kingdom

[38] CIBA-GEIGY Plastics and Additives Company. Low Temperature Curing Pre-Preg for Composites with Outstanding Environmental Resistance. CIBA-GEIGY Information Sheet No. FTA.46d, 1983

[39] Structural Polymer Systems Ltd. Information Sheet on 150° Epoxy Laminating System SP695

[40] ESDU W 01.01.01. Lift Curve Slope of Swept and Tapered Wings, 1981

[41] Fielding, J. P. Design Specification for A-90 500 Seater Short Haul Airliner, College of Aeronautics. Cranfield Institute of Technology, 1990

[42] Larrive, L. Design of Variable Camber Inner Flaps for the A-90 Project. College of Aeronautics, Cranfield Institute of Technology, 1991

[43] Landry, J. G. N. Variable Camber Outer Flaps for the A-90 Project. College of Aeronautics, Cranfield Institute of Technology, 1991

APPENDIX A

PRELIMINARY DESIGN OF THE FUTURE LARGE AIRCRAFT (BASELINE CONFIGURATION)

NOTATION

A	Wing Aspect ratio
AMC	Aerodynamic mean chord (m)
b	Wing span (m)
b_{HT}	Span of the horizontal tail unit (m)
b_{VT}	Span of the vertical tail unit (m)
C_D	Drag coefficient
C_L	Lift coefficient
C_r	Wing root chord (m)
C_t	Wing tip chord (m)
D_f	External diameter of the fuselage (m)
GMC	Geometric mean chord (m)
h_c	Aircraft service ceiling (m)
L/D	Lift top drag ratio
l_f	Fuselage length (m)
L_{RUN}	Landing run (ft)
L_{50}	Landing from 50 feet screen (ft)
M_F	Fuel mass (Kg)
M_L	Aircraft landing mass (Kg)
M_{PL}	Payload mass (Kg)
MTOM	Maximum take off mass (Kg)
M_O/S	Wing loading (Kg/m^2)
N	Normal acceleration factor
OEM	Operating empty mass (Kg)
R_F	Maximum fuel range (nm)
R_{PL}	Maximum payload range (nm)
S	Wing planform area (m^2)
S_{HT}	Horizontal tail area (m^2)
S_{VT}	Vertical tail area (m^2)
$T\text{-}O_{RUN}$	Take off run (ft)
$T\text{-}O_{35}$	Take off to 35 ft screen (ft)
T_o/M_O	Thrust to weight ratio
$(t/c)_r$	Wing thickness to chord ratio at the root
$(t/c)_t$	Wing thickness to chord ratio at the tip
V_C	Cruise speed (Knots or m/s)
V_{CE}	Economic cruise speed (Knots or m/s)
V_{SI}	Stalling speed (Knots or m/s)
V_D	Design diving speed (Knots or m/s)
λ	Wing taper ratio
ρ	Air density (Kg/m^3)

A.1 BRIEF HISTORY OF THE FUTURE LARGE AIRCRAFT (FLA)

In 1982 Aerospatial in France, British Aerospace (BAe) in United Kingdom, Lockheed Georgia in the USA and Messerschmitt-Bolkow-Blohm (MBB) in Germany (all companies with transport aircraft manufacturing experience) teamed to carry out preliminary studies for future military transport needs. Aeritalia in Italy and CASA in Spain joined the team in 1987. The FIMA (Future International Military Airlifter) group (as it was then called), has since been reorganised and is now known as EuroFLAG (European Future Large Aircraft Group), because Lockheed is no longer an active member of the team. Euroflag partners are currently engaged in joint studies to address the need to replace the existing transporters with the European air forces at the turn of the century. The Euroflag sponsored Future Large Aircraft (FLA) is aimed primarily at replacing the C-130 in the Royal Air Force; and the Transall C.160 in the German Air Force and French Air Force[A1].

Both C-130 and C.160 are optimised for shorthaul and their cargo compartments are relatively small for the needs of the modern army and air force customer. for example, the stretched version of the C-130 bulks out at the 14-16 tonne mark. Helicopters have to be stripped down to fit in the Hercules, and personnel transport has always been uncomfortable. It is cramped, noisy and either very hot or absolutely freezing inside. The Hercules was designed in 1950's and Transall suffers from the same basic comfort problems.

In general the basic design criteria for the FLA are improved payload/range/ cruise speed over the present generation of airlifters, a wide optimised cargo hold including a load bearing tail ramp, very good field performance and improved crew and passenger comfort. FLA seeks to develop an aircraft from a common airframe that could perform freighter transport or advanced early warning (AEW) roles.

A.2 INITIAL AIRCRAFT SPECIFICATION AND PRELIMINARY REQUIREMENTS

Owing to the nature of the role of the aircraft and the fact that it is a new and a joint pursuit, information regarding the overall specification and geometric details of the FLA could not be released by any of the partners. In the absence of a firm requirement an initial specification was developed based on the information obtained from several sources. This included journal and magazine articles and computer literature data base.

It followed that the FLA could be thought of as a derivative of BAe 146, implying that there will be similarities between the two aircraft in terms of wing design and general aircraft arrangement. The aircraft is to have a longer (approximately 15ft) fuselage than the stretched Hercules C-130H-30 (Table A.1) and a wider (between 12ft and 15ft) cargo hold floor. It is to have a high 'T' - tail arrangement.

Transit speed of the FLA will be approximately 400 knots which will compare well with 325 knots for the C-130H-30. Economic cruise speed will be 300 knots. High speed dash capabilities of Mach No. of 0.7 to 0.75 are envisaged.

The FLA would be powered by four contra-rotating propfan engines. The baseline powerplant is the Alison 578D engine with four plus four Hamilton standard swept blade propellers. It is to have "fairly good" field performance with minimum take-off run of 3000 to 4000ft being talked about. Thus rough field performance will be slightly improved on the C-130H-30's take-off roll and landing runs will be within 2,500-3000ft. Maximum take-off mass (MTOM) is suggested to be between 192,000 and 200,000 lb's. Payload requirements in terms of both weight and bulk, are aimed at doubling the airlift capabilities provided by the C-130. In fact the tentative plan is for FLA to carry 25 tonnes of cargo, with an increase of 1000-1500 nm range over the C-130 with minimum of 5 % fuel reserves and an additional 30min at sea-level.

State-of-the-art avionics will allow day/night all-weather operations from semi-prepared grass field or desert strips. The aircraft will be rugged and built for the low-level tactical role. Survivability close to forward edge of the battle area (FEBA) must be improved by good and reliable airframe/structural design.

Primary missions for the aircraft are:-

- Air-lifting and air-landing of ammunition, general stores, military vehicles, weapon systems and helicopter.
- Air-lifting of troops and other military passengers.
- Air-dropping of troops, palletised stores, ammunition, weapons and other equipment.
- Casualty and medical evacuation.

The FLA is to have in-flight refuelling capabilities. Short take-off and landing (STOL) capabilities will be achieved using conventional high lift devices such as slotted flap. Spoilers will be employed for roll control.

A.3 CONCEPTUAL AND PRELIMINARY DESIGN STUDY (BASELINE CONFIGURATION)

The information given above is obviously very limited in identifying the exact features of the aircraft and its loading requirements. In order to determine the parametric details with regards to aircraft configuration, mass balancing, performance targets, etc, it was necessary to carry out a preliminary design study. It must be noted that this study was undertaken before the aerodynamic data on the two aerofoil was available and therefore the details should not be compared.

It was thought that the design of the overall aircraft, regarding fuselage layout, tail section design/layout, under carriage configuration, etc, would be time-consuming and not necessary for the final development of the VC system. Thus initial work largely concentrated on the design and layout of the wing, performance analysis and weights/loading estimates.

Details of the parametric studies made of the aircraft comparable to military/commercial airlifter application are presented in Table A.1.

The initial specification and the study of previous designs together with informative

discussions with BAe (Commercial Aircraft Ltd) provided the starting point for some layout schemes. These were an attempt to bring together the main features of the aircraft into feasible configuration. Several alternatives with regards to wing loading and geometry were considered. Table A.2 contains the initial specification target figures for the FLA.

A.3.1 Initial Aircraft Layout

The basic form of wing for an airlifter type of aircraft would be one of high aspect ratio and large planform area to enable it to achieve moderately low wing loading and small induced drag. The wing would require some amount of sweepback to allow a transit cruise Mach number of 0.7 - 0.75 without suffering drag rise effects.

It was envisaged that a modern supercritical aerofoil would be used to obtain the advantages of both reduced wing sweep and increased structural depth.

The location of the wing relative to the fuselage is in most cases dependent on the operational requirements. For transport airlifters the wing is often mounted on top of the fuselage, i.e, high wing arrangement. This is true for the C-130, Ilyushin 11-76, Lockheed C-5A Galaxy and many other transport aircraft[A2]. Such an arrangement allows sufficient ground clearance for the engines (wing mounted). It also helps to have the fuselage fairly close to the ground to assist in the loading/unloading of cargo. With this low ground clearance it is possible to design a simple undercarriage units that could be installed within the fuselage. These arguments therefore suggest that the FLA will have a high wing arrangement. An artist impression of the FLA (taken from reference [A1]) shown in Figure A.1 support this suggestion.

Tactical and strategic mission requirements for the FLA call for an optimised cargo hold volume with the design payload mass and large rear loading door. The aircraft must have a constant height and width cargo hold. Details of the overall layout of the fuselage were not available accept that length would be approximately 15ft longer than the C-130H-30. It was therefore assumed at this stage to retain the external shape of the Hercules C-130 and increase the length accordingly.

A trimming 'T' tail arrangement would be required for maximum tail arm and freedom from wing and engine induced turbulence.

A.3.2 Towards the Solution

In an attempt to establish a preliminary design specification and the detailed wing geometry of the FLA, it was decided to use the methods given in reference [A3], [A4], and [A5].

A.3.2.1 Wing loading and aircraft performance

<u>Low speed lift requirement</u>

Maximum attainable lift coefficient (C_{Lmax}) with the supercritical section design by

Mackinnon [A6] (see Chapter Two) is 1.25. It was necessary to include a leading edge (LE) nose slat and a trailing edge (TE) flap in order to increase this value such that the low speed requirements for both the tack-off (T-O) and landing conditions are satisfied. Preliminary estimations were made using the method given in reference [A3]. The proposed aerofoil with high lift devices has the following characteristics:

The aerofoil requires a LE slat of 17% chord which is to be deflected at 15° for both the take off and landing conditions. The aerofoil experiences an increment in C_L of about 0.6.

Towards the aft region a single slotted flap of 30% chord is required. This is to be deflected through 10° and 30° for T-O and landing conditions respectively. The possible C_L increment with these settings being 0.272 (10°) and 0.724 (30°). Total 3-D C_{Lmax} attainable for the aerofoil is therefore 2.122 and 2.574 for T-O and landing conditions respectively. It was decided to limit the required C_{Lmax} to 1.875 for the former and 2.5 for the latter.

Take off (T O) field distance

For the C-130 the take off distance to 35 ft screen is 5160 ft (Table A.1). Since the FLA is required to have a slightly better performance it is assumed that the distance should be restricted to 4000 ft. For this distance reference [A4] (figure 3.7) gives the following take off parameter;

$$\frac{\frac{M_G}{S}}{\delta C_{L_T}\left(\frac{T_O}{M_G}\right)} = 106$$

The variation of thrust to weight (T_o/M_G) ratio with wing loading is shown in Figure A.2.

Since the FLA wing is a derivative of the BAe 146 wing, it was assumed that the maximum wing loading on the two aircraft is likely to be of the same order. The wing loading (M_G/S) for the BAe 146 variants is as follows:
BAe 146 - 100 = 493 kg/m^2 (103 lb/ft^2)
BAe 146 - 200 = 546 kg/m^2 (119 lb/ft^2)
BAe 146 - 300 = 610 kg/m^2 (125 lb/ft^2).

It was decided to design the wing based on a relatively lower wing loading than these values. A value of 100 lb/ft^2 (488.2 kg/m^2) was considered to be quite appropriate to give reduced take off and landing field lengths. The thrust to weight ratio (T_o/M_G) for this wing loading is therefore = 0.503

Drag estimation

On achieving the near final design of the aircraft an initial drag predictions were made using the method given in reference [A3]. Thus the economic cruise drag is,

$C_D = 0.0171 + 0.04188C_L^2$,

Cruise $C_{Lmax} = (0.0171/0.04188)^{1/2} = 0.639$, and

$(L/D)_{max} = 18.68$

The high value of C_{Lmax} implies that the aircraft could be in the buffet region, therefore this value of $(L/D)_{max}$ could be reduced.

Cruise performance

To maintain the $(L/D)_{max}$ value while steadily climbing to maximum service ceiling the wing loading must increase and the cruise T_o/M_G decreases. Reference [A4] gives generalised curves (figure 3.13) for high compression ratio turbofan engines which illustrate this variation. The variation of T_o/M_G with M_G/S for aspect ratios of 9.0, 9.5 and 10.0 is shown in Figure A.2. Thus for a wing aspect ratio of 9.5:

M_G/S	T_o/M_G	H x 10^3 (ft)
60	0.3619	45.60
70	0.3197	42.50
80	0.2837	40.05
90	0.2635	38.15
100	0.2368	36.10
110	0.2180	34.18
120	0.1998	32.00

It is noticed that the service ceiling for the required $(M_G/S)_{max}$ is over 36,000 ft. The maximum ceiling for the FLA was assumed to be 36,500 ft.

Landing field distance

The FLA is required to have a good field performance, i.e STOL characteristics. The landing distance from 50 ft screen had to be less than 3000 ft. In order to check whether this is possible an estimation was made using an empirical relationship given in reference [A5]. Thus the overall field length from 50 ft screen,

$$L_{50} = 7.1V_A + \left[\frac{1.6}{\mu + \frac{T_R}{M_{TO}}} - 1\right] V_A x 10^{-2} ft.$$

where:

$V_A = 1.3V_{SI}$

μ = 0.3 - Assume good disc brakes

T_R/M_{TO} = 0.2 - Thrust reversal

where:

$C_L = C_{LMAX} = 2.5$

$$V_{SI}=\frac{\frac{M_L}{S}}{\frac{1}{2}\rho C_L}$$

M_L/S is the landing wing loading. This can be estimated from M_L/M_{TO}. From the mass estimation this ratio = 0.847.

Thus M_L/S = 84.7 lb/ft^2 (413.5 kg/m^2),

V_{SI} = 100 Knots,

V_A = 130 Knots = 219 ft/s, and

L_{50} = 2613 ft.

This falls between the required target of 2500-3000 ft

A.3.2.3 Mass estimation

An initial mass estimation was made based on the empirical relationship developed by Howe[A5]. This was used to give the aircraft maximum take off weight by considering the breakdown of the individual components. Thus

Wing:

For long range transport aircraft

$$M_W=C_1\left[\frac{bS}{\cos\Lambda_{1/4}}\frac{(1+2\lambda)}{(3+3\lambda)}\left[\frac{V_D}{\tau}\right]^{0.5}N^{0.3}\frac{M_G}{S}^{0.3}\right]^{0.9}$$

where C_1 = 0.028

Substitution of the relevant parameters gives;

M_W = 1.885572 x 10^{-3} $M_{TO}^{1.35}$ KG

Fuselage:

M_B = 0.024 $[2L_fD_fV_{D0.5}]^{1.5}$
= 6419 KG

Tail unit:

M_{TU} = 0.142 $M_{TO}^{0.83}$

Undercarriage:

$$M_{UC} = 0.38\ M_{TO}$$

Powerplant and installation:

Total of 4 engines @ 2600 KG each[A7]

$$M_{ENG} = 2600 \times 4 \times 1.3 = 13520\ KG$$

System equipment and furnishing etc:

Fuel system	$= 0.04 M_{TO}$
Flying control	$= 0.16 M_{TO}^{0.75}$
Hydraulic and Pneumatic	$= 3.2\ M_{TO}^{0.5}$
Electric power	$= 0.17\ M_{TO}^{0.84}$
APU	$= 0.005\ M_{TO}$
Instrumentation and Automatic controls	= 250 KG (Assumed)
Radio and Navigation equipment	$= 0.025\ M_{TO}$
De-icing system	$= 0.16\ M_{TO}^{0.7}$
Fire and Tank protection	$= 0.006\ M_{TO}$
External paint	$= 0.5\ S = 0.5\ M_G/S$
	$= 1.0244 \times 10^{-3} M_{TO}$
Furnishing	= 75 Kg (Assumed)
Air conditioning	$= 0.009 M_{TO}$
3 Crew members averaging 100 KG	= 300 KG
Payload	= 25000 KG

Fuel:

Assumption was made that the fuel will be allocated for use in the following proportions:

Take off and climb	= 18 %
Cruise	= 60 %
Reserves	= 17 %
Landing	= 5 %

For flights in stratosphere the cruise range (from Breguet range equation) is given by:

$$S = 1320 \frac{\overline{M}}{C_2} [L/D]_{max} \log_{10} \frac{M_1}{M_2}$$

where,
M_1 is the mass of the aircraft at start of the cruise and M_2 is the mass at the end of the cruise, C is the specific fuel consumption estimated to be 0.4057 (Calculated from the engine data given in reference [A7]), and S is calculated as maximum payload range less 200 nm for climb and descent, thus S = 3046 - 200 = 2846 nm.
Evaluation of the above equation gives $M_1 = 1.1546\ M_2$.

Since the cruise fuel mass (M_F) is 60 % of the total M_F, the actual $M_F = 0.2577\ M_2$ or $0.2232\ M_1$. Take off is 18 % of M_F or $0.04017\ M_1$. Therefore,

$$M_1 = M_{TO} - 0.04017\ M_1,$$

or

$$M_F = 0.2146\ M_{TO}.$$

Landing mass, $M_L = M_2 - 0.05\ M_F = 0.8327\ M_{TO}$.

Evaluation of Gross take off mass, M_{TO}:
The above constituents are fixed masses or mass terms of various power of the M_{TO}. These were summed and solved iteratively to give a M_{TO} of 94540 KG. Table A.3 contains the mass of each component listed above.

A.3.2.3 Estimation of the geometric parameters

Wing

Wing Quarter chord sweep angle, $\Lambda_{1/4}$:

The FLA wing requires moderate wing sweepback to allow a cruise Mach number of 0.75, without suffering the drag rise effects.
The 3-D Mach number is related to $\Lambda_{1/4}$ (reference [A6]) by

$$M_D = \frac{M_{D(\Lambda=0)}}{(Cos\Lambda_{0.25})^2}$$

where $M_{D(\Lambda=0)}$ is the 2-D value of the drag rise Mach number, and is calculated from,

$$MD_{(\Lambda=0)} = 1 - 0.66(t/c)^{1/2} - 0.2C_{Lmax}$$

where (t/c) is the minimum value across the wing, assumed to be 0.125 (which compares well with the $(t/c)_{min}$ of 0.122 for the BAe 146-300), and $C_{Lmax} = 0.639$ (see Drag estimation). Evaluation of the above two equations gives $\Lambda_{1/4} = 22.5°$ for M_D not to exceed 0.75.

Torsional stiffness checks:

Reference [A5] gives a relationship to check whether torsional stiffness is likely to be a significant consideration. It is based only on design speed, (t/c) ratio and aspect ratio.

This states that;

$$\frac{A^{3/2}}{(t/c)^2} < \frac{3x10^8}{V_D^2 \cos\Lambda_{1/4}}$$

With V_D equivalent to M = 0.81 @ 36,500 ft, this criteria is satisfied for (t/c) = 0.15 (at the root), A = 9.5 and $\Lambda_{1/4} = 22.5°$.

Wing area:

The actual wing size is determined simply as the gross take off weight divided by the take off wing loading.

Thus Wing Area = M_{TO} / (M_G/S) = 193.73 m^2

Wing Taper Ratio (C_t/C_r):

This was simply assumed to be 0.3 by comparison with similar aircraft.

Fuselage sizing

Discussions with BAe concluded that the diameter of the fuselage must be higher than that of the C-130 in order to give favourable wing body aerodynamic characteristics. Assumption was made that the finesse ratio (l_f/D_f) of the FLA would be the same as the aircraft designed by Whitford[A8] (see Table A.1), i.e l_f/D_f = 8.73. With this ratio the new fuselage length and the diameter ware calculated as l_f = 34.047 m, D_f = 3.9 m respectively.

Empennage

These were simply obtained by matching the tail and fin volume coefficients with the few of the existing transport aircraft.

A.3.2.5 Engine sizing and location

Information regarding the power plant to be installed on the FLA was not available. Decision was made to install the Rolls-Royce RB509-05-FPTCR PUSHER as the base line powerplant for which appropriate information was available. Calculations with regards to the engine thrust ratings, specific fuel consumption (c), engine performance, etc were made using reference [A7].

The propeller diameter was assumed to be 13ft. This was in keeping with the propeller blade diameter for the C-130H engines. The position of the engine was judged on the basis that the blades of the adjacent engine cleared each other and the side of the fuselage.

A.3.3 Description of the Final Design

A general arrangement drawing of the final configuration is shown in Figure A.3 and some points are discussed below:-

Wing geometry

A moderately sweep back combined with thick and relatively low cambered wing section enable cruise Mach number of up to 0.75 to be achieved.

There is sufficient fuel tankage in the wing for a range of 5250 nm with reserves. Tanks on each half of the wing extend from 9% to 70% semi-span, with 5% reduction between tanks and engines. The chordwise size of the tanks is between 17% and 65% chord. The front spar was placed at 17 % chord while the rear spar was placed at 65 % chord. These were changed slightly for the FLA wing with the VC system. Details of the planform arrangement are given in Chapter Four. Conventional devices for the base line configuration include, a single slotted flap system, a LE slat, an aileron and spoilers.

Gross area, S = 193.73 m^2
Aspect ratio, A = 9.5
Span, b = 42.9 m
Sweep of 0.25c line = 22.5°
Leading edge sweep = 25.22°
Aerofoil section (see Chapter Two)
Thickness ratio,
Root = 15.98 %
Tip = 13.14 %
@ 70% semi-span = 14.0 %
Taper ratio = 0.3
Wing mean aerodynamic chord (M A C) = 4.952 m @ 41% semi-span
Wing geometric mean chord (G M C) = 4.5158 m
Root chord = 6.947 m
Tip chord = 2.084 m

Trailing edge device:
Type:- Single slotted, 3 position flap
Flap chord/wing chord = 30 %
Take off flap setting = 10°
Landing flap setting = 30°
Inboard end of the flap from C/L = 1.95 m
Outboard end of the flap from C/L = 17.16 m

Ailerons:
Type:- Round nose
Aileron chord/wing chord = 25 %
Movement +/- 25°
Inboard end of aileron from C/L = 17.16 m

Outboard end of aileron from C/L = 21.45 m

Spoilers:
Three equal length segments spoilers are installed, extending from the side of the fuselage to 80 % semi-span.
Chord = 15 %
Maximum movement relative to the top surface = 50°
Distance of spoiler LE from wing TE = 25 %

Tailplane and fin

	Tailplane	Fin
Span	16.05 m	7.161 m
Area	49.00 m	21.680 m
Root chord	4.136 m	5.1869 m
Tip chord	2.068 m	3.1121 m
Leading edge sweep		
Thickness ratio	10 %	10 %
Taper ratio	0.5	0.6
MAC	2.8952 m	4.2311 m

Weights and loading

Maximum payload	= 25000 kg (55125 lb)
Maximum fuel mass	= 20288 kg (44735 lb)
Maximum take off mass	= 94540 kg (208461 lb)
Maximum landing mass	= 80075 kg (176565 lb)
Maximum wing loading	= 488 kg/m (100 lb/ft)
Normal load factor	= 2.5g

Powerplant

Thrust rating (all engines)

Maximum take-off thrust	= 520768 N (240751 lbf)
Optimum cruise thrust	= 107874 N (49871 lbf)

Inboard powerplants:
Distance of engine centre line below datum at front face = 1.5m
Distance of engine centre line from aircraft centre line at front face = 6.6066 m
Location of engine front face aft of fuselage nose = 17.325 m
Engine Propeller diameter = 13 ft. (3.9624 m)
Total engine length = 5.936 m

Outboard powerplants:
Distance of engine centre line below datum at front face = 1.5 m
Distance of engine centre line from aircraft centre line at front face = 11.7975 m

Location of engine front face aft of fuselage nose = 19.725 m
Engine Propeller diameter = 13 ft. (3.9624 m)
Total engine length = 5.936 m

Performance requirements

Standard mission profile for maximum payload range is shown in Figure A.4, for which the fuel is proportioned as follows:

Take-off and climb	= 18 %
Cruise	= 60 %
Reserves	= 17 %
Landing	= 5 %

The take-off run is limited to 4000 ft. This will be taken as the maximum take-off distance to 11 m (35 ft.) altitude. Landing distance from 15 m (50 ft.) altitude is 2620 ft.

Maximum fuel range	= 5250 nm (cruise and climb)
Maximum payload range	= 3050 nm
Optimum operating cruise altitude	= 36500 ft. (11125 m)
Service ceiling	= 39300 ft. (11979 m)
Economic cruise Mach No	= 0.70
High speed dash Mach No	= 0.75
Airdrop speeds[A1]	= 115 and 250 knots at sea-level
	= 200 and 250 knots at 25,000 ft.

REFERENCES FOR APPENDIX A

[A1] Wanstall, B. Norris, G. Europe Defines Airlifter Needs. Interavia Aerospace Review, Sept 1991

[A2] Janes all the Worlds Aircraft. Janes Publication Company, London 1989

[A3] Torenbeek, E. The Synthesis of Subsonic Airplane Design. Delft University Press, 1986

[A4] Loftin, L. K. Subsonic Aircraft: Evaluation and Matching of Size to Performance, NASA Publication 1060, August 1980

[A5] Howe, D. Fielding, J. P. College of Aeronautics Lecture Notes on Aerospace Vehicle Design and Initial Project Design. Cranfield Institute of Technology

[A6] Mackinnon, A. V. An Experimental Study of a Variable Camber Wing, Ph D Thesis 1992 Cranfield Institute of Technology

[A7] Rolls Royce Limited. The RB509-05 FPT CR PUSHER Project Turbo-Shaft Engine. Published by Brochures & Specifications Group, 1984

[A8] Whitford, R. Design of a Medium Military Airlifter. Published by the American Institute of Aeronautics, AIAA-89-2064, 1989

Table A.1: Parametric data of the aircraft used for military and commerciai airlift application.

Aircraft Type	b (m)	AR	$C_{R\ (m)}$	S (m^2)	$\Lambda_{1/4\ (Deg)}$
C-130H-30	40.41	10.09	4.88	162.12	0
C-17	50.29	7.17	-	353.00	25
Nimrod MR	35.00	6.20	9.00	197.00	20
Ilyushin 11-76	50.50	8.50	-	300.00	25
Lockheed C-5	67.88	7.75	13.85	576.00	25
BAe 146	26.34	8.97	-	77.30	15
Transall C-160	40.00	10.00	4.84	160.00	-
A300	44.84	7.73	-	260.00	28
A310	43.89	8.80	8.38	219.00	28
B 747-200F	59.64	6.96	16.56	511.00	37
ATLAS*	38.75	9.00	6.15	166.79	

Aircraft Type	b_{HT} (m)	S_{HT} (m^2)	S_{VT} (m^2)	l_f (m)	D_f (m)
C-130H-30	16.05	49.40	27.87	34.47	3.30
C-17	-	-	-	53.39	5.49
Nimrod MR	14.51	52.98	16.63	38.63	2.95
Ilyushin 11-76	-	-	-	46.59	3.40
Lockheed C-5	20.94	113.76	110.35	75.54	5.79
BAe 146	11.09	25.64	20.81	28.60	3.56
Transall C-160	14.50	43.80	46.20	32.40	4.30
A300	16.62	-	45.20	53.30	5.64
A310	16.26	64.00	45.20	46.66	5.64
B 747-200F	22.17	169.10	100.00	70.66	6.13
ATLAS*	15.50	47.70	-	35.79	4.10

Table A1: (Cont..)

Aircraft Type	TO_{Run} (ft)	TO_{35ft} (ft)	L_{Run} (ft)	L_{50} (ft)	$h_{C\ (m)}$
C-130H-30	1091	1573	518	838	10060
C-17	2320	-	823	-	-
Nimrod MR	1463	-	1615	-	12800
Ilyushin 11-76	850	-	450	-	15500
Lockheed C-5	2530	2987	725	1164	10895
BAe 146					
Transall C-160	715	990	550	869	8230
A300	-	2347	-	1536	12121
A310	-	1768	-	1478	11212
B 747-200F	-	3170	-	2109	13715
ATLAS*	1031	1500	-	1660	11000

Aircraft Type	$R_{PL\ (nm)}$	R_F (nm)	V_C (Knots)	V_{CE} (Knots)	V_{SI} (Knots)
C-130H-30	2046	4250	325	300	100
C-17	2400	-	350	M = 0.77	-
Nimrod MR	-	5000	500	425	-
Ilyushin 11-76	2700	3617	432	-	-
Lockheed C-5	2892	5618	496	450	104
BAe 146	1176	1476		383	92
Transall C-160	-	4780	M = 0.64	-	95
A300	3546	-	480	-	134
A310	2800	-	483	-	132
B 747-200F	2700	7100	523	-	-
ATLAS*	1750	4080	415	-	100

Table A.1: (Cont..)

Aircraft Type	OEM (Kg)	M_{TO} (Kg)	M_F (Kg)	M_{PL} (Kg)	M_G/S (Kg/m^2)
C-130H-30	36397	70310	28540	17645	434.50
C-17	117480	258547	-	78110	-
Nimrod MR	39000	80510	38940	54430	-
Ilyushin 11-76	-	170000	-	40000	-
Lockheed C-5	169643	379657	150815	118388	659.00
BAe 146	22861	42184	9362	10478	545.70
Transall C-160	29000	51000	15295	16000	319.00
A300	88928	165000	50499	41072	635.00
A310	76107	132000	44236	32393	-
B 747-200F	175540	362875	159320	90720	710
ATLAS*	-	83000	24600	22300	498.00

* Design study carried out in reference [A8]

Table A.2: Initial specification targets for the FLA

Cruise Mach No. Range	0.70 - 0.75
Take off run	3000 to 4000 feet
Landing run	2500 to 3000 feet
Maximum take off mass	Around 200,000 lbs
payload mass	25000 Kg

Table A.3: Mass breakdown

Component	Mass (Kg)	% MTOM
Wing (inc. auxiliary surfaces structure)	9829	10.40
Fuselage	6419	6.79
Tail unit	1915	2.03
Under carriage	3593	3.80
Engine	13520	14.30
Fuel system	3782	4.00
Flaying control	863	0.91
Hydraulic system	984	1.04
Electrical Power	2570	2.72
Auxiliary power unit	423	0.45
Radio and navigation	2614	2.77
De-icing	487	0.52
Fire protection	621	0.66
Paint and furnishing	172	0.18
Air-conditioning	851	0.90
Crew	300	0.32
Payload	25000	26.44
Fuel	20288	21.46
Total	94540	100

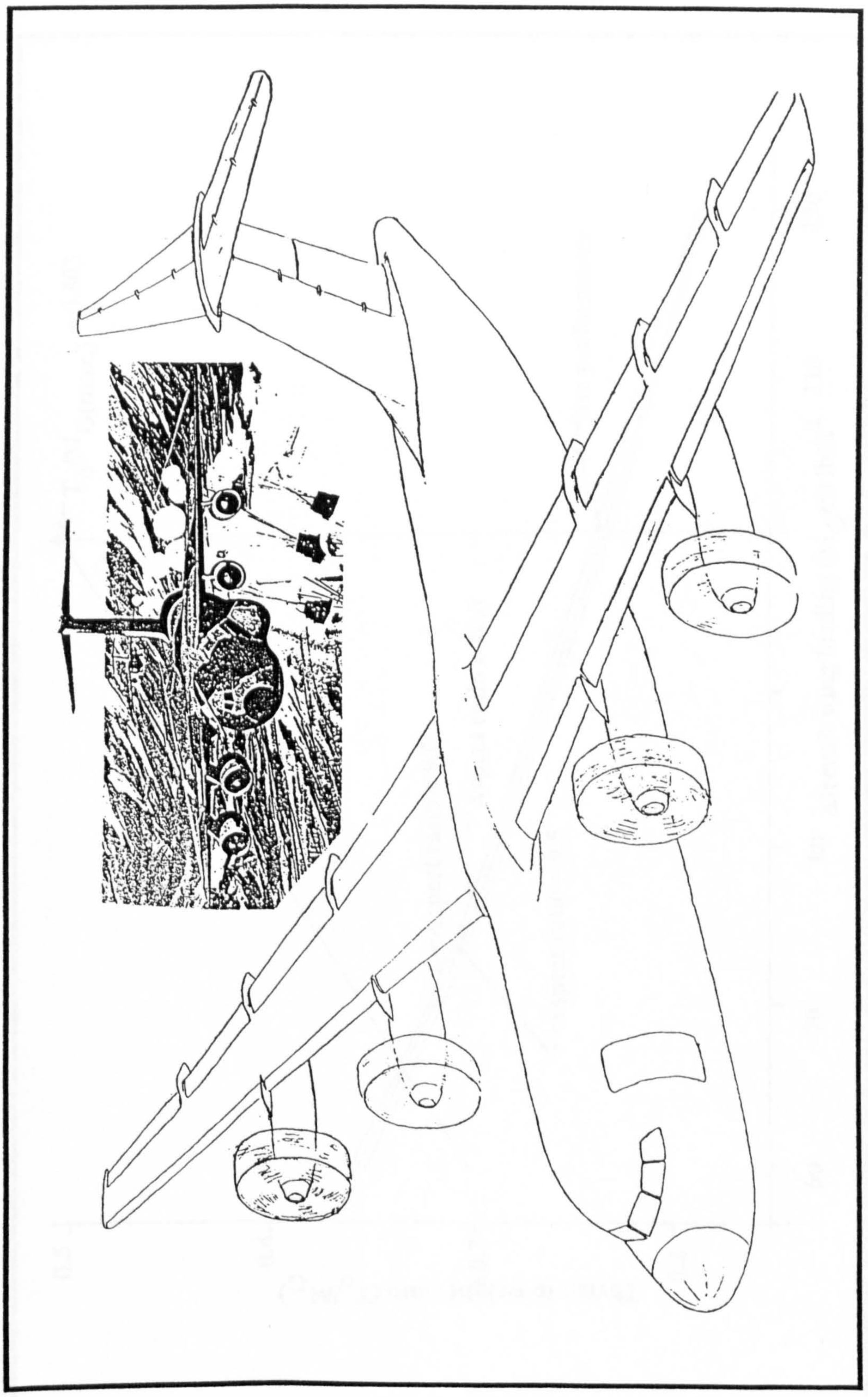

Figure A.1: Artists impression of the FLA

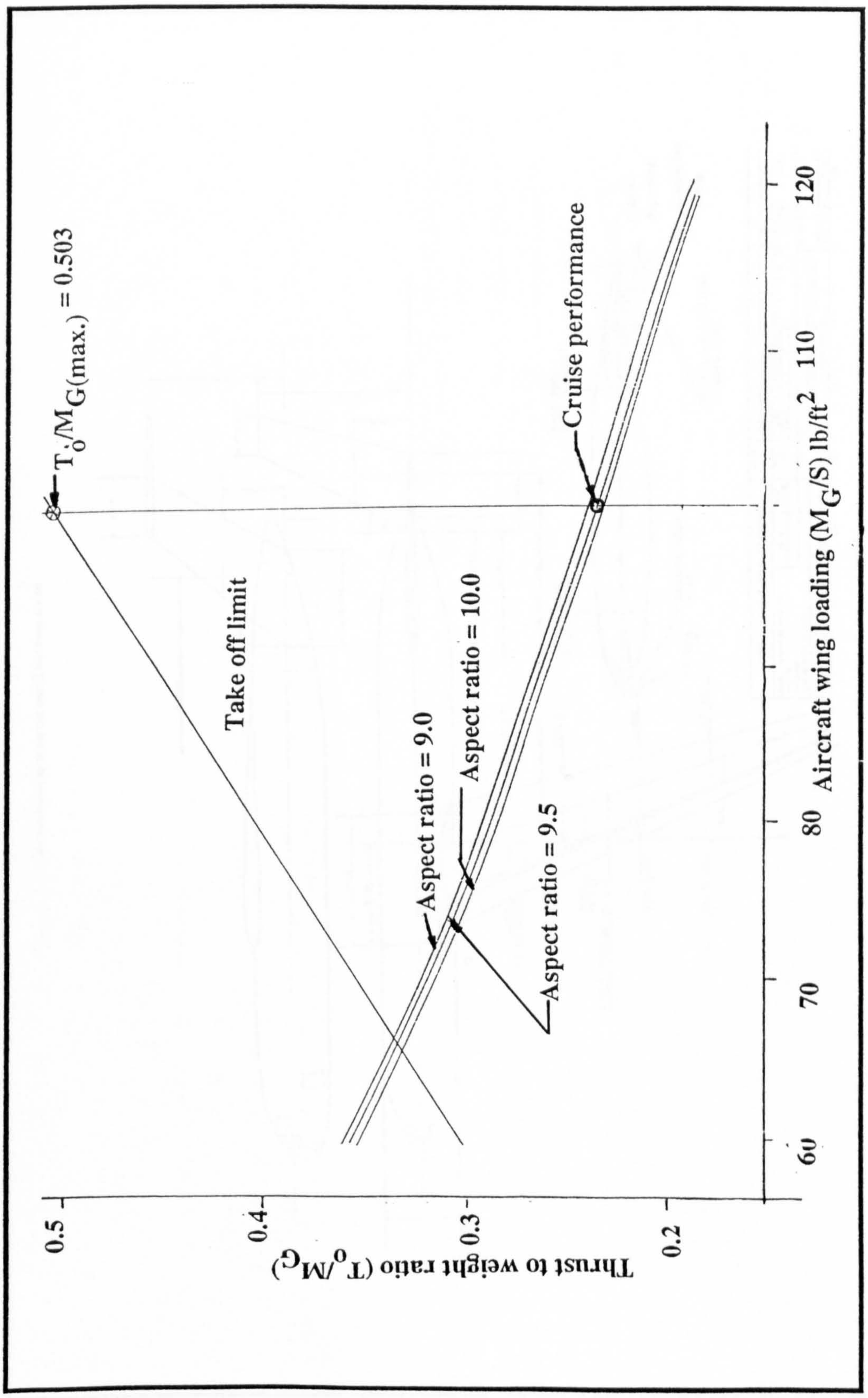

Figure A.2: FLA performance: Thrust to weight variation with wing loading

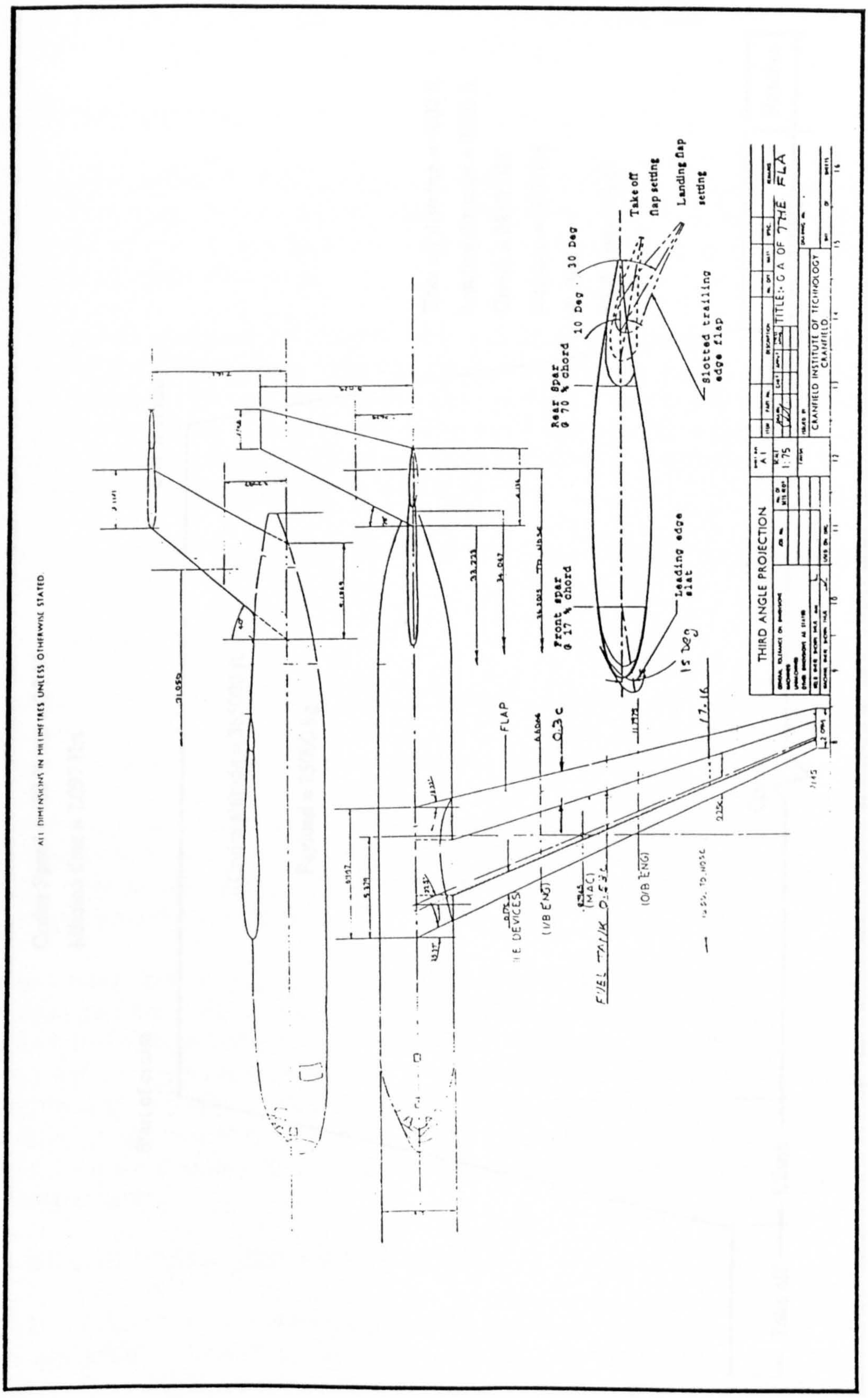

Figure A.3: General arrangement drawing of the FLA

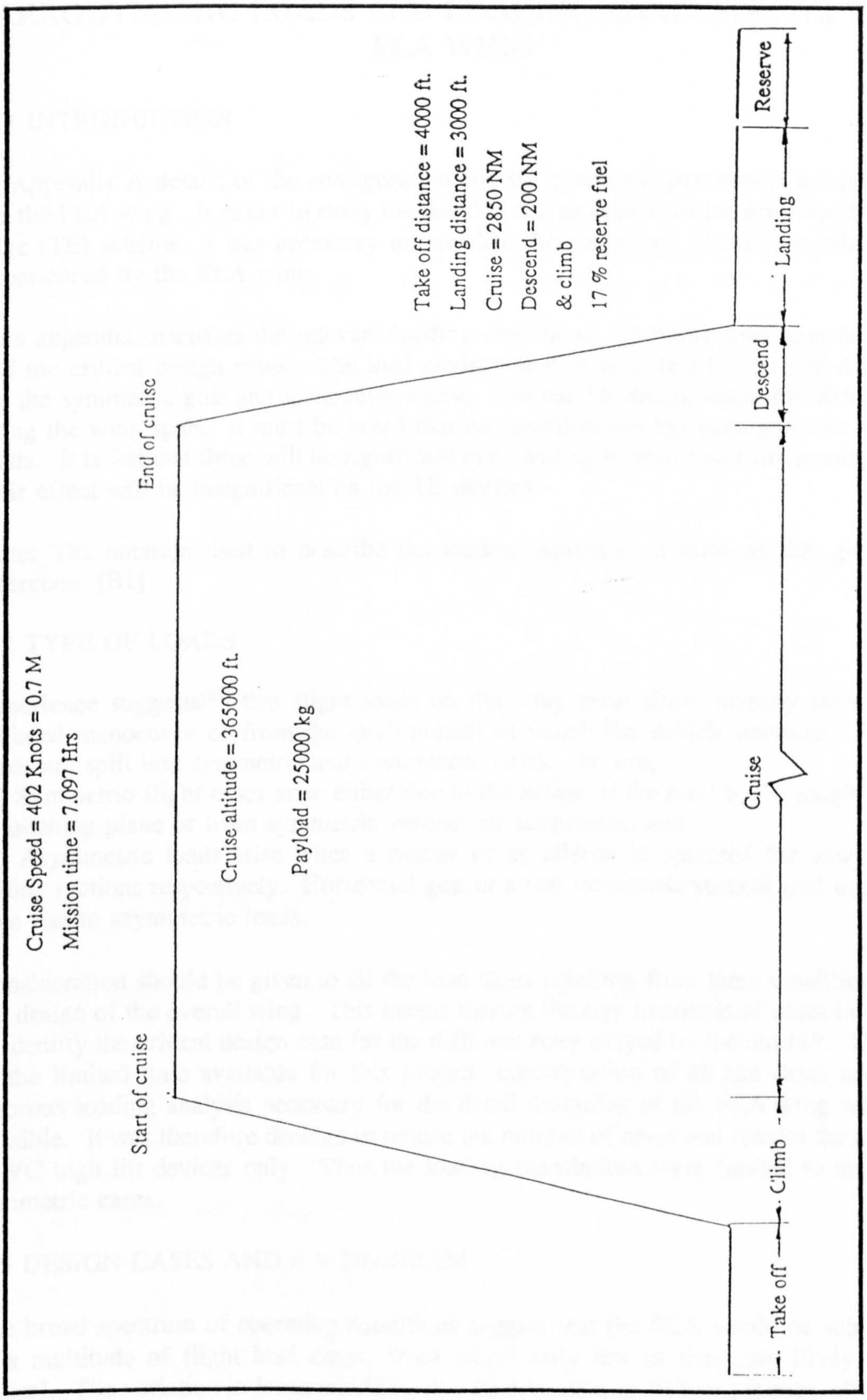

Figure A.4: Standard mission profile for maximum payload range

APPENDIX B

AERODYNAMIC LOADS AND LOADING ANALYSIS FOR THE FLA WING

B.1 INTRODUCTION

In Appendix A details of the configuration and the geometric parameters are outlined for the FLA wing. In order to study the detailed design aspects of the proposed trailing edge (TE) scheme, it was necessary to calculate the magnitude of aerodynamic loads experienced by the FLA wing.

This appendix discusses the relevant loading conditions, operating load environment, and the critical design cases. The load environment is described by the n-V diagram for the symmetric gust and manoeuvre cases. Critical TE design loads are distributed along the wing span. It must be noted that no consideration has been given to inertia loads. It is felt that these will be significant in providing inertial relief to the wing, but their effect will be insignificant on the TE devices.

Note: The notation used to describe the loading equations is same as that given in reference [B1]

B.2 TYPE OF LOADS

Experience suggests[B1] that flight loads on the wing arise either directly from pilot initiated manoeuvre or from the environment in which the vehicle operates. These loads are split into symmetric and asymmetric cases. Where,
(1) Symmetric flight cases arise either due to the action of the pilot in the longitudinal or pitching plane or from symmetric vertical air turbulence, and
(2) Asymmetric loads arise when a rudder or an aileron is operated for yawing or rolling motions respectively. Horizontal gust or a non symmetric vertical gust will also give rise to asymmetric loads.

Consideration should be given to all the load cases resulting from these conditions for the design of the overall wing. This means sieving through hundreds of cases in order to identify the critical design case for the different roles played by the aircraft. Owing to the limited time available for this project, consideration of all the cases and the rigorous loading analysis necessary for the detail designing of the FLA wing was not possible. It was therefore decided to reduce the number of cases and restrict the design to VC high lift devices only. Thus the loading calculations were limited to only the symmetric cases.

B.3 DESIGN CASES AND n-V DIAGRAM

The broad spectrum of operating conditions suggest that the FLA would be subjected to a multitude of flight load cases, from which only few of them are likely to be critical. The variation in loads would be due do operation at different speeds, altitudes and weights. Airworthiness requirements[B2],[B3] give formulated guidance and recommendation (which are based on past experience) that would appreciably reduce

the load cases.

Requirements for symmetric load cases suggest that the aircraft must operate within the boundaries of the manoeuvre acceleration (n-V) diagram.

B.3.1 Speed Envelope

B.3.1.1 Speed variation with altitude

The FLA is to fly at cruise Mach No. of 0.7 with a dash capability of 0.75. The design diving Mach No. is given by[B1] MC + 0.05 = 0.8. The economic cruise altitude is 36500ft, thus true airspeed (TAS) varies as a result of variation in temperature with increase in altitude. Where,

$$V_{TAS} = M\,(\alpha RT)^{1/2}$$

And $V_{EAS} = V_e = TAS\,(\rho/\rho_o)^{1/2}$

$\rho_o = 1.225\ KG/m^3$

$\alpha = 1.4$

$R = 287.1\ KG/KJ\ K$

Figure B.1 shows the variation of both the TAS and the EAS with altitude.

B.3.1.2 Flap design speed

B.3.1.2.1 Requirements as given in reference [B2]

Design flap speed V_F is defined as not less than:

i) 1.6 V_{SI} with the flaps in the take off position, zero engine power and maximum design mass.

ii) 1.8 V_{SI} with the devices in approach position at, zero engine power and maximum landing mass,

iii) 1.8 V_{SI} with the devices fully extended, zero engine power and maximum design landing mass.

Note, no approach position for the flaps was defined so requirements i) and iii) are used.

Where,

V_{SI} = Equivalent stalling airspeed.

B.3.1.2.2 Flap speed calculations

i) At design landing mass (M_L = 80075 KG)

$$V_{SI} = \sqrt{\frac{(Mg)}{(\frac{1}{2}\rho S C_{L_{Max}})}}$$

$M = M_L = 80075$ KG
$S = 193.73$ m^2
$C_{LMAX} = 2.5$
$V_{SI} = 51.46$ m/s
and $V_F = 1.8\ V_{SI} = 92.63$ m/s

ii) At design take off mass (94540 KG)

$M = M_{TO} = 94540$ KG
$S = 193.73$ m^2
$C_{LMAX} = 1.875$
$V_{SI} = 64.56$ m/s
and $V_F = 1.6\ V_{SI} = 103.0$ m/s

B.3.2 Critical Altitude

Three altitudes were considered for setting the critical design cases. These are at sea-level, 20,000ft and 36,500ft.

B.3.3 Design Mass

Vehicle weights considered to give high wing loads were[B1],[B4], operating empty mass, maximum take off mass, zero fuel mass (ZFM), and maximum landing mass.

B.3.4 n-V Diagram

The technique involved in constructing the n-V diagram for military aircraft are detailed in reference [B2]. These techniques were used to calculate the limiting boundaries for the FLA for symmetric loading due to both the manoeuvre and gust.

Thus, For the manoeuvre envelope following requirements are specified:

$n_2 = 1 - 0.3n_1$,
$n_3 = -0.6\ (n_1 - 1)$,
$n_4 = 0.75n_1$,
$V_A = V_{SI}(n_1)^{1/2}$,
$V_E = 0.7V_D$,
$V_C = 0.8V_D$,

$$\therefore \quad V_{SI} = \left(\frac{2nMg}{\rho S C_{L_{MAX}}}\right)^{\frac{1}{2}}$$

The normal load factor n_1 for a transport aircraft is limited to 2.5g for normal manoeuvre and its restricted to 2.0g for flapped configurations.

The value of n for stall boundary (n_s) is given by,

$$n_s = \frac{\frac{1}{2}\rho_o V_{EAS}^2 S C_{L_{MAX}}}{Mg}$$

where,

$$0 \leq V_{EAS} \leq V_A,$$

and C_{LMAX} is the maximum lift coefficient for appropriate wing configuration, i.e

C_{LMAX} = 2.5 for landing,
= 1.875 for take off, and
= 1.25 for clean nested wing.

Increment to the normal load factor due to sharp edge gust is given by,

$$n_G = \frac{\frac{1}{2}\rho V^2 \left(\frac{FU}{V}\right) a_1 S}{Mg}$$

where,

$$F = \frac{0.88\mu}{5.3+\mu},$$

and

$$\mu = \frac{2M}{\rho \bar{S} c a_1},$$

U is the sharp edge gust velocity for which the following values are suggested:

Aircraft Flight Speed m/s	Gust Speed EAS (0 - 6100m) m/s	Gust Speed EAS (@ 15200m) m/s
V_B	20	11.6
V_C	15.2	7.6
V_D	7.6	3.8

U varies linearly from 6100m to 15200m, Thus

Aircraft Flight Speed	Gust Speed EAS (@ 11125.2m)
m/s	m/s
V_B	15.36
V_C	11
V_D	5.5

Where $V_B = V_{SI} (n_G + 1)1/2$,
or it is determined from the intersection of the 20 m/s gust line with the static stall boundary.

Example gust calculation:

Design case 1

$c = 4.5158$ m
$S = 193.73$ m^2
$M = 0.511$
a_1 varies with the Mach No $= 5.542$ / rad
$V_C = 174$ m/s
$U = 15.2$ m/s
$\mu = 31.836$
$F = 0.7544$
$n_G = 1.41512$

Table B.1 summarise the conditions for the preliminary symmetric design loads. These conditions are thought to be representative of the likely high load conditions suitable for preliminary design of the wing structural box and the control (flap and VC) surface. Figure B.2 illustrate examples of the manoeuvre and gust n-V diagram for the FLA for two flight conditions. The formulation of the n-V diagram for the flight conditions of Table B1 indicate a total of 32 design cases that would give highest wing loads. These case are detailed in Table B2.

B.4 LOADING ANALYSIS

B.4.1 Loading Actions

Several methods are established and available for calculating the overall wing loads. For the purpose of estimating the loads on the FLA use was made of the simplified approach given in reference [B1]. It suggests that the lifting force on the aircraft wing body combination can be found from;

$$L_{WB} = \frac{1}{2} \rho_o V_{EAS}^2 \left(a\alpha + a_B S_B \frac{\alpha_B}{S} \right)$$

assuming

$$\alpha_B=0$$

$$\therefore L_{WB}=\frac{1}{2}\rho_o V_{EAS}^2 Sa\alpha$$

Contribution due to tail load is not included in the this expression but does play a substantial role in the overall loading of the wing. This tail load (L_T) is found from;

$$L_T=[M_o+ngM(h-H_o)\,\bar{c}+Tz_T-Mk_B^2\ddot{\theta}]\,/\,l_t$$

For steady symmetric manoeuvres

$$\ddot{\theta}=0$$

The total load on the wing is now given by;

$$L_{WB} = ngM - L_T$$

B.4.1.1 Wing loads sample calculation

Case 1

Mass	=	M_{TO}	= 94540 KG
Alt	=	Sea level	
EAS	=	V_D	= 190 m/s
cofg	=	h	= 0.2771 MAC
S	=		193.73 m^2
S_T	=		49.8 m^2
Izz	=	I_{Pitch}	= 3077.317x103 KGm^4
H_o	=		0.24 MAC
c	=		4.952 m
l_t	=		21.878 m
M	=	Mach No	= 0.5583
a_{1W}	=		5.75 /rad
a_{1T}	=		4.2 /rad
C_{Mo}	=		-0.0622
z_T	=		-0.8649 (above datum)

When the aircraft is in its steady state position.

Lifting force L = nMg = $\frac{1}{2}\rho V^2 S C_L$

$$C_L = \frac{2nMg}{\rho V^2 S}$$

For level flight @ 1g;

C_L = = 0.2165

C_D = = 0.0171 + 0.04188C_L^2

= 0.019060

Aircraft thrust T = Drag D_1

$= \frac{1}{2}\rho V^2 S C_D$

= 81659 N

The value of ngm(h - Ho)c = 170388 Nm

Pitching moment at zero lift M_o

$= \frac{1}{2}\rho V^2 S \bar{C} C_{M_o}$

= - 1319414 Nm

L_T = [-1319414 + 170388 - 70627] / 21.878

= - 55748 N

L_{WB} = ngm - L_T = 983185 N

For 2.5g case:

C_L = 0.5413

C_D = 0.0294

T = 125825 N

ngm(h - Ho)c = 425970 Nm

M_o = -1319414 Nm

L_T = -45812 N

and L_{WB} = 2364406 N (Total)

B.4.1.2 Results

Loads for the 32 design cases given in Table B2 were evaluated using the above equations. The results of these calculations together with the required variables are also given in Table B2.

B.4.1.3 Critical loads

Observation of Table B.2 suggests that from the design cases considered, the highest loads on the wing occur at the following conditions:

Design case 1
Aircraft operating at M_{TO}, manoeuvring from 0 to 2.5g at V_D at sea level. In this condition the wing lift is 2.37 MN, the C_L = 0.54127 and flight Mach No. = 0.588.

Design case 15
Aircraft operating at M_L, landing flap setting, manoeuvring to 2.0g at V_F (landing) at sea level. In this condition the wing lift is 1.59 MN, the C_L = 1.5431 and flight Mach

No. = 0.272.

Design case 16
Aircraft operating at M_{TO}, take off flap setting, manoeuvring to 2.0g at VF (take off) at sea level. In this condition the wing lift is 1.86 MN, the C_L = 1.4649 and flight Mach No. = 0.304.

Design case 20
Aircraft operating at M_{TO}, in a symmetric gust of 3.343g acceleration at VC at 6096 m. In this condition the wing lift is 3.13 MN, the C_L = 0.8832 and flight Mach No. = 0.544.

B.4.2 Load Distribution

Loads calculated above were distributed along the wing in both the spanwise and chordwise directions.

To estimate the distribution across the span an empirical method given in reference [B5] was used. This method gives a unit load distribution which can be factored to suit a particular design condition.

The exact percentage of the load acting on individual component can only be estimated from the chordwise pressure distribution. For the basic aerofoil section and for the section with the VC settings, pressure distributions obtained by Mackinnon[B6] were used. In the case when high lift device was used the distribution had to be obtained with a panel method program developed by Lesoine[B7].

The chordwise load was split between the wing body, the trailing edge device and the 25% flap piece (on the inboard). The TE was taken to be aft of 64.5% chord position. Therefore all the loads on the TE variable camber device are assumed to act aft of the wing rear spar. The calculated percentage loads over the system for the four design cases are as follows:

Case No	Load (%)	Position (% x/c)
1	27	93.5
15	51	97.0
16	42	100.0
20	27	91.0

All the loads on the TE variable camber device are assumed to act aft of the wing rear spar.

The spanwise unit distribution curves were factored for the design cases in accordance with the percentage loads calculated from the chordwise distribution. Illustration of these factored curves is given in Figure B.3 for the four design cases.

REFERENCES FOR APPENDIX B

[B1] Howe, D. College of Aeronautics Lecture Notes on Loading Actions. Cranfield Institute of Technology

[B2] Defence Standard 00-970

[B3] Joint Airworthiness Requirements - 25. Design of Civil Aircraft, Civil Aviation Authority

[B4] Torenbeek, E. The Synthesis of Subsonic Airplane Design. Delft University Press, 1986

[B5] Engineering and Science Data Unit. Method for the Rapid Estimation of Theoretical Spanwise Loading Due to Change in Incidence. Transonic Data Memorandum (TDM) 6403, 1982

[B6] Mackinnon, A. V. An Experimental Study of a Variable Camber Wing, Ph D Thesis, College of Aeronautics, Cranfield Institute of Technology

[B7] Lesoine, M. Msc Project thesis on Slat Design for the A88 Aircraft, Cranfield Institute of Technology, 1989

Table B.1: Preliminary symmetric design cases

Case No	Alt (m)	Mass	V_C (m/s)	V_D (m/s)	V_A (m/s)	V_{SI} (m/s)	n_1	Conf
1	0	M_{TO}	174	190	125	79	2.5	Clean
2	0	OEM	174	190	90	57	2.5	"
3	0	ZFM	174	190	110	70	2.5	"
4	6096	M_{TO}	172	188	125	79	2.5	"
5	6096	OEM	172	188	90	57	2.5	"
6	6096	ZFM	172	188	110	70	2.5	"
7	11256	M_{TO}	108	123	125	79	2.5	"
8	11256	OEM	108	123	90	57	2.5	"
9	11256	ZFM	108	123	110	70	2.5	"
10	0	M_L	174	190	73	52	2.0	Land
11	0	M_{TO}	174	190	91	65	2.0	T-O

Table B.2a: Symmetric wing body loads due to pitching manoeuvre

Case No	Alt (m)	Mass	V_{EAS} (m/s)	CofG	C_{mo} (-ve)	n_1	L_{WB} (MN)
1	0	M_{TO}	190	0.277	0.0645	2.5	2.37
2	0	M_{TO}	174	0.277	0.0627	2.5	2.37
3	0	M_{TO}	125	0.277	0.0570	2.5	2.33
4	0	OEM	190	0.193	0.0645	2.5	1.28
5	0	OEM	190	0.193	0.0645	-1.0	-0.42
6	0	ZFM	190	0.316	0.0645	2.5	1.84
7	6096	M_{TO}	172	0.277	0.0639	2.5	2.36
8	6096	M_{TO}	188	0.277	0.0660	2.5	2.37
9	6096	M_{TO}	125	0.277	0.0583	2.5	2.33
10	6096	M_{TO}	172	0.277	0.0639	-1.0	-0.86
11	6096	ZFM	172	0.316	0.0639	2.5	1.82
12	11126	M_{TO}	123	0.277	0.0588	2.5	2.33
13	11126	M_{TO}	108	0.277	0.0568	2.5	2.33
14	11126	OEM	90	0.193	0.0543	2.5	1.23
15	0	M_L	93	0.250	0.0530	2.0	1.59
16	0	M_{TO}	103	0.277	0.0546	2.0	1.86

Table B.2b: Symmetric wing body loads due to vertical gust

Case No	Alt (m)	Mass	V_{EAS} (m/s)	CofG	C_{mo} (-ve)	n_1	L_{WB} (MN)
17	0	OEM	174	0.193	0.0627	3.433	1.71
18	0	OEM	174	0.193	0.0627	-1.433	-0.63
19	0	ZFM	174	0.316	0.0627	2.700	2.01
20	6096	M_{TO}	172	0.277	0.0639	3.343	3.13
21	6096	M_{TO}	172	0.277	0.0639	-1.343	-1.20
22	6096	OEM	172	0.193	0.0639	5.414	2.66
23	6096	OEM	188	0.193	0.0639	3.267	1.64
24	6096	OEM	188	0.193	0.0660	-1.267	-0.54
25	6096	OEM	172	0.193	0.0660	-3.414	-1.60
26	6096	ZFM	172	0.316	0.0639	4.152	3.00
27	6096	ZFM	172	0.316	0.0639	2.152	1.58
28	6096	ZFM	188	0.316	0.0639	2.611	1.92
29	6096	M_{TO}	108	0.277	0.0568	2.225	2.07
30	11126	OEM	108	0.193	0.0568	2.899	2.69
31	11126	ZFM	108	0.316	0.0568	2.820	1.39
32	11126	ZFM	106	0.316	0.0565	2.5	1.79

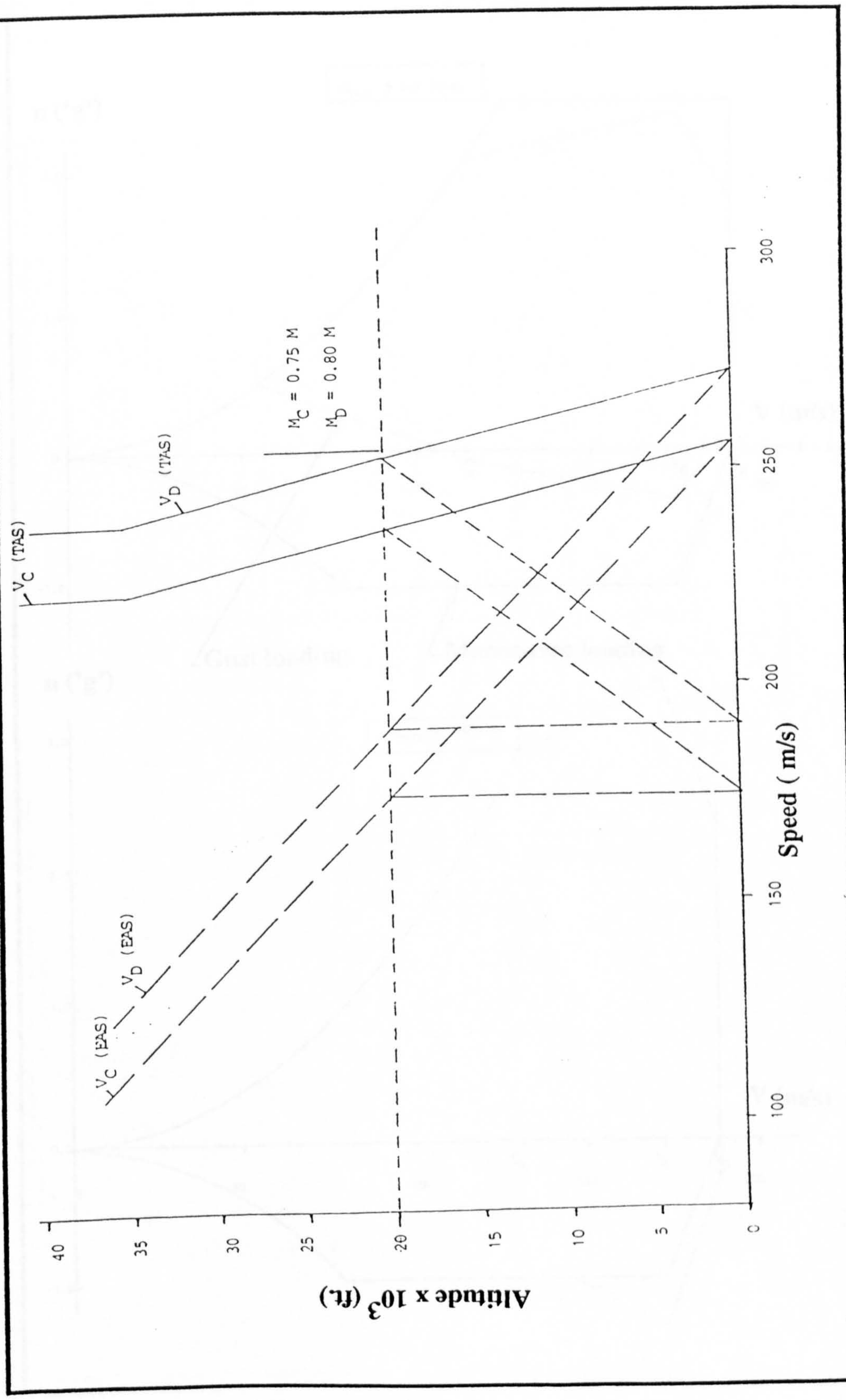

Figure B.1: Speed variation with altitute

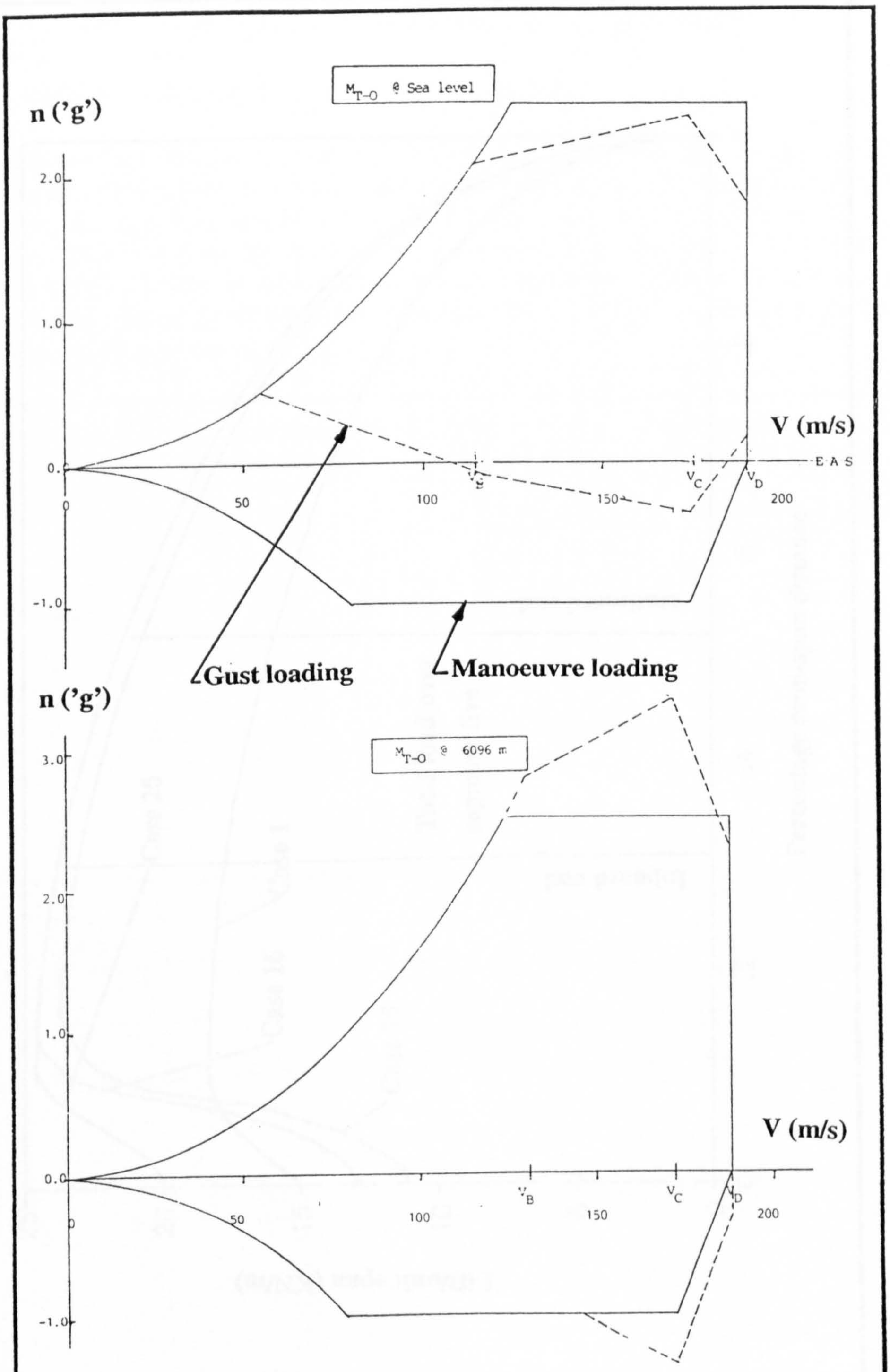

Figure B.2: Examples of n-V diagrames

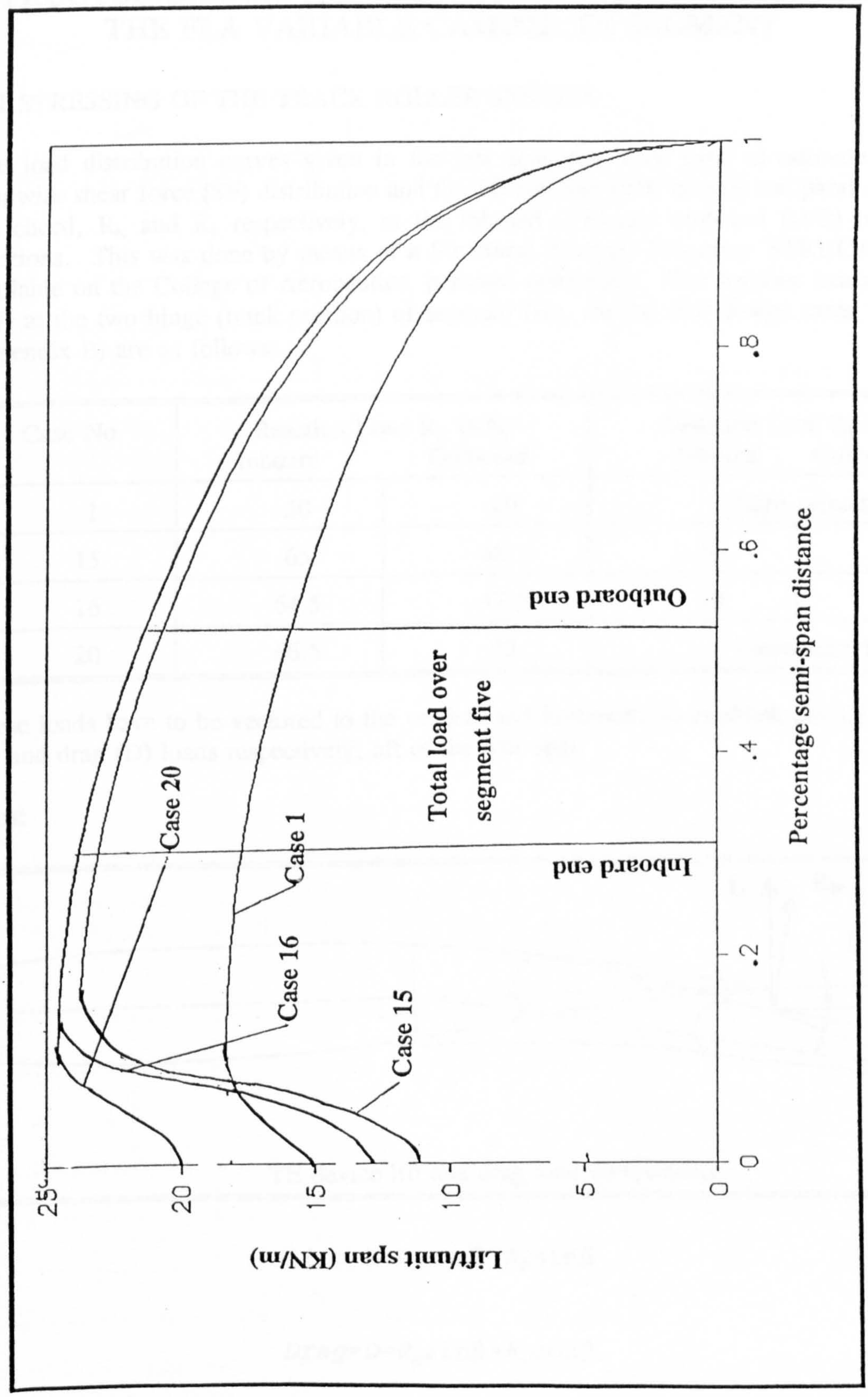

Figure B.3: Spanwise lift distribution aft of 64.5% chord line

APPENDIX C

STRUCTURAL ANALYSIS AND STRESS CALCULATIONS FOR THE FLA VARIABLE CAMBER TE SEGMENT

C.1 STRESSING OF THE TRACK ROLLER SYSTEM

The load distribution curves given in the last appendix were used to estimate the spanwise shear force (SF) distribution and the TE reaction loads normal and parallel to the chord, R_N and R_P respectively, at the inboard (I/B) and outboard (O/B) track positions. This was done by means of a Structural Analysis Program, 'STRUCT'[C1] available on the College of Aeronautics, personal computers. The reaction loads (in KN) at the two hinge (track position) of segment five, for the four design cases (see Appendix B) are as follows:

Case No.	Reaction Load R_N (KN) Inboard	Outboard	Reaction Load R_P (KN) Inboard	Outboard
1	50	40	Flaps retracted	
15	65	48.5	14	11.5
16	64.5	47.5	10	8
20	66.5	49	Flaps retracted	

These loads have to be vectored to the vertical and horizontal to establish the TE lift (L) and drag (D) loads respectively, aft of the rear spar.

Thus:

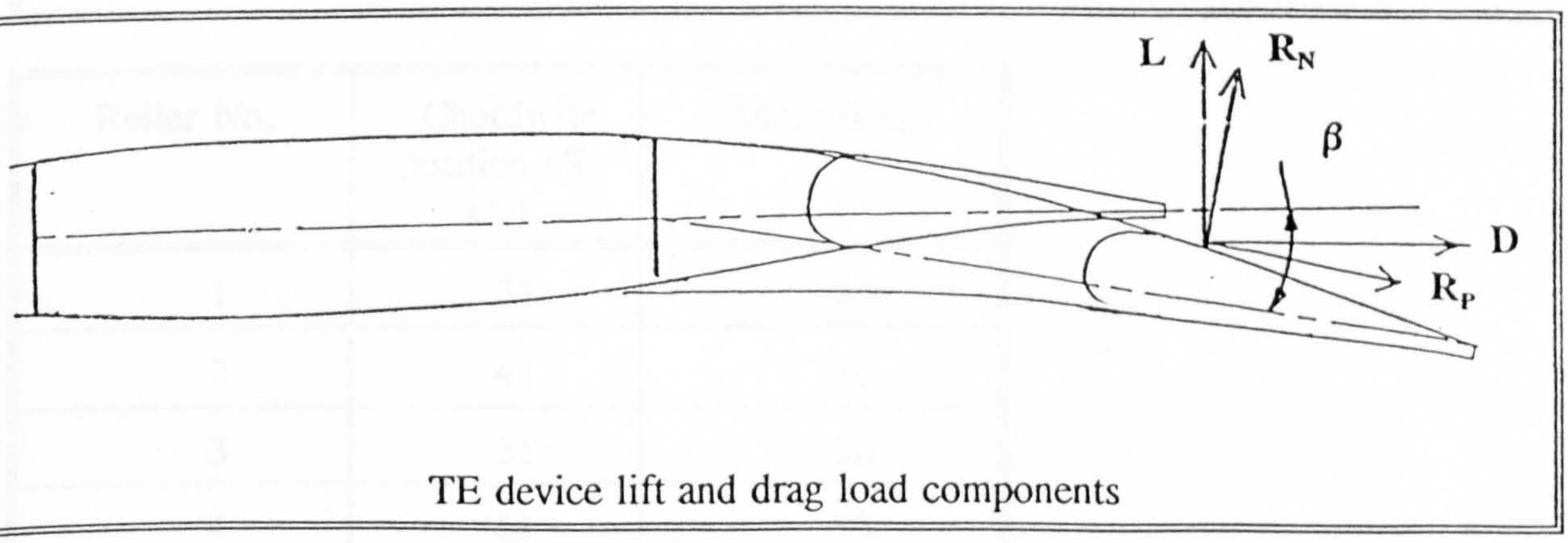

TE device lift and drag load components

$$Lift = L = R_N \cos\beta - R_P \sin\beta$$

$$Drag = D = R_N \sin\beta + R_P \cos\beta$$

where $\beta = 30°$ and $10°$ for cases 15 and 16 respectively, and for cases 1 and 20 $\beta = 0°$.

Evaluation of the above equations gives:

Case No.	Lift Reaction L (KN)		Drag Reaction D (KN)	
	Inboard	Outboard	Inboard	Outboard
1	50	40	-	-
15	63.5	47	25	20
16	63	46	18	13
20	66.5	48.5	-	-

Six twin roller sets are arranged along the track (chord) to react the lift loads. To estimate these reactions, the position of the rollers must be known.

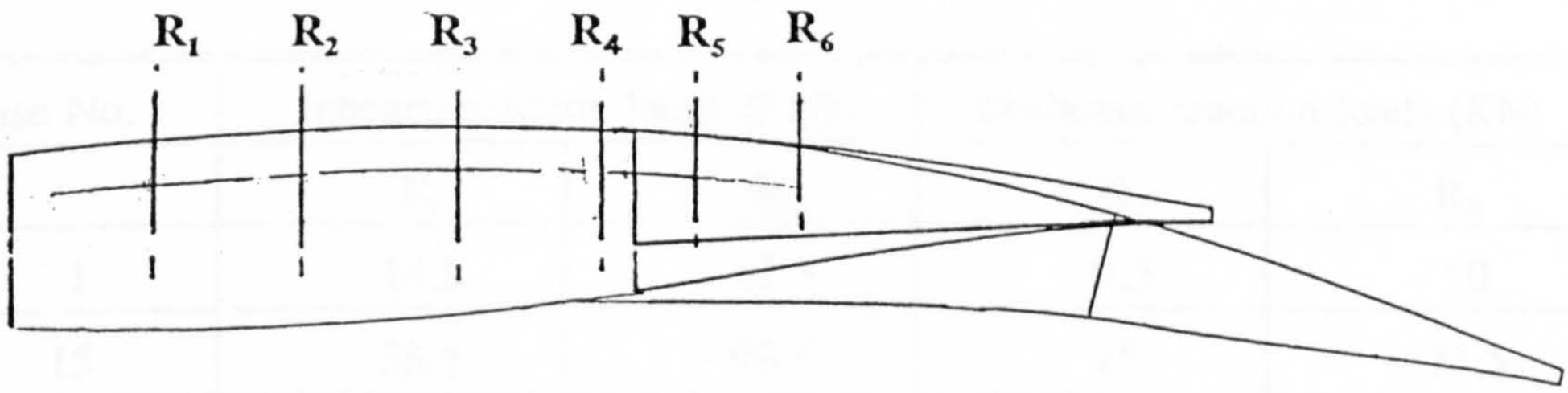

Roller position along the track length

Roller No.	Chordwise position (% x/c)	Angle (Deg)
1	31	83
2	41	86
3	51	90
4	61	93
5	71	97
6	81	101

From these, only two sets of rollers (front and rear) will experience the greatest loads. R_1 becomes the front roller (R_F) for Cases 1 and 20, while the rear roller (R_R) is represented by R_6. For Cases 15 and 16, R_1 and R_3 represent R_F and R_R respectively.

Roller reaction loads

For Case 1

$$\uparrow \Sigma F_V = 0 = R_F \cos(83-90) + R_R \cos(101-90) + L$$

$$\circlearrowleft \Sigma M \text{about} R_F = 0 = -L(0.935-0.31) - R_R(.81-.31)$$

$R_R = -1.2584L$ and $R_F = 0.2383L$

Similarly:

For Case 15 $R_R = -1.5568L$ and $R_F = 0.5296L$,

For Case 16 $R_R = -1.6474L$ and $R_F = 0.6189L$, and

For Case 20 $R_R = -1.2010L$ and $R_F = 0.1809L$

The calculated reaction loads for the four cases are as follows:

Case No.	Inboard reaction loads (KN)		Outboard reaction loads (KN)	
	R_F	R_R	R_F	R_R
1	14.5	- 62.5	9.5	- 50
15	33.5	- 98.5	25	- 73.5
16	39	-104	28.5	- 76
20	12	- 80	9	- 58.5

Maximum roller reaction loads are therefore due to take off variable camber (VC) setting and loading condition.

Bearing Size

The design has a double bogie cam stud type roller arrangement at all roller positions.

Rollers bearings were chosen from INA KR Series[C2]. It was assumed that one roller in a set should take the full load in-case the other one fails.

The required roller has 80 mm outside diameter with a static load rating of 120 KN which is just sufficient to sustain the applied load of 104 KN.

Extending Track Cross Section

This is forged from an aerospace grade titanium, TA48, and has the following cross-sectional and material properties (taken from reference [C3]):
$I = 31794587\ mm^4$
$Z = 397432\ mm^3$

f_n =831 N/mm^2, $1/\epsilon_n$ = 140, m = 27, and
t_5 = 927 N/mm^2

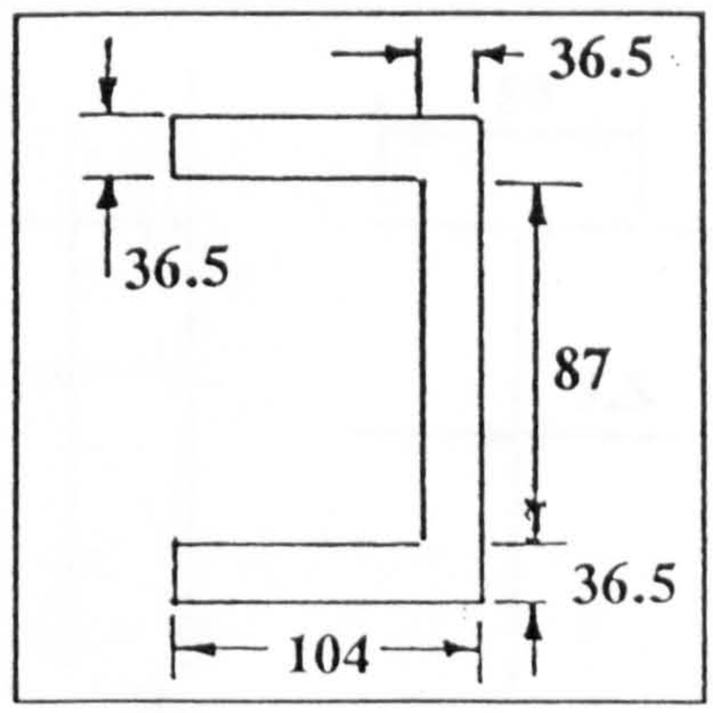

Flange instability check

From reference [C3]

$$\frac{\sigma_{cr}}{f_n}\frac{1}{\epsilon_n}=0.58\frac{1}{\epsilon_n}(t/b)^2=1.0$$

and σ_{cr} = 897.5 N/mm$_2$

Allowable bending moment, M_{all} = σ_{cr} Z = 357 KNM.

Maximum applied bending moment, M_{app} will be experienced near the rear roller position, at the inboard track. Thus,

$$M_{app} = 63.3 \text{ x } (0.97 - 0.81)c_\eta$$

Where $0.97c_\eta$ is the position of the centre of lift due to aft loading (see Appendix B), and c_η is the chord at the inboard end of the segment five.

M_{app} = 55.2 KNM (Limit)
= 55.2 X 1.5 = 82.5 KNM (Ultimate)
RF = 357/82.5 > 2.0

Carriage Shear Loads

The carriage is fixed to the side support structure with a 3/4" S96 shearing pin. The pin goes through a spherical bearing placed inside the side support rib. Maximum ultimate applied load = 104 x 1.5 = 156 KN

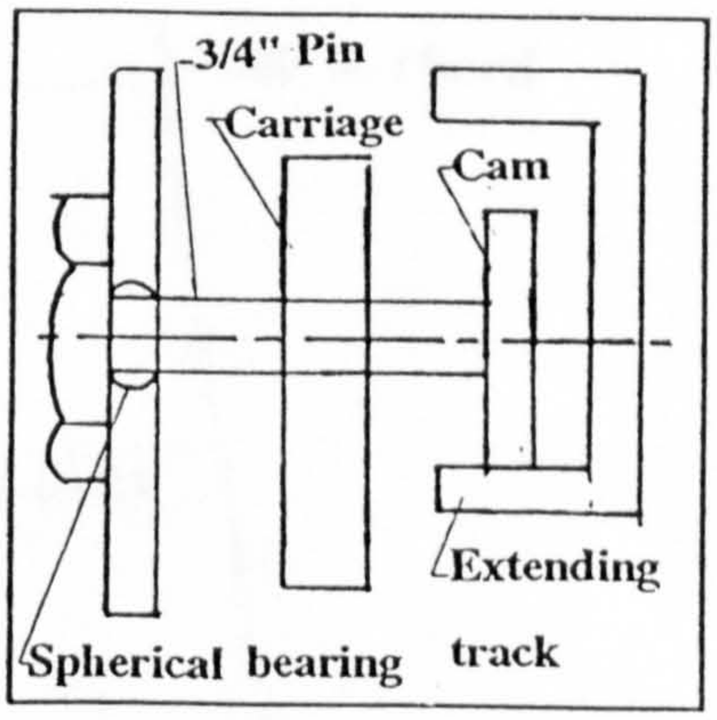

Pin in shear

Maximum allowable load = 159 KN.
RF = 159/156 = 1.02

Spherical bearing

This was chosen from reference [C4], Part no 11 AWG 12 3/4 " outside diameter.
Static Load rating = 178 KN
RF = 178/104 = 1.71

Side Support Structure Bending

Roller reaction loads are transferred through to the main wing box via the side ribs. The rib section accepting these loads is an 'I' beam assumed to be cantilevered at 17 % chord position.

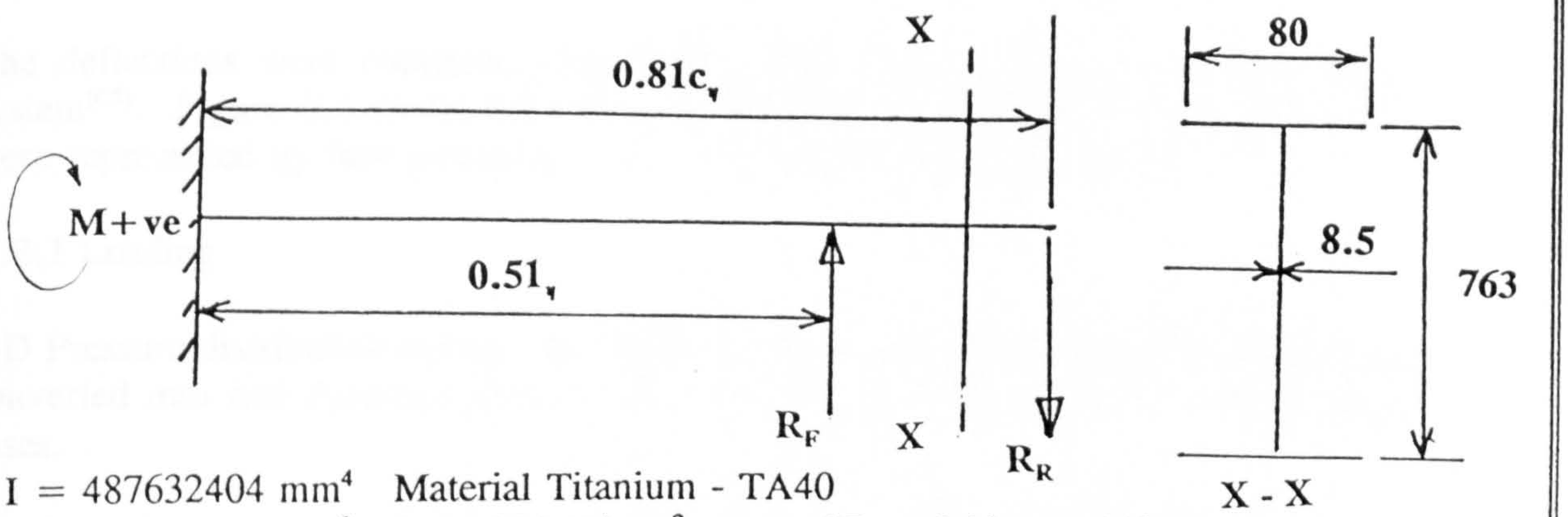

I = 487632404 mm^4 Material Titanium - TA40
Z = 1278198 mm^3 fn = 831 N/mm^2, m = 27, and 1/ϵn = 140

Maximum bending moment due to loads at R_F and R_R is;

$M_{app} = (0.81R_R + 0.51R_F)\, c_\eta$ = 354 KNM (Limit)
= 531 KNM (Ultimate)

For flange instability, σ_{cr} is worked out (as before) to be 863 N/mm^2.

Therefore $M_{all} = Z\, \sigma_{cr}$ = 1103 KNM
RF = 1103/531 = 2.07

C.2 FLEXIBLE UPPER SURFACE SKIN STIFFNESS CHECK

The upper surface skin at the TE is made from carbon fibre reinforced plastic (CFRP) material with the ply arrangement of $([(0/90)_2/0/\ 45]_2/0/90)_s$. Each ply is 0.125 mm thick, giving an overall thickness of 4mm to the laminate.

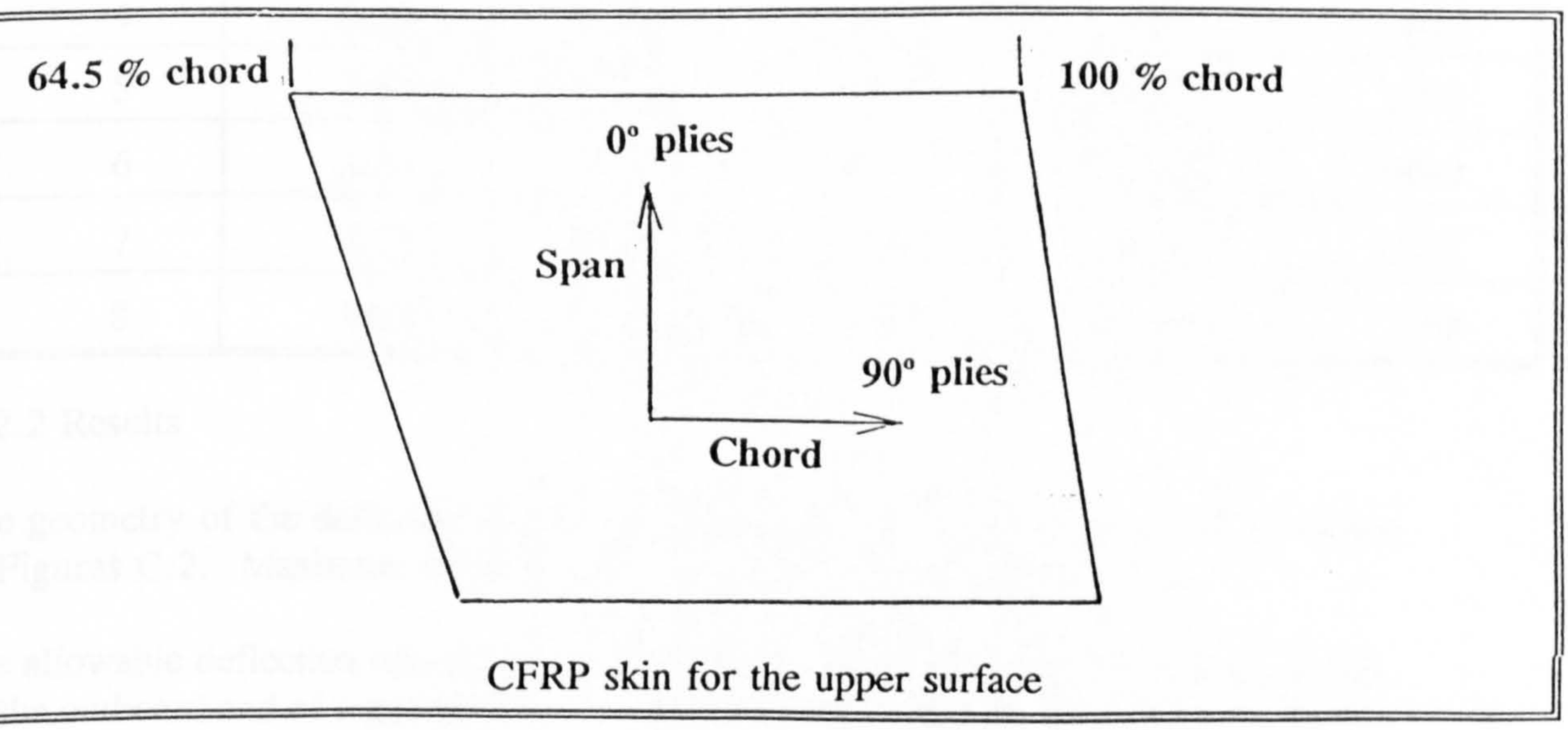

CFRP skin for the upper surface

Greater number of 0° plies are placed in the laminate in order to alow the surface to flex in chord.

A check on the stiffness of the skin suggested that in order to be aerodynamically clean, there should be a number of retainers (rollers) positioned in rails along the chord on

several spanwise stations to hold the skin.

The deflections were obtained using SDRC Ideas™ finite element analysis (FEA) system[C5]. Figure C.1 shows the FE model used for the analysis. Loads on the skin were represented by face pressures on thin quadrilateral shell elements.

C.2.1 Loading

2-D Pressure distribution curves were obtained from reference [C6]. These were than converted into real dynamic pressure loads for the low speed and high speed design cases.

Where low speed loading is due to takeoff at 103.3m/s and high speed loads arises from flying at 190 m/s.

$$AppliedPressure P_{app} = \frac{1}{2} \rho V_{EAS}^2 C_P$$

Pressure coefficients (C_P) and the applied pressures (P) due to suction on the upper surface, for the two cases are contained in the following table:

Strip NO	Width (%c_η)	C_P Low	P (N/mm$^{2)}$	C_P High	P (N/mm$^{2)}$
1	1.65	0.7883	5122	0.7745	17125
2	3.724	0.8051	5232	0.6493	14357
3	3.65	0.8160	5302	0.5678	12555
4	3.55	0.8058	5236	0.4804	10622
5	3.44	0.7792	5063	0.3954	8743
6	3.30	0.7403	4811	0.3142	6047
7	3.16	0.6906	4488	0.2337	5167
8	3.03	0.6597	42887	0.1650	3648

C.2.2 Results

The geometry of the deflected skin due to the loads for the high speed case is shown in Figures C.2. Maximum obtained deflection for this cases is 8.31 mm.

The allowable deflection was limited to 2 % of the maximum depth (d) of the aerofoil. At the outboard end of segment five, d = 598 mm. Therefore, 2 % of d = 11.96 mm
Thus, RF = 11.96/8.31 = 1.44

Conforming Rollers and Link sizing

The upper surface skin is conformed via a roller link arrangement. A set of links are attached to the upper surface skin at one end while the other end of each link has a

roller running inside a conforming track.

From the FE results the maximum applied load (L) at the link is 5.4 KN. Suitable cam track roller[C2] has 16 mm outside diameter and 6 mm inside diameter with a static load rating for the bearing is 6.5 KN.

Link lug stress (Light Alloy - L168)

Applied stresses:-

Tensile Stress = L / (2ct) = 226N/mm^2

Shear Stress = L / (2at) = 148 N/mm^2

Bearing Stress = L / (dt) = 429 N/mm^2

Allowable Stresses (N/mm^2):-

	Fail	Proof	RF
Tensile	424	380 x 1.5 x 0.7 = 399	1.77
Shear	180	142 x 1.5 x 0.7 = 149	1.01
Bearing		570 x 1.5 x 0.7 = 599	1.04

Buckling of the link

The link is likely to buckle along the Y axis.
Where, Iyy = $(2t)^3$ 2a/12 = 107 mm^4
radius of gyration k^2 = Iyy/A =1.464

$$\sigma_{cr}=\frac{P_{cr}}{A}=\frac{\pi^2 E_T I}{L^2 A}=\frac{\pi^2 E_T k^2}{L^2}$$

From reference [C3]

$$\frac{\sigma_{cr}}{E_T}\frac{1}{\epsilon_T}=2.569x10^{-3}x171$$

$$\frac{\sigma_{cr}}{f_n}=0.439\therefore\sigma_{cr}=186N/mm^2$$

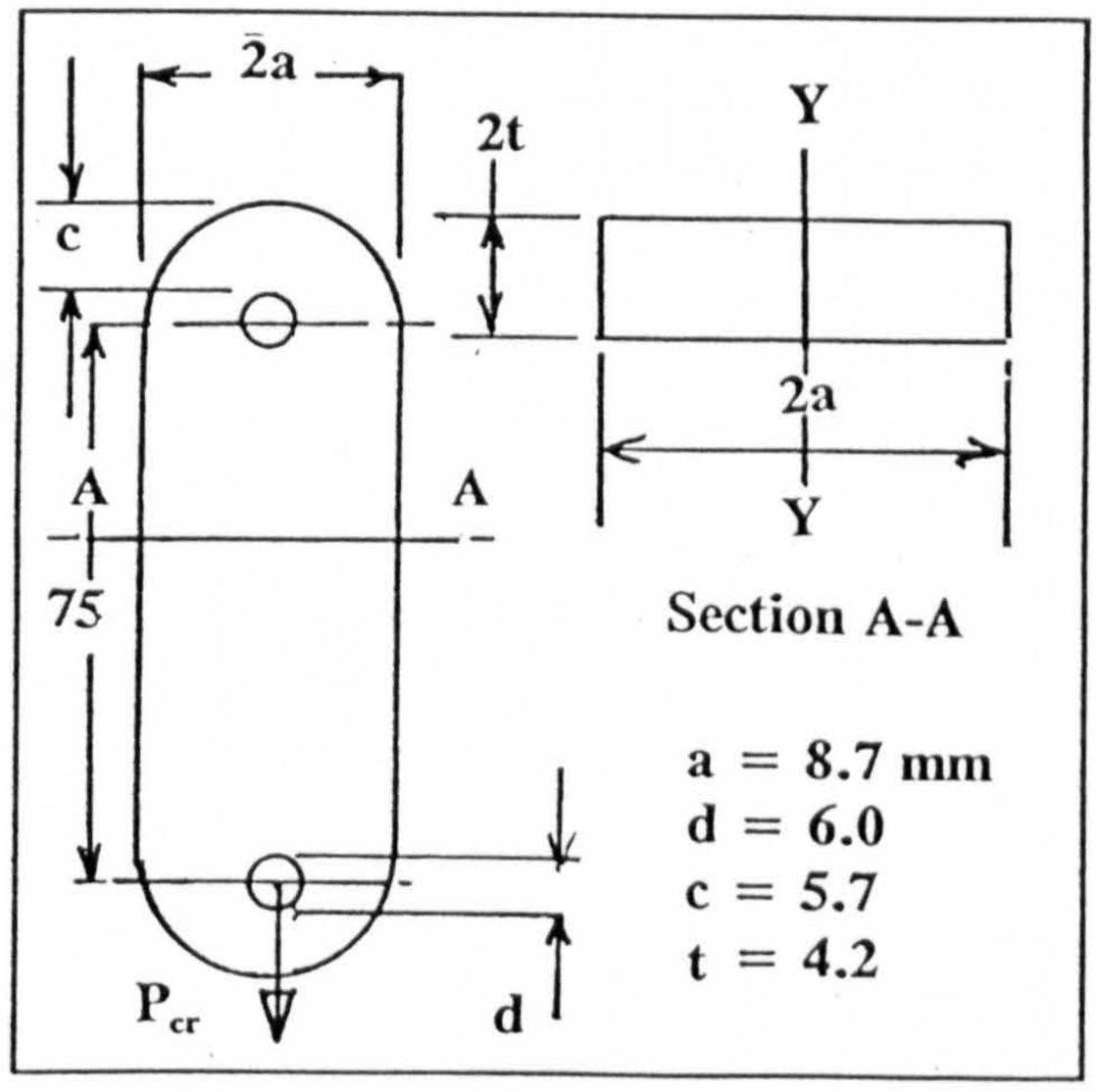

Thus, P_{cr} = 13612 N

RF = 13612/5406 = 2.5

REFERENCES FOR APPENDIX C

[C1] Young, J. B. 'STRUCT' Structural Analysis Computer Code. Available on the College of Aeronautic's Personal Computer Network System, Cranfield Institute of Technology

[C2] INA Bearing Company Limited. Roller Bearings INA 305.

[C3] Young, J. B. College of Aeronautics Detail Stressing Notes and Design Data Sheets. Cranfield Institute of Technology

[C4] Ampep Aerospace Bearings, Ampep PLC, Cleveden England

[C5] SDRC-IDEAS Finite Element Modelling™. Users Guide, 1990

[C6] Mackinnon, A. V. An Experimental Study of a Variable Camber Wing. Ph D Thesis, Cranfield Institute of Technology, 1992

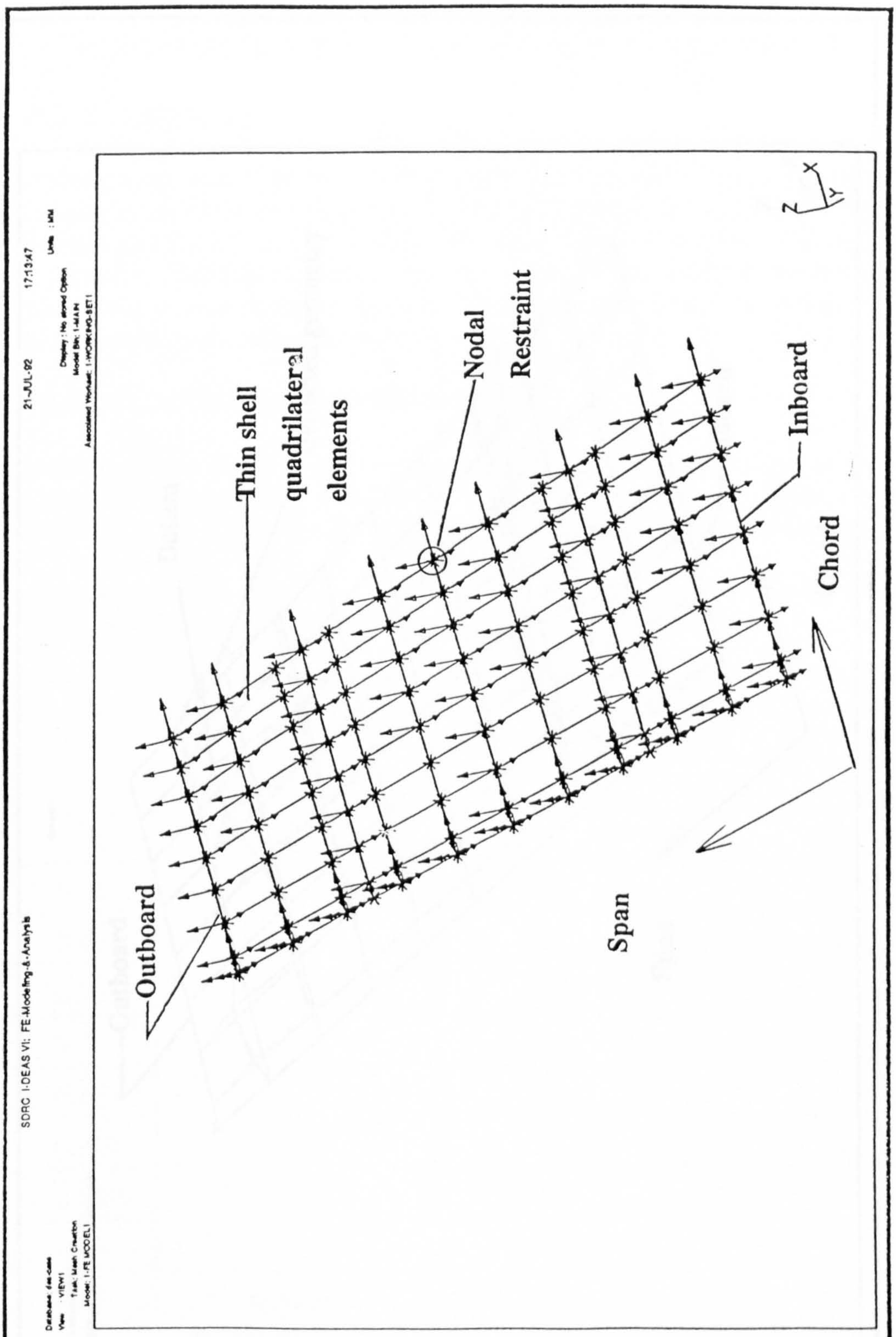

Figure C.1: Finite element model of the upper surface skin

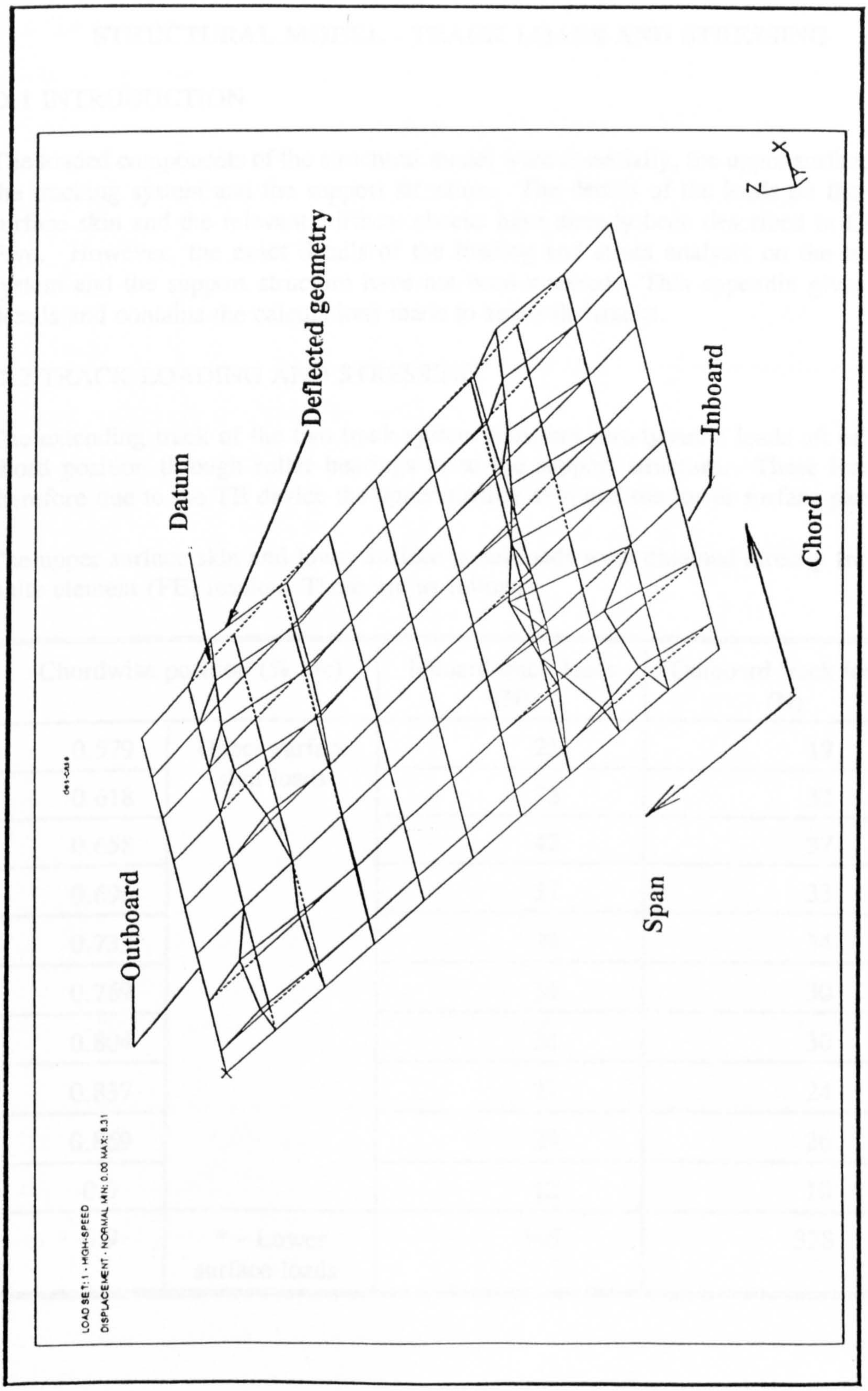

Figure C.2: Deflection geometry for high speed loading

APPENDIX D

STRUCTURAL MODEL - TRACK LOADS AND STRESSING

D.1 INTRODUCTION

The loaded components of the structural model were essentially, the upper surface skin, the tracking system and the support structure. The details of the loads on the upper surface skin and the relevant stiffness checks have already been described in Chapter Five. However, the exact details of the loading and stress analysis on the tracking system and the support structure have not been covered. This appendix gives these details and contains the calculations made to stress the tracks.

D.2 TRACK LOADING AND STRESSING

The extending track of the two track system transfers aerodynamic loads aft of 54 % chord position through roller bearings in to the support structure. These loads are therefore due to the TE device the upper surface skin and the lower surface panel.

The upper surface skin and lower surface panel loads were obtained directly from the finite element (FE) results. These are as follows:

Chordwise position (% x/c)		Inboard track loads (N)	Outboard track loads (N)
0.579	Upper surface skin loads	25	19
0.618		38	32
0.658		42	37
0.696		37	33
0.733		39	34
0.769		34	30
0.804		34	30
0.837		27	24
0.869		29	26
0.9		12	10
0.9	* - Lower surface loads	345	328

The TE device loads on the upper and lower side were assumed to act at the inboard (I/B) and outboard (O/B) ends of the TE segment in 2/3 and 1/3 proportions respectively. Thus,

		Loads (N)	
	Chordwise position % x/c	I/B track	O/B track
TE upper side	0.987	979	489
TE lower side	1.060	841	421

The total track loading is therefore as follows:

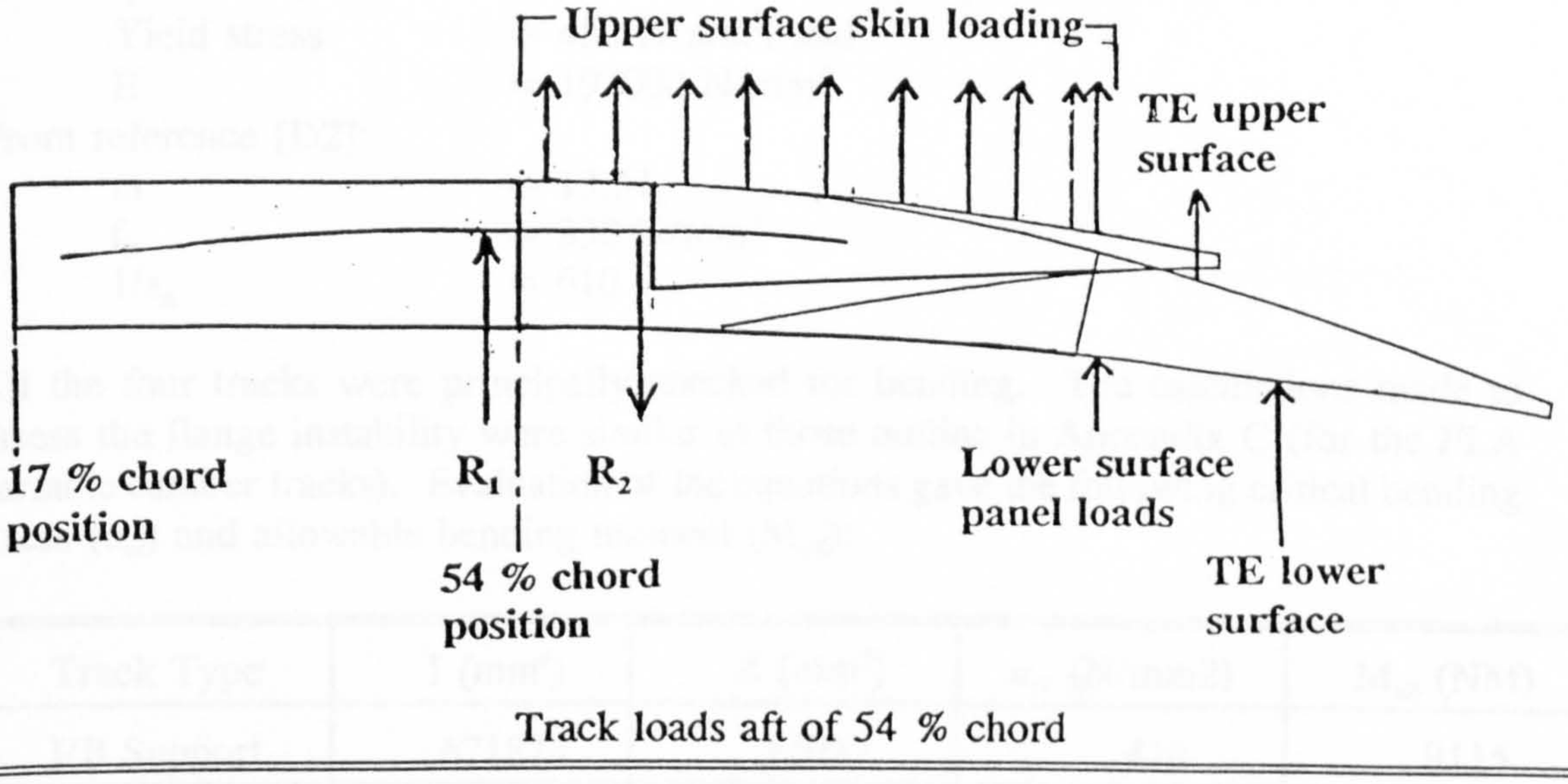

Track loads aft of 54 % chord

Where R_1 and R_2 represent the cam roller positions for reacting the above loads. From the force and moment balance the total reaction loads (N) at these positions is worked out as:

Roller No.	Chordwise position % x/c	Inboard end	Outboard end
R_1	0.511	6733	3821
R_2	0.625	-9175	-5325

The maximum applied bending moment (M_{app}) to the tracks is 341 NM (I/B) and 668 NM (O/B).

Cam Bearing Size

A double roller bogie arrangement is used at all roller positions. Thus assuming a fail safe system, if one roller fails the other should sustain the full load.

From the INA bearing range[D1], the required bearing diameter for the I/B and O/B track rollers is 35 mm and 26 mm respectively. The later has a static load rating of 23 KN while the former has a static load rating of 11.3 KN.

Track Stressing

The tracks are machined from a commercial mild steel, EN8M with a 0.4 % carbon content. The properties for this material are as follows:

f_t	= 620-770 N/mm^2,
t_2	= 370 - 415 N/mm^2,
t_1	= 0.95 t2 = 394 N/mm^2,
Yield stress	= 450 N/mm^2, and
E	= 193000 N/mm^2

From reference [D2]:

m	= 13.51,
f_n	= 338 N/mm^2
$1/\epsilon_n$	= 610

All the four tracks were principally checked for bending. The calculations made to assess the flange instability were similar to those outline in Appendix C (for the FLA variable camber tracks). Evaluation of the equations gave the following critical bending stress (σ_{cr}) and allowable bending moment (M_{all}):

Track Type	I (mm^4)	Z (mm^3)	σ_{cr} (N/mm2)	M_{all} (NM)
I/B Support	671824	22027	414	9115
I/B Extending	568593	15882	388	6157
O/B Support	285516	11897	409	4863
O/B Extending	315138	10505	400	4198

As is seen, M_{all} is greater than M_{app} for all the tracks. Therefore these tracks are not likely to fail in bending.

REFERENCES FOR APPENDIX D

[D1] INA Bearing Company Limited. Rolling Bearings INA 305

[D2] ESDU Validated Engineering Data. ESDU Item No. 76016, ESDU International Limited, 1976

APPENDIX E

MANUFACTURING DRAWINGS FOR THE STRUCTURAL MODEL

Drawings.

VCW-TE/1	Wing structural box
VCW-TE/2	Upper surface mould
VCW-TE/3	Flexible upper surface skin
VCW-TE/4	Trailing edge device
VCW-TE/5	Hinged lower surface box
VCW-TE/6	Variable camber tracks
VCW-TE/7	Upper surface conforming strip
VCW-TE/8	Actuator attachment to the trailing edge device

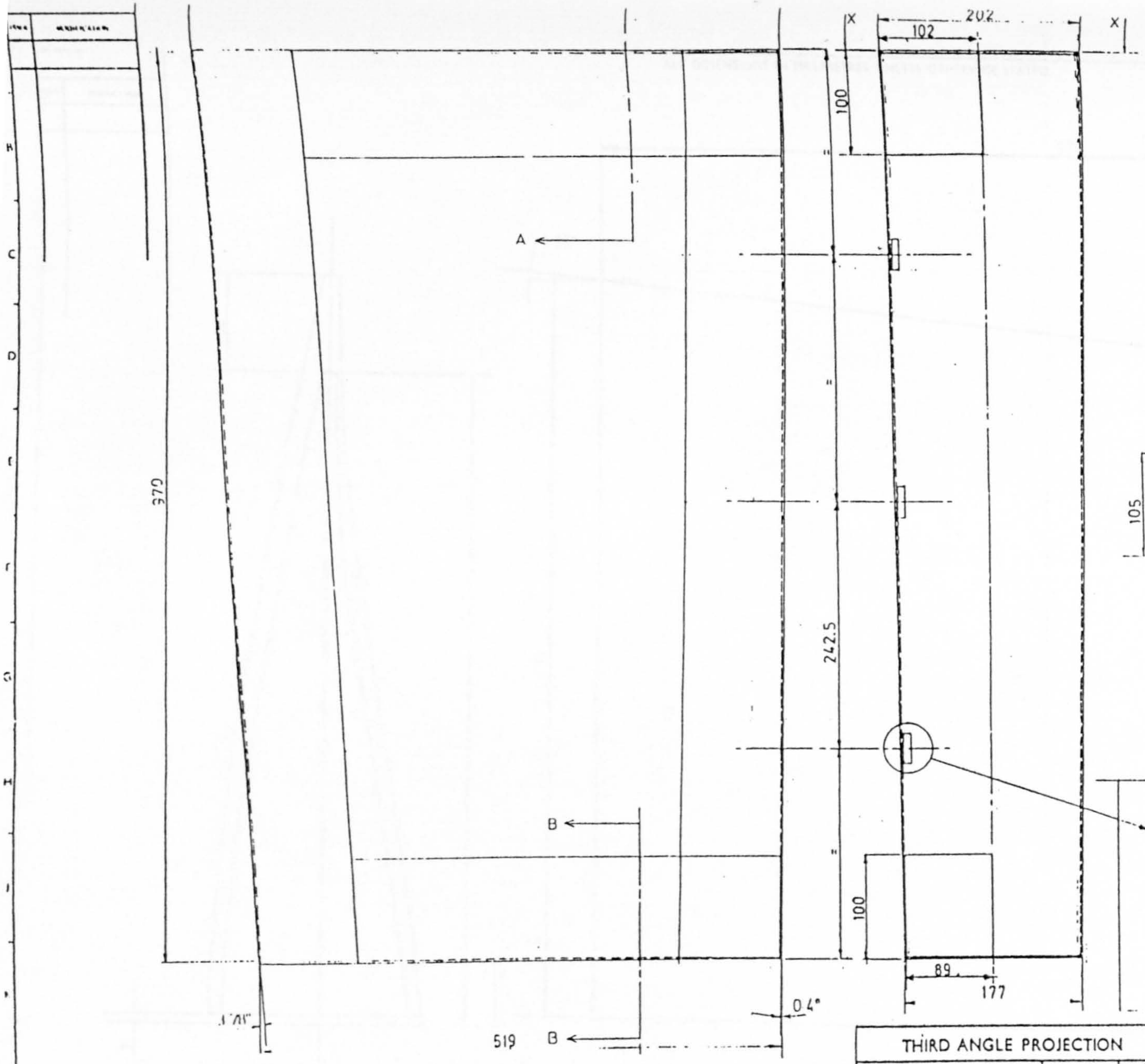

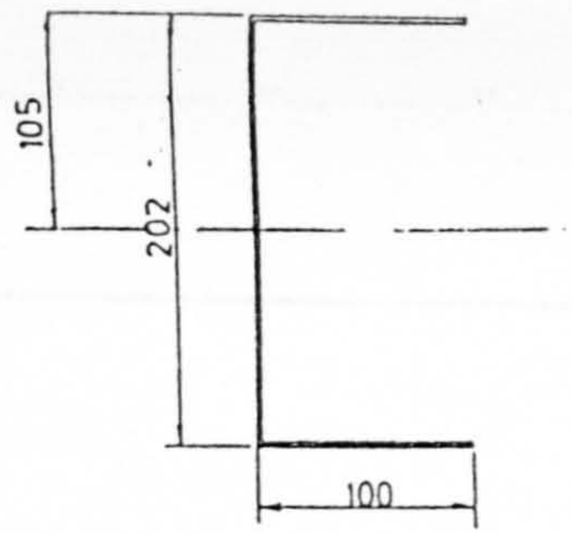

VIEW X-X

WING REAR SPAR (54% x/c)

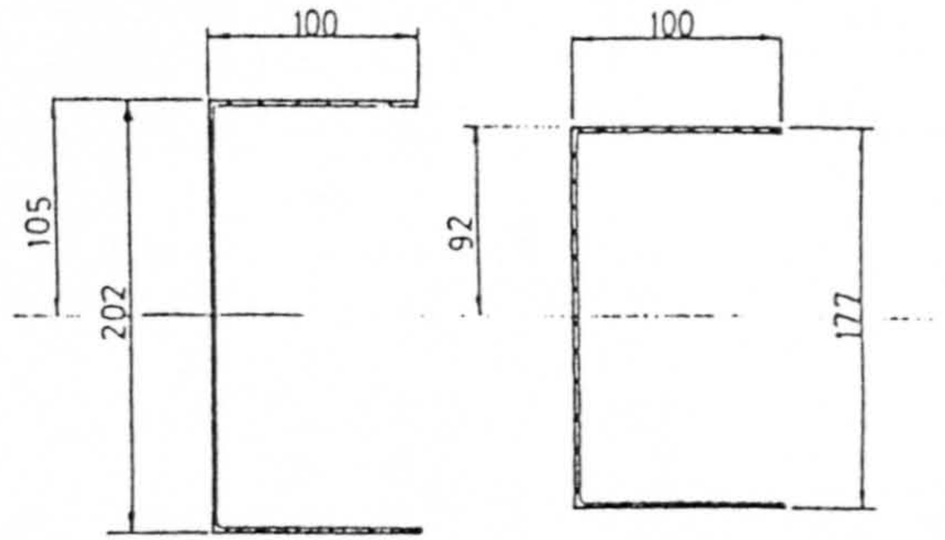

SECTION A - A

SECTION B-B

ALL CHANELS ARE 3mm THICK

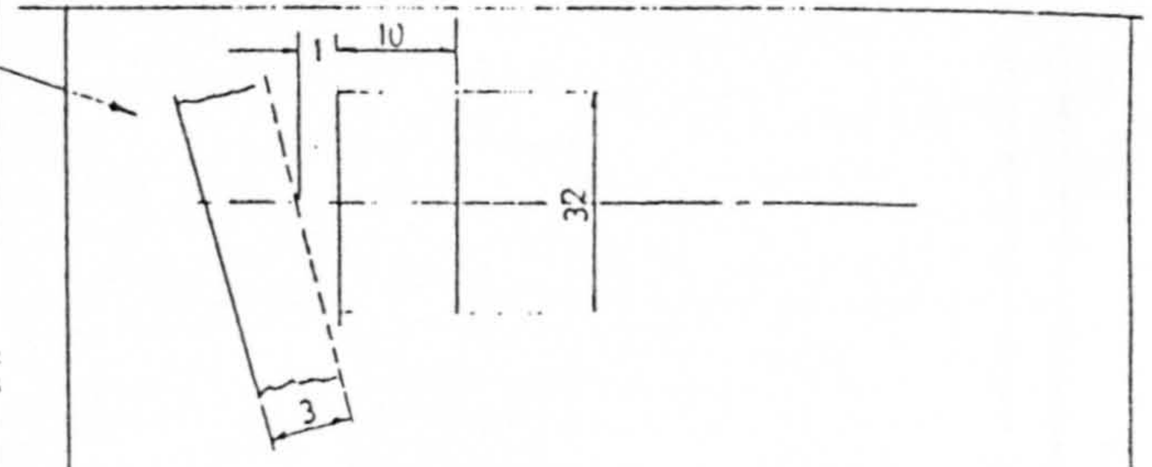

THIRD ANGLE PROJECTION			SHEET SIZE A1	ITEM	PART NO.	DESCRIPTION	NO. OFF	MATL	SPEC.	REMARKS			
GENERAL TOLERANCE ON DIMENSIONS: MACHINED, UNMACHINED, OTHER DIMENSIONS AS STATED	JOB NO.	NO. OF SHTS IN SET	SCALE 1/2										
WELD WHERE SHOWN THUS			FINISH	DRAWN	CHK'D	APP'D	STRESS OFFICE	TITLE:- WING STRUCTURAL BOX					
MACHINE WHERE SHOWN THUS	USED ON (NO.)			ISSUED BY: CRANFIELD INSTITUTE OF TECHNOLOGY, CRANFIELD.				DRAWING NO. VCW - TE/1					
								SHT	OF	SHTS			

225

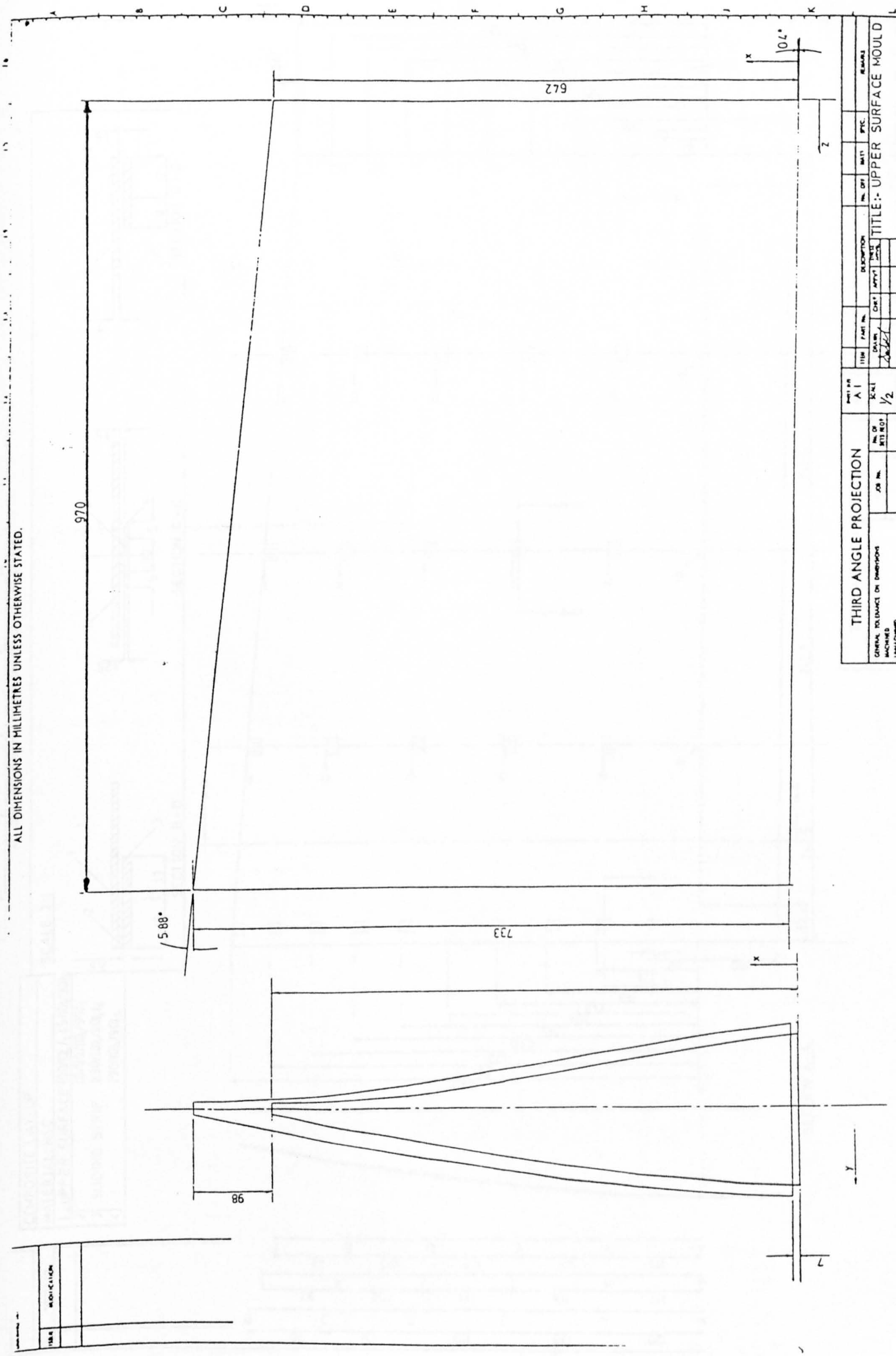
A
B
C
D
E
F
G
H
J
K
L
642
1°
07°
Z
970
5·88°
733
X
Y
98
7
ALL DIMENSIONS IN MILLIMETRES UNLESS OTHERWISE STATED.
THIRD ANGLE PROJECTION
TITLE:- UPPER SURFACE MOULD
CRANFIELD INSTITUTE OF TECHNOLOGY
VCW-TE/2
SCALE 1/2
SIZE A1

ALL DIMENSIONS IN MILLIMETRES UNLESS OTHERWISE STATED.

ISSUE	MODIFICATION

COMPOSITE LAY-UP		
MATERIAL: HSC		
1. UPPER SURFACE		$(90/(0)_4/\pm 45/(0)_4/90)_S$
2	SLIDING STRIP	$(0/90/(0)_2/90)_S$
3	SLIDING STRIP	$((90/(0)_4/90)_4)_S$
4	SLIDING STRIP	$(90/(0)_4/90)_S$

SCALE 2:1

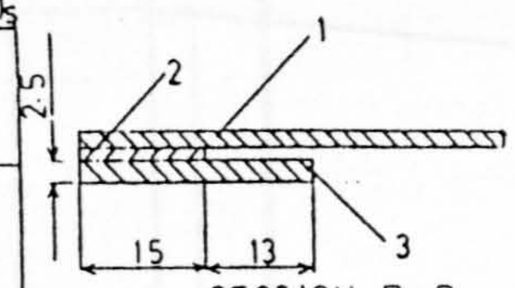

SECTION B-B

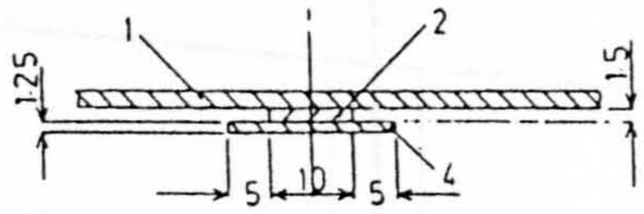

SECTION C-C

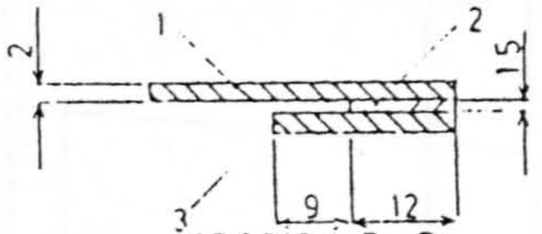

SECTION D-D

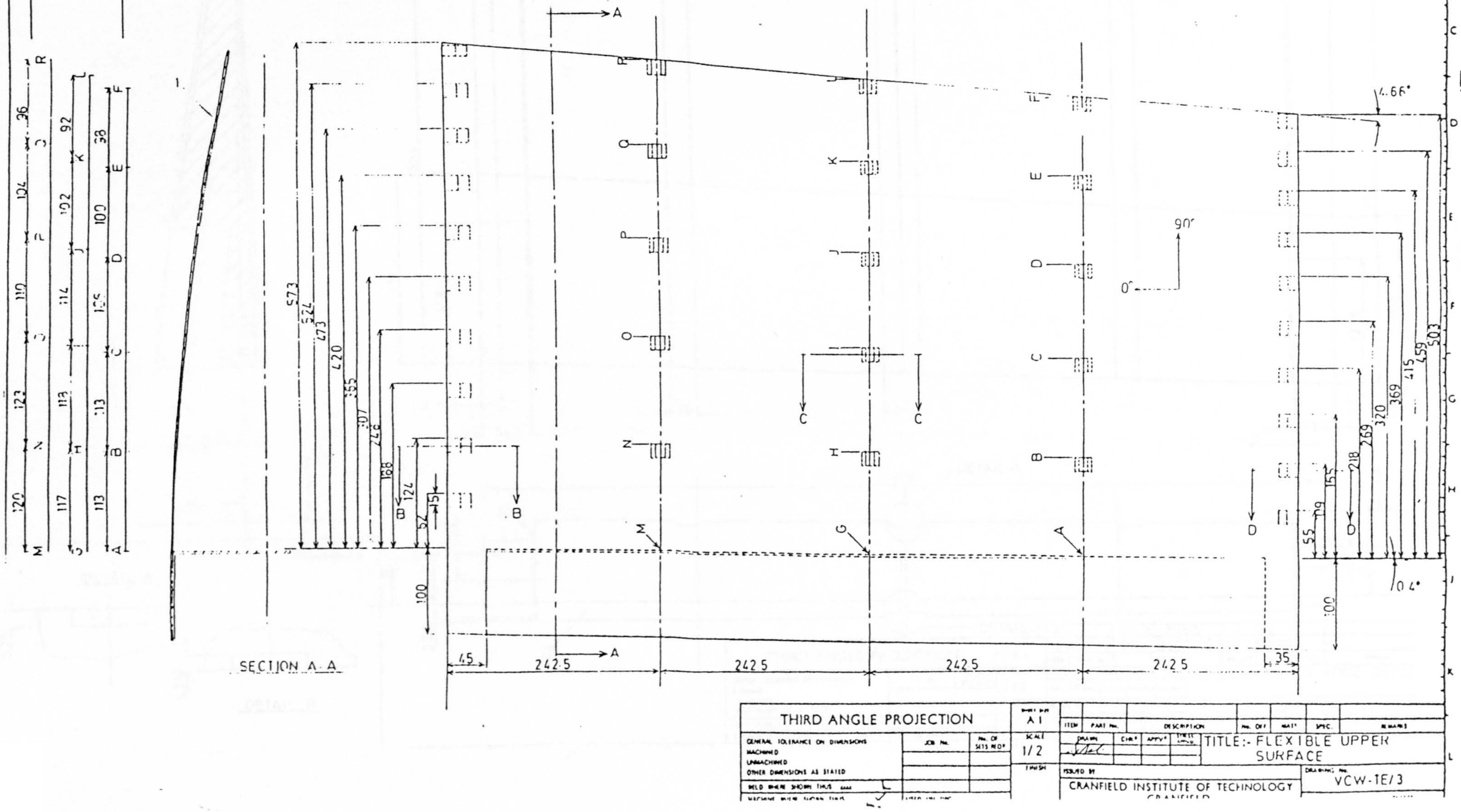

SECTION A-A

THIRD ANGLE PROJECTION			SHEET SIZE A1	ITEM	PART No.	DESCRIPTION	No. OFF	MAT'L	SPEC.	REMARKS
GENERAL TOLERANCE ON DIMENSIONS	JOB No.	No. OF SETS REQ'D	SCALE 1/2	DRAWN	CHK'D	APPV'D	TITLE:- FLEXIBLE UPPER SURFACE			
MACHINED										
UNMACHINED										
OTHER DIMENSIONS AS STATED										
WELD WHERE SHOWN THUS ~~~~			FINISH	ISSUED BY			DRAWING No.			
MACHINE WHERE SHOWN THUS				CRANFIELD INSTITUTE OF TECHNOLOGY CRANFIELD			VCW-1E/3			

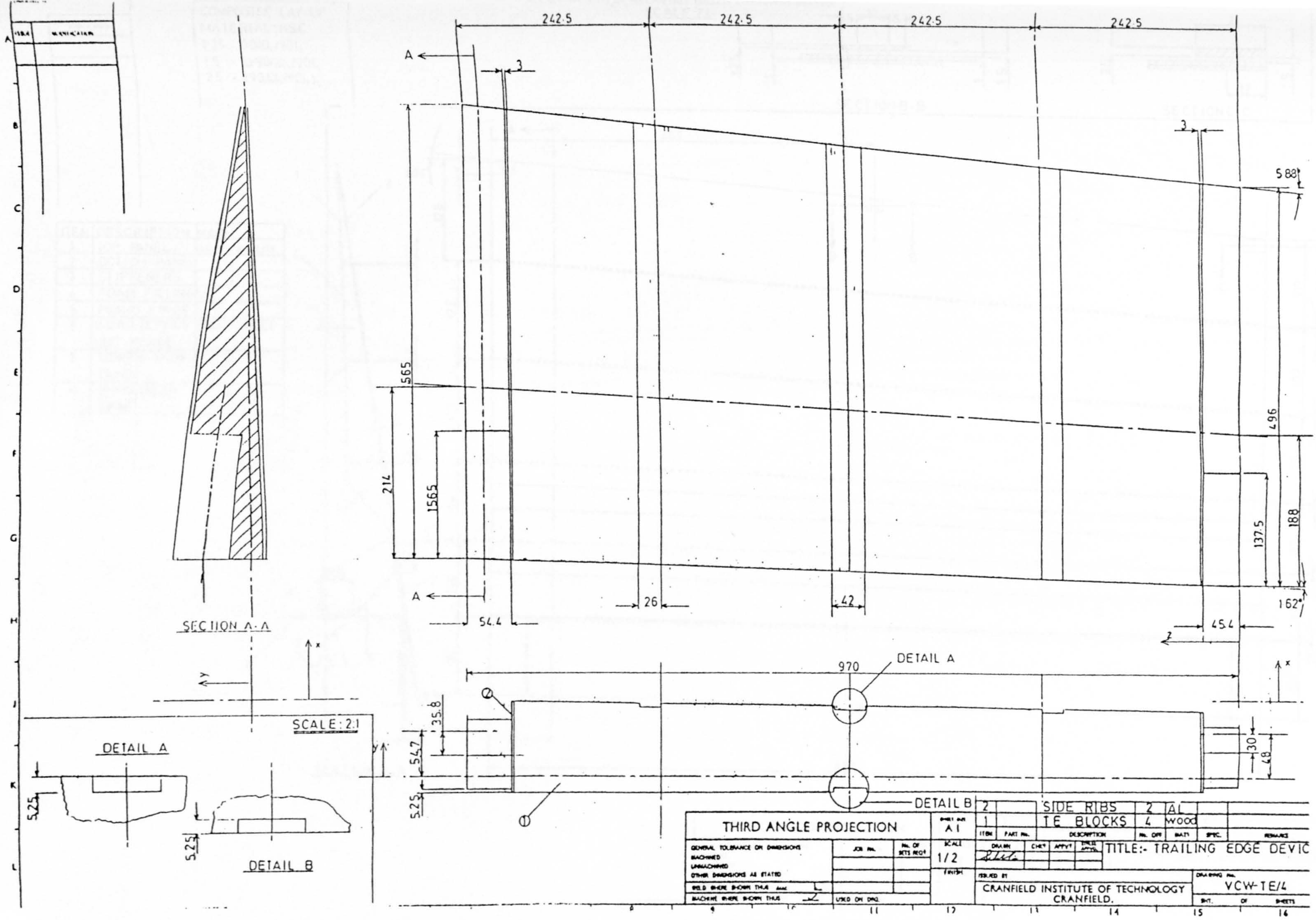

ITEM	PART No.	DESCRIPTION	No. OFF	MATL	SPEC.	REMARKS
2		SIDE RIBS	2	AL		
1		TE BLOCKS	4	wood		

THIRD ANGLE PROJECTION

SHEET SIZE A1

SCALE 1/2

DRAWN | CHK'D | APPV'D | DWG APPV'D

TITLE:- TRAILING EDGE DEVIC

GENERAL TOLERANCE ON DIMENSIONS
MACHINED
UNMACHINED
OTHER DIMENSIONS AS STATED
WELD WHERE SHOWN THUS
MACHINE WHERE SHOWN THUS

JOB No. | No. OF SETS REQ'd | USED ON DWG.

FINISH

ISSUED BY
CRANFIELD INSTITUTE OF TECHNOLOGY
CRANFIELD.

DRAWING No. VCW-TE/4

SHT. OF SHEETS

828

ALL DIMENSIONS IN MILLIMETRES UNLESS OTHERWISE STATED.

SCALE 2:1

COMPOSITE LAY-UP
MATERIAL : HSC
1 25 - $(90/10_h/90)_s$
1 5 - $(0/90/(0)_1/90)_s$
2 5 - $((90/10)_3/90)_2)_s$

ITEM	DESCRIPTION	MAT-
1	TOP PANEL	ALUMINIUM
2	BOTTOM PANEL	"
3	STIFFENERS	"
4	FOAM FILLING	
5	PIANO HINGE	
6	LOAD DIFFUS-ING PLATE	MILD STEEL
7	LOWER SKIN PANEL	"
8	WING REAR SPAR	"

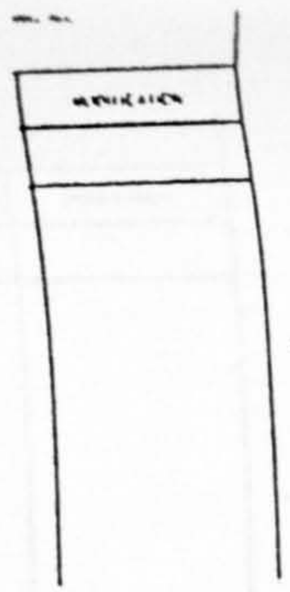

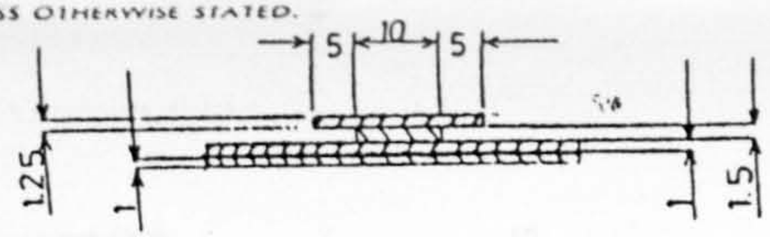

SECTION B-B

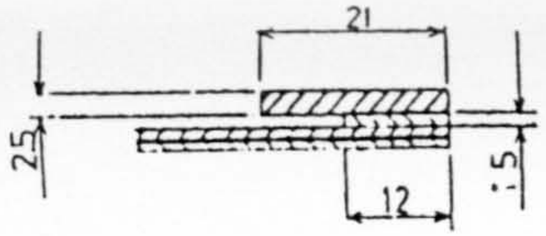

SECTION C-C

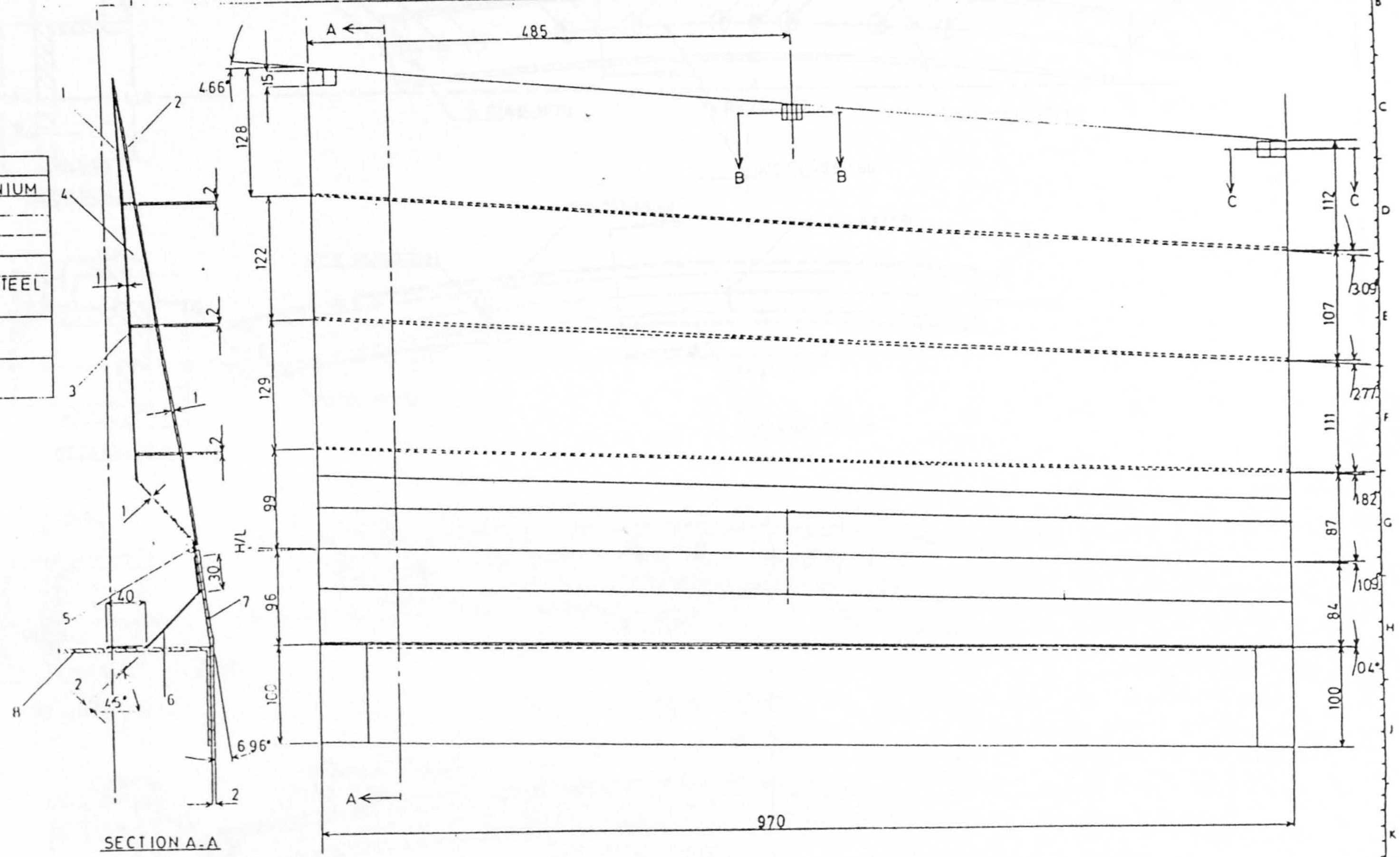

SECTION A-A

THIRD ANGLE PROJECTION	SHEET SIZE A1	ITEM	PART No.	DESCRIPTION	No. OFF	MATL	SPEC.	REMARKS
GENERAL TOLERANCE ON DIMENSIONS: MACHINED, UNMACHINED, OTHER DIMENSIONS AS STATED; WELD WHERE SHOWN THUS; MACHINE WHERE SHOWN THUS	SCALE 1/2	DRAWN	CHK'D	APPV'D	FINISH SPEC.	TITLE:-HINGED LOWER SURFACE		
JOB No. / No. OF SETS REQ'D / USED ON ENG.	FINISH	ISSUED BY: CRANFIELD INSTITUTE OF TECHNOLOGY, CRANFIELD.				DRAWING No. VCW-TE/5		
						SHT. OF SHEETS		

229.

POINTS	x-y COORDINATES	
1	442.14,	38.33
2	466.73,	39.92
3	499.85,	45.61
4	533.64,	47.92
5	622.67,	58.81
6	656.55,	59.5
7	690.03,	62.72
8	779.95,	65.18
9	813.81,	63.8
10	847.42,	64.97
11	937.32,	61.94
12	971.03,	58.49
13	1004.65,	57.6
16	1027.07,	54.27
15	289.13,	11.51
14	1183.31,	35.96
17	389.34,	34.1
16	409.19,	35.31
19	438.21,	40.48
20	469.88,	42.33
21	545.90,	52.25
22	575.64,	52.67
23	604.98,	55.67
24	683.86,	57.84
25	713.57,	56.44
26	743.03,	57.65
27	821.89,	54.99
28	851.47,	51.79
29	880.95,	51.2
32	900.61,	48.09
30	1037.65,	32.03
31	253.38,	10.57

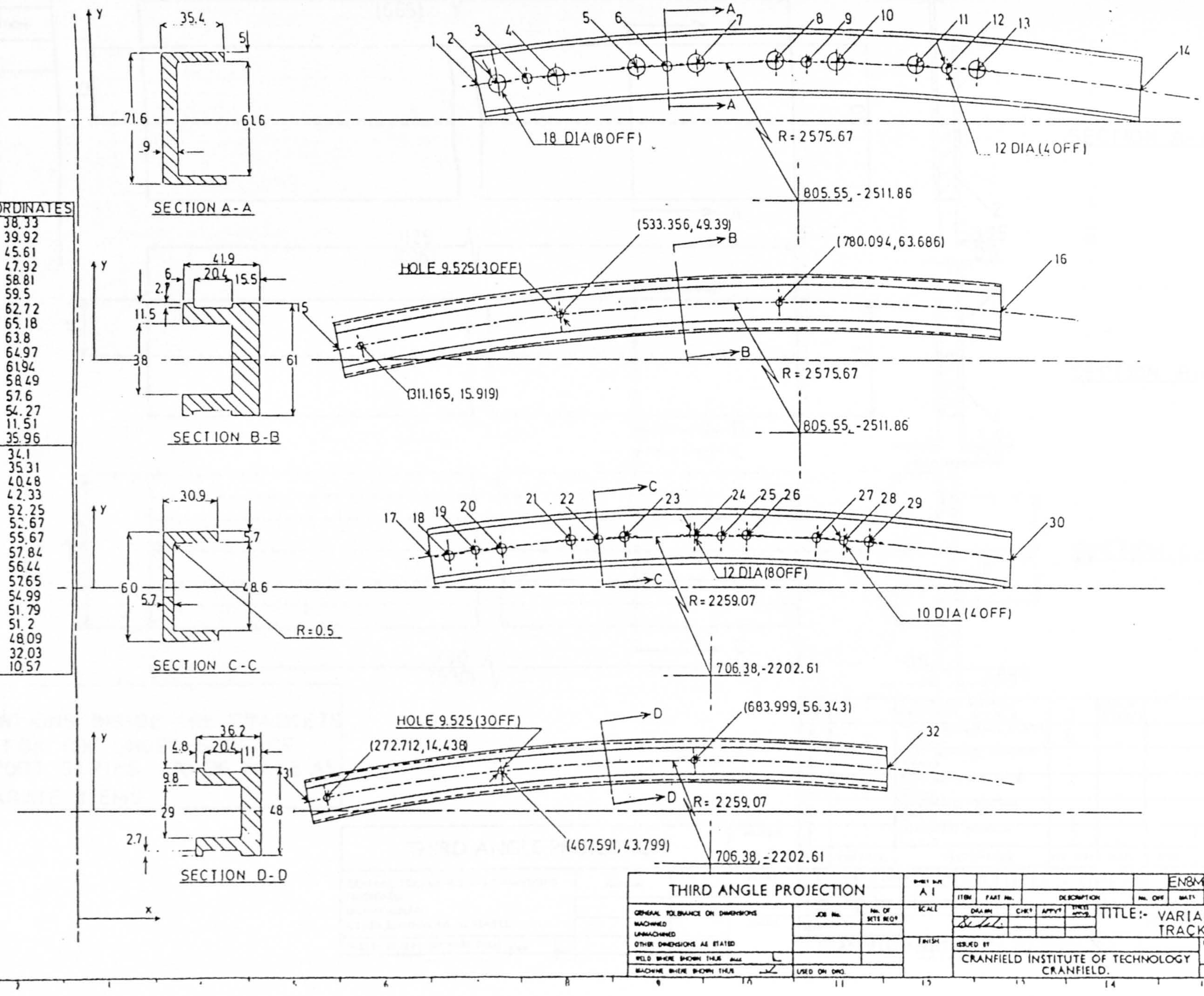

DRAWING No.

ISSUE	MODIFICATION

ALL DIMENSIONS IN MILLIMETRES UNLESS OTHERWISE STATED.

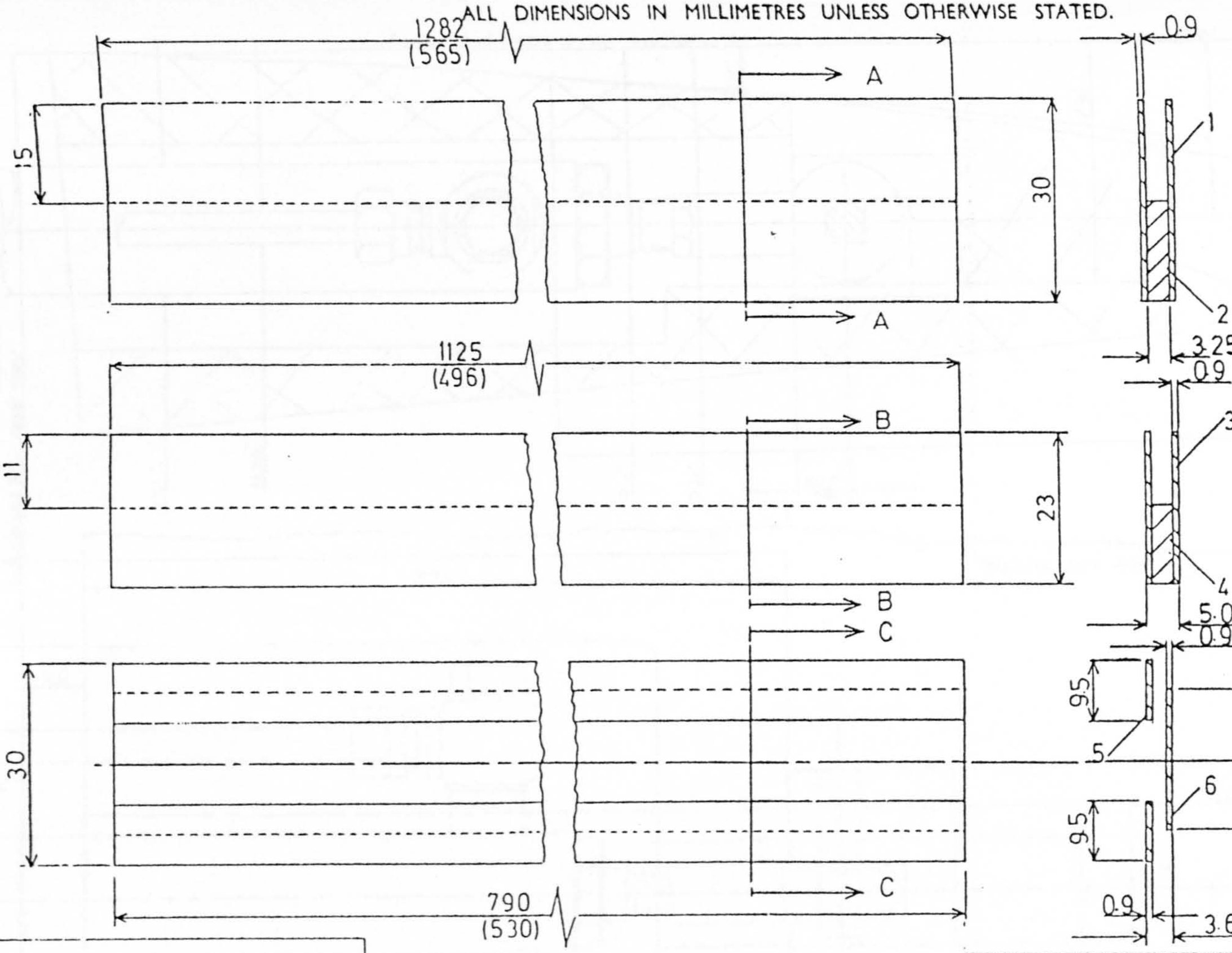

SECTION A-A

SECTION B-B

SECTION C-C

NOTE
DIMENTIONS INSIDE THE BRACKETS ARE FOR THE UNDER SURFACE SUPPORT STRIPS. TO BE MADE AS SEPARATE ITEMS

ITEM	PART No.	DESCRIPTION	No. OFF	MAT'L	SPEC.	REMARKS
6		BOTTOM INTER-MEDIATE STRIP	3	MILD STEEL		
5		TOP INTERMEDIATE STRIP	6	"		
4		OUTBOARD INNER STRIP	1	"		
3		OUTBOARD OUTER STRIP	2	"		
2		INBOARD INNER STRIP	1	"		
1		INBOARD OUTER STRIP	2	"		

THIRD ANGLE PROJECTION

SHEET SIZE A 2

GENERAL TOLERANCE ON DIMENSIONS
MACHINED
UNMACHINED
OTHER DIMENSIONS AS STATED
WELD WHERE SHOWN THUS

JOB No.	No. OF SETS REQ'D

SCALE 2:1

FINISH

DRAWN	CHK'D	APP'D	STRESS APP'D
[illegible] 4 APR 91			

TITLE:- UPPER SURFACE CONFORMING STRIP

ISSUED BY
CRANFIELD INSTITUTE OF TECHNOLOGY

DRAWING No. VCW-TE/7

231

ISSUE	MODIFICATION

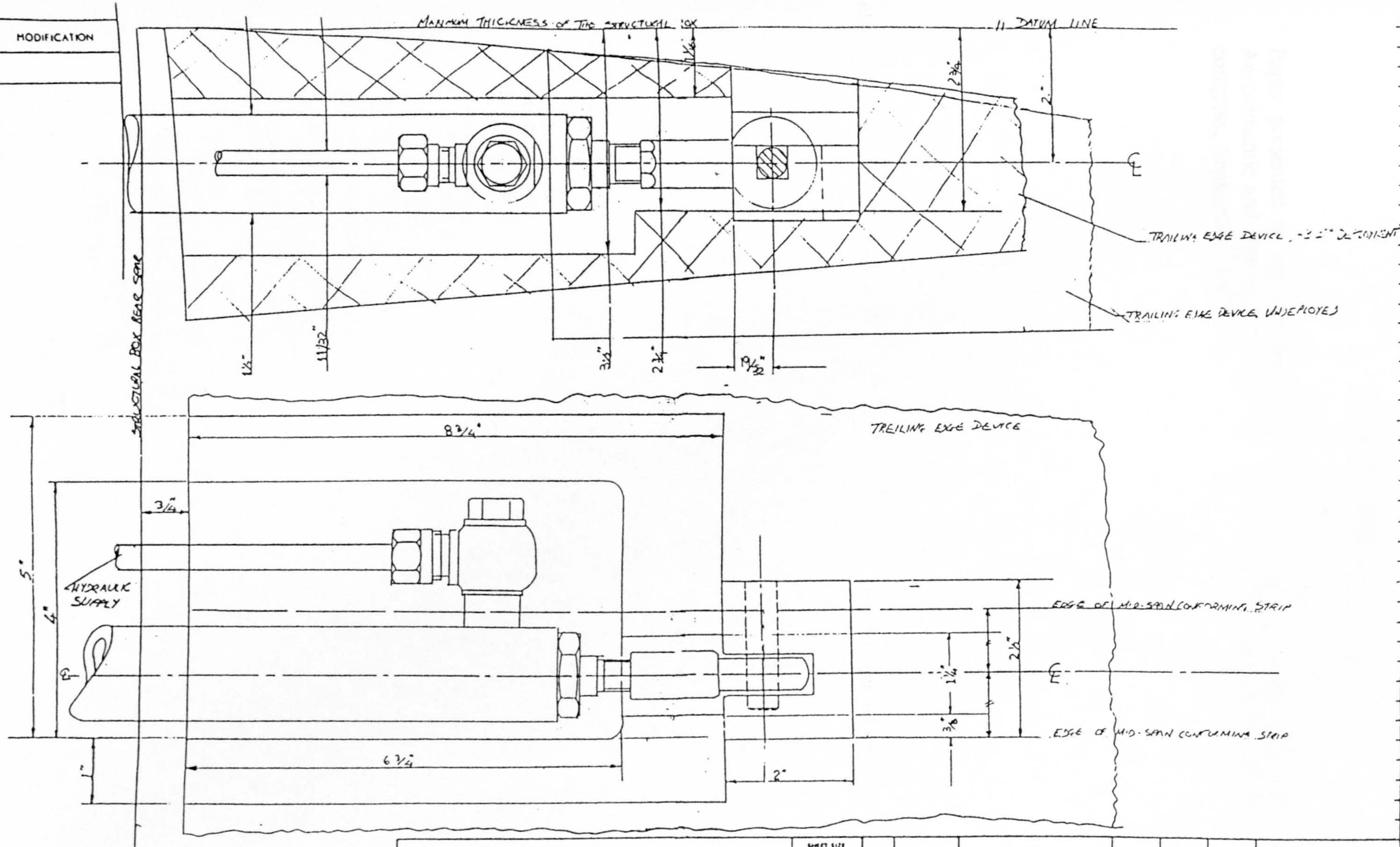

THIRD ANGLE PROJECTION			SHEET SIZE A 2	ITEM	PART No.	DESCRIPTION	No. OFF	MAT'L	SPEC.	REMARKS
GENERAL TOLERANCE ON DIMENSIONS MACHINED UNMACHINED OTHER DIMENSIONS AS STATED	JOB No.	No. OF SETS REQ'D	SCALE FULL SCALE	DRAWN	CHK'D	APPV'D	STRESS APPV'D	TITLE :- ACTUATOR ATTACHMENT TO THE TRAILING EDGE DEVICE		
WELD WHERE SHOWN THUS ⌒			FINISH	ISSUED BY				DRAWING No.		
MACHINE WHERE SHOWN THUS ✓	USED ON DRG.			CRANFIELD INSTITUTE OF TECHNOLOGY CRANFIELD.				VCW-TE 8		
								SHT. OF SHEETS		

APPENDIX F

Paper presented at the 18th International Council of the Aeronautical Sciences. "The Aerodynamic and Structural Design of a Variable Camber Wing", ICAS 1.6.4, 18th ICAS congress, September 1992.

THE AERODYNAMIC AND STRUCTURAL DESIGN OF A VARIABLE CAMBER WING (VCW)

J P Fielding
S H M Macci
A V Mackinnon
J L Stollery

Cranfield Institute of Technology, Cranfield,
Bedfordshire, MK43 OAL
England

ABSTRACT

Current trends in the design of transport (civil/military) aircraft have shown that in order to be economically viable it is necessary to investigate technologies which may give an improvement in performance and operational flexibility. It is believed that the application of variable camber (VC) to a wing would assist in achieving such a goal.

With the aim of developing a system which satisfies the conflicting structural and aerodynamic requirements, investigations have been made to:-

1) Study the low and high speed theoretical and experimental aerodynamic effects of continuously changing the wing profile to suit all flight conditions.
2) Examine the practical (structural/mechanical) implications of applying such a concept to a real aircraft.

The two dimensional (chordwise) variation in camber is obtained by simultaneous rotation and extension of the trailing edge element near the aft region, and by simple droop of the leading edge (LE) element towards the front of the aerofoil. Thus a family of aerofoils of varying camber may be generated. Two dimensional experimental tests indicate that with increase in lift coefficient, gradual variation of camber results in lower drag compared with the basic undeployed section.
On a three dimensional wing it is necessary to divide the wing span into multi-segmented leading and trailing edge pieces. Experimental tests show that variation in spanwise lift distribution can be achieved if these spanwise segments are deployed independently. The root bending moment associated with gust loads or pilot initiated manoeuvre loads is significantly reduced by altering the spanwise lift distribution in such a way to cause inboard movement of the centre of pressure. This is achieved by selection of a highly cambered wing root portion combined with low or negatively cambered tip segments.

This paper:

1) Reports on the encouraging results found from the theoretical and experimental aerodynamic work,
2) Presents a design solution of a practical system which satisfies the aerodynamic requirements, and
3) Describes the tests carried out to verify the overall design concept.

Notation

LE - Leading edge
TE - Trailing edge
VCW - Variable Camber Wing
C_{TE} - Chordwise length of the trailing edge element
E - Youngs modulus of elasticity (N/mm^2)
C_L - Lift coefficient
C_{Le} - Local lift coefficient
C_D - Drag coefficient
C_{Dinc} - Drag coefficient increment
C_{Rinc} - Roll coefficient increment
C_P - Coefficient of pressure
δ - Camber angle of rotation (Degrees)
α - Angle of incidence (Degrees)
η - Spanwise position of centre of pressure
$[90/0_2]_s$ - Orientation, No. and lay-up of carbon fibres. Subscript 's' refers to symmetric lay
[Note : all non dimensionalised coefficients are calculated based on the undeployed reference chord].

Segment No	1 Root	2	3	4 Tip	Symbol
Camber angle of rotation, δ (Degrees)	0	0	0	0	✱
	5	5	5	5	○
	10	10	10	10	◇
	5	5	0	0	□
	10	10	0	0	△
	5	5	0	-3.5	×

1. INTRODUCTION

The objective of this research was to investigate the problems and benefits of applying a variable camber wing (VCW) system to transport aircraft.

Spillman (Reference 1) pioneered a novel method of camber variation by means of rotation and translation of leading edge (LE) and trailing edge (TE) elements. The top surface was kept smooth and continuous to generate a family of cambered aerofoil sections. The proposal was tested experimentally by Rao (Reference 2) using a quasi two dimensional (2-D) wing. The work presented in this paper maintains the same deployment programme for the aft camber variation.

A supercritical aerofoil of 14 % thickness to chord ratio (t/cmax) was designed with generous section thickness between 50% and 70% chord and significant TE thickness. This was perceived to assist in accommodating the camber actuation equipment.

The details of the change in section profile are depicted in Figure 1. The position of maximum curvature on the upper surface lies at 64.5% chord and so was chosen as the junction between the centre body and the TE element. The origin of this curvature was selected as the centre of rotation and the camber angle, δ, was prescribed as the angle of rotation of the TE element in a circular arc about this origin. A flexible upper surface plate joins the centre body and the TE element to permit extension yet maintain curvature. The lower surface was a simpler system in which a rigid closing plate is hinged from the centre body at 60% chord and held by spring loads to the TE element. This geometry maintains a smooth top surface when deployed.

The purpose of LE deployment is to control the LE suction pressure peak caused by variations in circulation due to camber changes. Deployment of the LE element on a circular arc presented insurmountable design problems. These are overcome (see Figure 1) by simply drooping the LE element without extension, similar to the RAEVAM system. A description of this concept is given in Figure 2 (taken from Reference 3).

For a finite wing, spanwise variation of camber is possible by dividing the camber controlling devices into several segments along the span, each of which can be deployed independently. The geometric implications of achieving such a variation in wing camber are discussed in Section 3.2.

2. AERODYNAMIC DESIGN

2.1 VARIABLE CAMBER WING WIND TUNNEL MODEL

The variable camber (VC) half wing wind tunnel model shown in Figure 3 was of a rectangular planform swept at 25°. A semi-span distance of 1.6m and reference chord of 0.6m gave an aspect ratio of 5.33 which combined with a tunnel speed of 50 m/s resulted in a test Reynolds No. of two millions (2×10^6).

Discrete chordwise camber settings of -3.5°, 0°, 5° and 10° rotation were tested using detachable trailing edge (TE) pieces for each camber. The span was divided into four equal segments, thus any number of camber settings and spanwise positions could be achieved.
One TE piece of each camber setting was pressure tapped along with a leading edge segment and the centre body. The pressure distribution over the entire wing could therefore be measured by moving the appropriate pressure tapped segments along the span.

A series of tests was carried out with both uniform spanwise camber and discontinuous spanwise settings measuring forces and moments and recording pressure distributions at twelve spanwise stations.

2.2 FORCES AND MOMENTS

The notation used to describe the value of camber settings (rotation of the TE element about the origin) at each of the four span positions is simply done by stating the camber settings from root to tip (eg 10 10 0 0 describes a wing configuration of two 10 degree camber settings at the root portion combined with two undeployed settings at the tip).

Figure 4 displays the graph of lift coefficient (C_L) against incidence, α, for three uniform spanwise camber cases namely, 0°, 5° and 10°. Also shown are two cases with discontinuous spanwise camber settings, these being 10 10 5 5 and 5 5 0 0. It was found that the experimental lift curve slope of 3.86/rad compared well with the theoretical value of 3.87/rad (Reference 4) for the basic section. Subsequent increase in uniform camber across the span to 5° and 10° resulted in a parallel shift of the C_L vs α curve. Thus C_L at zero incidence rose from 0.092 to 0.342 for the 5° case and up to 0.646 for the 10° case.

The slope of both the discontinuous spanwise camber settings is greater than those of the uniform camber distribution. Examining the 5 5 0 0 case it would be expected that the lift against incidence curve would lie directly between that of 5° and 0° uniform case as the mean camber would be 2.5° across the span. These tests however show that for positive incidence the 5 5 0 0 lift against incidence curve lies nearer the 5° than the 0° curve. A similar pattern is repeated for the 10 10 0 0 case. This indicates that a large portion of the spanwise loading is carried by the segments at, or adjacent to the root of the wing.

Figure 5 shows the graph of drag coefficient against lift coefficient (C_D vs C_L) for the three uniform camber settings (namely 0°, 5° and 10°). There appears to be little difference between the three curves but a trend can be seen. At low C_L an increase in camber results in an increase in C_D. As the C_L rises this drag difference reduces and at C_L of approximately 0.8 the drag of the 5° case equals that of the 0° case. Above this value of C_L it is seen that the more cambered sections produce less drag than the basic section. Thus at the higher values of C_L the C_D vs C_L curves overlap one another. To maintain the minimum drag the camber setting would have to be increased gradually with increasing C_L above 0.8.

To amplify the difference between these curves the drag increments with respect to the basic section, $C_{D_{inc}}$, were plotted against C_L, as depicted in Figure 6. It is clearly seen that the higher the camber setting the larger the drag increment at zero lift. As C_L increases the drag increment for the 5° and 10° cases reduces. The 5° case matches drag with the basic section at C_L of 0.8 and the 10° case at C_L of 0.9. Above these values drag benefit is gained. Figure 6 also shows the drag increment for the aforementioned discontinuous camber cases plus a further case with the camber setting of 5 5 0 -3.5, which has two camber discontinuities across the span. For these three cases the reduction in drag increment with increased C_L is much sharper. For the configuration 5 5 0 0 the drag cross-over occurs at a C_L of approximately 0.42, whilst for the 10 10 0 0 case it occurs at a C_L of 0.8. This is a little

surprising as it was suspected that the configuration with mid-span camber discontinuity would generate additional vortex drag due to the geometry step between adjacent camber segments. However the reason is indicated by the spanwise lift distribution shown in Figure 11. With the spanwise change of camber (eg 5 5 0 0) the distribution is more nearly elliptic. The load distribution was further altered by introducing a second spanwise camber discontinuity with the configuration 5 5 0 -3.5. This condition results in almost the same drag as the 5 5 0 0 single camber discontinuity case.
In an attempt to reduce drag further, small fences were introduced between each of the TE segments to straighten cross flow. Over the entire C_L range the results show an extra drag increment due to the increased wetted area.

Figure 7 shows a graph of rolling moment coefficient increment with respect to the basic section, $C_{R_{inc}}$, against C_L. It demonstrates that little rolling moment change is experienced between uniform spanwise camber cases. This was to be expected as the planform remains rectangular and hence the spanwise loading are of similar shape. The 5 5 0 0 configuration shows a reduction in rolling moment coefficient of 20% at a C_L of 0.3 and further reduction is achieved with the 5 5 0 -3.5 and 10 10 0 0 configurations. This effect is more clearly shown in Figure 8, where the spanwise centre of pressure, η, is plotted against C_L. It is seen that the combination of large wing root cambers and low wing tip camber causes large inboard movements of the centre of pressure.

2.3 PRESSURE DISTRIBUTIONS

The pressure distributions were measured at twelve spanwise positions. From each chordwise distribution the local lift coefficient was calculated and as before was based on the reference chord.
Comparing the pressure distributions at spanwise station 7 (See Figure 9) for the three uniformly cambered wing cases identifies the need for an efficient and well controlled LE camber device. The rise in the LE suction pressure peak due to the increased circulation produced by the aft camber variation is significant. Early theoretical calculations confirmed the need for a LE device and a deployment method which maintained a smooth change in curvature, similar to that at the junction between the centre body and deployed TE element. It is also seen that significantly more aft loading results from the larger camber. This is due to the rotation and extension of the TE element and much of the additional lift is carried by the chord extension.
On the lower surface for the larger camber cases a discontinuity of slope of pressure coefficient, C_p, appears at 60% chord. This position is the joint between the hinged lower surface closing plate and the centre body and this peak was accepted in order to simplify the structural design. Theoretical calculations indicated negligible drag penalty which was insufficient to warrant modification.
Figure 10 shows the pressure distributions at stations 1, 7 and 12 for the uniform spanwise camber configuration 5 5 5 5 at zero incidence. It is seen that the root pressure distribution has a slightly lower LE suction peak compared to the mid-span pressure distribution at station 7. This is probably due to the existence of a small gap (3mm) between wing root and reflection plate to prevent rigging load interference. This gap allows a small passage of air from the lower surface to the upper surface reducing lift near the LE and increasing aft loading due to the presence of a small root vortex. At the tip of the wing C_L is zero and at station 12, 30mm from the tip, the pressure distribution is severely altered by the presence of the tip vortex. This increases the aft loading considerably and could be reduced by 'wash-out' near the tip. For a VCW this would be achieved by camber reduction of the tip segment.
It was found that the shape of the pressure distribution was similar for all the spanwise stations except station 12, the only difference being the gradual reduction of lift towards the tip. This suggested that the vortex influence was strongest over the outer 10 % of the span.
Figure 11 shows an almost rectangular spanwise lift distribution for the three uniform spanwise camber cases. Altering the spanwise camber by decreasing the tip camber and increasing the root camber changes the lift distribution significantly. This results in a large loss of lift in the outboard region. Consequently the centre of lift is moved inboard.

2.4 DISCUSSION

These results raised several points:

1) The C_L at which the uniform spanwise camber cases 5 5 5 5 and 10 10 10 10 cross-over in Figure 6 to indicate lower drag compared to the basic section are very high (greater than 0.8). The C_L range over which variable camber would be desirable would be between 0.2 and 0.6 for most civil aircraft at cruise. However theoretical calculations indicate that little more than 2° of camber rotation would be needed to cover this C_L range, therefore the 5° case would suit a high lift situation. The 10° case would be more applicable to the low speed take off and landing conditions where it is felt little or no additional assistance would be required from auxiliary high lift devices.

2) The selection of the origin of rotation based on the maximum curvature of the upper surface at 64.5% chord results in a large amount of chord extension for a given rotation. It is felt that the chord extensions of 13.6% and 27.7% for the 5° and 10° cases respectively are too great resulting in a large increase in the total wetted area. These values may be reduced by choosing an origin with a smaller radius of rotation resulting in more camber and less extension. The penalty for this would be a local increase in curvature on the upper surface at the junction between the centre body and the TE segment increasing the possibility of wave drag at transonic speeds.

3) The neglect of the LE camber deployment during wind tunnel tests results in large LE suction peaks. Whilst these may be tolerated to some extent at low speed the resulting wave drag at transonic speeds would be a severe penalty.

4) It is seen that spanwise variations of camber is a powerful tool for two reasons;

a) the rolling moment and hence the wing root bending moment can be significantly reduced by the deployment of large root cambers in conjunction with low tip cambers. Typically high lift manoeuvre situations would benefit greatly, as would the gust load alleviation problem.

b) The drag advantages of the 5 5 0 0 and 5 5 0 -3.5 configuration cases at C_L above 0.4 compared to the basic section indicates how the operational flexibility of a variable camber wing can allow the lift distribution to be altered to become more elliptic hence minimising vortex drag.

3. STRUCTURAL AND MECHANICAL DESIGN

3.1 TWO DIMENSIONAL (2-D) TRAILING EDGE (TE) DESIGN SCHEME

Aerodynamic investigations suggest that the predicted aerofoil performance improvements can best be achieved if the upper surface curvature is kept smooth and continuous. These geometric constraints therefore governed the practical, structural, and mechanical design of the VCW.

Figure 12 shows the essential features of the proposed scheme. It comprises of the following elements:

1) a solid trailing edge (TE) device,
2) a flexible upper surface,
3) a hinged lower surface,
4) an extending/conforming track,
5) a support track, and
6) a set of rolling elements for controlling the profile of the upper surface.

The necessary deployment curvature for the TE device is provided by attaching it to a curved extending track which slides within the support track of the same profile. The shape of these tracks is in keeping with the deployment arc A-B. Continuity between the TE device and the wing structure is provided by a flexible skin on the upper side and a hinged flap panel on the lower side. The flexible skin is clamped at the rear spar position and sits in a conforming track by means of a set of rolling elements. The conforming track is grooved in both the curved extending track and the TE device. It therefore matches the upper surface of the un-deployed TE device from point C to point D and curves from point C forward to match the shape of the extending track. The upper surface thus slides within the track during the TE deployment. The under side is kept continuous by means of a spring loaded lower surface closing plate hinged at 60% chord. Computational calculations showed no significant aerodynamic effects due to a slight kink at the lower surface hinge link.

The practical size of the upper surface skin restricts the range of deflection to either 0° to +10° or -3.5° to +7°. The position of the wing rear spar for the former range is 64.5% while for the later it is placed at 54%. The negative deflection was required for the flap to contribute to the roll control and wing root bending moment control.

3.2 THREE DIMENSIONAL (3-D) GEOMETRIC AND PRACTICAL DESIGN CONSIDERATIONS

Spanwise variation in camber is possible by dividing the control devices (LE and TE) into several segments similar to high lift devices on conventional wings. The resulting discontinuity between the differentialy deployed camber segments means that the motion should be in-line of flight. Figure 13a illustrates the planform arrangement of a typical transport aircraft wing, with the TE split in to six segments. The three inboard segments are deployed through positive angles only, while the three outboard segments have both positive and negative deflections. In reality this geometry is impossible to achieve for a swept and tapered wing, since the local radius of curvature varies along the span, increasing from tip to root. The deployment line joining the points of maximum curvature thus lies on a frustum of a cone.

If the segments are to move backwards in a line of flight direction with their edges streamwise, and at the same time rotate to give angular deflection, the axes of rotation, and the forward and aft end of the TE device must be unswept. The necessary changes to be made to the wing planform are shown in Figure 13b (the radius of curvature matches the outboard end of the segment). With such an arrangement the chord of the TE device, C_{TE} (see Figure 12) decreases rapidly as the span of the segment increases.

From these arguments it is apparent that a true VC profile could only be achieved by placing the segments perpendicular to the hinge line and deploying them conically as shown in Figure 13c.

The conical nature of the deployment requires the support tracks to be attached at an angle to the vertical, as illustrated in Figure 13d (dashed lines). This angle is equivalent to the angle made by the segments to the line of flight. Such an arrangement gives a lateral movement to the TE device which is;

a) aerodynamically unsatisfactory; requiring large cover fairings (Figure 13c), and
b) structurally impossible to give differential deployment of adjacent segments.

The attachment of the tracks should be directly on to the wing structural box side ribs, as shown by full lines in Figure 13d. Deployment of a solid TE is obviously not possible with such an arrangement, unless the TE box is made to flex and warp or be supported by a suitable universal joint system.

It is apparent from Figure 12 that in order to have negative deflections the rear spar position must be moved forward (to 54% chord). If some of the segments were to have both negative and positive deployment while the rest only had positive deployment the rear spar must be staggered, as shown in the planform drawings of Figure 13. This is an obvious drawback since the structural efficiency of the system will be much lower than say the continuous spar arrangement. The structural efficiency is further reduced by introducing cutouts to allow the tracks to run in and out of the main wing section.

Most modern transport aircraft make use of the wing structural box for fuel storage. An obvious disadvantage of the proposed concept is the positioning of the tracks on the side ribs inside the wing box, thus invading the fuel space.

3.3 THREE DIMENSIONAL (3-D) STRUCTURAL MODEL DESIGN AND TESTING

From the above discussions it is clear that the key features of the design are:

1) The desire to have both conical and parallel deployment, and
2) The requirement for flexibility and controlled curvature of the upper surface.

It was decided therefore to design, construct and test a scaled prototype model of one TE segment with the following aims:-

a) Highlight the problems associated with a 3D deployment geometry.
b) Assess how the system (track/roller) behaves when actuated and deployed under applied loads.
c) Check the suitability of designing the upper surface with varying stiffness in span and chord.

The second and third objectives required the tracking system and the upper surface to be designed to meet suitable stiffness criteria.

3.3.1 Model Design

An illustration of the design of the proposed system is given in Figure 14.

Upper Surface Design

The design of the upper surface is critical to the whole concept. The most important aspect being spanwise stiffness and chordwise flexibility. The upper surface skin must have sufficient stiffness in order to hold shape without excessive warping due to the applied aerodynamic loads. At the same time flexibility along the chord is needed for it to conform without sticking and binding. The undesired warping can be prevented by any, or combination, of the following three ways:

1) The attachment of spanwise stiffeners across the chord of the upper surface,
2) The placement of several chordwise rails across the span,
3) The design of the surface in appropriate fibre reinforced plastic (FRP) material.

For the structural model it was decided to combine the second and third alternatives. The skin was made from carbon composite fibres and restrained along the chord at 5 segmental spanwise stations. The longitudinal (spanwise) and transverse E values of the material are 0.8175×10^5 N/mm^2 and 0.499×10^5 N/mm^2 respectively. The laminate is 2mm thick and has 8 (0.25 mm thick) plies orientated in $[90/0_2/+45/0_2/90]_s$ direction. The 0° plies are placed along the span to give chordwise flexibility.
The upper surface skin profile is changed through a series of tags (rolling elements) positioning the skin in strips (rails). At the inboard and outboard ends the rails are attached to the extending tracks and the TE device, while in the intermediate span position they are attached to the TE device only. On actuation of the TE device, the extending track moves aft, carrying the conforming strips. Thus the upper surface skin effectively slides within the aforementioned strips.
The design of the upper surface was based on a stiffness criterion which restricted the maximum deflection to be less than 2% of the maximum local spar depth. The deflection predictions were made using Finite Element (FE) analysis techniques by simulating face pressures on thin shell elements.

Tracking system

A two track system is adapted with an extending track sliding on top of a support track with the assistance of cam and needle rollers (See section drawing in Figure 14). The rollers are sized to react to aerodynamic loads, whilst the design of the tracks is based on their ability to transfer shear and bending loads to the support structure (wing box).

TE Device

Structural design of the TE was not necessary since its basic function was only to display the 3-D geometric problems associated with conical and parallel deployment of a solid body. It was therefore simply machined from laminated wood.

Actuation

Initially it was intended to have two actuators placed, one at either end of the segment. However such an arrangement can only be implemented if the TE device is made to flex along the chord and warp along the span. Since the TE device was designed as a solid body which was envisaged to experience a lateral movement during deployment, only a single actuator could be implemented. This actuator was placed in a mid-span position.

3.3.2 Structural Testing and Results

In view of the three test objectives, the testing had to be divided into three distinct phases:

Phase I - Stiffness testing of the upper surface and comparison of the results with the FE predictions.
Phase II - Observation of the TE deployment unloaded.
Phase III - Observation of the deployment with representative applied loads.

Phase I Testing

Verifications of the FE results could only be possible by testing the upper surface under similar loading conditions.
Illustrations of the test apparatus is shown in Figure 15a. The test was carried out by supporting the upper surface on five chordwise formers along the span (simulating the tracks and conforming strips). The distributed load was applied by means of sand bags and the deflection measurements were made with dial gauges. 48 deflection measurements were recorded along the span and chord of the skin. An illustration of the measured and analysed deflections along the span at one chordwise station is given in Figure 15b. The miss-match of the results is due to slight miss

representation of the stiffness parameters and the loading between the two systems. In general the two sets of results correlate well with very little difference.

Phase II Testing

Once assembled, the TE was actuated in order to observe its translational motion. Figure 16 displays a photograph of the model in its maximum possible positive deployed position. Initial observations of the system suggested that the TE deployed smoothly. The upper surface was seen to conform smoothly and continuously without wrinkling or binding. The expected lateral movement across the span (from inboard to outboard) was evident. This was because of the different track radius at the two ends of the segment, which tends to twist the TE element. The TE element was obviously riding more on the larger radius (inboard) than it was on the smaller one.

The maximum measured extensions (for 7° of camber rotation) at the inboard and outboard ends were found to be approximately 270 mm and 261 mm respectively. In comparison the required extension at the two ends were 301 mm (inboard) and 264 mm (outboard). The difference in the two sets of figures implies that the TE device is too stiff to twist in order to flex for maximum parallel deployment. The TE device had a tendency to bind above 6° of deflection.

Phase III Testing

Figure 17 displays a photograph taken while operating the system under applied loads. The purpose of this exercise was to simply monitor the changes in deployment behaviour of the TE and the tracks due to applied loads. Observations indicated no real difference in the deployment of the loaded model in comparison with the unloaded model, except that the former system was much slower. This had been expected and is primarily due to rolling friction between the needle rollers and the two tracks.

3.4 DISCUSSION

A totally new design concept has been developed to satisfy the given geometric constraints of the aerofoil section and flap deployment set by aerodynamic requirements.
Extension of the concept to a 3-D wing showed how the desired conical and parallel deployments are possible only if a warping TE flap box or universal joints are used. This point is highlighted by designing the TE device of the structural model in laminated wood and operating under unloaded and loaded conditions. Deployment checks indicated no problems of achieving VC with continuous curvature tracks. The translational motions were observed to be smooth, and the upper surface flexed without wrinkling or binding.
FE analysis and initial static tests of the flexible upper surface suggest that it is possible to satisfy the stiffness requirements, provided that an appropriate number of chordwise rails are positioned along the span. The close proximity between the two sets of results indicates that much confidence can be placed in FE analysis, thus future work may not require separate stiffness checks for the upper surface.

4 RECOMMENDATIONS

1) The TE device structural box needs to be redesigned so that it flexes and has adequate stiffness such that it is not prone to flutter.

5 CONCLUSIONS

The outcome of this work was to design a variable camber wing which accommodates many of the conflicting structural and aerodynamic problems. The wind tunnel model demonstrated the possibility of improving the performance by means of both chordwise and spanwise camber variation. The structural model tested proved that such type of variation was a practical possibility.

ACKNOWLEDGEMENT

This project was a joint venture involving British Aerospace (Commercial Aircraft Division), the Department of Trade and Industry (DTI) and Cranfield Institute of Technology.
It provided a unique opportunity to blend the extensive design experience of British Aerospace with Cranfield's research and testing facilities to produce a workable design solution. DTI's involvement was of great assistance to the aerodynamic design of the wind tunnel model and with its testing.
The authors wish to express their appreciation to all involved and especially to Professor J J Spillman, who originated the project and whose enthusiasm and experience contributed greatly to all aspects of the work.

REFERENCES

1) J. J. Spillman, The use of variable camber to reduce drag, weight and cost of transport aircraft. Aeronautical Journal, January 1992 Royal Aeronautical Society Paper No. 1844

2) A. J. Rao Variable camber wing for transport aircraft, PhD Thesis 1989 Cranfield Institute of Technology

3) Pierce and Treadgold A simple mechanical system to vary a wing section shape to suit various flight conditions. RAE TM 1149, 1969

4) Engineering and Science Data Unit (ESDU) ESDU Item 70011 - Lift curve slope and aerodynamic centre position of wings in inviscid

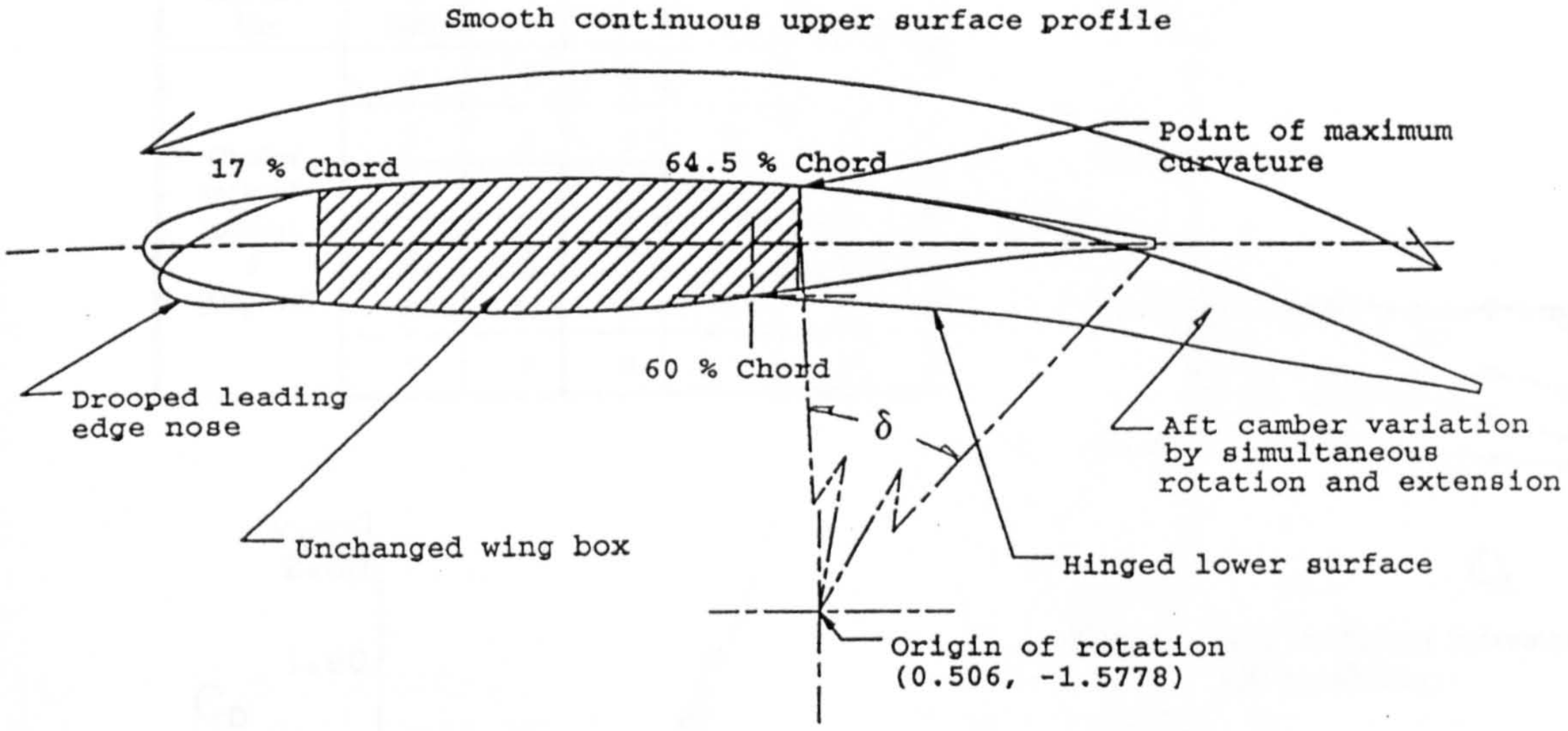

Figure 1: Basic aerofoil section indicating proposed camber variation scheme

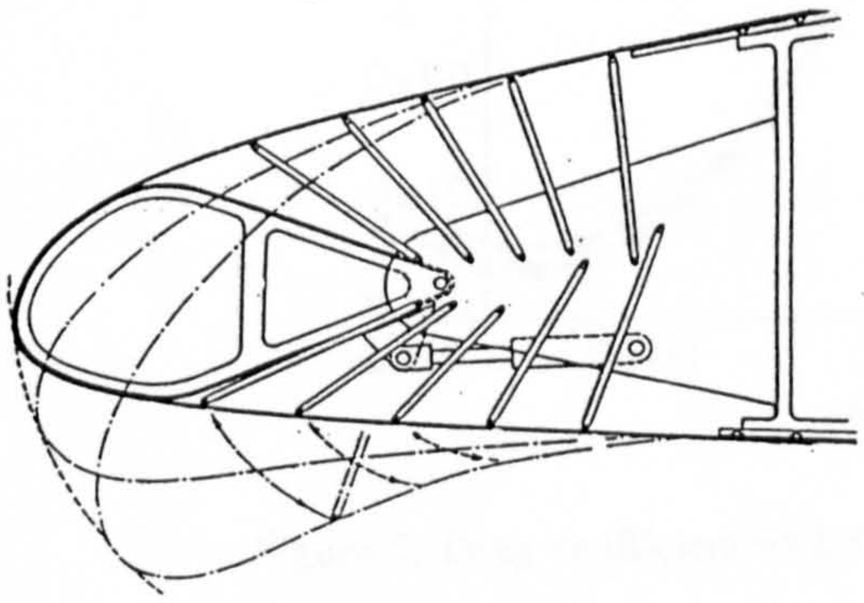

Figure 2: The RAEVAM leading edge droop

Segment No	1 Root	2	3	4 Tip	Symbol
Camber angle of rotation, δ (Degrees)	0	0	0	0	✱
	5	5	5	5	○
	10	10	10	10	◇
	5	5	0	0	□
	10	10	0	0	△
	5	5	0	-3.5	×

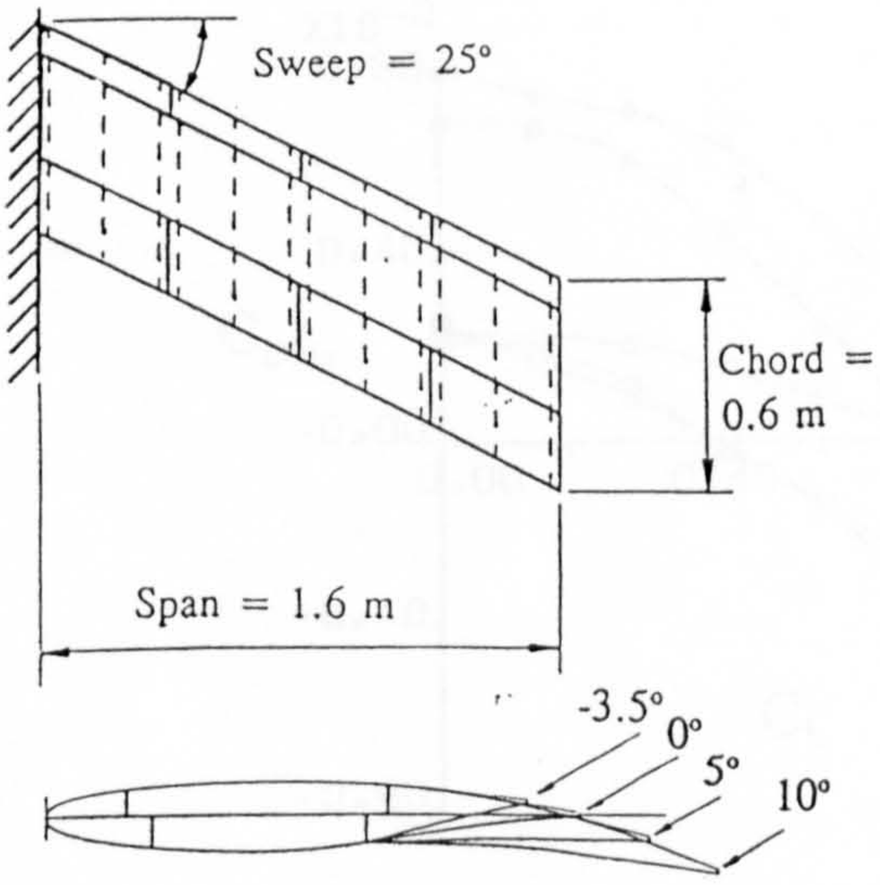

Figure 3: Four segment variable camber wind tunnel model

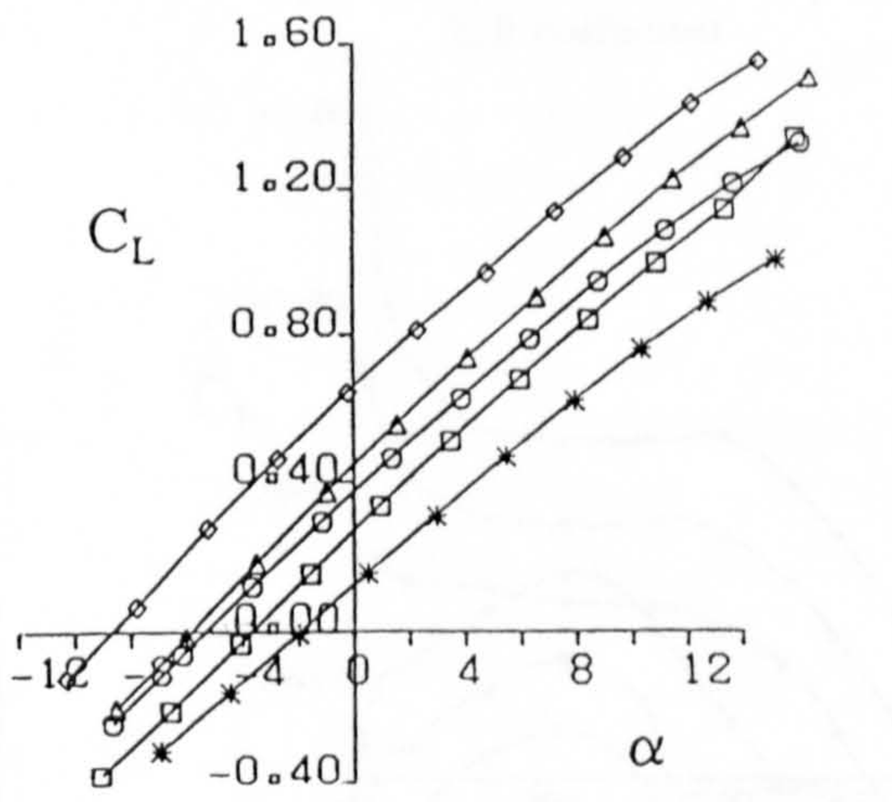

Figure 4: Lift coefficient vs Incidence

Segment No	1 Root	2	3	4 Tip	Symbol
Camber angle of rotation, δ (Degrees)	0	0	0	0	✱
	5	5	5	5	○
	10	10	10	10	◇
	5	5	0	0	□
	10	10	0	0	△
	5	5	0	-3.5	×

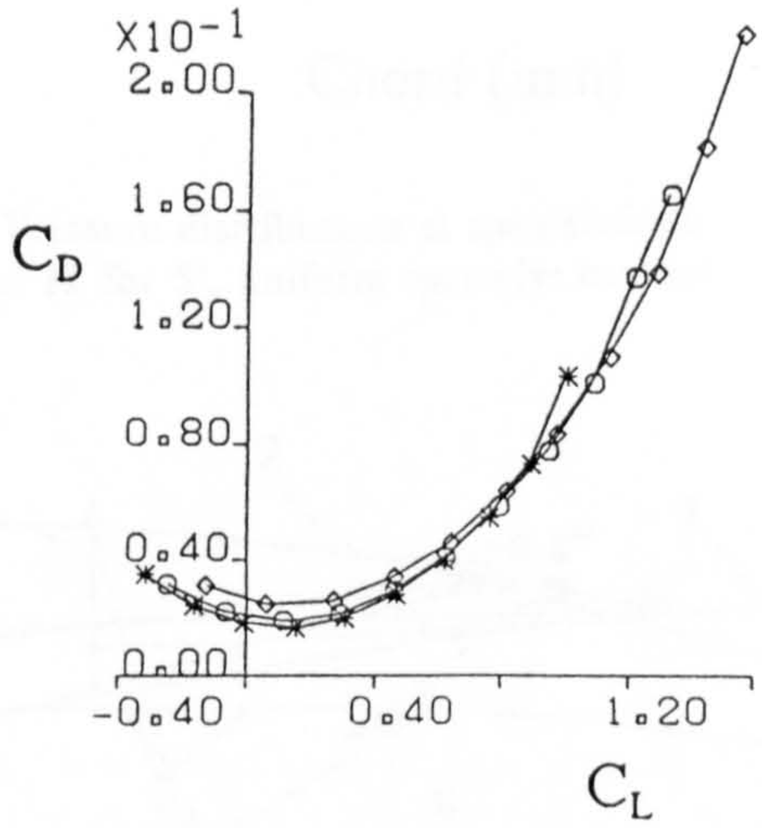

Figure 5: Drag coefficient vs Lift coefficient

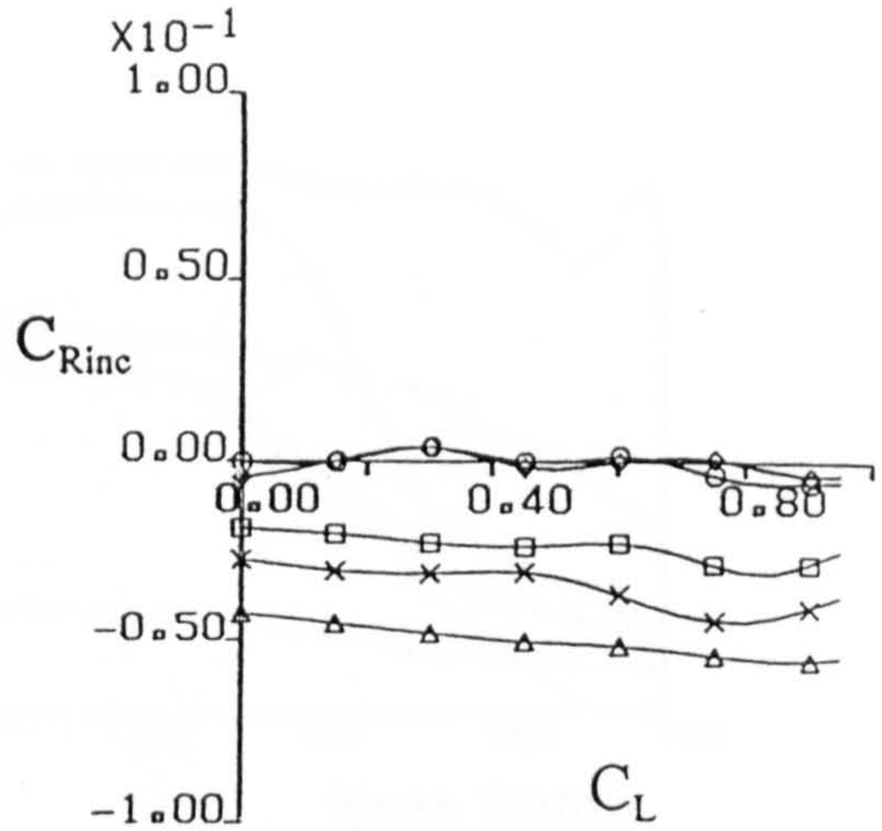

Figure 7: Roll coefficient increment vs Lift coefficient

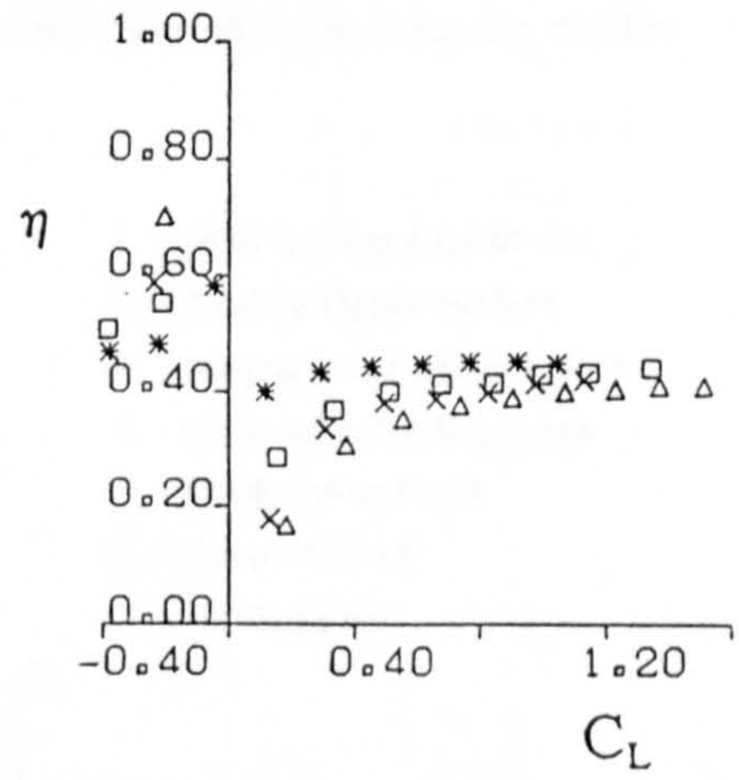

Figure 8: Spanwise centre of pressure vs Lift coefficient

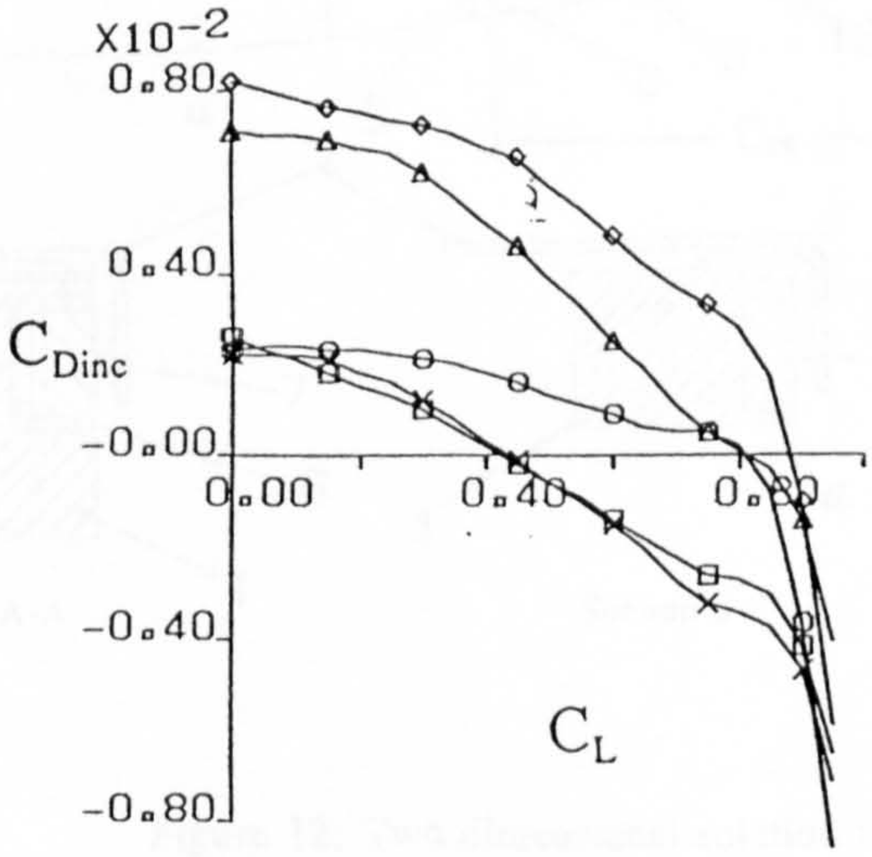

Figure 6: Drag coefficient increment vs Lift coefficient

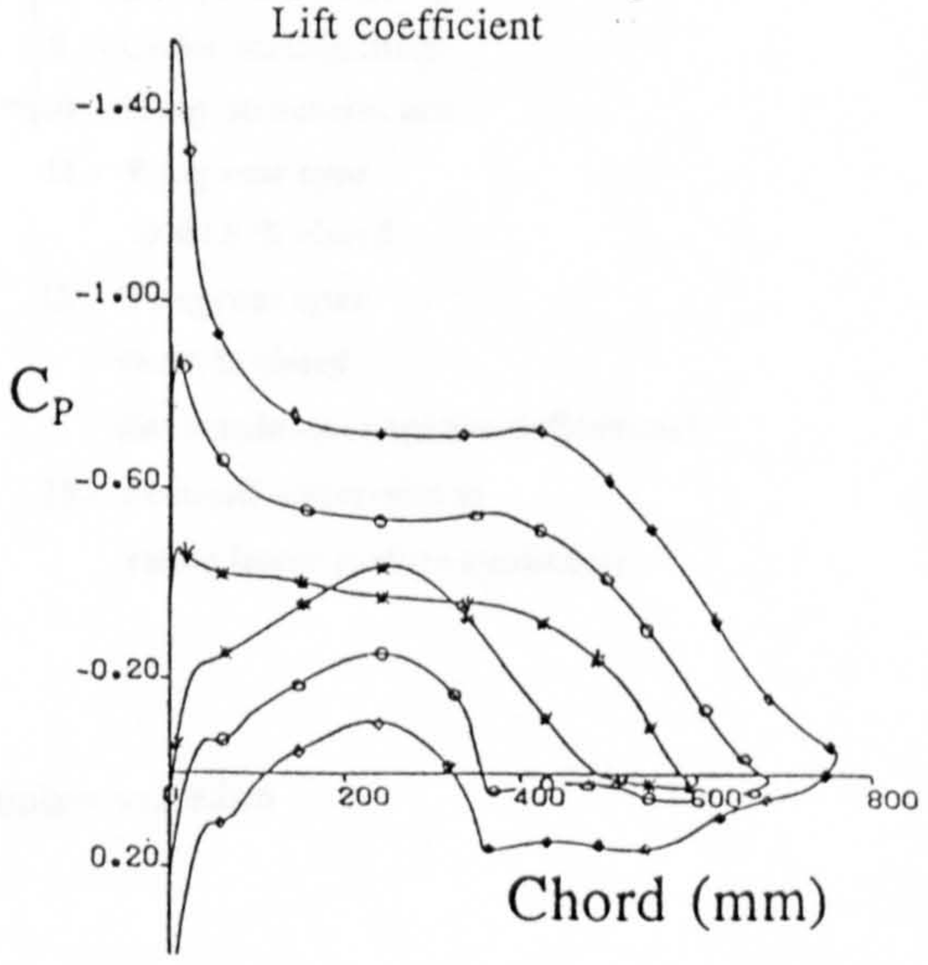

Figure 9: Pressure distributions at span station 7 for 0°, 5°, and 10° uniform spanwise camber

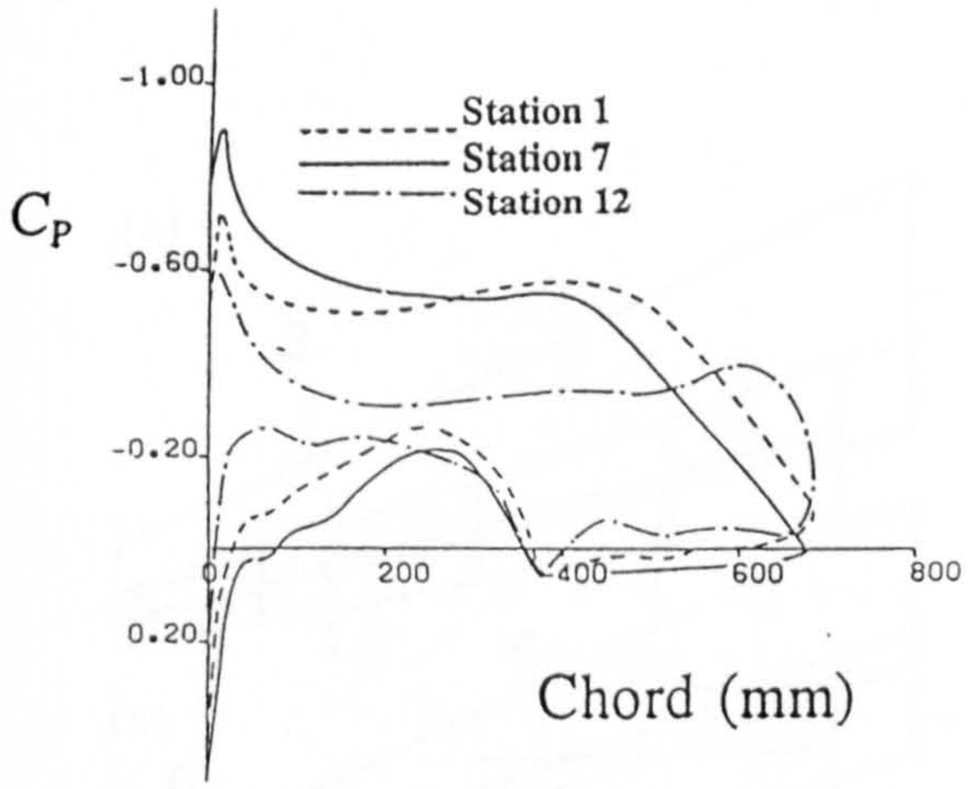

Figure 10: Pressure distributions at span stations 1, 7 and 12 for 5°, uniform spanwise camber

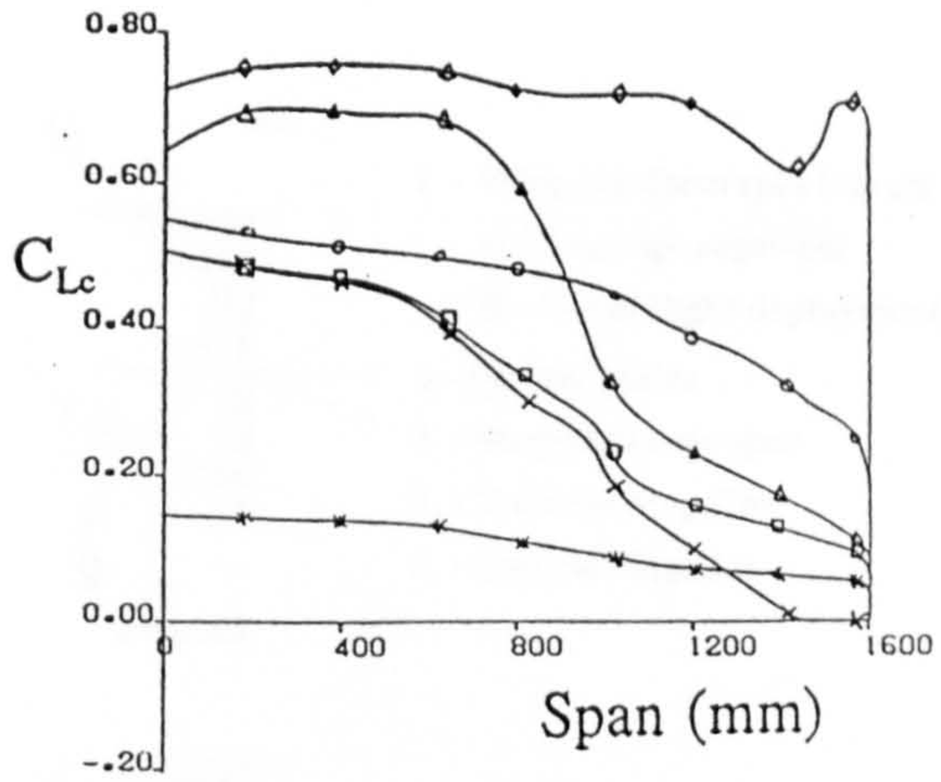

Figure 11: Spanwise lift distribution for various uniform and discontinuous spanwise camber

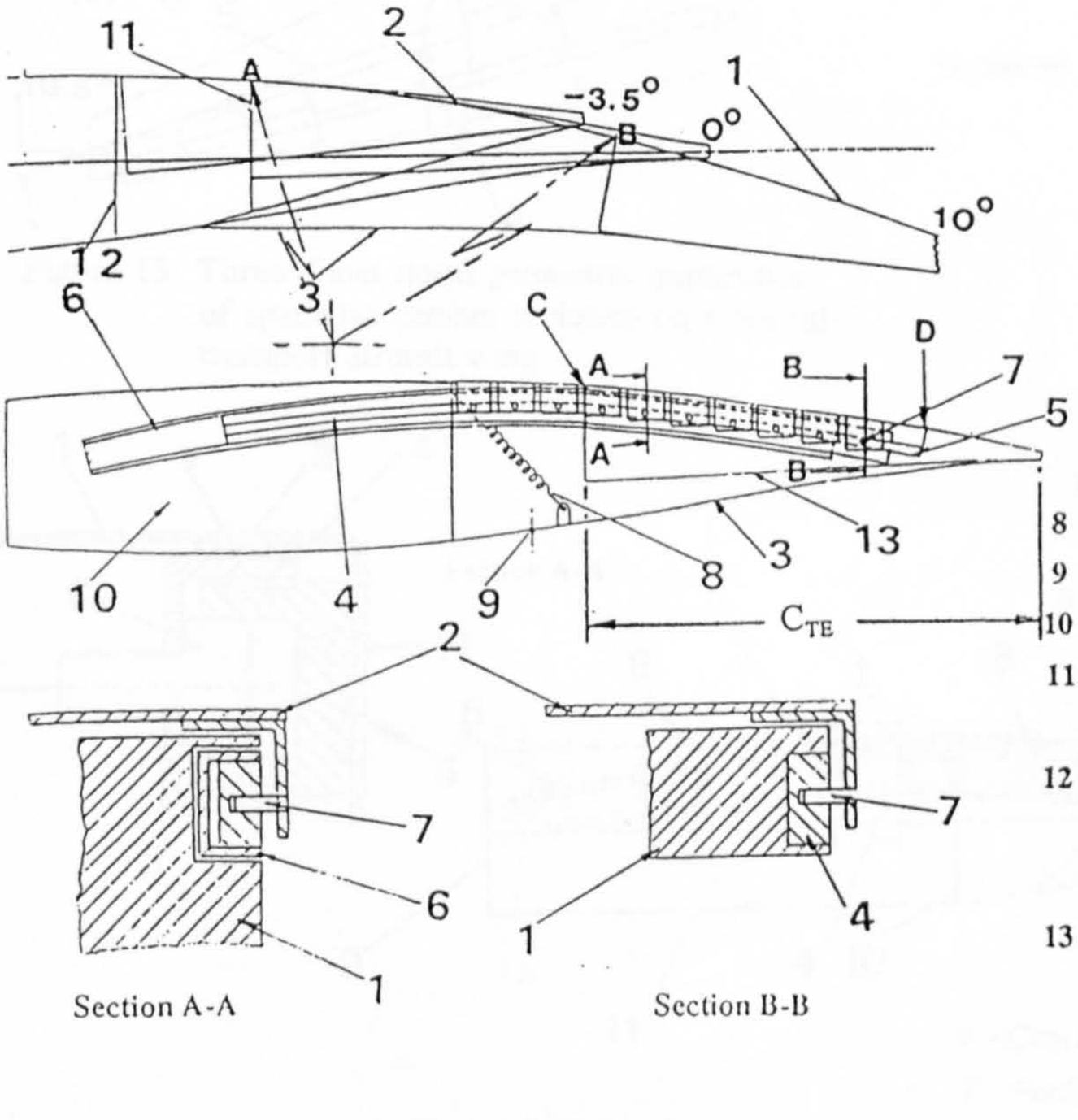

1 - Solid trailing edge device
2 - Flexible Upper surface
3 - Hinged lower surface plate
4 - Grooved extending track
5 - Conforming track
6 - Support track
7 - Rolling pins
8 - Compression spring
9 - Under surface hinge
10 - Wing structural box
11 - Wing rear spar @ 64.5 % chord
12 - Wing rear spar @ 54 % chord (for maximum negative deflections)
13 - Reduced under-side to retain lower surface continuity

Figure 12: Two dimensional solution for aft camber variation

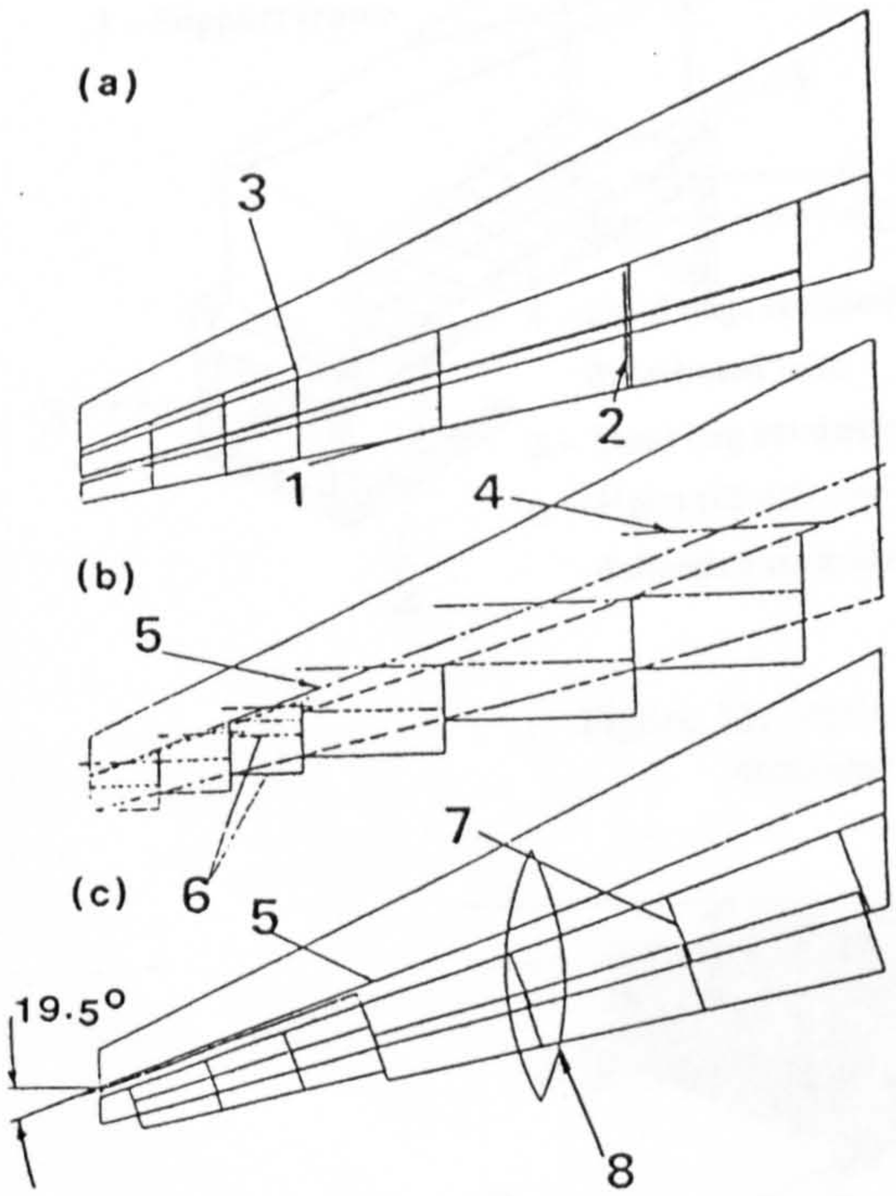

Figure 13: Three dimensional geometric implication of spanwise camber variation on a typical transport aircraft wing

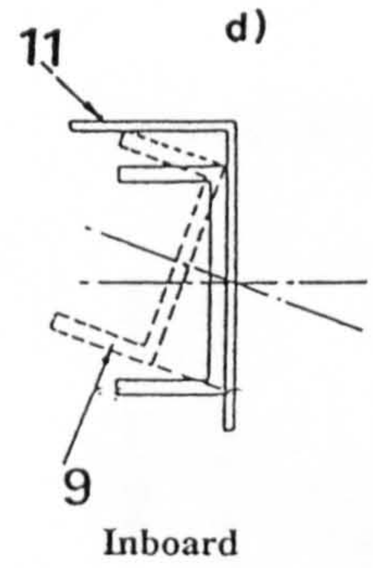

1 - Wing planform split into six trailing edge segments (in-line of flight deployment)
2 - Splitter plates
3 - Staggered rear spar
4 - Unswept hingeline
5 - Conical hingeline
6 - Unswept trailing edge device
7 - Conicaly deployed segments
8 - Fairings to cover lateral movement of the segments
9 - Support tracks mounted at an angle
10 - Support tracks mounted direct of the wing side ribs
11 - Wing side ribs

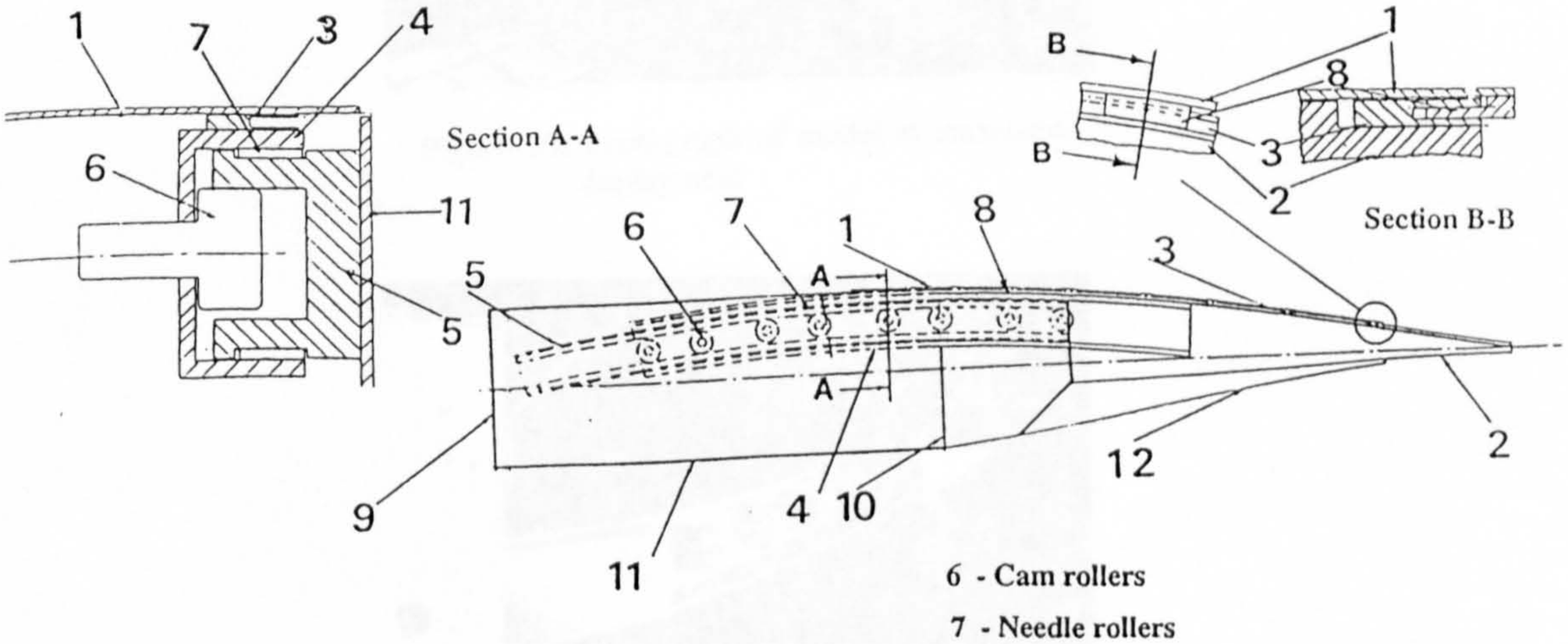

1 - Carbon fibre upper surface skin
2 - Solid trailing edge device
3 - Conforming strip
4 - Extending track
5 - Support track
6 - Cam rollers
7 - Needle rollers
8 - Rolling elements
9 - Front spar
10 - Rear spar
11 - Side support rib
12 - Lower surface flap panel

Figure 14: Three dimensional structural model

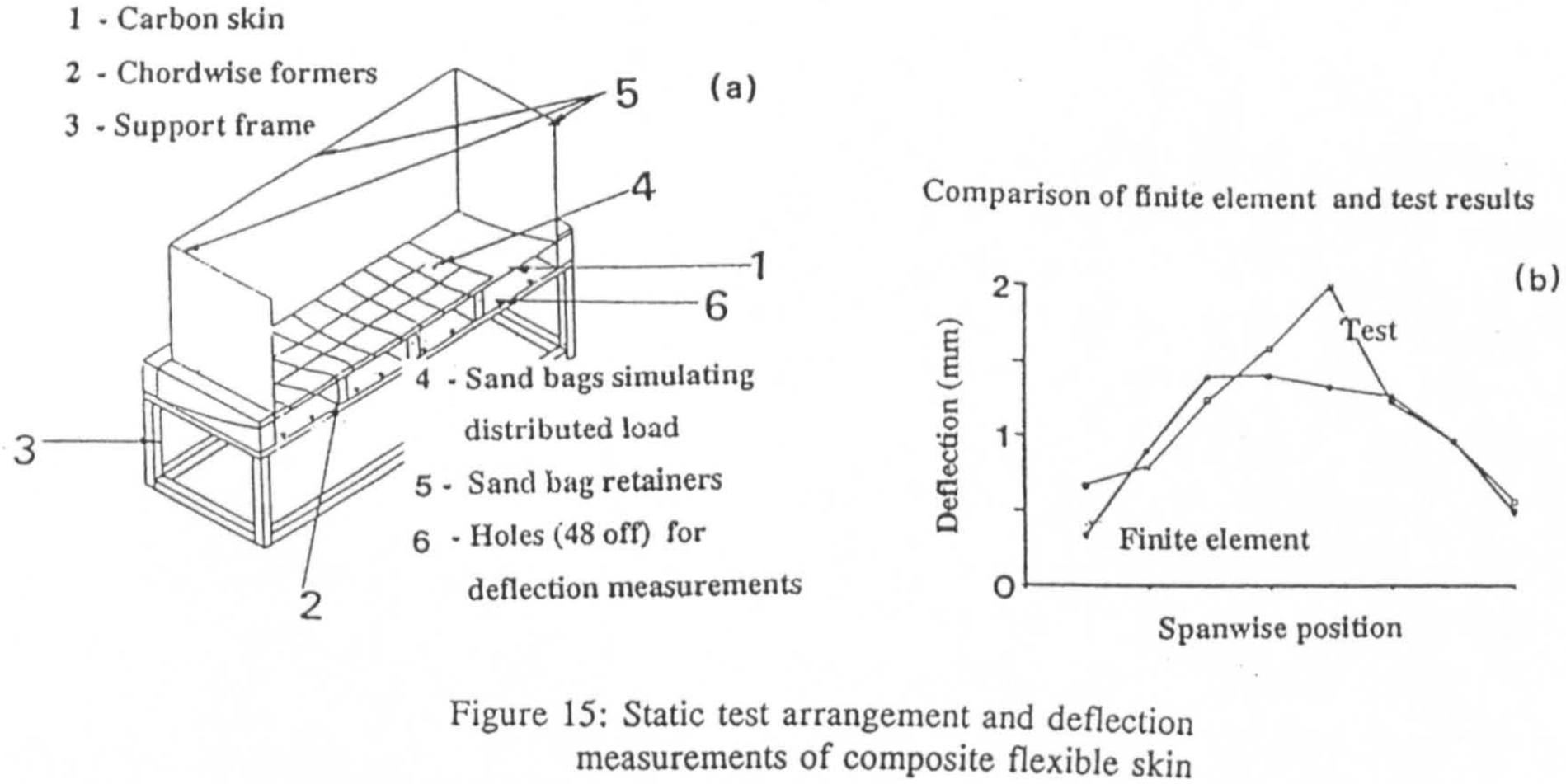

Figure 15: Static test arrangement and deflection measurements of composite flexible skin

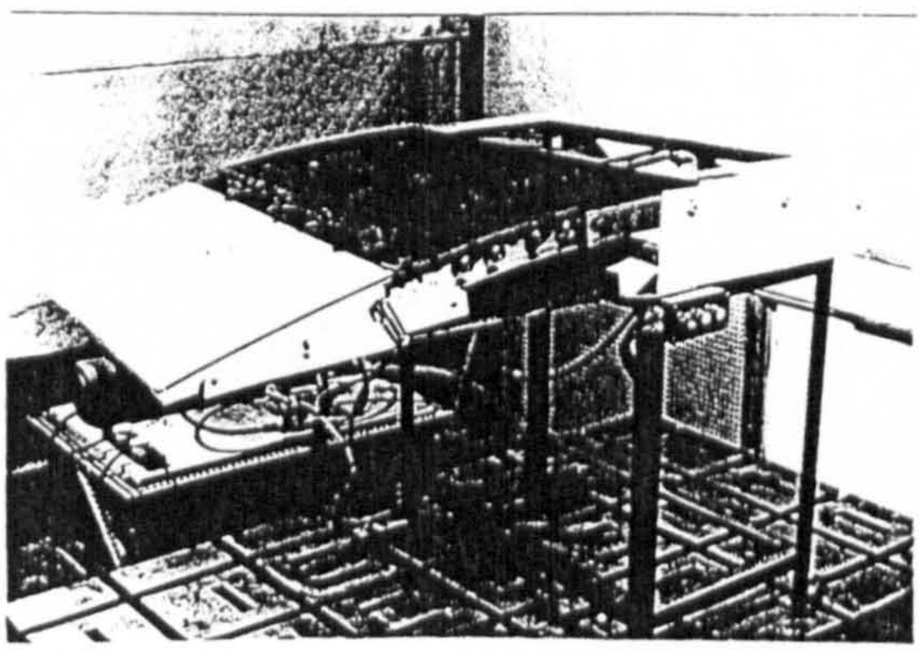

Figure 16: Photograph of model at maximum deployment

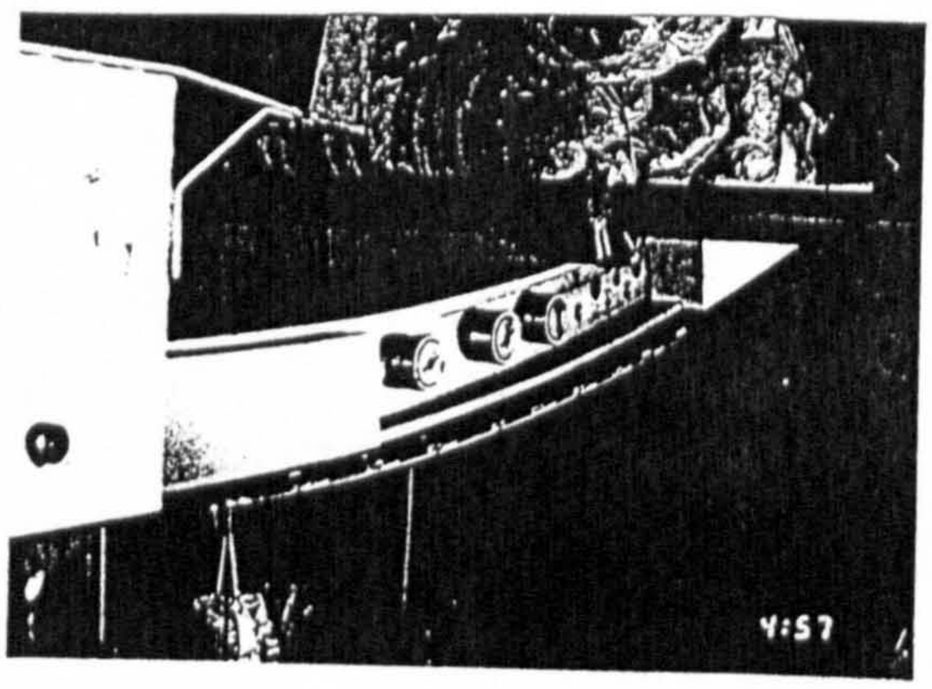

Figure 17: Operation of the structural model under applied load